

**Characterization of Dendritic
Changes Induced by Elevated
Intraocular Pressure in a Chronic
Glaucoma Model**

Thesis submitted for the degree of Doctor of Philosophy (PhD)

University College London

March 2011

Meng Liu

Visual Neuroscience, University College London, Institute of
Ophthalmology, London

Declaration of Own Work

I, Meng Liu, confirm that the work presented in this thesis is my own. Where information has been derived from other sources, I confirm that this has been indicated in the thesis.

Signature: MENG LIU Date: 8/3/2011

Abstract

Visual information is sent from the retina to central visual targets through the optic nerve which is formed of retinal ganglion cells' (RGCs) axons. In rodents, the superior colliculus (SC) is the major site of termination of retinal axons and the lateral geniculate nucleus (LGN) is another target of retinal axons. Glaucoma is a progressive optic neuropathy, characterized by RGC death. Dendrites are fine neuronal processes which support postsynaptic contact elements and are responsible for receiving synaptic signals. Accordingly, the morphology of dendrites has a profound impact on integrating neuronal input to the central nervous system from peripheral targets. Previous studies have documented dendritic changes in neuronal degenerative processes including those occurring in ageing and diseases. However, the morphological changes of dendrites in the visual pathway in glaucoma have not been well characterized.

This thesis characterizes morphological changes of dendrites in the retina and the central visual targets in an experimental rat model of glaucoma for the first time.

Dendritic labelling was achieved using the fluorescent dye DiI with *in vivo* and *in vitro* techniques. Dendrites of neurons in the SC and LGN were labelled *in vitro* using 0.1% DiI solution, and those of the RGCs were labelled using the biolistic technique. Confocal microscopy was next performed to image neurons, and dendrites were traced and quantified using Image J. Dendritic parameters including the mean dendritic length and the number of dendrites per neuron were analyzed in baseline, glaucoma animals and age-matched controls. Dendritic morphologies were studied in

five types of neurons in the SC (including horizontal (H); piriform (P); narrow field vertical (V); wide field vertical (W) and stellate (S) cells), two types of neurons in the LGN (including the relay neuron type I (LG1) and type II (LG2)) and three types of RGCs (including type I (RI), type II (RII) and type III (RIII)).

In this thesis, both age-related and glaucoma-related dendritic changes were demonstrated in the RGCs, SC cells and LGN cells in our rat model of experimental glaucoma. Firstly, the mean dendritic length and dendritic number of RGCs, SC cells and LGN cells were significantly reduced during ageing in normal animals, and more pronounced changes were observed in glaucoma animals. Secondly, significant dendritic shrinkage and losses were also shown in glaucoma animals compared with age-matched controls. Thirdly, the RGC was the first site to show dendritic changes following elevated IOP, but the most prominent changes were visible in the SC.

The results in this study implicated that both the RGC and SC are potential sites for an early diagnosis strategy. Additionally, the glaucoma-related dendritic degeneration was demonstrated not only in the RGCs, but also in the SC and LGN, indicating that both the retina and the brain should be targeted when considering therapies for glaucoma.

In conclusion, this thesis characterizes dendritic changes in the visual pathway in rats with chronic glaucoma, demonstrating that both ageing and elevated intraocular pressure (IOP) can affect dendritic morphology in the RGCs, SC cells and LGN cells. The findings in this study have contributed to the understanding of retinal and central neuronal degeneration in glaucoma, providing new insights into potential diagnosis and therapeutic strategies.

Acknowledgments

First and foremost, I would like to express my sincere gratitude to my supervisor, Professor Francesca Cordeiro, for giving me the opportunity to study for this PhD. I gratefully acknowledge Professor Cordeiro for her enthusiasm, inspiration, and thoughtful guidance over the past years. I also want to thank Francesca for supporting me to present my research at international conferences, and for her invaluable advice and patience that I have received for writing this thesis. I would also like to thank Professor Tom Salt for his continual encouragement, patience and constructive suggestions throughout this work. I'm deeply grateful to his great insights and immense knowledge, especially his expertise in neuroscience, and his guidance from the early stage of this research. The general support from the Medical Research Council and Visual Farma which make this PhD work possible is also greatly appreciated.

I would like to extend my warmest thanks to all those who have helped me with my research in the Institute of Ophthalmology, University College London. They have been constant sources of help, encouragement and companionship during my PhD journey. I would like to thank Dr Li Guo for preparing all the animal models that have been used in this thesis. Special thanks to Dr Anne Georgiou, who was the PhD student in our lab, for her encouragement, helpful suggestions and her friendship throughout these years. Many thanks to Shereen Nizari, the laboratory technician in our lab, for her help to complete the blind analysis, for her support and friendship. A huge thank you goes to Anne and Shereen for their precious time spent

proofreading this thesis. I would also like to acknowledge our previous and current fellow labmates Dr Annelie Maass, William Cheung, Nick Wood, Sarah Borrie, Dr. David Lara, Dr James Duggan, Dr Katy Coxon, Dr Eduardo Normando and Dr Abeir Baltmr, for all of their support, encouragement and for sharing their knowledge to help me complete my thesis. Other members of staff in the institute who have been of great help during this project also deserve a mention. Staffs in the BRU who have taken care of my animals, Peter Munro who has helped me with the confocal imaging, Rosalind, Heidi and Christine who have taught me the histology techniques, also deserve a big thank you.

Furthermore, I wish to express my sincere gratitude to Professor David Becker, Department of Cell and Developmental Biology, University College London, for allowing me to complete the RGC staining in his lab, and for his guidance and warm encouragement.

I'm always greatly indebted to my parents, for raising me, believing in me and supporting me to pursue my interests. I also wish to thank my grandma, my aunts, and of course my lovely cousins, for their understanding and encouragement. Without my family's boundless love and incredible support, this thesis would not have been possible. Last, but not least, I would like to thank Nick Hsieh for his love and support over the years.

Table of Contents

Declaration of Own Work	2
Abstract	3
Acknowledgments.....	5
Table of Contents	7
List of Figures	15
List of Tables.....	22
List of Abbreviations.....	26
Chapter 1: Introduction.....	31
1.1 Visual System.....	31
1.1.1 The Neurons.....	31
1.1.2 The Pathway of Light in Retina.....	32
1.1.2.1 The Structure of Retina.....	32
1.1.2.2 The Visual Pathway in Retina.....	34
1.1.2.3 Retinal Ganglion Cells.....	36
1.1.2.3.1 Primate Ganglion Cells.....	36
1.1.2.3.2 Feline Ganglion Cells.....	37
1.1.2.3.3 Rodent Ganglion Cells.....	37
1.1.3 The Visual Pathways in the Brain.....	41
1.1.3.1 Retinal Projections to the Central Visual Targets in Primates.....	41
1.1.3.1.1 Parallel Pathways in the Lateral Geniculate Nucleus in Primates.....	43
1.1.3.1.2 Neurons in the Primate Lateral Geniculate Nucleus.....	45
1.1.3.1.3 Retinal Input to the Superior Colliculus in Primates.....	47

1.1.3.2 Retinal Projections to the Central Visual Targets in Felines	48
1.1.3.2.1 Retinal Input to the Lateral Geniculate Nucleus in Felines.....	49
1.1.3.2.2 Neurons in the Feline Lateral Geniculate Nucleus.....	49
1.1.3.2.3 Retinal Input to the Superior Colliculus in Felines	50
1.1.3.2.4 Neurons and Layers in the Superior Colliculus in Felines	51
1.1.3.3 Retinal Projections to the Central Visual Targets in Rodents.....	52
1.1.3.3.1 Retinal Input to the Superior Colliculus in Rodents.....	52
1.1.3.3.2 Neurons in the Rodent Superior Colliculus.....	56
1.1.3.3.3 Retinal Input to the Dorsal Lateral Geniculate Nucleus in Rodents	60
1.1.3.3.4 Neurons in the Rodent Lateral Geniculate Nucleus	60
1.1.4 Glaucoma	65
1.1.4.1 Epidemiology of Glaucoma Disease	65
1.1.4.2 Intraocular Pressure and Types of Glaucoma	66
1.2 Neuronal Atrophy in Visual Pathways in Glaucoma.....	67
1.2.1 Dendritic Degeneration in the RGCs in Glaucoma.....	68
1.2.1.1 Dendritic Changes in Human Glaucoma and Primate Glaucoma Model	68
1.2.1.2 Dendritic Changes in Feline Glaucoma Model	69
1.2.1.3 Dendritic Changes in Rodent Glaucoma Model	70
1.2.2 Dendritic Degeneration in Glaucoma Brain	74
1.2.3 Dendritic Alterations in Other Neurodegenerative Conditions	75
1.2.3.1 Cerebral Trauma.....	75
1.2.3.2 Alzheimer’s disease.....	77
1.2.3.3 Amyotrophic Lateral Sclerosis.....	78
1.2.4 Dendritic Changes during Development.....	80

1.2.5 Age-related Dendritic Changes.....	81
1.3 Summary and Aims of the Study.....	83
Chapter 2: Materials and Methods.....	85
2.1 Animals.....	85
2.2 Glaucoma Model	86
2.2.1 Anaesthesia of Animals	86
2.2.2 Induction of Ocular Hypertension	86
2.3 Dendritic Changes in the Superior Colliculus	88
2.3.1 Animal Preparation	88
2.3.1.1 Animals	88
2.3.1.2 Animal Sacrifice and Removal of Brains.....	89
2.3.2 Preparation of Brain Slices	90
2.3.3 DiI Labelling Method	92
2.3.3.1 DiI.....	92
2.3.3.2 Comparison of Different DiI Dilutions	93
2.3.3.3 Staining Procedure	94
2.3.3.3.1 Immersion Labelling	94
2.3.3.3.2 Injection Labelling	94
2.3.4 Mounting.....	95
2.3.5 Blind Analysis.....	95
2.3.6 Laser Confocal Microscopic Imaging.....	97
2.3.7 Morphological Analysis of Cells in the Superior Colliculus	97
2.3.7.1 Groups of Cells in the SC.....	97
2.3.7.2 Classification of Cells in the SC	98
2.3.7.3 ImageJ software.....	99

2.3.7.4	Procedures for Analyzing Dendritic Parameters.....	100
2.3.8	Statistical Analysis.....	101
2.4	Dendritic Changes in the Lateral Geniculate Nucleus.....	102
2.4.1	Animal Preparation	102
2.4.2	Preparation of Brain Slices	103
2.4.2.1	Preparation of Parasagittal Slices.....	104
2.4.2.2	Preparation of Pseudo-Parasagittal Slices.....	104
2.4.3	DiI Labelling Method	107
2.4.3.1	Staining Procedure	107
2.4.3.1.1	Injection Labelling.....	107
2.4.3.1.2	Retrograde Labelling of LGN.....	109
2.4.4	Mounting, Blind Analysis and Confocal Imaging.....	111
2.4.5	Morphological Analysis of Cells in the Lateral Geniculate Nucleus	114
2.4.5.1	Groups of Cells in the LGN	114
2.4.5.2	Classification of Cells in the LGN.....	114
2.4.5.3	Morphological Analysis.....	116
2.4.6	Statistical Analysis.....	116
2.5	Dendritic changes in the Retina.....	117
2.5.1	Animal Preparation	117
2.5.1.1	Animals	117
2.5.1.2	Animal Sacrifice and Eye Enucleation.....	117
2.5.1.3	Retina Dissection.....	119
2.5.1.4	Retina Flat-mounting.....	119
2.5.1.5	Removal of Vitreous and Inner Limiting Membrane.....	120
2.5.2	DiI Labelling.....	121

2.5.2.1 Preparation of Shooting Bullets	121
2.5.2.1.1 Pre-coating Tubing with PVP	121
2.5.2.1.2 Coating Particles with Dye.....	122
2.5.2.1.3 Loading the Bullets	122
2.5.2.2 Gene Gun Labelling	123
2.5.3 Mounting, Blind analysis and Confocal Imaging	125
2.5.4 Morphological Analysis.....	126
2.5.4.1 Groups of Retinal Ganglion Cells	126
2.5.4.2 Classification of Retinal Ganglion Cells.....	127
2.5.5 Statistical Analysis.....	128
Chapter 3: Results.....	129
3.1 IOP Measurements	129
3.2 Dendritic Changes in the Superior Colliculus	130
3.2.1 DiI Labelling Method	130
3.2.1.1 Immersion Labelling and Injection Labelling.....	130
3.2.1.2 Comparison of Different DiI Dilutions	131
3.2.2 Comparison of Different Fixation Methods for Rat Brains	133
3.2.3 Classification of Cells in the Rodent Superior Colliculus	134
3.2.4 Morphological Changes of Dendrites in the Superior Colliculus.....	136
3.2.4.1 Dendritic Changes in Control Animals	136
3.2.4.1.1 Changes in Mean Dendritic Length.....	136
3.2.4.1.2 Changes in Dendritic Number	144
3.2.4.2 Dendritic Changes in Glaucoma Animals.....	151
3.2.4.2.1 Changes in Mean Dendritic Length.....	151
3.2.4.2.2 Changes in Dendritic Number	158

3.2.4.3 Comparison of Dendritic Parameters between Glaucoma and Control Animals	165
3.2.4.3.1 Comparison of Mean Dendritic Length.....	165
3.2.4.3.2 Comparison of Dendritic Number	168
3.3 Dendritic Changes in the Lateral Geniculate Nucleus.....	173
3.3.1 DiI Labelling Methods.....	173
3.3.2 Classification of Cells in the Rat LGN	175
3.3.3 Morphological Changes of Dendrites in the Lateral Geniculate Nucleus	176
3.3.3.1 Dendritic Changes in Control Animals	176
3.3.3.1.1 Changes in Mean Dendritic Length.....	176
3.3.3.1.2 Changes in Dendritic Number	181
3.3.3.2 Dendritic Changes in Glaucoma Animals.....	185
3.3.3.2.1 Changes in Mean Dendritic Length.....	185
3.3.3.2.2 Changes in Dendritic Number	189
3.3.3.3 Comparison of Dendritic Parameters between Glaucoma and Control Animals	193
3.3.3.3.1 Comparison of Mean Dendritic Length.....	193
3.3.3.3.2 Comparison of Dendritic Number	196
3.4 Dendritic Changes in the Retina.....	199
3.4.1 DiI Labelling Method	199
3.4.2 Classification of Retinal Ganglion Cells in the Retina	199
3.4.3 Morphological Changes of Dendrites in the Retina.....	201
3.4.3.1 Dendritic Changes in Control Animals	201
3.4.3.1.1 Changes in Mean Dendritic Length.....	201
3.4.3.1.2 Changes in Dendritic Number	206
3.4.3.2 Dendritic Changes in Glaucoma Animals.....	210

3.4.3.2.1 Changes in Mean Dendritic Length.....	210
3.4.3.2.2 Changes in Dendritic Number	215
3.4.3.3 Comparison of Dendritic Parameters between Glaucoma and Control Animals	220
3.4.3.3.1 Comparison of Mean Dendritic Length.....	220
3.4.3.3.2 Comparison of Dendritic Number	224
3.5 Comparison of Dendritic Changes in RGCs, SC cells and LGN cells	227
3.5.1 Dendritic Changes in Control Animals.....	227
3.5.1.1 Changes in Mean Dendritic Length	227
3.5.1.2 Changes in Dendritic Number	231
3.5.2 Dendritic Changes in Glaucoma Animals.....	235
3.5.2.1 Changes in Mean Dendritic Length	235
3.5.2.2 Changes in Dendritic Number	239
3.5.3 Comparison of Dendritic Parameters between Glaucoma and Control Animals	244
3.5.3.1 Comparison of Mean Dendritic Length	244
3.5.3.2 Comparison of Dendritic Number	248
Chapter 4: Discussion	252
4.1 The Methodologies of Dendritic Labelling and Analysis	254
4.1.1 Dendritic Labelling	254
4.1.2 Analysis of Dendritic Parameters	257
4.2 Classification of the SC cells, LGN cells and RGCs.....	258
4.2.1 Classification of Neurons in the SC.....	258
4.2.2 Classification of Neurons in the LGN	260
4.2.3 Classification of the RGCs.....	262
4.3 Age-related Dendritic Changes in Normal Animals.....	263

4.3.1 Dendritic Changes in the Superior Colliculus	264
4.3.2 Dendritic Changes in the Lateral Geniculate Nucleus.....	266
4.3.3 Dendritic Changes in the Brain.....	268
4.3.4 Functional Changes in the SC and LGN during Ageing.....	274
4.3.5 Dendritic Changes in the Retinal Ganglion Cells	275
4.3.6 Comparison of Dendritic Changes in the RGCs, SC cells and LGN cells	280
4.4 Dendritic Changes in Glaucoma Animals	282
4.4.1 Age-related Dendritic Alteration in Glaucoma Animals	283
4.4.1.1 Dendritic Changes in the Superior colliculus.....	283
4.4.1.2 Dendritic Changes in the Lateral Geniculate Nucleus	286
4.4.1.3 Dendritic Changes in the Retinal Ganglion Cell.....	289
4.4.1.4 Comparison of Dendritic Changes in the RGCs, SC cells and LGN cells.....	294
4.4.2 Glaucoma-related Dendritic Changes	296
4.4.2.1 Dendritic Changes in the Superior Colliculus.....	299
4.4.2.2 Dendritic Changes in the Lateral Geniculate Nucleus	301
4.4.2.3 Dendritic Changes in the CNS in Neurodegenerative Conditions	302
4.4.2.4 Functional Changes in the SC and LGN in Glaucoma.....	306
4.4.2.5 Dendritic Changes in the Retinal Ganglion Cells	308
4.4.2.6 Comparison of Dendritic Changes in the RGCs, SC Cells and LGN Cells.....	314
Chapter 5: Summary and Future Perspectives	317
References	324
Appendix	348

List of Figures

Figure 1.1: The structure of a typical neuron.	32
Figure 1.2: The anatomy of the eye and arrangements of retinal layers.	33
Figure 1.3: The layers and basic circuitry of the retina.....	35
Figure 1.4: The primate visual pathways from the retina to the central visual targets.	42
Figure 1.5: The function and eye specific organization of primate LGN.	44
Figure 1.6: The visual pathways from the retina to the brain in rats.....	54
Figure 1.7: A diagram of sagittal view of rat brain.	55
Figure 1.8: A diagram of sagittal view of the superior colliculus (SC) from rat brain.	56
Figure 1.9: Classification of neurons in the upper layers of superior colliculus.....	57
Figure 1.10: Diagrams of the main types of relay neurons and the interneuron in the rodent dLGN.	61
Figure 2.1: Sagittal view of a rat brain slice containing superior colliculus (SC)	91
Figure 2.2: Absorption and fluorescence emission spectra of DiI bound to phospholipid bilayer membranes	92
Figure 2.3: Diagram of DiI injection method.....	96
Figure 2.4: The sample image and tracings by NeuronJ in ImageJ software.....	101
Figure 2.5: The sagittal view of the brain slice and the location of dLGN.	105
Figure 2.6: The preparation of Pseudo-sagittal slices containing the dLGN.	106
Figure 2.7: The injection site of fluorescent dye DiI for labelling dLGN neurons of rat mid-brain slices	108

Figure 2.8: The Kopf Stereotaxic Apparatus	112
Figure 2.9: The in vivo retrograde labeling method.....	113
Figure 2.10: The flat-mount retina	120
Figure 2.11: The Helios Gene Gun	124
Figure 2.12: Electroporation set up.....	125
Figure 3.1: Average IOPs with age in the operated eyes (os) and unoperated controls (od).	129
Figure 3.2a-h: Comparison of VyDiI dilutions for labelling neurons in the superior colliculus.	132
Figure 3.3a, b: Comparison of the fixation methods for rat brains.	134
Figure 3.4a-e: Classification of cell types in the rat superior colliculus.	135
Figure 3.5a-e: Comparison of the mean dendritic length of SC cells between control groups at different time points.	139
Figure 3.6a-e: Scatter plots of percentage reductions in the mean dendritic length of SC cells in control groups.	141
Figure 3.7a-e: The exponential decay of the mean dendritic length of SC cells in control rats.....	143
Figure 3.8a-e: Comparison of the dendritic number of SC cells between control groups at different time points.	146
Figure 3.9a-e: Scatter plots of percentage reductions in the dendritic number of SC cells in control groups.	148
Figure 3.10a-e: The exponential decay of the dendritic number of SC cells in control groups.....	150

Figure 3.11a-e: Comparison of the mean dendritic length of SC cells between glaucoma groups at different time points.	153
Figure 3.12a-e: Scatter plots of percentage reductions in the mean dendritic length of SC cells in glaucoma animals.	155
Figure 3.13a-e: The exponential decay of the mean dendritic length of SC cells in glaucoma groups.	157
Figure 3.14a-e: Comparison of the dendritic number of SC cells between glaucoma groups at different time points.	160
Figure 3.15a-e: Scatter plots of percentage reductions in the dendritic number of SC cells in glaucoma animals.	162
Figure 3.16a-e: The exponential decay of the dendritic number of SC cells in glaucoma groups.	164
Figure 3.17a-e: Comparison of the mean dendritic length of SC cells between glaucoma and control animals.	166
Figure 3.18a-e: Scatter plots of percentage reductions in the mean dendritic length of SC cells after glaucoma surgery.	168
Figure 3.19a-e: Comparison of the dendritic number of SC cells between glaucoma and control animals.	170
Figure 3.20a-e: Scatter plots of percentage reductions in the dendritic number of SC cells after glaucoma surgery.	172
Figure 3.21a, b: Comparison of different methods for labelling cells in the dLGN: (a) Method I; (b) Method II.	174
Figure 3.22a, b: Classification of cell types in the rat dorsal lateral geniculate nucleus.	175
Figure 3.23a, b: Comparison of the mean dendritic length of LGN cells between control groups at different time points.	178

Figure 3.24a-e: Scatter plots of percentage reductions in the mean dendritic length of LGN cells in control groups.....	179
Figure 3.25a, b: The exponential decay of the mean dendritic length of LGN cells in control groups.....	180
Figure 3.26a, b: Comparison of the dendritic number of LGN cells between control groups at different time points.	181
Figure 3.27a-e: Scatter plots of percentage reductions in the dendritic number of LGN cells in control groups.....	183
Figure 3.28a, b: The exponential decay of the dendritic number of LGN cells in control groups.....	184
Figure 3.29a, b: Comparison of the mean dendritic length of LGN cells between glaucoma groups at different time points.	186
Figure 3.30a, b: Scatter plots of percentage reductions in the mean dendritic length of LGN cells in glaucoma groups.....	187
Figure 3.31a, b: The exponential decay of the mean dendritic length of LGN cells in glaucoma groups.	188
Figure 3.32a, b: Comparison of the dendritic number of LGN cells between glaucoma groups at different time points.	190
Figure 3.33a-e: Scatter plots of percentage reductions in the dendritic number of LGN cells in glaucoma groups.....	191
Figure 3.34a, b: The exponential decay of the dendritic number of LGN cells in glaucoma groups.	192
Figure 3.35a, b: Comparison of the mean dendritic length of LGN cells between glaucoma and control groups.	194
Figure 3.36a, b: Scatter plots of percentage reductions in the mean dendritic length of LGN cells after glaucoma surgery.	195

Figure 3.37a, b: Comparison of the dendritic number of LGN cells between glaucoma and control groups.	197
Figure 3.38a, b: Scatter plots of percentage reductions in the dendritic number of LGN cells after glaucoma surgery.	198
Figure 3.39a-c: Classification of RGC types in the rat retina: (a) RI; (b) RII; (c) RIII	200
Figure 3.40a-c: Comparison of the mean dendritic length of RGCs between control groups at different time points.	203
Figure 3.41a-c: Scatter plots of percentage reductions in the mean dendritic length of RGCs in control groups.....	204
Figure 3.42a-c: The exponential decay of the mean dendritic length of RGCs in control groups.....	205
Figure 3.43a-c: Comparison of the dendritic number of RGCs between control groups at different time points.	207
Figure 3.44a-c: Scatter plots of percentage reductions in the dendritic number of RGCs in control groups.....	208
Figure 3.45a-c: The exponential decay of the dendritic number of RGCs in control groups.	209
Figure 3.46a-c: Comparison of the mean dendritic length of RGCs between glaucoma groups at different time points.	212
Figure 3.47a-c: Scatter plots of percentage reductions in the mean dendritic length of RGCs in glaucoma groups.....	213
Figure 3.48a-c: The exponential decay of the mean dendritic length of RGCs in glaucoma groups.	214
Figure 3.49a-c: Comparison of the dendritic number of RGCs in glaucoma groups at different time point.....	216

Figure 3.50a-c: Scatter plots of percentage reductions in the dendritic number of RGCs in glaucoma groups.....	218
Figure 3.51a-c: The exponential decay of the dendritic number of RGCs in glaucoma groups.....	219
Figure 3.52a-c: Comparison of the mean dendritic length of RGCs between glaucoma and control animals.....	221
Figure 3.53a-c: Scatter plots of percentage reductions in mean dendritic length of RGCs after glaucoma surgery.....	223
Figure 3.54a-c: Comparison of the dendritic number of RGCs between glaucoma and control animals.....	224
Figure 3.55a-c: Scatter plots of percentage reductions in the dendritic number of RGCs after glaucoma surgery.....	226
Figure 3.56: Comparison of the mean dendritic length of RGCs, SC cells and LGN cells in control groups.....	228
Figure 3.57: Scatter plot of percentage reductions in the mean dendritic length of RGCs, SC cells and LGN cells in control groups.....	229
Figure 3.58a-c: The exponential decay of the mean dendritic length of RGCs, SC cells and LGN cells in control groups.....	231
Figure 3.59: Comparison of the dendritic number of RGCs, SC cells and LGN cells in control groups.....	232
Figure 3.60: Scatter plot of percentage reductions in the dendritic number of RGCs, SC cells and LGN cells in control groups.....	233
Figure 3.61a-c: The exponential decay of the dendritic number of RGCs, SC cells and LGN cells in control groups.....	234
Figure 3.62: Comparison of the mean dendritic length of RGCs, SC cells and LGN cells in glaucoma groups.....	236

Figure 3.63: Scatter plot of percentage reductions in the mean dendritic length of RGCs, SC cells and LGN cells in glaucoma groups.	237
Figure 3.64a-c: The exponential decay of the mean dendritic length of RGCs, SC cells and LGN cells in glaucoma groups.	238
Figure 3.65: Comparison of the dendritic number of RGCs, SC cells and LGN cells in glaucoma groups.	241
Figure 3.66: Scatter plot of percentage reductions in the dendritic number of RGCs, SC cells and LGN cells in glaucoma groups.	242
Figure 3.67a-c: The exponential decay of the dendritic number of RGCs, SC cells and LGN cells in glaucoma groups.	243
Figure 3.68a, b: Comparison of the mean dendritic length of RGCs, SC cells and LGN cells between glaucoma and control groups.	246
Figure 3.69: Scatter plot of percentage reductions in the mean dendritic length of RGCs, SC cells and LGN cells after glaucoma surgery.	247
Figure 3.70a, b: Comparison of the dendritic number of RGCs, SC cells and LGN cells between glaucoma and control groups.	249
Figure 3.71: Scatter plot of percentage reductions in the dendritic number of RGCs, SC cells and LGN cells after glaucoma surgery.	250
Figure a1: A sample neuron was analyzed using the Neuron J programme.	349
Figure a2: A sample neuron was analyzed using the Sholl analysis.	350
Figure a3: Comparison of the Neuron J programme to the Sholl analysis on eleven dendrites.	351

List of Tables

Table 1.1: The morphological classification of main types of RGCs in rodents.	38
Table 1.2: Comparison of primary RGC types in Primates, Felines and Rodents.	40
Table 1.3: Summary of the main types of neurons in the SC and LGN in Primates, Felines and Rodents.	64
Table 1.4: Primary rodent models used for glaucoma study currently	74
Table 2.1: Animals used for studying dendritic changes in the superior colliculus...	89
Table 2.2: Summary of brain slices and neurons analyzed in the study of dendritic changes in the superior colliculus.	98
Table 2.3: Animals used for studying dendritic changes in the dorsal lateral geniculate nucleus.	103
Table 2.4: Summary of brain slices and neurons analyzed in the study of dendritic changes in the dorsal lateral geniculate nucleus.....	115
Table 2.5: Animals used for studying dendritic changes in the retinal ganglion cells.	118
Table 2.6: Summary of retinae and neurons analyzed in the study of dendritic changes in the retinal ganglion cells.	127
Table 3.1: Characteristics of different types of SC cells analyzed in this thesis.....	136
Table 3.2: Summary of the rates of dendritic shrinkage in glaucoma and control animals	156
Table 3.3: Summary of the rates of dendritic in glaucoma and control animals.....	163
Table 3.4: Characteristics of different types of LGN cells analyzed in this thesis. .	176

Table 3.5: Summary of the rates of dendritic shrinkage in glaucoma and control animals	189
Table 3.6: Summary of the rates of dendritic loss in glaucoma and control animals	193
Table 3.7: Characteristics of different types of RGCs analyzed in this thesis.....	200
Table 3.8: Summary of the rates of dendritic shrinkage in glaucoma and control animals	215
Table 3.9: Summary of the rates of dendritic loss in glaucoma and control animals	220
Table 3.10: Comparison of the rates of dendritic shrinkage in glaucoma and control animals.....	239
Table 3.11: Comparison of the rates of dendritic loss in glaucoma and control animals	244
Table 4.1: Comparison of percentage dendritic changes in the SC cells from normal animals at different time points.....	264
Table 4.2: Comparison of percentage dendritic changes in the LGN cells from normal animals at different time points.....	266
Table 4.3: Comparison of age-related dendritic changes found in this thesis and in published literature: (a) dendritic shrinkage; (b) dendritic loss.	273
Table 4.4: Comparison of percentage dendritic changes in the RGCs from normal animals at different time points.....	276
Table 4.5: Comparison of RGC age-related changes shown in this thesis and in published literature.....	278
Table 4.6: Comparison of age-related dendritic changes in the RGCs, SC cells and LGN cells.	281

Table 4.7: Comparison of average rates of age-related dendritic changes in the RGCs, SC cells and LGN cells.	282
Table 4.8: Comparison of percentage dendritic changes in the SC cells of glaucoma and control animals.	284
Table 4.9: Comparison of the rates of dendritic changes in the SC cells from glaucoma and control animals.	286
Table 4.10: Comparison of percentage dendritic changes in the LGN cells from glaucoma and control animals.	287
Table 4.11: Comparison of the rates of dendritic changes in the LGN cells from glaucoma and control animals.	288
Table 4.12: Comparison of percentage dendritic changes in the RGCs from glaucoma and control animals.	290
Table 4.13: Comparison of the rates of dendritic changes in the RGCs from glaucoma and control animals.	291
Table 4.14: Comparison of dendritic changes in the RGCs, SC cells and LGN cells from glaucoma animals at different time points.	295
Table 4.15: Comparison of the rates of dendritic changes in the RGCs, SC cells and LGN cells from glaucoma and control animals.	296
Table 4.16: Comparison of dendritic changes in the SC cells after OHT induction.	299
Table 4.17: Comparison of dendritic changes in the LGN cells after OHT induction.	301
Table 4.18: Comparison of dendritic changes in glaucoma and neurodegenerative conditions in this thesis and in published literature: (a) dendritic shrinkage; (b) dendritic loss.	304
Table 4.19: Comparison of dendritic changes in the RGCs after OHT induction ...	309

Table 4.20: Comparison of structural changes of RGCs following elevated IOP shown in this thesis and in published literature.....	311
Table 4.21: Comparison of dendritic changes in the RGCs, SC cells and LGN cells after OHT induction.	314
Table a: Comparison of the Neuron J programme to the Sholl analysis on eleven dendrites.	351

List of Abbreviations

A	Amacrine cell
ACG	Angle closure glaucoma
AD	Alzheimer's disease
ALS	Amyotrophic lateral sclerosis
AMT	Age-matched control
ANOVA	Analysis of variance
BC	Bipolar cell
BDNF	Brain derived neurotrophic factor
BL	Baseline control
C	Cone
CA	Catecholamine
C1q	Component 1Q
CNS	Central nervous system
CNTF	Ciliary neurotrophic factor
CO	Cytochrome oxidase
CPu	Caudate-putamen
CRAO	Central retinal artery occlusion
DA	Dark agouti
DiI	1,1'-Dioctodecyl-3,3',3'-tetramethylindocarbocyanine perchlorate
dLGN	Dorsal lateral geniculate nucleus
DMSO	Dimethyl sulfoxide
ECM	Extracellular matrix
fEPSP	Field excitatory post-synaptic potentials

GABA	γ -aminobutyric acid
GCL	Ganglion cell layer
GDNF	Growth derived neurotrophic factor
GFAP	Glial fibrillary acidic protein
H	Horizontal cell
HD	Huntington's disease
HRP	Horseradish peroxidase
IC	Inferior colliculus.
ILM	Inner limiting membrane
INL	Inner nuclear layer
IOP	Intraocular pressure
IP	Intraperitoneal
IPL	Inner plexiform layer
KCl	Potassium chloride
KH₂PO₄	Potassium dihydrogen phosphate
K pathway/layer/cell	Koniocellular pathway/layer/cell
LGB	Lateral geniculate body
LGN	Lateral geniculate nucleus
LG1	Relay neuron type 1 in the dLGN
LG2	Relay neuron type 2 in the dLGN
LHA	Lateral hypothalamic area
M	Marginal cell
MAP2	Microtubule-associated protein-2
M pathway/layer/cell	Magnocellular pathway/layer/cell
MRI	Magnetic resonance imaging
MSN	Medium spiny neuron
MTN	Medial terminal nucleus

NaCl	Sodium chloride
NaHCO₃	Sodium bicarbonate
NFL	Nerve fibre layer
NGF	Nerve growth factor
NMDA	N-methyl-D-aspartate
NO	Nervus opticus
NT-3	Neurotrophic-3
NT-4/5	Neurotrophin-4/5
OFL	Optic fiber layer
OHT	Ocular hypertension
OPT	Olivary pretectal nucleus
ON	Optic nerve
ONH	Optic nerve head
ONL	Outer nuclear layer
ONT	Optic nerve transection
OPL	Outer plexiform layer
OT	Optic tract
OX	Optic chiasm
P	Pyriiform cell
P pathway/layer/cell	Parvocellular pathway/layer/cell
PAC	Primary angle closure
PACG	Primary angle closure glaucoma
PBS	Phosphate buffered saline
PD	Parkinson disease
PFA	Paraformaldehyde
PFC	Prefrontal cortex
PGN	Pergeniculate nucleus

POAG	Primary open angle glaucoma
POS	Photoreceptor outer segment
PT	Pretectum
R	Rod
RGC	Retinal ganglion cells
RG_A	Retinal ganglion cell type A
RG_B	Retinal ganglion cell type B
RG_C	Retinal ganglion cell type C
RG_D	Retinal ganglion cell type D
RI	Retinal ganglion cell type I
RII	Retinal ganglion cell type II
RIII	Retinal ganglion cell type III
RNFL	Retinal nerve fibre layer
RPE	Retinal pigment epithelium
RTN	Reticular thalamic nucleus
SAI/InWh	Stratum album intermediale (intermediate white layer)
SAP/DpWh	Stratum album profundum (deep white layer)
SC	Superior colliculus
SCN	Suprachiasmatic nucleus
SD	Standard deviation
SGI/ InG	Stratum griseum intermediale (intermediate gray layer)
SGP/ DpG	Stratum griseum profundum (deep gray layer)
SGS/SuG	Stratum griseum superficial (superficial grey layer)
SN	Substantia nigra
SO/Op	Stratum opticum (Optic layer)
SPSS	Statistical package for the social sciences
SSP	Staurosporine

SZ/Zo	Stratum zonale (Zonal layer)
TCR	Thalamo-cortical relay neuron
TM	Trabecular meshwork
V	Narrow field vertical cell
W	Wide field vertical cell

Chapter 1: Introduction

1.1 Visual System

1.1.1 The Neurons

Neurons are essential components of the nervous system, which are able to receive, integrate and transmit electro-chemical signals to other cells (Purves et al., 2001). Based on their different functions, neurons are generally classified into three categories including sensory neurons which are sensitive to various non-neural stimuli; motor neurons which are able to stimulate muscle cells throughout the body; and interneurons which provide connections between sensory and motor neurons, as well as between themselves (Nicholls et al., 1992).

A typical neuron consists of a cell body (soma), a large number of dendrites and an axon. The cell body contains the nucleus, coordinating the metabolic activities of the neuron (Lodish et al., 2000). Virtually, all neuronal proteins and membranes are synthesized in the soma. The dendrites appear as branches or spikes extending outward from the cell body, acting as signal receivers. It is primarily the surfaces of the dendrites that receive chemical and electrical messages from other neurons. Neurons in central nervous system (CNS) have long dendrites with complex dendritic trees, allowing them to receive signals from a large amount of other neurons. One unique extension, the axon, is specialized for transmitting an electro-chemical signal away from the cell body, toward the axon terminus, which could connect to other cells. Longer axons are usually covered with a myelin sheath which

coats and insulates the axon (except for periodic breaks called nodes of ranvier), increasing transmission speed along the axon (Fig. 1.1).

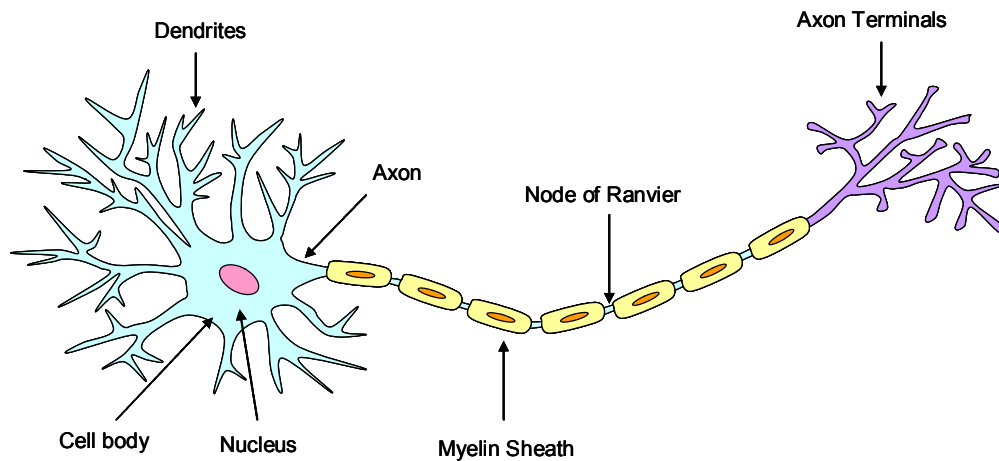


Figure 1.1: The structure of a typical neuron.

A typical neuron is comprised of a cell body containing nucleus, a large number of dendrites and an axon covered with myelin sheath.

1.1.2 The Pathway of Light in Retina

1.1.2.1 The Structure of Retina

The vertebrate retina is a thin tissue film that lines the back of the eye (Fig. 1.2). When light enters the eye and strikes the retina, the decomposition of pigments in the photoreceptors (rods and cones) of the retina converts the light rays into electrical signals that are processed in the retina and are sent to the brain through the

optic nerve (ON). There are three layers of nerve cells and two layers of synapses in the vertebrate retina. The outer nuclear layer (ONL) contains photoreceptors, including rods and cones, which respond to light. In human retina, there are on average 57.4 million rods and 3.3 million cones (Glaser, 1999). The inner nuclear layer (INL) contains the bipolar, horizontal and amacrine cells. The ganglion cell layer (GCL) contains ganglion cells and displaced amacrine cells. Dividing these nerve cell layers are two other layers where synaptic contacts occur: the outer plexiform layer (OPL) providing connections between ONL and INL, and the inner plexiform layer (IPL) acting as a relay station between INL and GCL (Fig. 1.2) (Margalit and Sadda, 2003; Paxinos, 2004).

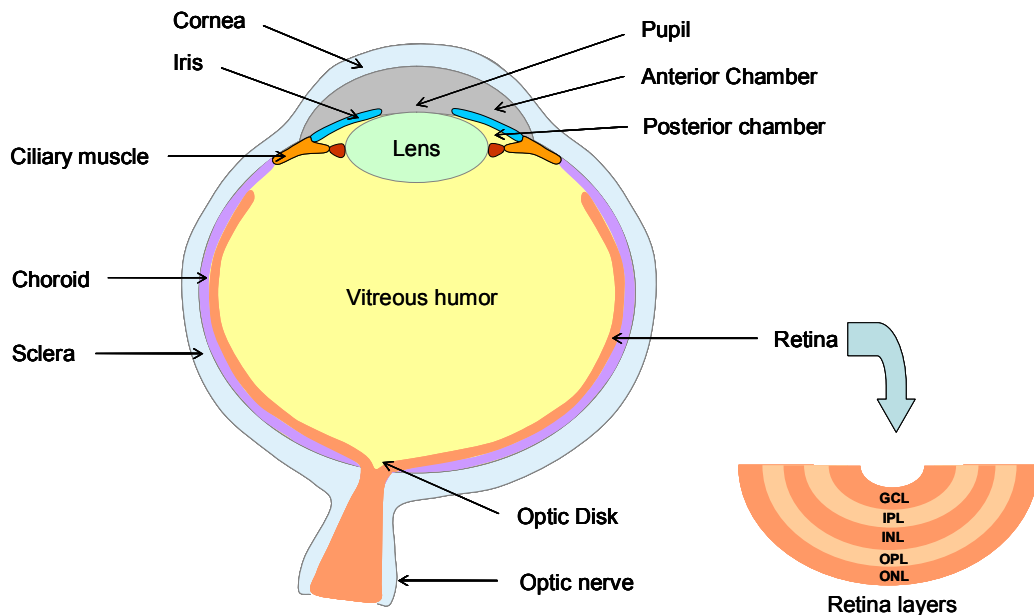


Figure 1.2: The anatomy of the eye and arrangements of retinal layers.

The retina is composed of five layers: the ganglion cell layer (GCL); inner plexiform layer (IPL); inner nuclear layer (INL); outer plexiform layer (OPL) and outer nuclear layer (ONL).

1.1.2.2 The Visual Pathway in Retina

Retinal ganglion cells (RGCs) are neurons located in the ganglion cell layer that receive visual information from photoreceptors via various intermediate neuronal cells including bipolar, amacrine, and horizontal cells (Purves et al., 2001). RGC dendrites are responsible for receiving the synaptic inputs from bipolar and amacrine cells, integrating, processing and sending the visual information to the central visual targets through the optic nerve. RGC axons become myelinated when they leave the eye, forming the optic nerves, which converge at the optic chiasm before becoming the optic tracts, providing the connection between the eye and the central nervous system (CNS).

The photoreceptor cells connect to the “ON centre” or “OFF centre” ganglion cells through “ON-type” or “OFF-type” bipolar cells (Schiller, 1982; Schiller et al., 1986). The “ON-type” bipolar cells become depolarized in response to light and receive visual signals from rods or cones (Schiller et al., 1986). They excite “ON” RGCs or inhibit “OFF” RGCs and vice versa. The OFF-types bipolar cells become hyperpolarized on exposure to light. Thereby, the visual signals for both incremental and decremental light are transferred efficiently with equal sensitivity via the ON and OFF channels. These two pathways were also suggested to facilitate high contrast sensitivity. In addition to passing the visual signal to RGCs, bipolar cells also connect to horizontal or amacrine cells which are interneurons providing lateral interactions (Masland, 1986) (Fig. 1.3).

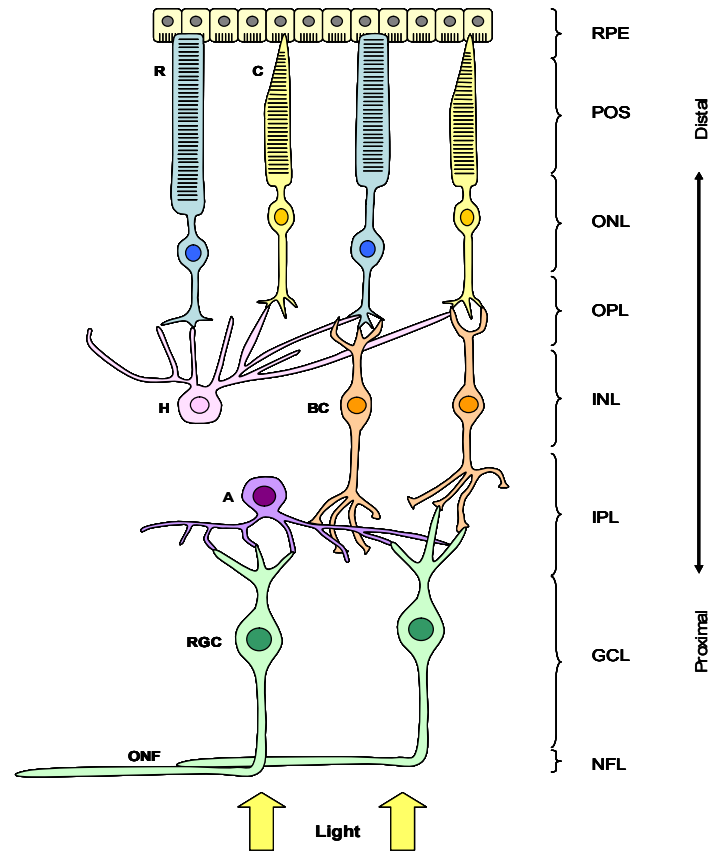


Figure 1.3: The layers and basic circuitry of the retina.

The diagram shows the arrangement of the retinal layers. The neuron chain composed of photoreceptor, bipolar cell, and ganglion cell is the most direct route for transmitting visual information to brain. RPE: Retinal Pigment Epithelium; POS: Photoreceptor Outer Segments; ONL: Outer Nuclear Layer; OPL: Outer Plexiform Layer; INL: Inner Nuclear Layer; IPL: Inner Plexiform Layer; GCL: Ganglion Cell Layer; NFL: Nerve Fibre Layer; R: Rod; C: Cone; H: Horizontal Cell; BC: Bipolar Cell; A: Amacrine Cell; RGC: Retinal Ganglion Cell; ONF: Optic Nerve Fibre.

1.1.2.3 Retinal Ganglion Cells

1.1.2.3.1 Primate Ganglion Cells

There are several different types of ganglion cells with distinct dendritic morphologies in the primate retina. Of those the midget and parasol cells have been described most completely. The midget cells are small cells with a compact dendritic arbor, representing approximately 80% of the ganglion cells in the primate retina. Parasol cells in contrast have a much larger cell body and dendritic arbor, making up approximately 10% of the total population of primate RGCs (Perry et al., 1984; Watanabe and Rodieck, 1989). Midget cells were also termed Type III cells, B cells and P β cells, whereas parasol cells were also termed Type II cells, A cells, P α cells and stratified diffuse in other studies (Leventhal et al., 1981; Rodieck et al., 1985; Watanabe and Rodieck, 1989). The other 10% RGCs were estimated to project to the superior colliculus (SC) which has only very few projections from parasols, but no projection from midget ganglion cells (Perry et al., 1984; Watanabe and Rodieck, 1989). Axons of midget cells project to the dorsal, parvocellular layers of the lateral geniculate nucleus (LGN), whilst those of parasol cells project to the ventral magnocellular layers of the LGN. Functionally, parasol cells are the high contrast sensitive RGCs, representing the M-pathway of the primate visual system; whilst midget cells represent the P-pathway. Midget cells have small receptive fields whereas parasol cells have large receptive fields (Watanabe and Rodieck, 1989). The receptive field of a ganglion cell refers to the retinal region within which the visual stimuli causes the alteration in this cell (Glaser, 1999).

1.1.2.3.2 Feline Ganglion Cells

In cat retina, RGCs are morphologically classified into β -, α - and γ - cells: α -cells have the large soma, large dendritic field area, and the thickest dendrites; β -cells have medium-sized soma, small dendritic field area, and a bushy dendritic arbor; γ -cells contain the smallest soma and less dendritic arbors (Boycott and Wassle, 1974). The β -, α - and γ - cells were assumed to correspond to X-, Y-, and W- cells physiologically (Fukuda and Stone, 1975; Fukuda et al., 1985). It has also been demonstrated that Y-, X-, and W- cells have large, intermediate and small cell bodies respectively. X-cells have the smallest receptive-field centres, whilst W-cells and Y-cells have similar sizes of the receptive-field centres, which were both larger than those of X-cells. A fourth morphological class of RGC is the δ -cell, which is found relatively infrequently. The δ -cells have a soma size comparable to the β -cell but their dendritic arbors are much more extensive (Boycott and Wassle, 1974). It has been evidenced that W- (γ -) and X- (β -) which have smaller cell bodies are more numerous than Y- (α -) cells with large soma (Stone, 1965). There were approximately 40% W-cells, 50%-60% X-cells, and less than 10% Y-cells of the total RGCs in feline retina. X-cells and W-cells predominantly project to the lateral geniculate nucleus of the forebrain, and the superior colliculus in the midbrain; Y-cells project to both of these two sites in the brain (Fukuda and Stone, 1974).

1.1.2.3.3 Rodent Ganglion Cells

The RGCs of rat retina have been classified into three groups based on their morphological diversity (Perry, 1979; Dreher et al., 1985; Paxinos, 2004). Perry grouped cells in the GCL into four types based on soma and dendritic-field size, and

the dendritic branching pattern demonstrated with Golgi-staining (Perry, 1979). Three of these cell types were regarded as analogous to α -, β -, and γ -cells described in the cat retina. The fourth cell type was thought to be a displaced amacrine cell. Dreher et al. also found three types of ganglion cells regarded as class I, II, and III and added a subclass to Perry's types II and III by retrograde HRP labelling (Dreher et al., 1985; Paxinos, 2004). The large cells, class I cells, were further divided into α and β cells similar to the feline RGCs (Peichl, 1989). Huxlin and Goodchild classified the ganglion cells into three groups, RG_A , RG_B and RG_C using intracellular Neurobiotin injection and retrograde DiI labelling (Huxlin and Goodchild, 1997).

These previous studies characterized the ganglion cells according to their soma size and dendritic-field size. As shown in Table 1.1, the rodent RGCs were mainly classified into four types. Type RG_A (type I, class I) refers to cells with a large soma and a large dendritic field. Type RG_B (type II, class II) contains cells with a small soma and a small dendritic field. In addition, type RG_C (type III, class III) are cells that have small-to-medium soma, but a large dendritic field (Table 1.1).

RGC types	Soma Size	Dendritic Area
Type I (RG_A , class I)	Large	Large
Type II (RG_B , class II)	Small	Small
Type III (RG_C , class III)	Small to medium	Large

Table 1.1: The morphological classification of main types of RGCs in rodents.

A fourth type RG_D cells were described as bistratified cells using the DiOlistic method (Sun et al., 2002b). In Perry's study, the type IV cells were rarely stained in their entirety using Golgi staining. Unlike that on type I, II and III cells, there was no axon stained on type IV cells (Perry, 1979; Gan et al., 2000; Sun et al., 2002b). In Perry's study, the mean diameters of rat RGC soma size were $20.4\mu\text{m}$ (RI), $13.5\mu\text{m}$ (RII), and $12.1\mu\text{m}$ (RIII). The mean diameter of dendritic fields were $312\mu\text{m}$ (RI), $150\mu\text{m}$ (RII) and $339\mu\text{m}$ (RIII) respectively. Sun et al., also further divided the mouse and rat RGCs into subtypes using the DiOlistic staining method (Sun et al., 2002b, a). In rats, RG_A cells were subdivided into RG_{A1} and RG_{A2} with mean soma diameter of $24\mu\text{m}$ and $23\mu\text{m}$; RG_B cells were subdivided into RG_{B1} , RG_{B2} , RG_{B3} and RG_{B4} , with mean soma diameter ranging from $14\mu\text{m}$ to $17\mu\text{m}$; RG_C were subdivided into six types as RG_{C1} to RG_{C6} , with mean soma diameter ranging from $15\mu\text{m}$ to $17\mu\text{m}$; and RG_D cells were subdivided into RG_{D1} and RG_{D2} , with mean soma diameter of $15\mu\text{m}$ (Sun et al., 2002b).

In rodents, there are few correlations among morphology of the RGCs, their targets and functions due to the technical difficulties of recording from the small eyes. The three morphological groups may be related to different conduction velocity peaks recorded in the optic nerve (Paxinos, 2004). So far, α -type cells are the best described group and found to be conserved throughout mammalian species. RG_A (type I, class I) type cells correspond to α -type cells (Sun et al., 2002a). RG_B cells have very small and dense dendritic fields, which may be functionally equivalent to cat β -type cells (Wassle et al., 1981). A subtype of RG_C cells, named as RG_{C1} , is very similar in morphology to the medial terminal nucleus (MTN)-

projecting RGCs described in Dann and Buhl's paper (Dann and Buhl, 1987; Sun et al., 2002b).

It has been shown that the soma size of cells projecting to the SC is smaller than that of cells projecting to dLGN. Cells projecting to MTN are similar to RG_c (type III) cells. Most cells projecting to the olivary pretectal nucleus (OPT) are small cells as RG_c (type III), while some appear as RG_A (type I). A few small cells of RG_c (type III) project to the hypothalamus (Moore et al., 1995; Paxinos, 2004).

In this thesis, the primary types of RGCs in primate, feline and rodent were summarized and compared based on their morphological classification, as shown in Table 1.2.

Species	Primary types of RGCs
Primate	Midget cell (Type III cells, B cells and P β cells); Parasol cell (Type II cells, A cells, P α cells).
Feline	β -cell (X-cell); α -cell (Y-cell); γ -cell (W-cell).
Rodent	Type I (RG _A , class I); Type II (RG _B , class II); Type III (RG _C , class III).

Table 1.2: Comparison of primary RGC types in Primates, Felines and Rodents.

1.1.3 The Visual Pathways in the Brain

1.1.3.1 Retinal Projections to the Central Visual Targets in Primates

In primates, visual information is mainly sent from the retina to the LGN of the thalamus via the optic nerve, which then connects to more than 120 million neurons in the primary visual cortex (V1). There are additionally three other targets of RGC axons: the pretectum responsible for the pupillary light reflex; the suprachiasmatic nucleus of the hypothalamus which regulates the circadian rhythms; and the superior colliculus which coordinates head and eye movements (Fig. 1.4). In addition to receiving synaptic input from the retina, the LGN also receives return projections from the visual cortex, ascending projections from different brain-stem nuclei and perigeniculate nucleus (PGN) which is a component of the reticular nucleus (RTN) of the thalamus (McIlwain, 1996). In humans, the LGN, is also the largest primary visual nucleus. It acts as the termination of the optic tract, and the axons of neurons in the LGN form the geniculocalcarine radiations. The axons of the RGCs constitute the optic nerve fibres which pass through the optic chiasm to the LGN. A little more than half of the optic fibres cross at the chiasm, whilst the remaining optic fibres do not cross. The axons of cells in the LGN then form the output of the geniculate to the striate cortex (also known as visual cortex or V1) through the white matter of the cerebral hemispheres (Hubel and Wiesel, 1977). The LGN is divided into two parts: the larger dorsal LGN (dLGN) and the smaller ventral LGN (vLGN), with most studies in human and non human primate LGNs mainly referring to the dLGN (Polyak, 1957; Glaser, 1999).

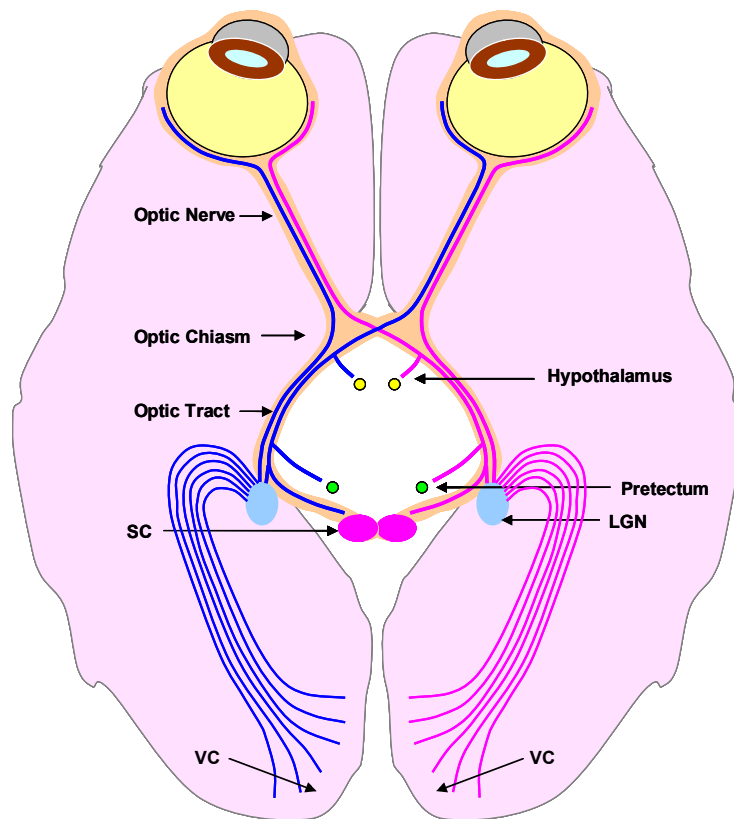


Figure 1.4: The primate visual pathways from the retina to the central visual targets.

Forming the nerve pathway from the eyes to the brain, ganglion cell axons terminate at four subcortical regions in the brain: the lateral geniculate nucleus (LGN) of the thalamus, the superior colliculus (SC), the pretectum and the hypothalamus. The axons of cells in the LGN then form the output of the geniculate to the visual cortex (VC).

1.1.3.1.1 Parallel Pathways in the Lateral Geniculate Nucleus in Primates

Studies that link the structure and function of these pathways would help to understand how these parallel signals are processed by the visual cortex. The LGN consists of six layers. Layers 1 and 2 are ventral layers receiving input primarily from parasol RGCs, forming the M-pathway, whilst layers 3, 4, 5, 6 are dorsal layers receiving input primarily from midget ganglion cells, forming the P-pathway (Callaway, 2005). A third distinct part in the LGN, the koniocellular (K) division, intercalates between the main laminae, and is comprised mainly of small cell bodies. The “W-like” cells possessing relatively large dendritic fields and diverse cortical projections are assumed to project to the K division, comprising the K pathway (Kaas et al., 1978; Szmajda et al., 2008). Unlike P and M pathways which have been studied in detail, the exact function of the Koniocellular (K) pathway in vision is still not clearly documented but it has been proposed to be involved in colour vision in new world monkeys (Casagrande, 1994). There are six K layers in the macaque LGN with different sizes, of which the most ventral layer is the most robust one. In macaque monkeys, axons from K layer 1 and 2 appear simple with less bouton like swellings (synaptic bouton) and branch into cortical layers 1 and 3A, whilst those from K layers 3 to 6 appear complex with more synaptic bouton projecting into the cytochrome oxidase (CO) blobs in cortical layer 3Ba (Casagrande et al., 2007). These pathways include the axons of RGCs and their synaptic connections to neurons in the LGN, the axons of geniculate cells that carry information to the primary visual cortex (V1), and the fibres from the visual cortex that connect to higher brain centres.

In addition to this function-specific organization, each LGN layer has an eye-specific input: LGN layers 1, 4 and 6 receive input from the contralateral eye, whilst layers 2, 3 and 5 receive input from the ipsilateral eye (Fig. 1.5).

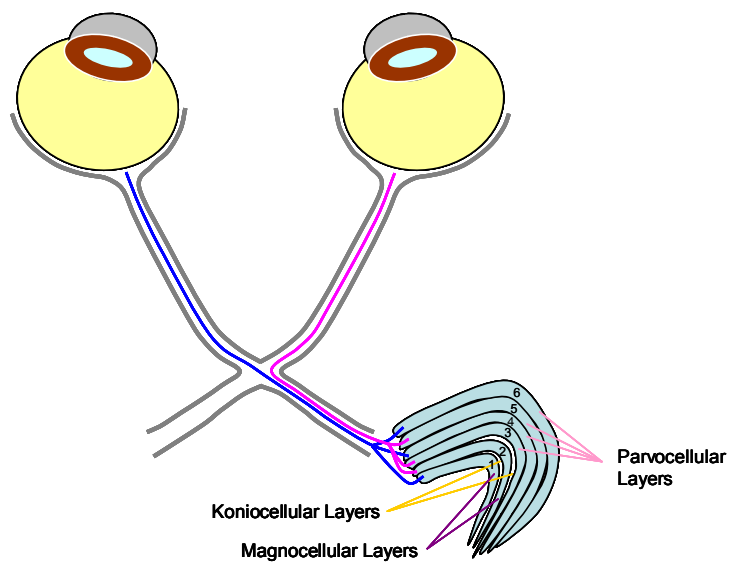


Figure 1.5: The function and eye specific organization of primate LGN.

Each of the six LGN layers receives inputs from either the ipsilateral or contralateral eye. The ganglion cells of the left eye project to layer 1, 4 and 6 of the right LGN, and the right eye ganglion cells project to its layer 2, 3 and 5.

1.1.3.1.2 Neurons in the Primate Lateral Geniculate Nucleus

The types of neurons in the dorsal LGN have been investigated in squirrel monkey by Golgi staining, and classified into four types according to their morphology (Wong-Riley, 1972).

The type I and II cells are characterized as geniculo-cortical relay neurons. Type I cells are large to medium sized neurons depending whether they are located in the parvocellular or the magnocellular regions. Their perikaryal diameter ranges from 15 to 30 μm , with six to ten primary dendrites which further branch into secondary and tertiary dendrites. The dendrites are orientated either perpendicular or parallel to the plane of the lamina, extending a long distance of about 300 μm . No protrusions are observed in the proximal dendrites, whereas spines and small protrusions are seen along the distal dendritic trunks. Type II cells are the most common type of neurons, with a soma size ranging from 16 to 29 μm and 23 to 37 μm in diameter in the parvocellular and magnocellular layers respectively (Wong-Riley, 1972). They have three to five primary dendrites orientated perpendicular or parallel to the plane of the lamina similar to type I cells. The most characteristic feature of the type II cell is the spherical or ovoid protrusions observed along the primary and secondary dendrites. These protrusions are especially clustered at the branching points, giving a grape-like appearance. The type I and II cells correspond to class 1 and 2 cells described in cats (Guillery, 1966).

Type III and IV cells are suggested as interneurons. Type III cells are small neurons. They have round or spindle shaped soma, ranging from 9 to 16 μm in diameter. There are three or four primary dendrites which rarely branch. The dendrites are orientated parallel, perpendicular or even oblique to the plane of the

lamina, running a longer distance compared to type I and II cells. Type IV cell is the smallest sized neurons, resembling glial cells. They have a very small cell body from 6.5 to 8 μm in diameter, with small and fine dendrites radiating in various directions. However, they are not easily distinguishable.

Four main types of neurons in the LGN of old- and new-world monkeys were also described (Saini and Garey, 1981). The multipolar and bipolar neurons were most numerous and presumed to be relay neurons. The multipolar neurons have small to large soma, bearing radiate or tufted dendritic arbors. The bipolar neurons have large soma and two thick primary dendrites. The other two types of cells with small soma and axon-like or beaded dendrites were presumed to be interneurons.

Relay neurons identified in the LGN are also classified into three types: the M (magnocellular); P (parvocellular); and K (koniocellular) types, representing M, P and K pathways to visual cortex respectively (Perry et al., 1984; Martin et al., 1997; Callaway, 2005) (Figure 1.5). M, P and K cells receive the visual input from the parasol, midget and blue-ON RGCs respectively. M cells are distributed in the two ventral layers of the LGN, and the P cells are located in the four dorsal layers of the LGN. The third type K cells are found within and between these layers.

Neurons found in the two ventral layers have larger and highly contrast sensitive receptive fields; whereas those in the four dorsal layers have smaller and poorly contrast sensitive receptive fields (Leventhal et al., 1981; Perry et al., 1984; Shapley and Perry, 1986; Rodieck and Watanabe, 1993). The M cells have more dendrites and dendritic branches, and longer dendrites than those of P cells in macaque LGN (Wilson, 1989). RGCs projecting to the K layers are W-like cells with relatively larger dendritic areas and various cortical projections compared to midget

and parasol cells (Hendry and Reid, 2000; Casagrande et al., 2007; Szmajda et al., 2008). K cells have distinct neurochemical and morphological properties, making up the third functional pathway in primate LGN.

The interneurons have thin dendrites extending long distances in primate LGN (Wilson, 1989). They contain gamma-aminobutyric acid (GABA) and contact relay neurons via dendro-dendritic synapses. In primate LGN, the number of interneurons were estimated to be less than 15% of neurons (Norden and Kaas, 1978). Norden et al. have identified that almost all neurons in the main relay layers of the LGN of owl and rhesus monkeys are relay cells. The fact that only very few interneurons exist in primate LGN indicates the organization of the primate LGN in primates may be quite different from that of other mammals.

1.1.3.1.3 Retinal Input to the Superior Colliculus in Primates

Unlike the lateral geniculate nucleus, the superior colliculus is not the major target of retinal axons in primates (Bunt et al., 1975; Perry et al., 1984). Virtually all RGCs project to the LGN in primates. Perry et al. studied the projection from RGCs to the SC by retrograde axoplasmic transport using horseradish peroxidase (HRP). They found there were up to 10% of all RGCs sending their axons to the SC in macaque monkeys. Most cells projecting to the SC were termed as P γ and P ϵ cells, which have small to medium sized soma and sparsely branched dendritic tree with thin dendrites. The P γ and P ϵ cells were similar to γ - and ϵ -cells in the cat. There was no evidence that P β cells projected to the SC, and only a few P α cells' axons were

revealed to terminate at the SC. The $P\alpha$ cells were also termed parasol cells and A cells, whilst $P\beta$ cells were also termed midget cells and B cells (Watanabe and Rodieck, 1989). In Leventhal's et al. study, they termed RGCs as A, B, C, E cells and some unclassified cells (Leventhal et al., 1981; Perry et al., 1984). A cell with a large cell body and medium sized dendritic field projects to the magnocellular laminae of the LGN in primate. Some A cell, C cell and unclassified cell's axons terminated in the SC. B cells with a small cell body and the smallest dendritic field project to the parvocellular laminae of the LGN. These findings were in agreement with the earlier results from Bunt et al.'s study (Bunt et al., 1975).

Three main types of neurons in the SC of squirrel monkeys have been described: L, X and T neurons (Moschovakis et al., 1988). L neurons are small to medium sized cells, primarily located in the superficial SC. They have triangular or ovoid soma, bearing relatively elaborate dendritic trees. X neurons are multipolar cells with large soma and complex dendritic trees, which are usually located within the intermediate gray layer. T neurons are small or medium sized cells, mainly located in the ventral optic or dorsal intermediate gray layers. They have trapezoid or ovoid soma and simple radiating or vertical dendritic trees.

1.1.3.2 Retinal Projections to the Central Visual Targets in Felines

Both the dLGN and SC are primary visual targets in cats (Garey and Powell, 1968). Approximately 50% of all RGCs send their axons to the SC, and many RGCs have axon collaterals projecting to the LGN (Wassle and Illing, 1980).

1.1.3.2.1 Retinal Input to the Lateral Geniculate Nucleus in Felines

The LGN is composed of six laminae (A, A1, C, and C1-C3) and the medial interlaminar nucleus. The three dorsal laminae, A, A1 and C, are termed as magnocellular layers containing small to large cells. The other three laminae, C1-C3, are referred as parvocellular layers containing small neurons (Guillery, 1970; Payne and Peters, 2002; Nakamura et al., 2005).

Y- and X- RGCs project to Y- and X- type relay cells separately to form parallel pathways of visual information. These relay cells are in laminae A and A1 of the dLGN. The pathway is similar to the magnocellular and parvocellular pathways in the primate visual system (Fukuda and Stone, 1974; So and Shapley, 1981). The lamina C and the medial interlaminar nucleus consist of large and small cells, receiving Y- and W-cell projections. The ventral laminae C1–C3 are composed of small cells. Laminae C1–C2 receives projections from the larger subtype of W-cells (Wilson and Stone, 1975). Recently, Nakamura et al. reported that rather than receiving retinal projections, the lamina C3 of the dLGN receives visual input from the small subpopulation of W- type ganglion cells via the upper substratum of the superficial gray layer of the superior colliculus (Nakamura et al., 2005).

1.1.3.2.2 Neurons in the Feline Lateral Geniculate Nucleus

Hajdu et al. have classified the LGN neurons into two types: the large thalamo-cortical relay neuron (TCR) that projects to the primary visual cortex (V1) and the small interneuron which is confined to the LGN (Hajdu et al., 1974). The relay neurons in the feline LGN are classified into three groups: the X-, Y- and W-

type relay cells. Each type of cell receives visual input from the corresponding type of RGCs (Wilson and Stone, 1975; Wilson et al., 1976; Leventhal, 1979; Payne and Peters, 2002). The interneurons involved in the LGN were also classified into intrageniculate and perigeniculate interneurons based on the location of their cell bodies. Intrageniculate refer to the neurons with cell bodies within the LGN, whilst perigeniculate refer to those with soma above the LGN (Dubin and Cleland, 1977). The perigeniculate nucleus (PGN) is a specialized part of reticular thalamic nucleus (RTN) and associated closely with the A-laminae of the dLGN (Sherman and Koch, 1986; Fitzgibbon et al., 1999). Dubin et al. suggested that the intrageniculate interneurons have smaller, precise and concentric receptive fields compared to perigeniculate interneurons which have generalized, diffuse receptive fields. There were approximately 25-57% of all neurons in LGN were interneurons in feline (Norden and Kaas, 1978).

1.1.3.2.3 Retinal Input to the Superior Colliculus in Felines

There are at least three types of retinal ganglion cells that have been classified in cat retina, which are the X- (β -), Y- (α -) and W- (γ -) type cells based on their soma size, dendritic field area as well as the receptive-field properties (Boycott and Wässle, 1974; Fukuda and Stone, 1974). Hoffmann has described three functionally different pathways from the retina to superior colliculus in the cat, including two direct retinocollicular pathways and another indirect pathway involving the visual cortex (Hoffmann, 1972, 1973). Y-cells had fast-conducting axons bifurcating in the optic tract. One branch of these fast-conducting axons

terminated in the superior colliculus, forming a fast direct retinocollicular pathway, whilst the other branch terminated in the lateral geniculate nucleus. W-cells had slowly-conducting axons terminating in the colliculus, constituting a slow direct retinocollicular pathway. Y-cells were found to project indirectly to the SC via the LGN and visual cortex, forming a fast-indirect retinocollicular pathway. The axons of X-cells terminated at the LGN, however, no direct or indirect projections of X-type to the superior colliculus were observed. In contrast, other studies recorded one tenth of X-cells projecting to the SC of the midbrain (Wassle and Illing, 1980; Sawai et al., 1985). Wassle and Illing investigated the retinal projections using the method of retrograde axonal transport by injecting horseradish peroxidase (HRP) to the superior colliculus (Wassle and Illing, 1980). Almost all α -cells and at least 80% of γ -cells projected to the SC. In addition, approximately 10% of the β -cells projected to the SC. Considering Kelly's et al. earlier findings which revealed that almost all α -cells send axons to the SC, the α -cells must have axon collaterals projecting to both SC and LGN (Kelly and Gilbert, 1975).

1.1.3.2.4 Neurons and Layers in the Superior Colliculus in Felines

In cats, the SC is a laminated structure, and the layers could be generally grouped into the superficial and deep layer. Most projections from the retina and visual cortex terminate in the superficial gray layer of the feline superior colliculus (Sterling, 1971; Lund, 1972). The superficial layer was further divided into the upper and lower parts. The upper superficial layer, together with the zonal layer, was termed as the zone of horizontal cells by Cajal; whilst the lower superficial gray

layer was termed as the zone of vertical fusiform cells (Cajal, 1955). The cells varied in size, shape and dendritic structure. Compared to cells in the upper superficial layer with their dendrites restricted within the region, cells in the lower part have their dendrites extending to either upper or lower parts, or both. In addition, horizontal, pyriform and small stellate cells have been identified in the superficial SC in the cat using GABA (γ -aminobutyric acid) immunohistochemistry (Mize et al., 1982).

1.1.3.3 Retinal Projections to the Central Visual Targets in Rodents

In rodents, the LGN only receives about 30% of RGC axons. Instead, the SC acts as the major target (Dreher et al., 1985; Paxinos, 2004; Guerin et al., 2006) (Fig. 1.6). The SC has long been studied as a center for visual sensory and motor responses. In addition, it is also involved in orienting attention and multimodal processing (Hemelt and Keller, 2007). Most axons of RGC in the retina project contralaterally to the SC and the LGN. In addition, 5-10% of RGCs send projection fibers ipsilaterally to the SC and LGN (Kondo et al., 1993).

1.1.3.3.1 Retinal Input to the Superior Colliculus in Rodents

In rats, more than 90% of retinal ganglion cells project to the contralateral SC, which is located at the dorsal surface of the midbrain (Dreher et al., 1985; Guerin et al., 2006) (Fig. 1.7). The SC has a laminated structure, consisting of zonal (stratum zonale) (Zo/SZ), superficial gray (stratum griseum superficiale) (SuG/SGS), optic (stratum opticum) (Op/SO), intermediate gray (stratum griseum intermediale)

(InG/SGI), intermediate white (stratum album intermediale) (InWh/SAI), deep gray (stratum griseum profundum) (DpG/SGP), and deep white (stratum album profundum) layers (DpWh/SAP) (Huber and Crosby, 1933; Paxinos and Watson, 1998) (Fig. 1.8). The visual input goes directly from the retina to the superficial gray and upper optic strata of the colliculus. The cells in these layers project to intermediate and deep layers. The output from the SC then goes to motor centers responsible for orienting behaviors (Binns, 1999).

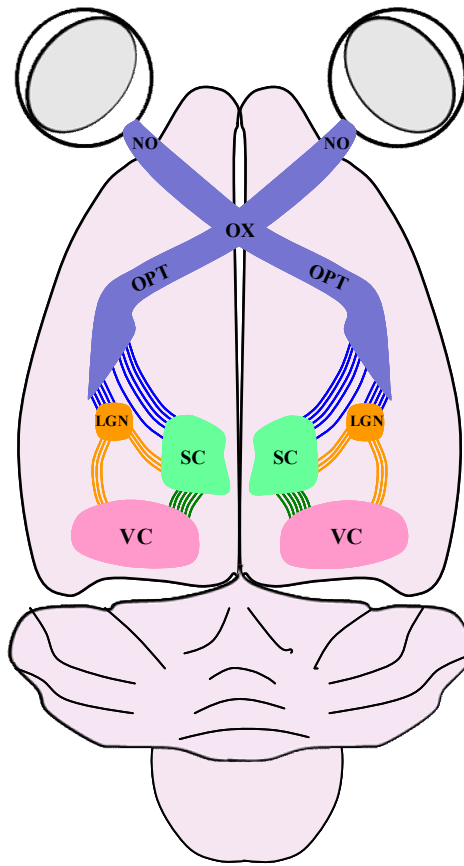


Figure 1.6: The visual pathways from the retina to the brain in rats.

In rats, the superior colliculus (SC) acts as the major target of retinal axons. NO: nervus opticus; OX: optic chiasm; OPT: optic tract; SC: superior colliculus; LGN: lateral geniculate nucleus; VC: visual cortex.

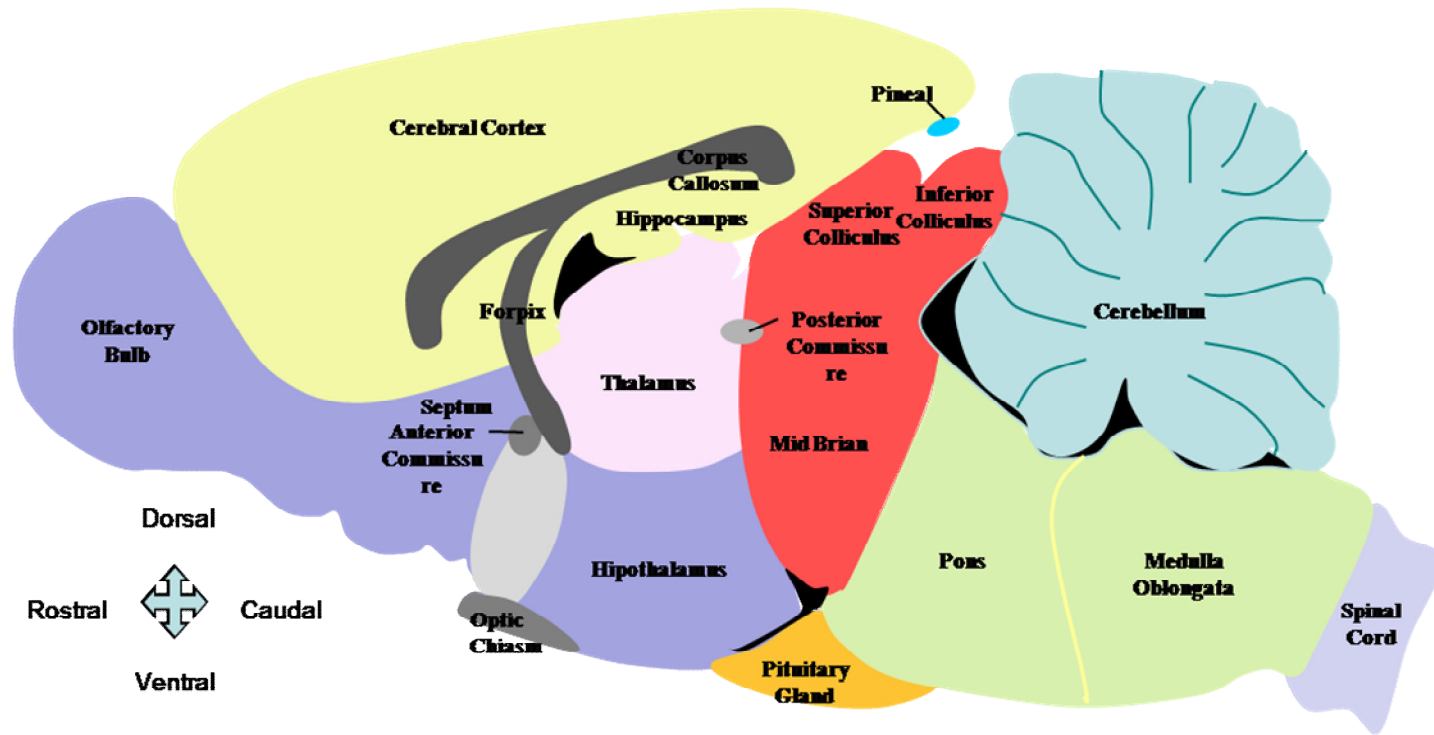


Figure 1.7: A diagram of sagittal view of rat brain.

In rodents, the SC is located at the dorsal surface of middle brain

Superior Colliculus in Rat Brain

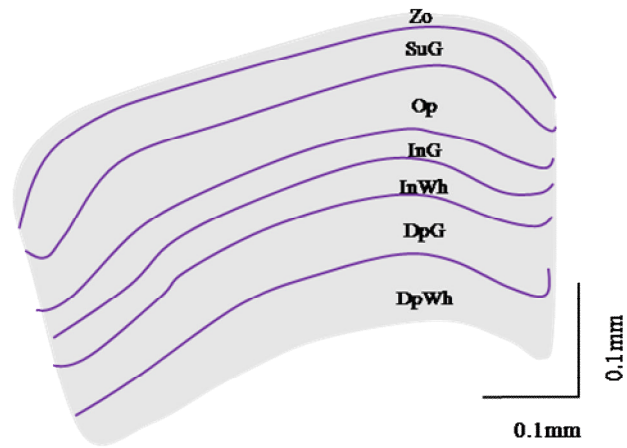


Figure 1.8: A diagram of sagittal view of the superior colliculus (SC) from rat brain.

The layers of Superior Colliculus in rat, from the surface are Zo: zonal layer; SuG: superficial gray layer; Op: optic layer; InG: intermediate gray layer; InWh: intermediate white layer; DpG: deep gray layer; DpWh: deep white layer (Paxinos and Watson, 1998).

1.1.3.3.2 Neurons in the Rodent Superior Colliculus

Cajal described the cells of the rat's SC in 1911 using Golgi-staining (Cajal, 1911). Four decades ago, Langer et al. labeled neurons in the SC in young adult white rats using the Golgi-method. They described the morphologies of cells located in the upper layers of the SC including marginal, horizontal, piriform, narrow and wide field vertical, pyramidal and stellate cells, as well as some subtypes of these cells. In general, cells in the upper layer of the SC were classified into horizontal,

vertical and stellate cells according to the orientation of their dendrites (Langer and Lund, 1974; Tokunaga and Otani, 1976; Labriola and Laemle, 1977) (Fig. 1.9).

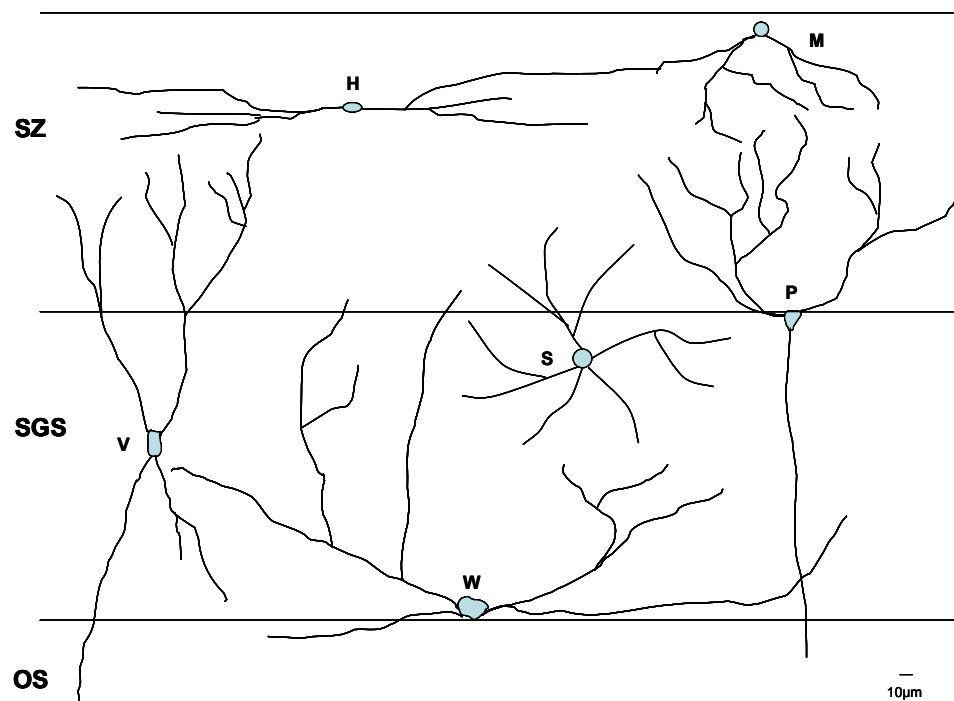


Figure 1.9: Classification of neurons in the upper layers of superior colliculus.

Typical cell types in the upper layers of superior colliculus (SC) in rat, their dendritic fields and distribution in the superficial layers. H, horizontal cell; M, marginal cell; P, piriform cell; V, narrow field vertical cell; W, wide field vertical cell; S: stellate cell; SZ: zonal layer; SGS: superficial gray layer; OS: optic layer. The diagram was drawn based on figures shown in Langer et al.'s study (Langer and Lund, 1974).

The marginal cells have the smallest ovoid cell body with a diameter of 5-8 μ m. The cell bodies are the most superficially located soma in the SC, within or just beneath the anteroposterior coursing fibers of the stratum zonale (SZ). They usually have two primary dendrites arising from the deeper part of cell body, branching several times to form a dense dendritic tree. The dendrite could extend for as far as 150 μ m (Langer and Lund, 1974). Some horizontal and marginal neurons with their axons confined to the upper layers of the SC appear to be interneurons.

Most horizontal cells have fusiform cell bodies that are about 10 μ m in diameter. Their dendrites are tangential to or parallel with the surface of the colliculus, and are usually confined within the same zone of horizontal cells. Generally, there are two primary dendrites arising from opposite sides of the cell body. The primary dendrites run for 10-50 μ m before branching into the higher order dendrites which may run over 300 μ m (Langer and Lund, 1974).

In the superficial gray and optic layers, vertical cells have been found as relay cells projecting to deeper layers of SC, including wide-field vertical cells, piriform cells as well as some narrow field cells (Isa et al., 1998). The piriform cells have ovoid or cup-shaped cell bodies with 10-15 μ m in diameter. Their cell bodies are located at the junction between the zonal layer and superficial gray. These cells usually have 2-5 primary dendrites which are either ascending or descending. The ascending dendrites branch more frequently as they approach the surface. Their dendrites could extend for about 150-350 μ m in width and slightly less than 200 μ m in depth (Langer and Lund, 1974).

The narrow field vertical cells have narrow, fusiform cell bodies ranging from 10 to 20 μm in diameter. Their dendritic fields are narrow and vertically orientated, which are about 100-200 μm in width. There are three types of narrow field vertical cells termed as superficial, intermediate and deep vertical fusiform cells based on their location. The pyramidal cells are very similar as the narrow field vertical cells. They have narrow and vertically elongated cell bodies, which are about 15 μm in diameter. Their dendritic fields are about 100-25 μm in diameter, appearing in narrow and cylindrical shapes as those of narrow field vertical cells (Langer and Lund, 1974).

There are two populations of wide field vertical cells in Langer and Lund's study, which were termed as type II and type III ganglion cells. The type II and III ganglion cells may correspond to Cajal's ovoid, triangular cells or stellate cells (Cajal, 1911). The type I ganglion cells are referred to piriform cells. The type II ganglion cells have cell bodies in diameter of 15-25 μm , and 3-7 primary dendrites. The dendrite fields may be 400 μm in diameter, formed by the vertically or obliquely orientated dendrites. Almost all of the dendritic fields are superficial to the cell body. Type III ganglion cells are very much similar to the type II ganglion cells. They also have multipolar cell bodies in diameter of 20-25 μm , 3-6 primary dendrites, and large dendritic field which may be over 1000 μm in diameter. However, unlike the type II ganglion cells, the type III ganglion cells have some dendrites extending below the cell body (Cajal, 1911; Langer and Lund, 1974)

Stellate cells have multipolar cell bodies with dendrites arising from the cell body symmetrically. The size of their cell bodies and dendritic fields are similar to those of other cells at the same location (Langer and Lund, 1974).

1.1.3.3.3 Retinal Input to the Dorsal Lateral Geniculate Nucleus in Rodents

The LGN is another major target of retinal projections in rodents apart from the SC. It is a striated structure occupying the dorsolateral part of the dorsal thalamus and transmits visual information to the visual cortex. Unlike that in primate and feline, no lamination has been described in the dLGN of rats (Paxinos, 2004). RGCs have been shown mainly projecting toward the contralateral dorsal lateral geniculate nucleus (dLGN). It has been demonstrated that the somal sizes of RGCs projecting to either the dLGN only or both SC and dLGN are generally larger than those projecting strictly to the SC (Dreher et al., 1985; Moriya and Yamadori, 1993).

1.1.3.3.4 Neurons in the Rodent Lateral Geniculate Nucleus

Cajal has studied cell types in the dLGN of the rabbit and mouse and observed two classes of cells: Golgi type I and II cells. The type II cells are smaller than type I cells, and lack an axon (Cajal, 1911; Paxinos, 2004).

Kriebel investigated the neuron types in rat dLGN and the morphologic patterns of their dendrites and dendritic appendages by Golgi staining (Kriebel, 1975). In this study, the cells in dLGN were classified into three types according to their soma size, distribution and dendritic characteristics and architecture of dendritic appendages. The predominant cells are type 1 neurons which are distributed throughout the dLGN. They have multipolar perikarya with mean diameters of 25 μm , giving off four to eight primary dendrites. The type 1 neurons have a tufted dendritic pattern which is typical of thalamocortical relay neurons (Ramón-Moliner, 1968). The dendrites of the type 1 cells are relatively straight and mostly orientated

perpendicular to the optic fibres passing through the dLGN, extending 108 to 120 μ m. The primary dendrites are smooth whilst the dendritic appendages show a short-stalked appearance with large terminal swellings (Kriebel, 1975) (Fig.1.10a). The multiple rounded protrusions observed at the distal dendrites of type 1 neurons are suggested to provide a greater surface area for synaptic contact. The type 1 cells may correspond to the class 1 cells in the cat, and they also resemble the type I neurons in the squirrel monkey (Guillery, 1966; Wong-Riley, 1972).

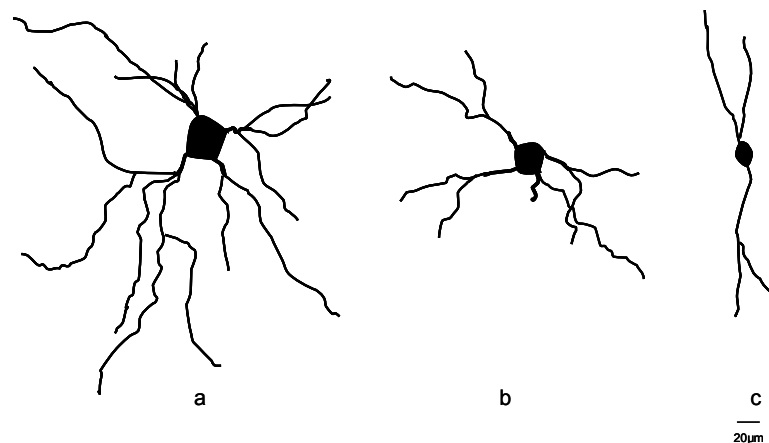


Figure 1.10: Diagrams of the main types of relay neurons and the interneuron in the rodent dLGN.

There are two main types of relay neurons in rodent dLGN were observed by Golgi staining: the relay neuron type I have larger somas (about 25 μ m in diameter) (a); and relay type II with smaller soma (about 20 μ m in diameter) (b). The soma of the interneuron shows an ovoid or spindle shape (about 10 μ m in diameter) (c) (Kriebel, 1975; Paxinos, 2004).

Type 2 neurons are distributed only within the superficial zone of the middle third of the dLGN. They have smaller soma (mean diameter of 20 μm), with dendrites parallel to the optic fibres but less numerous and shorter compared to type 1 cells. However, primary dendrites of type 2 cells extend further than those of type 1, prior to branching into secondary dendrites (Fig. 1.10b). The type 2 cells also correspond to class 2 neurons in the cat and similar neurons, termed as the type II neurons, were also observed in the primate (Guillery, 1966). The amount of type 2 neurons was less than the type 1 neurons in the dLGN. In contrast, there were more type II neurons observed in the dLGN than the type I neurons in the primate.

Type 3 neurons are distributed throughout the dLGN but not as frequently as the other types. They have small round perikarya which are 14 μm in mean diameter. The type 3 neurons show a radiating dendritic pattern with reduced dendritic arbors, and lack the parallel orientation to retinal or cortical afferents. Their dendritic appendages have long pedicles (Ramón-Moliner, 1968; Kriebel, 1975). This type of neuron may correspond to Golgi type II interneuron.

The interneurons in dLGN represent about 22% of overall amount of cells (Gabbott et al., 1986). They are found mostly in the lateral region of dLGN and are orientated dorsoventrally parallel to the lateral border of the nucleus. They have smaller cell bodies which are about 10 μm in diameter and show an ovoid or spindle shape. They have only two to four primary dendrites but no axon (Webster and Rowe, 1984; Gabbott and Bacon, 1994). Parnavelas et al. also described a group of cells, Golgi class B cells, which may represent the interneurons. They branch only rarely and extend a considerable distance, with no axon identified for most of the cells (Parnavelas et al., 1977) (Fig. 1.10c).

In summary, both the SC and LGN are central targets for retinal projections in primates, felines and rodents. In rodents, the SC is the major site of termination of retinal axons; whilst in primates, it is the LGN. In felines, both the SC and LGN are primary visual targets. Previous studies have described the main types of neurons in the SC and LGN in primates, felines and rodents and proposed different morphological classifications (Cajal, 1911; Cajal, 1955; Guillery, 1966; Wong-Riley, 1972; Langer and Lund, 1974; Kriebel, 1975; Wilson and Stone, 1975; Tokunaga and Otani, 1976; Wilson et al., 1976; Labriola and Laemle, 1977; Leventhal, 1979; Mize et al., 1982; Perry and Cowey, 1984; Moschovakis et al., 1988; Wilson, 1989; Martin et al., 1997; Hendry and Reid, 2000; Payne and Peters, 2002; Paxinos, 2004; Callaway, 2005; Casagrande et al., 2007; Szmajda et al., 2008), as shown in Table 1.3.

Species	Primary visual targets in the brain	Main types of neurons in the central visual targets	
Primate	LGN	LGN	Type I, II, III and IV cells; The multipolar, bipolar relay neurons and small interneurons; M, P and K cells.
		SC	L, X and T neurons
Feline	LGN and SC	LGN	X-, Y- and W- type cells; Class 1 and 2 cells
		SC	Horizontal, Vertical fusiform, Pyriform and Stellate cells
Rodent	SC	SC	Marginal, Horizontal, Piriform, Narrow and Wide field vertical, Pyramidal and Stellate cells.
		LGN	Golgi type I and II cells; Type 1, 2 and 3 cells

Table 1.3: Summary of the main types of neurons in the SC and LGN in Primates, Felines and Rodents.

This table summarises the primary types of neurons in the SC and LGN in three different species: primates, felines and rodents according to their morphologies (Cajal, 1911; Cajal, 1955; Guillery, 1966; Wong-Riley, 1972; Langer and Lund, 1974; Kriebel, 1975; Wilson and Stone, 1975; Tokunaga and Otani, 1976; Wilson et al., 1976; Labriola and Laemle, 1977; Leventhal, 1979; Mize et al., 1982; Perry and Cowey, 1984; Moschovakis et al., 1988; Wilson, 1989; Martin et al., 1997; Hendry and Reid, 2000; Payne and Peters, 2002; Paxinos, 2004; Callaway, 2005; Casagrande et al., 2007; Szmajda et al., 2008).

1.1.4 Glaucoma

1.1.4.1 Epidemiology of Glaucoma Disease

Glaucoma refers to a group of diseases where the optic nerve is damaged, resulting in vision loss and irreversible blindness. It has been shown that visual loss in glaucoma is attributed to RGC death, and elevated intraocular pressure (IOP) is defined as the major modifiable risk factor (Anderson, 1977; Sommer, 1989; Guo and Cordeiro, 2008; Cordeiro et al., 2010).

As a second leading cause of blindness worldwide, glaucoma is a serious disease with a significant socio-economic burden which is predicted to get worse as the population ages (Quigley, 1996). The number of people with open angle glaucoma (OAG) and angle closure glaucoma (ACG) worldwide was estimated to be 60.5 million in 2010, and increased to 79.6 million by 2020 (Quigley and Broman, 2006). The National Eye Health Program has stated that approximately 120,000 are blind from glaucoma, accounting for 9% to 12% of all cases of blindness in the United States. It was predicted that there would be 2.79 million people with OAG in the United States in 2010 (Quigley and Broman, 2006). In the UK, glaucoma is the second most common cause of blindness after age-related macular degeneration, which is responsible for approximately 13% of wholly or partial blindness (Bunce and Wormald, 2006). As the most common type of glaucoma, OAG accounts for 75% to 95% of primary glaucoma in the UK (Quigley, 1996; Azuara-Blanco et al., 2007). About 1 in 50 people in the UK population aged over 40 have glaucoma, although it is estimated that only about 50% of these have been diagnosed and are under treatment. Therefore, it is important to establish methods for early diagnosis of

disease, and to identify early markers for the neurodegeneration process before significant visual loss occurs.

1.1.4.2 Intraocular Pressure and Types of Glaucoma

IOP is maintained by the balance between the secretion and drainage of aqueous humour in the eye. Elevated IOP is one major risk factor for glaucoma (Weinreb and Khaw, 2004). Aqueous humour is secreted posteriorly to the iris by the ciliary body and then flows anteriorly to the anterior chamber through the trabecular meshwork. It provides nutrients to the iris, lens, and cornea. There are two main types of glaucoma: primary open angle glaucoma (POAG) and primary angle closure glaucoma (PACG) (Coleman, 1999).

POAG is the most frequent type of glaucoma defined by an open angle between the iris, cornea and sclera at the anterior chamber angle. The aqueous humour accesses the trabecular meshwork freely and the anterior chamber angle has a normal appearance (Newell, 1991). In the past, raised IOP was considered as one criterion to define POAG, however, recent population-based epidemiologic studies have stated that POAG can occur at any level of IOP. Therefore, increased eye pressure is no longer considered as the criterion for POAG but only a risk factor (Wolfs et al., 2000; Foster et al., 2002; Leske, 2007).

In PACG, the trabecular meshwork in the angle of the eye is obstructed by the iris and the drainage of aqueous humour from the anterior chamber is prevented, in contrast to POAG in which the trabecular meshwork is open and unobstructed (Newell, 1991; Coleman, 1999). This type of glaucoma is mainly caused by pupillary

block or plateau iris, which is a direct mechanical blockage of the drainage angle by the root of the iris (Newell, 1991).

Secondary glaucoma is used to define a disease other than glaucoma that causes or contributes to increased eye pressure, resulting in optic nerve damage and vision loss.

Though there is no cure for glaucoma yet, medication or surgery can slow or prevent progressive vision loss. Currently, lowering IOP is the only effective method in preventing or delaying the development of glaucoma in individuals with elevated IOP, which however does not completely stop the disease process (Heijl et al., 2002).

1.2 Neuronal Atrophy in Visual Pathways in Glaucoma

Glaucoma is increasingly recognized as a neurodegenerative disease, and has been shown to involve neuronal changes both in the retina and CNS. Neuronal degeneration refers to the death of cells from the primary injury, and death secondary to the primary damage (Schwartz, 2001).

Previous studies have shown that RGC loss is a hallmark of glaucoma, and that elevated IOP is regarded as a primary risk factor for the initiation and progression of glaucomatous optic neuropathy (Leske, 1983; Sommer, 1989). However, IOP does not always correlate with the loss of visual field in glaucoma patients, implicating that IOP is not the only cause of glaucomatous retinopathy and optic neuropathy. There are some other mechanisms involving the retina, optic nerve and brain that may also contribute to the RGC death, including neurotrophin deprivation, excitotoxicity, ischemia, glial activation, oxidative stress, mitochondrial

dysfunction and protein misfolding (Kass et al., 2002; Pang and Clark, 2007; Baltmr et al., 2010; Qu et al., 2010). The RGC apoptosis may either be a retrograde or anterograde death (Guerin et al., 2006). The lack of neurotrophin supply from the superior colliculus may cause the retrograde death of RGCs, whereas the presence of excessive glutamate or other excitotoxins released in the retina may lead to anterograde death of RGCs (Nickells, 1999).

1.2.1 Dendritic Degeneration in the RGCs in Glaucoma

1.2.1.1 Dendritic Changes in Human Glaucoma and Primate Glaucoma

Model

In primates, the structure and morphology of ganglion cells in the retina change during the degenerative process. The morphology of midget and parasol cells in the eyes of a primate glaucoma model was studied using Lucifer yellow demonstrating that RGCs undergo structural changes prior to cell death (Weber et al., 1998). The earliest structural signs of RGC degeneration involved abnormalities in the dendritic field, including a thinning of the proximal and distal dendrites, abrupt reductions in dendritic process diameter at branch points, as well as a general decrease in the complexity of the cell's dendritic tree which was followed by a reduction in axonal thickness and shrinkage of soma size. A reduction in RGC function, both spatially and temporally to visual stimuli has also been demonstrated and attributed to the significant changes in dendritic architecture, suggesting a direct link between dendritic pathology and visual dysfunction (Weber et al., 1998; Weber

and Harman, 2005). Some studies have suggested that there was a more pronounced reduction in larger RGCs and their axons than that in smaller cells and their axons in both primate and human glaucoma, indicating that large cells are more sensitive to the elevated IOP (Quigley et al., 1987; Quigley et al., 1988; Glovinsky et al., 1991; Glovinsky et al., 1993). On the other hand, Morgan *et al.* have shown that RGC loss is not selective but due to shrinkage of RGCs (Morgan et al., 2000; Morgan, 2002).

Dendritic alterations in the RGCs have also been investigated in advanced human glaucomatous retinas whereby the morphologic changes of RGCs that survive elevated IOP were examined by applying the fluorescent dye 1,1',di-octadecyl-3,3,3'3'-tetramethylindocarbocyanine perchlorate (DiI) into the optic fibre layer (OFL) (Pavlidis et al., 2003). This study revealed that the pruning of dendrites occurred in glaucoma-resistant RGCs. So far, there are only a few studies which have investigated the dendritic pathology in the retina in human glaucoma.

1.2.1.2 Dendritic Changes in Feline Glaucoma Model

Investigations of cell-type-differentiated dendritic shrinkage of RGCs in cats with chronic glaucoma showed a significant reduction in RGC density, soma size, maximum dendritic field radius, total dendritic length, and the number of branch bifurcations of dendrites in glaucomatous eyes compared to age-matched controls (Shou et al., 2003). In addition, they demonstrated ocular hypertension led to the progressive cell loss and dendritic damage in both RGCs and LGN cells, which were more pronounced in the Y- cells than the X- cells (Shou et al., 2003). Cell-type-differentiated dendritic shrinkage appeared more sensitive to IOP

elevation than soma atrophy, which was consistent with Weber's studies, confirming RGC degeneration commences with dendritic arbor changes, followed by a reduction in axonal thickness, and finally with shrinkage of the cell body (Weber et al., 1998).

1.2.1.3 Dendritic Changes in Rodent Glaucoma Model

During the past two decades, a variety of rodent glaucoma models have been developed in order to delineate the degenerative process and provide strategies to prevent or delay RGC loss. These glaucoma models are classified as acute vs. chronic models, and induced vs. spontaneously occurring damage models (Goldblum and Mittag, 2002; Morrison, 2005; Urcola et al., 2006). However, none of these models completely mirror the clinical disease. Several primarily used rodent models of glaucoma were summarised as shown in Table 1.4.

Schwartz et al. used an optic nerve crush model to quantitatively distinguish the damage due to secondary degeneration from primary degeneration (Yoles and Schwartz, 1998b; Schwartz and Yoles, 1999). Using this model, they found that intraocular glutamate and aspartate levels were significantly higher than that in normal or sham-operated-on eyes, and returned to normal after two weeks (Yoles and Schwartz, 1998a). Leung et al. also used a mouse model of optic nerve crush to investigate the longitudinal profile of RGC loss and suggested a two-phase exponential decay model for describing RGC degeneration (Leung et al., 2008).

Ischemic retinal injury achieved by complete irreversible central retinal artery occlusion (CRAO) leads to an inevitable course of necrosis of the retina (Hayreh and Weingeist, 1980). Antagonists of glutamate or its analogues were found to have

neuroprotective effects. Donello et al. stated that activation of the α_2 -adrenergic receptor may prevent the accumulation of extracellular glutamate and aspartate and finally reduce ischemic retinal injury (Donello et al., 2001).

The excitotoxin injection rat model has been used to further determine excitotoxic involvement in the pathogenesis of retinal ischemic injury (Vorwerk et al., 1996). Vorwerk et al.'s study suggested that chronic, low-dose elevations in vitreal glutamate for 3 months can be toxic to RGCs. Memantine was demonstrated effective at protecting RGCs from chronic low-dose glutamate toxicity. Previous studies have also shown that BDNF, nipradilol, MK-801, or eliprodil could protect inner retinal cells in this model (Morizane et al., 1997; Kapin et al., 1999; Kido et al., 2000; Mizuno et al., 2001). Honjo et al. used this model to examine the role of retinal muller cells in N-methyl-D-aspartate (NMDA)- or kainic acid (KA)-induced retinal damage. They found the upregulated expression of glial fibrillary acidic protein (GFAP) and ciliary neurotrophic factor (CNTF) in Muller cells in response to NMDA- and KA-induced neuronal death, indicating that production of CNTF in muller cells may be a part of the endogenous neuroprotective system in the retina (Honjo et al., 2000).

Since elevated IOP is regarded as a major risk factor for the initiation and progression of glaucomatous optic neuropathy (Leske, 1983), several rodent models with surgically induced chronically elevated IOP have been developed to investigate the disease. A variety of methods were devised to induce elevated IOP in the rat eye to impede the outflow of aqueous humor. Injection of hypertonic saline into limbal aqueous humor collecting veins to produce scarring of the tissue and the cautery of two or three episcleral/limbal veins are commonly used procedures (Shareef et al.,

1995; Johnson et al., 1996; Morrison et al., 1997). Using the rat model with elevated IOP, Guo et al. demonstrated that RGC apoptosis correlates strongly with elevated IOP and is significantly associated with IOP-induced changes in specific ECM components in the RGC layer, and showed a link between MMP-9, laminin degradation, RGC apoptosis, and IOP exposure in glaucoma (Cordeiro et al., 2004; Guo et al., 2005a). Chauhan et al. have characterized the effect of IOP on retinal function and axonal survival in a model of IOP-induced optic nerve damage in rats, showing a positive correlation of the loss of RGC axons to the level and the duration of IOP elevation in experimental rat glaucoma (Chauhan et al., 2002). Morgan et al. studied RGC remodelling using the episcleral vein injectin model, and found dendritic changes in RGCs prior to the onset of RGC death in glaucoma rats (Morgan et al., 2006).

Other studies also used laser photocoagulation of either the trabecular meshwork alone or in concert with episcleral veins to produce elevated intraocular pressure in rodents (Ueda et al., 1998; Levkovitch-Verbin et al., 2002; Grozdanic et al., 2003; Fu and Sretavan, 2009). However, using the laser treatment, the elevated IOP last for a shorter period compared to the methods of altering aqueous fluid dynamics in the anterior segment.

Recently, Sappington et al. also established a rodent glaucoma model by injecting small volumes of polystyrene microbeads into the anterior chamber to impede aqueous outflow and elevate the IOP (Sappington et al., 2010). In addition, the method of injecting latex microspheres into the eye anterior chamber to restrict the outflow of aqueous humor through the trabecular meshwork and induce chronic elevated IOP was also used in rats. This method has been used for establishing the

primate model of experimental glaucoma earlier (Weber and Zelenak, 2001; Urcola et al., 2006).

Another rodent model is the one with spontaneously elevated IOP. The DBA/2NNia, DBA/2J and AKXD-28/Ty inbred mouse strains develop a form of secondary glaucoma (pigment dispersion) spontaneously in almost 100% of mice (Sheldon et al., 1995; John et al., 1998; Anderson et al., 2001).

Jakobs et al. examined the neural changes that occur during elevated intraocular pressure using a mouse model of inherited glaucoma (strain DBA/2J). They found axonal atrophy, dendritic remodelling, and soma shrinkage prior to ganglion cell death in this glaucoma model. Some ganglion cells had clearly abnormal morphology including the loss of second and higher order dendrites. In some severely affected ganglion cells, only the cell body and the proximal part of the primary dendrites are visible (Jakobs et al., 2005). The findings that dendritic changes during the neurodegenerative processes are observed before cell body dysfunction, indicates a dendritic self-destruct mechanism apart from cell apoptosis (Whitmore et al., 2005). Morgan et al., also have shown the RGC remodelling with reductions in overall dendritic area and in the complexity of the dendritic tree in a rat model of experimental glaucoma (Morgan et al., 2006). The findings of dendritic shrinkage and remodelling prior to cell loss support the hypothesis that dendritic changes in RGCs precede the onset of RGC death in experimental glaucoma (Weber et al., 1998).

Rodent Models of Glaucoma	Damage
Crush Injury Model	Secondary degeneration
Ischemic Injury Model	Central retinal artery occlusion
Impedance of Aqueous Humor Outflow Model a) Episcleral cauterization b) Injection of Hypertonic Saline c) Laser photocoagulation d) Polystyrene microbeads/ Latex microsphere	Ocular Hypertension
Transgenic Animal Model (DBA-J)	Ocular Hypertension

Table 1.4: Primary rodent models used for glaucoma study currently (Goldblum and Mittag, 2002; Morrison, 2005; Urcola et al., 2006).

1.2.2 Dendritic Degeneration in Glaucoma Brain

So far, only a few studies have investigated the dendritic changes in glaucomatous brain, but in recent work dendrites of neurons in the LGN in an experimental primate model showed striking changes with thickened and shortened dendrites following chronically elevated IOP (Gupta et al., 2007). The dendrite complexity also decreased remarkably by 47% and 41% in magnocellular and parvocellular layers respectively in glaucoma monkeys. Recently, reductions in dendrite complexity and length were also shown in LGN relay neurons in a primate model of glaucoma (Ly et al., 2010).

The mechanisms involved in the dendritic degeneration are still not clear, however, the reduced axoplasmic transport may contribute to the dendritic changes. The axoplasmic flow consists of the transport organelles and metabolic substances

along the axon, and it could be partially obstructed by moderately elevated IOP in the region of the lamina cribrosa, optic nerve or LGN (Anderson and Hendrickson, 1974; Gupta et al., 2007). Distal axon injury has also been shown in early stages of mouse glaucoma, with RGC axons terminating in the SC displaying reduction of active transport in a retinopic pattern akin to vision loss in glaucoma (Crish et al., 2010). Transport loss progresses from distal-to-proximal, prior to axonal degeneration and therefore could represent an important therapeutic target. Loss of axoplasmic flow could cause the dendritic degeneration which would further proceed to the cell death.

1.2.3 Dendritic Alterations in Other Neurodegenerative Conditions

1.2.3.1 Cerebral Trauma

Dendritic lesions in cerebral ischemia have been demonstrated in the gerbil using MAP2 immunohistochemistry, with the loss of MAP2 immunostaining being considered an early indicator of neuronal pathology. MAP2 has been used as a marker to describe dendritic pathology including mild focal cortical trauma and spinal cord compression trauma, showing that MAP2 immunostaining is a sensitive method for identifying dendritic lesions of various CNS injuries in rats (Kitagawa et al., 1989; Li et al., 1995; Lewen et al., 1996; Li et al., 2000). Dendritic loss was also observed in the toxin-induced neurodegeneration in rat brain using tyrosine-hydroxylase (TH)-immunolabeling (Bywood and Johnson, 2000). Catecholamine (CA) neurons are essential neurons in motor control, attention and other brain

functions, which are also selected targets of several neurotoxins. Bywood and Johnson found the loss of dendrites in the degenerated substantia nigra (SN) CA neurons, suggesting dendritic changes as the characteristic early indicator of neurodegeneration. As the dendritic degeneration could precede the loss of nerve cell bodies, using the dendritic loss as the early indicator could be applied to study the mechanisms of cell death.

Dendritic spines are the postsynaptic morphological specializations at the excitatory synapse, protruding from the dendritic shaft of a neuron. The spines are responsible for the synaptic contacts in more than 90% of glutamatergic terminals in mature brain. The principal neurons of most brain regions are covered with dendritic spines, meaning that alteration of dendritic spines are characteristic of traumatized or diseased brain (Fiala et al., 2002; Kim et al., 2007). Alteration of spine distribution, including spine number, distorted spine shape, and abnormal position of spine origin on the neuron, has been documented following traumatic lesions. The loss of spines and their synapses have been found in pyramidal cells after undercutting cerebral cortex and in granule cells of the dentate gyrus following lesions of entorhinal cortex (Rutledge et al., 1969; Rutledge et al., 1972; Parnavelas et al., 1974; Fiala et al., 2002). Al-Abdulla et al. found dendritic atrophy and loss of dendritic protrusions in the dorsal lateral geniculate nucleus after axotomy using a unilateral occipital cortex ablation rat model (Al-Abdulla et al., 1998).

1.2.3.2 Alzheimer's disease

Dendritic pathology of neurons has also been clearly identified in Alzheimer's disease (AD). AD is a progressive neurodegenerative disease of the central nervous system, and accounts for approximately 80% of all dementia cases in the elderly (Terry, 2006).

Synaptic alterations are prominent in AD, correlated heavily with dendritic pathology, due to dendritic dystrophy being found frequently in AD (Gonatas, 1967; Terry et al., 1991). The presence of neuritic plaques in human dentate granule cells in AD brains generated significant differences between the morphology of dendrites in control and AD cases (Einstein et al., 1994). The dendrites of granule cells from AD cases appeared shorter, branched less profusely, and had fewer spines compared to those from age matched controls. This was in agreement with previous studies, showing the decrease in dendritic length, dendritic diameter, abnormal varicosities, and loss of dendritic spines in dentate granule cells (De Ruiter and Uylings, 1987; Flood et al., 1987). A progressive loss of dendritic spines from hippocampal pyramidal neurons has been documented in AD (el Hachimi and Foncin, 1990). The dendritic and spinal pathology has also been studied in the human acoustic cortex at early stages of AD (Baloyannis et al., 2007). Neurons in the acoustic cortex were stained by Golgi staining, following which the morphological changes of dendrites and dendritic spines were analyzed. This study revealed the loss of Cajal-Rezius cells in layer I and the remarkable decrease in dendritic arborization in layers III and V. The spine density and size also significantly declined in the majority of cells in layers II, III and V of the acoustic cortex. They also found the morphological alterations of mitochondrial and Golgi apparatus in soma and spines, indicating

oxidative stress in early stages of AD (Nunomura et al., 2001; Baloyannis, 2006, 2009). Further investigation of the dendritic abnormalities in human AD correlated the dendritic and spinal changes with mitochondrial alteration (Baloyannis, 2009). Most neurons in both acoustic and visual cortices still showed the primary apical dendrites and part of the secondary branches, however, the tertiary dendritic branches were significantly reduced. In addition, a decrease of dendritic spines and the loss of distal spines were also revealed in these cortical areas. The overall reduction of dendritic field and spines are 45% and 52% in acoustic and visual cortices compared to control groups (Baloyannis, 2009). Structural changes of mitochondria were found in some axonal and dendritic profiles, showing a prominent polymorphism of the mitochondria in AD cases. The mitochondrial alterations and dysfunction may contribute to the dendritic and spinal degeneration, since the normal distribution, morphology and function of dendritic mitochondria are essential in modulating synapse morphogenesis and spine formation (Li et al., 2004).

1.2.3.3 Amyotrophic Lateral Sclerosis

Dendritic alteration has also been documented in amyotrophic lateral sclerosis (ALS), a fatal progressive motor neuropathy characterized by the loss of spinal cord and cortical motoneurons (Nirmalanathan and Greensmith, 2005). Investigation of the changes of anterior horn cell processes in ALS patients revealed structural changes in anterior horn cells in the lumbar cords of patients with ALS and those of patients without neurological disease (Kato et al., 1987). In the ALS cases, the abnormalities of dendrites consisted of a poorly developed dendritic extension

from the cell body. The loss of dendrites in anterior horn cells, and the thin and short appearance of dendrites were also observed in the ALS cases. It was further hypothesized that the loss and atrophy of dendrites could precede the death of motor neuron in ALS, and the reduction of dendritic arborization could also lead to the loss of afferent synaptic inputs to the motoneurons (Karpati et al., 1988). The dendritic synapses of anterior horn neurons were also studied at the early stage of ALS, revealing thin and thread-like atrophic proximal dendrites (Sasaki and Iwata, 1996). Although the shortening of dendrites was not observed, significant degeneration of dendrite presynapses, including the aggregation of electron-dense presynaptic vesicles and mitochondria, and neurofilament bundles were found more frequent at the early ALS cases compared to controls. Recently, the prefrontal cortex (PFC) neuronal abnormalities were found in a mouse model of ALS (G93A mice) (Sgobio et al., 2008). The structural changes of the prelimbic/infralimbic (PL/IL) medial prefrontal cortex (mPFC) neurons consisted of the reduction in the length of basal dendritic arborization, the dendritic branching and a mild decrease of dendritic spine in G93A mice compared to control mice. These morphological alterations in mPFC neurons were found to be associated with fear extinction deficits in this mouse model of ALS before the onset of the motor symptoms. Based on the above results, it was suggested that the early diagnosis of ALS might be achieved by assessing the mPFC function using non-invasive brain imaging and neuro-psychological techniques.

1.2.4 Dendritic Changes during Development

RGC dendrites undergo highly dynamic rearrangement during dendritogenesis, both in the addition of dendritic arborization and loss of existing dendritic branches. During the development, several primary dendrites firstly extend to the inner plexiform layer (IPL), and then these primary dendrites branch actively to remodel the dendritic tree. During early postnatal development, RGC show a more complex morphology than their adult counterparts, with a remarkable decrease in the number of dendrites and their spines during development of the α - and β - retinal ganglion cells (Dann et al., 1987; Ramoa et al., 1987; Dann et al., 1988; Ramoa et al., 1988; Cohen-Cory and Lom, 2004). Dendritic remodelling of RGCs may be a generalized mechanism during maturation of mammalian retina with type I and II RGCs both undergoing extensive loss of dendritic spines and longer dendritic branches during maturation, indicating dendritic remodelling may be a generalized mechanism during maturation in developing rats (Yamasaki and Ramoa, 1993). Furthermore, synaptogenesis appears to occur in the inner plexiform layer of cat's retina during the dendritic remodelling, suggesting that the transient excessive dendritic branches and exuberant spines play a role in establishing the intraretinal connections (Ramoa et al., 1988; Wassle, 1988)

The structural remodelling of the dendritic arbor also appears to occur elsewhere in the visual system during development, with previous studies having investigated the principal features of dendritic morphology in the developing cortex and the molecular mechanisms that regulate the dendritic development (Houser et al., 1983; Katz, 1987; Koester and O'Leary, 1992). Neurotrophic factors, including

brain-derived neurotrophic factor (BDNF), nerve growth factor (NGF), neurotrophin-3 (NT-3) and neurotrophin-4/5 (NT-4/5), have been demonstrated to control dendritic growth and branching in cortical neurons (Huang and Reichardt, 2001). Neurotrophins are essential for regulating axonal and dendritic growth, guidance, synaptic connections and plasticity. They exert their functions through two different transmembrane-receptor signalling systems, the high-affinity Trk receptor tyrosine kinases and the low-affinity p75 neurotrophin receptor (Kaplan and Miller, 2000; Chao, 2003; Guerin et al., 2006; Kisiswa et al., 2010).

1.2.5 Age-related Dendritic Changes

Over the past four decades, age-related morphological changes of neurons in the brain have been recorded in different species such as monkeys, dogs and human.

Age-related synapse loss, neuronal loss, and cognitive decline are commonly found in neurodegenerative disorders such as AD. In addition, age-associated cognitive impairment without neuronal loss has also been found in many species. It is known that cognitive decline is accompanied by subtle changes in neuronal morphology, such as dendritic and synaptic alterations (Morrison and Hof, 2002). Neuronal dendrites play a vital role in the formation and maintenance of neural networks, the regulation of synaptic plasticity and the integration of electrical inputs. They are important in the functional properties of neuronal circuits, accordingly, any structural changes of the dendrites can result in profound and detrimental effects (Duan et al., 2003; Nguyen et al., 2004; Dickstein et al., 2007). There is a variation of dendritic shape and branching patterns among both neuronal classes and

individual cells in each class (Samsonovich and Ascoli, 2006).

Previous studies have shown irregularities in dendritic morphology, including the dendritic complexity, dendritic length, spine number during ageing without neuronal degeneration either in primate or non primate models (Dickstein et al., 2007). The structural changes of dendritic spines could reflect the alterations of synaptic densities.

In monkeys, the age-related reduction in the dendritic arbors and the dendritic spines of pyramidal neurons has been demonstrated. Cupp and Uemura found that entire branches or segments were lost from apical dendrites from the prefrontal region of rhesus monkeys with ageing. An approximate 25% loss of spines in that region was also detected in aged monkeys (Cupp and Uemura, 1980). Recently, regressive dendritic changes in apical dendrites were found in old macaque monkeys compared to young controls, as well as an age related reduction of spine number and density in both apical and basal arbors (Duan et al., 2003). The effects of ageing on two types of pyramidal neurons, the long projection neuron and local projection neuron, in the macaque prefrontal cortex showed a remarkable reduction in dendritic arborization, length and diameter in apical dendrites in the long projection neuron (Kabaso et al., 2009). Whereas in the local projection neuron the dendritic branches only decreased significantly at the most distal areas of the apical dendrites, with the dendritic diameter not being affected. In both two types of neurons, the spine number and density decreased significantly on basal and apical dendrites.

In human, the age-related changes of basal dendrites was demonstrated, showing a decline in the number of dendrites of the pyramidal cell with age in the motor cortex (Nakamura et al., 1985). An age-related decrease in total dendritic

length, total number of dendritic segments, and terminal dendritic length were also revealed in pyramidal cells in the human prefrontal cortex (De Brabander et al., 1998). In addition, the dendritic shrinkage and spine loss in canine neocortex were also reported in aged dogs (Mervis, 1978). The dendritic changes have also been investigated in aged rodent brain showing a shortening of the dendrites and a reduction in the dendritic arborization in the hypothalamus in old mouse (Machado-Salas et al., 1977). Xu et al, have also demonstrated an age-related decrease in the dendritic length in the rat visual cortex (Xu et al., 2007).

However, the functional repercussions of these dendritic changes are still not clear. The abnormalities in numbers of dendritic branches and dendritic length with ageing may alter the neuron's response to synaptic input, and ultimately cause detrimental effects in the absence of neuronal degeneration.

1.3 Summary and Aims of the Study

Glaucoma is a progressive optic neuropathy, characterized by RGC death, optic nerve damage and visual loss. There is accumulating evidence revealing retinal and central neuronal degeneration in glaucoma. Glaucomatous neurodegeneration also has similarities to other neurodegenerative conditions such as Alzheimer's disease (AD). Dendrites are fine neuronal processes which support postsynaptic contact elements and are responsible for receiving synaptic signals. Dendritic changes have been recorded in neuronal degenerative processes including those occurring in AD, amyotrophic lateral sclerosis (ALS) and ageing, and were suggested as an early indicator of neuronal degeneration. However, dendritic changes

in glaucoma have not been well investigated. The rodent glaucoma model is being used increasingly and can be a useful model for primate and human glaucoma. In rodents, the superior colliculus and (SC) and the lateral geniculate nucleus (LGN) are the central targets of retinal axons.

This study aimed to characterize the dendritic changes in the RGCs and cells in the SC and LGN in a rat model of experimental glaucoma. The investigation of dendritic morphologies in the RGC, SC and LGN will reveal whether dendritic changes in the RGCs can be early signs of retinal degeneration in glaucoma. In addition, the results will also help to reveal whether the retinal degeneration has an effect on central visual targets in the brain. Furthermore, dendritic changes with age in the RGCs and cells in the SC and LGN will also be delineated. The findings in this thesis will increase the understanding of retinal and central neuron degeneration in glaucoma; provide new sights for early diagnosis of neuronal degeneration to protect RGCs and neurons in the CNS prior to cell death; and suggest new therapeutic strategies in glaucoma.

Chapter 2: Materials and Methods

2.1 Animals

All animals were treated in compliance with the ARVO (Association for Research in Vision and Ophthalmology) statement for the Use of Animals in Ophthalmic and Vision Research. All conditions and experimental procedures were carried out in accordance with the UK Animals (Scientific Procedures) Act 1986. Adult male Dark Agouti (DA) rats were ordered from Harlan UK at the age of 6 to 8 weeks with the body weight of 150 to 200g. All animals were housed in the animal room with a 12 hour light/12 hour dark cycle, and were supplied with unlimited access to water and food pellets (RM1 Special Diet Services, Cambridgeshire, England).

In total 90 DA rats were used to study the dendritic changes in the visual pathway in this thesis. The morphological changes of dendrites were investigated in the superior colliculus (n = 42 rats), lateral geniculate nucleus (n = 37 rats) and retinae (n = 19 rats). Four rats in 8 weeks OHT group were used for both SC and RGC. Three rats in 4 weeks OHT group were used for both LGN and RGC study. One rat in 32 weeks OHT group was used for both LGN and RGC study.

2.2 Glaucoma Model

2.2.1 Anaesthesia of Animals

Animals were placed in the induction chamber for inhalation anaesthesia initially using analgesic 2-chloro-2-(difluoromethoxy)-1, 1, 1-trifluoro-ethane (Isoflurane) (Merial Animal Health Ltd, Harlow, Essex, UK), and then deeply anaesthetized by intraperitoneal (IP) injection with ketamine cocktail consisting of 37.5% Ketaset (Fort Dodge Animal Health Ltd., Southampton, UK), 25% Dormitor (Pfizer Animal Health, Pfizer limited, Kent, UK) and 37.5% sterile water (Pfizer Animal Health, Exton, PA) at 0.2ml/100g body weight.

2.2.2 Induction of Ocular Hypertension

Ocular Hypertension (OHT) was induced in rats only using the Morrison method, which has been previously used and validated in our lab to introduce the glaucoma model (Morrison et al., 1997; Cordeiro et al., 2004; Guo et al., 2005a; Guo et al., 2005b; Guo et al., 2006; Guo et al., 2007; Guo and Cordeiro, 2008; Cordeiro et al., 2010; Guo et al., 2010). The glaucoma surgery and the measurement of IOP were performed by Dr Li Guo in our lab.

OHT induction was performed on 42 animals under a dissecting microscope (Zeiss, Carl Zeiss microimaging, Munich, Germany). Animals were positioned onto a stereotaxic frame with a bite bar after anaesthesia and a drop of topical anaesthetic, 0.5% Proxymetacaine hydrochloride (Chauvin Pharmaceuticals Ltd., Surrey, UK), was administered on to each eye.

The IOP was unilaterally elevated in the left eye of each animal by injection of 50 μ L of hypertonic saline solution (1.80 M) into two episcleral veins. The left eye was opened by performing a lateral canthotomy. In the following, a small polypropylene ring was placed around the equator of the eye globe and an incision was made at the conjunctiva to expose the episcleral veins. The ring helps to clearly locate and insert the needle into the vein and also to prevent the saline flowing to the surrounding areas. The injection apparatus is composed of a 34-gauge 8mm glass micro-needle (Hamilton, Reno, NV), the polyethylene tubing on a Hamilton syringe (50 μ l, Hamilton), and the syringe pump (60 μ l /min; UMP2, World Precision Instruments, Sarasota, FL).

After the injection, ointments consisting of Chloramphenicol 1% and Hydrocortisone 0.5% (Martindale Pharmaceuticals Ltd, Romford, England) were applied on the eyes before the incision at the conjunctiva was sutured (10-0 12", ALCON Suture System, Alcon Laboratories, Inc., USA). The eyelids were then sutured once to keep the operated eye moist (6-0, Ethicon coated vicryl, Johnson and Johnson International, St-Stevens-Woluwen, Belgium).

The IOP was measured an hour later using a TonoLab-Tonometer (Icare Finland Oy, Helsinki, Finland) which has been specially designed for rodent IOP measurement. The tonometer is based on a measuring principle known as the rebound method (Icare Finland Oy, Helsinki, Finland). A very light probe is used in this method to make momentary contact with the cornea, and the IOP is displayed in mmHg instantly. There's very little discomfort caused from the measurement to the animals.

The recovery drug atipamezole consisting of 20% Antisedan, 80% sterile water (Pfizer Animal Health) was then administrated at a dose of 0.1mg/ 100g body weight. The animals were woken up and placed in the recovery room with a heated mat underneath the cage to keep them warm. Softened food pellets and drinking water were also provided at a reachable place. The suturing on the eyelid was taken off next morning.

2.3 Dendritic Changes in the Superior Colliculus

2.3.1 Animal Preparation

2.3.1.1 Animals

42 animals were used for studying the dendritic changes in the superior colliculus. All the glaucoma rats and age-matched controls were sacrificed at 0 (n=5 rats), 4 (n=10 rats), 8 (n=7 rats), 16 (n=10 rats) and 32 (n=10 rats) weeks after ocular hypertension (OHT) (Table 2.1).

In this study, we used different animals as controls rather than using the opposite half of brain. This is because although most retinal axons project contralaterally to the SC in rodents, there are still 5-10% of RGCs which send projection fibres ipsilaterally to the visual targets in the brain (Kondo et al., 1993). When the IOP was elevated in the left eye, there might be effects of OHT on both right and left halves of the brain. Therefore, we used different animals as controls in the study of dendritic changes in the SC.

Superior Colliculus study			
Group	OHT (week)	Age (week)	Number of Rats
0 CTL	N/A	7-8	5
4 OHT	4	11-12	5
4 CTL	N/A	11-12	5
8 OHT	8	15-16	4
8 CTL	N/A	15-16	3
16 OHT	16	22-24	5
16 CTL	N/A	22-24	5
32 OHT	32	39-40	5
32 CTL	N/A	39-40	5

Table 2.1: Animals used for studying dendritic changes in the superior colliculus.

The 0 week group is the baseline group. Animals in this group were sacrificed at the age of 7-8 weeks when the glaucoma surgery was usually performed for the OHT groups. OHT: Ocular Hypertension; CTL: Control animals.

2.3.1.2 Animal Sacrifice and Removal of Brains

The rats were sacrificed by carbon dioxide (CO₂) asphyxiation (Vet Tech Solutions LTD, UK). CO₂ has a direct narcotic effect therefore the exposure to a rising concentration of CO₂ results in unconsciousness in the animals. This is a widely accepted method of euthanasia for rodents.

10-15 minutes after the sacrifice, the animals were decapitated using a guillotine (Harvard Apparatus LTD, Kent, UK), and the whole procedure was performed inside a fume cupboard (Morgan and Grundy Ltd., Manchester, UK). The

animal was positioned so that its neck was placed under the raised blade, and the lever was pushed down firmly to decapitate behind the ears. The skin of the head was cut along the midline of the skull with scissors. The skull was then carefully broken off piece-by-piece using rongeurs until the dorsal surface of the brain was exposed. The whole brain was then lifted and taken out gently and fixed into 4% paraformaldehyde (PFA) immediately (Sigma-Aldrich, St. Louis, MO, USA).

2.3.2 Preparation of Brain Slices

The cerebellum, brainstem and a small amount of the frontal cortex were removed and the brain was cut into halves at the midline. As the intraocular pressure was induced in the left eye, the contralateral brain section was used for sectioning. The medial aspect of right brain half was then glued to the cutting stage of a Vibratome (Series 1000, Agar Scientific LTD., Essex, UK). The speed of the blade was set at 2 and the section blade angle was adjusted as 15~20°. The brain block was cut into 400µm thick parasagittal slices and the slices containing superior colliculus were picked for the subsequent staining (Fig. 2.1). Some of the brain blocks and slices used in this study were provided by Dr Anne Georgiou.

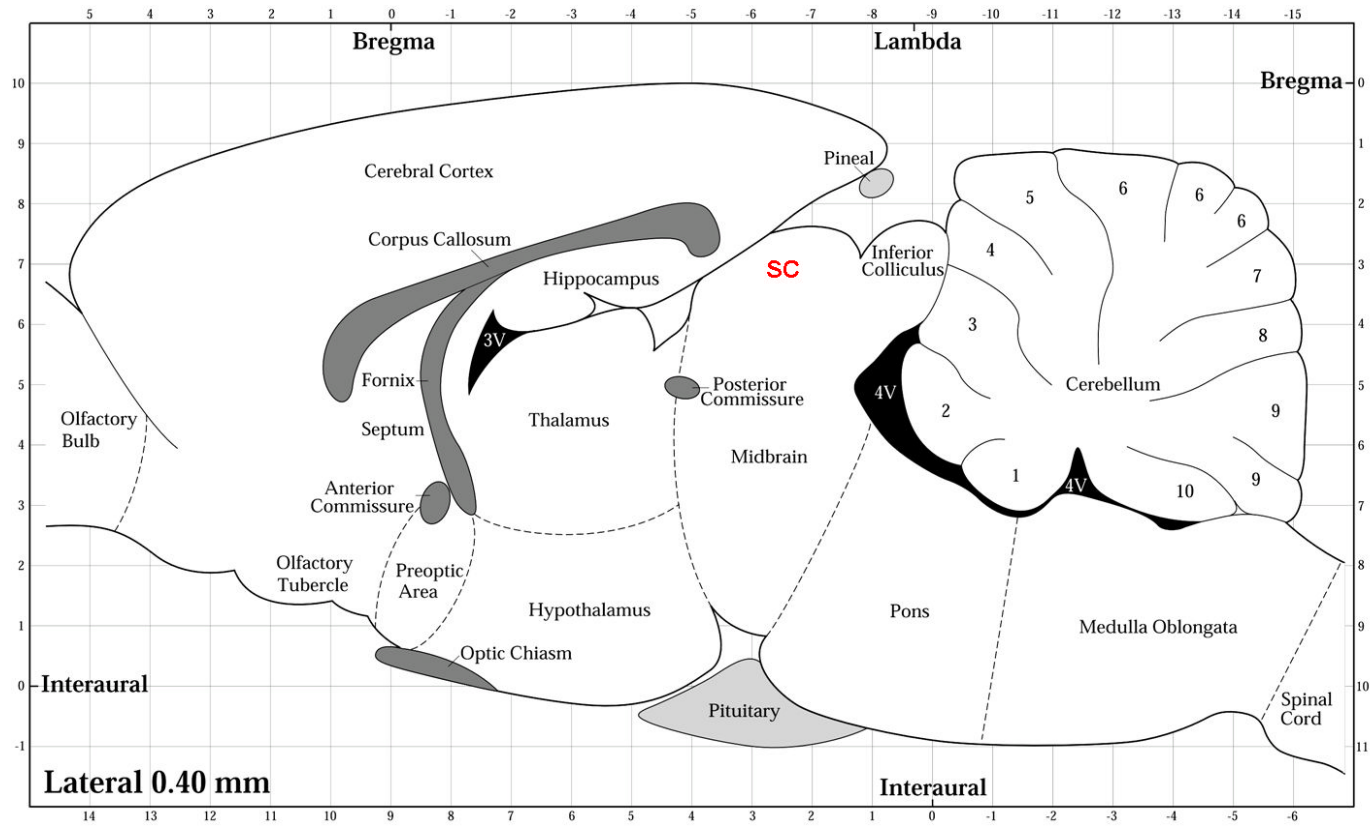


Figure 2.1: Sagittal view of a rat brain slice containing superior colliculus (SC) (Paxinos and Watson, 1998).

2.3.3 DiI Labelling Method

2.3.3.1 DiI

The fluorescent dye 1,1',di-octadecyl-3,3,3'3'-tetramethylindocarbocyanine perchlorate DiI was introduced as a neuronal tracer in fixed tissue by Godement et al. (Godement et al., 1987). This carboncyanine dye has a long carbon chain which is lipid soluble and thus can be incorporated into plasma membrane. It absorbs at 546 nm and emits at 563 nm in maximum, fluorescing bright red (Sims et al., 1974) (Fig. 2.2).

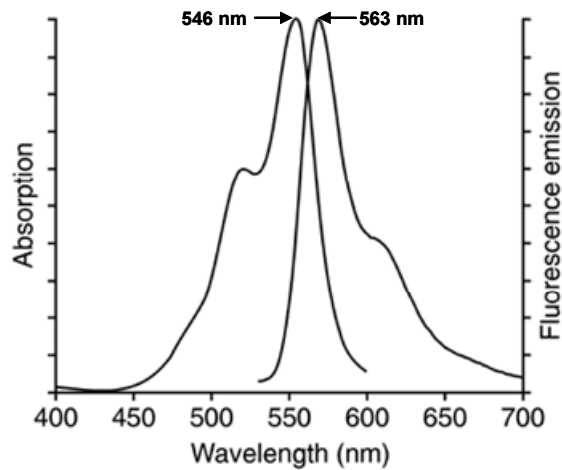


Figure 2.2: Absorption and fluorescence emission spectra of DiI bound to phospholipid bilayer membranes (Invitrogen Life Science).

DiI has been widely used for retrograde and anterograde labelling of the structures of cells and tracing projections (Honig and Hume, 1986; Elberger and Honig, 1990; Hofmann and Bleckmann, 1999). The fluorescent dye is transported in the membranes by lateral diffusion and labels the neuronal connections of structures which are difficult to access *in vivo*. In addition to staining the live tissue, DiI can also label fixed specimens as it labels cells by diffusion in the membrane rather than by axonal transport (Godement et al., 1987; Elberger and Honig, 1990). Since the advantages of DiI make it a convenient and effective cell marker, this fluorescent dye has been employed to label the structure of cells including dendritic arborizations and spine structures, extensively (Ragnarson et al., 1992; Hosokawa et al., 1995; Hofmann and Bleckmann, 1999; Kirov and Harris, 1999; Gan et al., 2000; Kim et al., 2007).

In our study, we applied DiI in the superior colliculus to label neurons and studied the dendritic changes in the superficial layer of the SC. The optimal concentration of DiI solution and staining method were investigated first.

2.3.3.2 Comparison of Different DiI Dilutions

In order to find out the optimal concentration of DiI solution, a series of Vybrant DiI dilutions (Invitrogen, UK) were applied to the fixed brain slices. DiI is highly hydrophobic, dissolving in the solvent dimethyl sulfoxide (DMSO) (Sigma Aldrich, UK). Different concentrations of DiI solution including 0.0001%, 0.001%, 0.01%, 0.1% (w/v) were tested and compared.

2.3.3.3 Staining Procedure

There are two major staining methods which have been applied on brain slices: Immersion labelling and Injection labelling. The effects of the two labelling methods were compared.

2.3.3.3.1 Immersion Labelling

Fresh brain specimens were used for immersion labelling. The rat brain was taken out of the skull without fixation and the sectioning was done immediately. Krebs' solution containing (mM) NaCl, 124; KCl, 2; KH₂PO₄, 1.25; MgSO₄, 1; CaCl₂, 2; NaHCO₃, 26 and glucose, 10 was made up freshly (BDH laboratory supplies, Poole, England). The brain slices were incubated in 2 ml of Krebs' solution containing 1 µl of DiI solution (50 µg of DiI / 50 µl of DMSO) for 10 min at 37°C in the laboratory incubator (Boro Labs Ltd., UK). When added to Krebs' solution, the dye solution forms a sparse suspension of droplets that settle on the surface of the tissue, labelling the cells beneath.

2.3.3.3.2 Injection Labelling

Carbocyanine dye DiI (0.1% w/v) was applied by gently and precisely stabbing the slices twice using a glass micropipette with a sharp tip. The fine micropipette was made using a Micropipette puller (Sutter Instrument Company, USA). The dye was injected at rostral and middle sites in the superficial layer of superior colliculus (Fig. 2.3). The slices were then incubated in phosphate buffer

solution (PBS) (Oxoid Ltd., Hampshire, England) at 37°C for seven days to allow the DiI to diffuse fully along the neuronal membranes.

2.3.4 Mounting

After incubating the specimen to allow the dye to fully diffuse, the slices were washed in PBS three times using a Gyro-Rocker shaker (Stuart Scientific, UK). The slices were then mounted on SuperFrost slides (VWR international, Leuven, Belgium) using the glycerol-based mounting medium Citifluor (Citifluor, Kent, UK). Citifluor was used to prevent possible dehydration-induced shrinkage of dendritic structures and dye bleaching. The slides were then labelled, wrapped in aluminium foil to avoid light and stored in the fridge at 4°C.

2.3.5 Blind Analysis

The blind analysis was performed in order to prevent outcomes from being influenced during the imaging and morphological measurement. All the slides were re-labelled by our laboratory technician before confocal imaging and morphological analysis performed. Measurements were made by the same person (Meng Liu) throughout the analysis to ensure reproducibility of measurements.

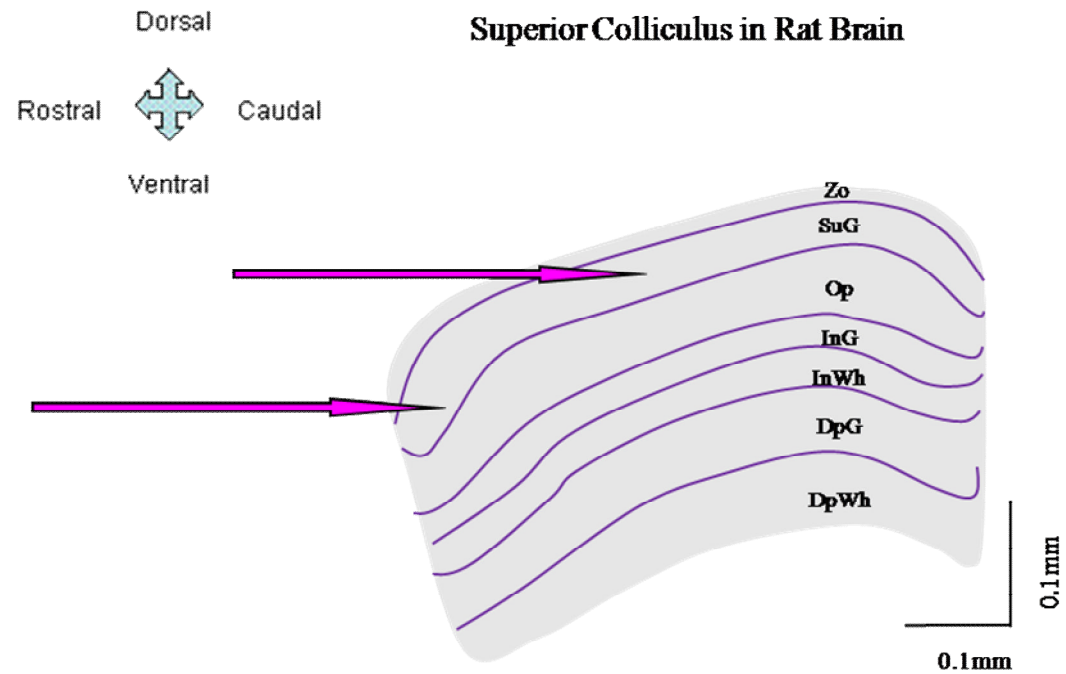


Figure 2.3: Diagram of DiI injection method.

The diagram shows layers of the superior colliculus from a sagittal brain slice. DiI was injected at the superficial layer of the SC by poking the brain slice twice at rostral and middle sites respectively. Zo: zonal layer; SuG: superficial gray layer; Op: optic layer; InG: intermediate gray layer; InWh: intermediate white layer; DpG: deep gray layer; DpWh: deep white layer (Paxinos and Watson, 1998).

2.3.6 Laser Confocal Microscopic Imaging

All images were taken using a Zeiss 510 confocal laser scanning microscope (CLSM 510 META, Zeiss, Gottingen, Germany) equipped with LSM image browser.

The microscope was focused on the superficial layer of the SC. A 543nm Helium/Neon laser was used to visualize fluorescence emitted by the DiI. The 1024×1024 pixel for frame size was used without zooming. Dendritic segments that were well separated from neighbouring neural processes were randomly sampled and imaged. Fifteen neurons were imaged for each type of neuron of each group. The image of a single neuron was taken using 16 x or 40 x oil-immersion lenses. The serial stack images were collected and projected to reconstruct three dimensional images for analysis.

2.3.7 Morphological Analysis of Cells in the Superior Colliculus

2.3.7.1 Groups of Cells in the SC

42 animals were divided into nine groups: (1) 0 week group which is the baseline group, (2) 4 weeks OHT, (3) 4 weeks CTL, (4) 8 weeks OHT, (5) 8 weeks CTL and (6) 16 weeks OHT, (7) 16 weeks CTL, (8) 32 weeks OHT and (9) 32 weeks CTL. There were 675 neurons (n=75 neurons per group, as this is the maximum amount of neurons that could be observed for all types of cells) were analyzed in the study of dendritic changes in the superior colliculus (Table 2.2).

Brain				Neuron
Group	Fixation	Slicing	Number of neurons	
1	Baseline CTL	4% PFA	P.S. 400 μ m	75
2	4 weeks OHT	4% PFA	P.S. 400 μ m	75
3	4 weeks CTL	4% PFA	P.S. 400 μ m	75
4	8 weeks OHT	4% PFA	P.S. 400 μ m	75
5	8 weeks CTL	4% PFA	P.S. 400 μ m	75
6	16 weeks OHT	4% PFA	P.S. 400 μ m	75
7	16 weeks CTL	4% PFA	P.S. 400 μ m	75
8	32 weeks OHT	4% PFA	P.S. 400 μ m	75
9	32 weeks CTL	4% PFA	P.S. 400 μ m	75

Table 2.2: Summary of brain slices and neurons analyzed in the study of dendritic changes in the superior colliculus.

PFA: paraformaldehyde; P.S. : parasagittal; CTL: control; OHT: ocular hypertension.

2.3.7.2 Classification of Cells in the SC

The neurons were further divided into five types as horizontal cell (H); piriform cell (P); narrow field vertical cell (V); wide field vertical cell (W) and stellate cell (S). The classification of cells was based on the shape of their soma and the orientation of their dendrites (Langer and Lund, 1974). The diagrams of these five types of neurons have been shown in Figure 1.9. In general, the horizontal cells have fusiform cell bodies, and dendrites that are tangential to or parallel with the surface of the colliculus. The piriform cells have ovoid or cup-shaped cell bodies and

2-5 primary dendrites. The primary dendrite are either ascending or descending. The ascending dendrites branch more frequently as they approach the surface. The narrow field vertical cells have fusiform cell bodies, and narrow, vertically orientated dendritic fields. The wide field vertical cells have multipolar cell bodies, and vertically or obliquely orientated dendrites. Both cell bodies and dendritic fields of the wide field vertical cells are larger compared to that of the narrow filed vertical cells. Stellate cells have multipolar cells bodies and their dendrites arising from the cell body symmetrically.

2.3.7.3 ImageJ software

In this study, the morphological characteristics of neurons were analyzed using ImageJ v3.91 software ([Http://rsb.info.nih.gov/ij](http://rsb.info.nih.gov/ij)). ImageJ is a java-based open-source image processing program developed at the National Institutes of Health, which is an essential tool for image processing and analysis (Collins, 2007).

Neuron J is one plugin in the ImageJ program, which is designed to facilitate the tracing and quantification of elongated structures, in particular neurites in fluorescence microscopy images (Abramoff et al., 2004; Meijering et al., 2004). After trialling several other software, we found the Image J program is a very useful and convenient tool especially for tracing and quantifying dendrites. Therefore, in this study, we chose to use ImageJ program with Neuron J plugin to analyze the dendritic parameters. The number of dendrites were counted and the mean dendritic length of dendrite were measured (Figure 2.4)

2.3.7.4 Procedures for Analyzing Dendritic Parameters

Although ImageJ can understand virtually any kind of image format, there are still a few restrictions that the content of the image must adhere to make the plugin to function properly. The first requirement is that the image must be an 8-bit grayscale image. Also the neurons must be in one solid colour in contrast to the rest part of the picture such as noise or background *etc.*. In order to meet these requirements, all the images were converted to 8-bit grayscale images using Image J. Then the brightness and contrast of the images were adjusted, and sometimes the thresholding was used in order to satisfy the second restriction. The correct scale information embedded in the image also needs to be set using Image J because the plugin will calculate and report the results based on this information. In the following the individual image was uploaded in the Neuron J program as it can only analyze one image at a time. Then using the ‘Add tracing’ tool, the single dendrite was traced automatically once the starting point was set, and the tracing can also be modified manually. The different types of neurites can be labelled in different colours and analyzed separately. After all dendrites of one neuron were traced, the tracings were saved and the measurements were performed and reported by Neuron J. In this study, we analyzed two dendritic parameters: the number of dendrites and the mean dendritic length of one neuron

2.3.8 Statistical Analysis

Statistical analysis was performed by SPSS 14.0 (Chicago, IL). One-way ANOVA was applied to compare the dendritic parameters in control groups and those in glaucoma groups at different ages. The difference in dendritic parameters between glaucoma animals and age-matched controls was also analyzed ($P < 0.05$ was considered to be significant).

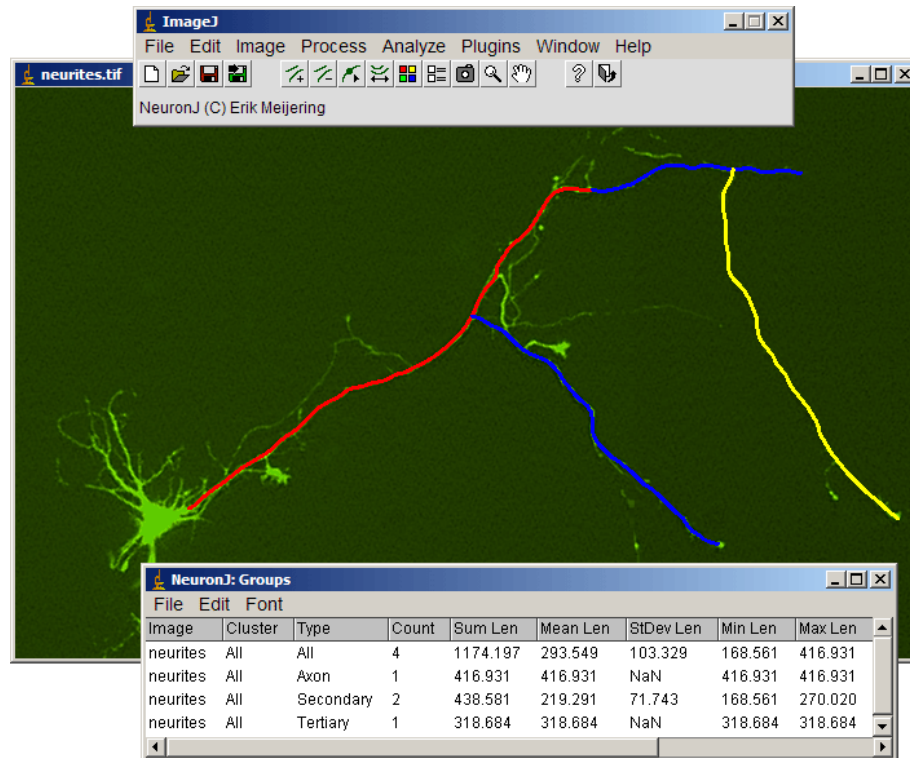


Figure 2.4: The sample image and tracings by NeuronJ in ImageJ software

Different types of neuritis are labelled in different colours and analyzed separately. The number of neurites is counted and the lengths of them are measured automatically (Meijering et al., 2004).

2.4 Dendritic Changes in the Lateral Geniculate Nucleus

2.4.1 Animal Preparation

There are 37 animals used for studying the dendritic changes in the dorsal lateral geniculate nucleus. All the glaucoma rats and age-matched controls were sacrificed at 4 (n=6 rats), 8 (n=7 rats), 16 (n=12 rats) and 32 (n=8 rats) weeks after ocular hypertension (OHT) (Table 2.3). We also have a 0 week control group (n=4 rats) used as baseline. The animals were sacrificed and the brains were removed as described previously.

In this study, there were two labelling methods used to stain neurons in the dLGN. One method is to inject the DiI crystals into the visual cortex *in vivo*, followed by sectioning the brains into parasagittal slices. The other method is to slice the brain blocks into pseudo parasagittal slices, followed by injecting the DiI solution into the brain slices *in vitro*.

The brain slices containing the lateral geniculate nucleus in this study were sectioned in a different way. Therefore, we can't use the same rat brains that have been used for the superior colliculus study.

I also used different animals as controls rather than using the opposite half of brain as explained before.

LGN			
Group	OHT (week)	Age (week)	Number of Rats
0 CTL	N/A	7-8	4
4 OHT	4	11-12	3
4 CTL	N/A	11-12	3
8 OHT	8	15-16	4
8 CTL	N/A	15-16	3
16 OHT	16	22-24	4
16 OHT-2	16	22-24	4
16 CTL	N/A	22-24	4
32 OHT	32	39-40	4
32 CTL	N/A	39-40	4

Table 2.3: Animals used for studying dendritic changes in the dorsal lateral geniculate nucleus.

The 0 week group is the baseline group. Animals in this group were sacrificed at the age of 7-8 weeks when the glaucoma surgery was usually performed for the OHT groups. OHT: Ocular Hypertension; CTL: Control animals.

2.4.2 Preparation of Brain Slices

The brains were sectioned in two ways to prepare parasagittal and pseudo-parasagittal slices.

2.4.2.1 Preparation of Parasagittal Slices

The preparations of parasagittal slices were performed after the DiI labeling. The animals had the DiI crystals injected into their visual cortex and were sacrificed at the certain age. The brains were removed and fixed in to 4% PFA for at least 24 hours. The fixed brain blocks were then cut into halves through the midline. The medial aspect of the right brain block was glued to the cutting stage of a Vibratome (Series 1000, Agar Scientific LTD., Essex, UK) and sliced into 400 μ m parasagittal slices. The slices containing the dLGN were chosen for the subsequent confocal imaging (Paxinos and Watson, 1998) (Fig. 2.5).

2.4.2.2 Preparation of Pseudo-Parasagittal Slices

The preparations of pseudo-parasagittal slices were performed before the DiI labelling. After the animals were sacrificed, the brains were removed and fixed in 4% PFA before sectioning. Firstly, two initial cuts were performed to produce the blocks of brain tissue (Paxinos and Watson, 1998; Turner and Salt, 1998). The blade was positioned at 3 ~ 5 degree to the sagittal plane either side of the mid-line, and angled outwards by 10 ~ 25 degree in the medio-lateral plane (Fig. 2.6). The right brain block containing dLGN was then ready for the subsequent slice preparation. This cutting method was designed to maintain the integrity of the sensory and cortical inputs (Bourassa and Deschenes, 1995). The medial aspect of the right brain half was glued to the cutting stage of a Vibratome (Series 1000, Agar Scientific LTD., Essex, UK) and sectioned into 400 μ m Pseudo-sagittal slices. The slices containing dLGN were chosen for subsequent staining using DiI solution.

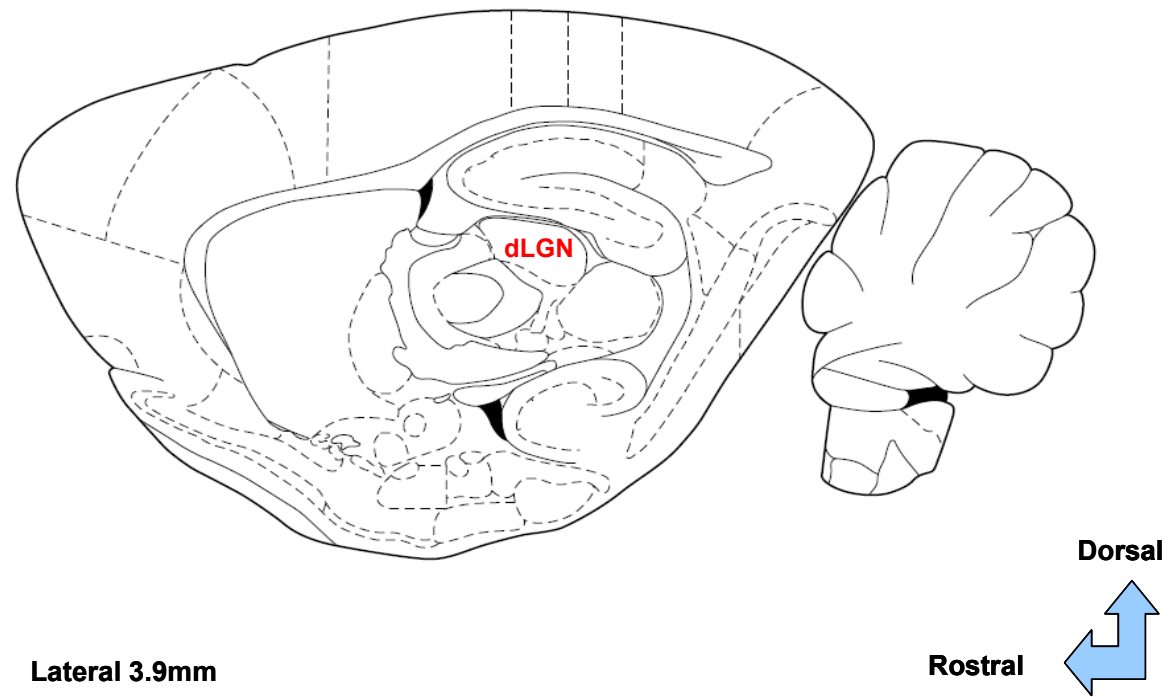


Figure 2.5: The sagittal view of the brain slice and the location of dLGN.

The diagram shows the sagittal view of a brain slice containing the dorsal lateral geniculate nucleus (labelled in red). The slice is located about 3.9mm lateral to the midline of the brain. dLGN: dorsal lateral geniculate nucleus.

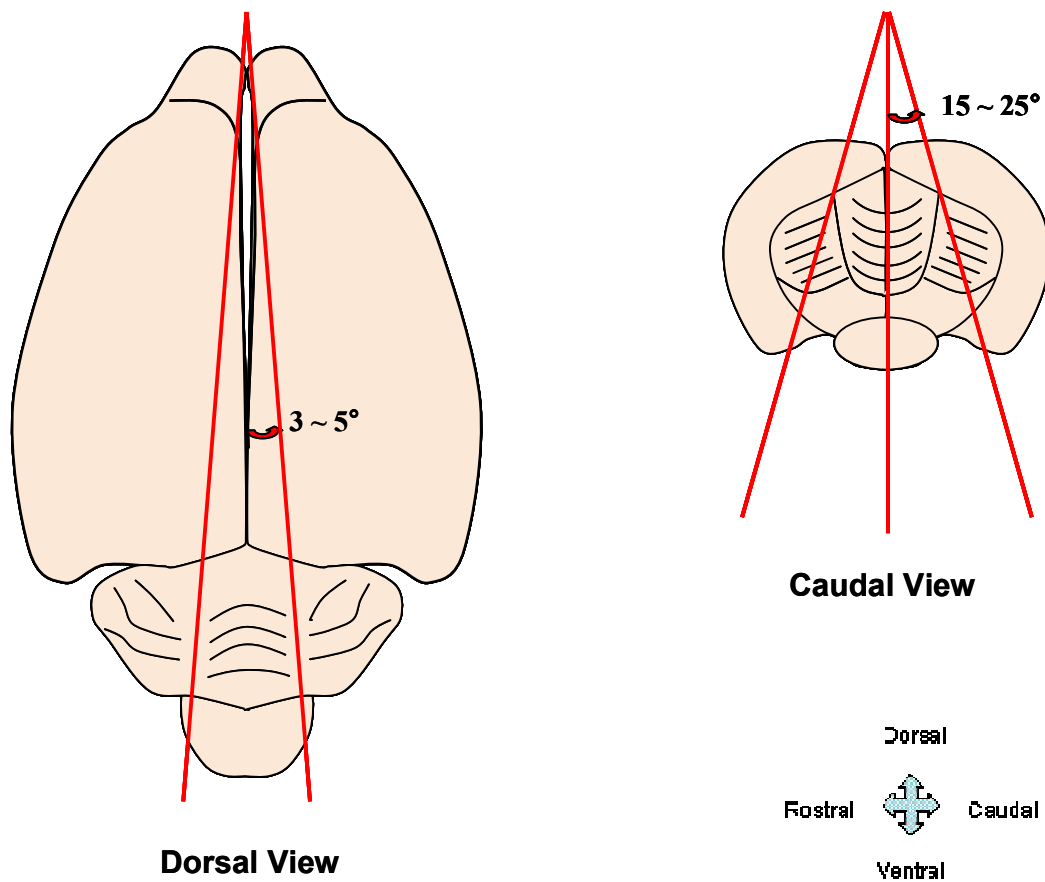


Figure 2.6: The preparation of Pseudo-sagittal slices containing the dLGN.

The figures show the dorsal and caudal view of the brain tissue and illustrate the position and angle of the two initial cuts used to produce the blocks for subsequent slice preparation (Turner and Salt, 1998).

2.4.3 DiI Labelling Method

2.4.3.1 Staining Procedure

In our study, we applied DiI in the dLGN to label neurons and studied the dendritic changes. The staining was achieved by two methods: *in vitro* injection labelling (Method I) and *in vivo* retrograde labelling of the LGN (Method II). The results of these two labelling methods were compared.

2.4.3.1.1 Injection Labelling

The injection labelling was performed on fixed brain slices *in vitro*. The brains were immersed in 4% PFA for fixation after being removed from the sacrificed animals. As the intraocular pressure was induced in the left eye, the contralateral brain section was used for sectioning. The brain block was cut into Pseudo-sagittal slices (400µm) for injection labelling. Carbocyanine dye DiI (0.1%) was applied to the optic radiation using a glass micropipette to retrogradely label the neurons in the dorsal lateral geniculate nucleus (dLGN) (Fig. 2.7). Slices were then incubated in PBS at 37 °C for 7 days.

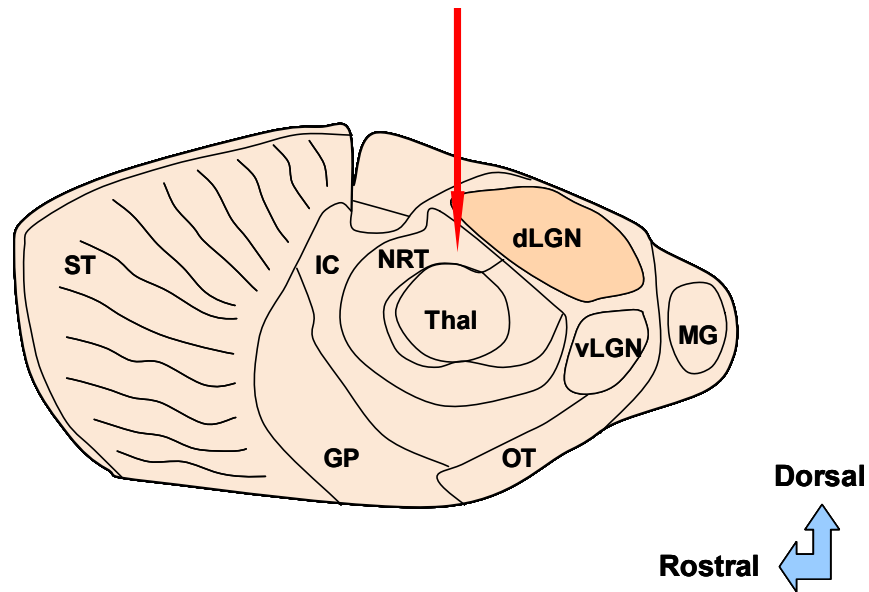


Figure 2.7: The injection site of fluorescent dye DiI for labelling dLGN neurons of rat mid-brain slices (Turner and Salt, 1998).

The diagram shows the injection site of the DiI in a pseudo-parasagittal slice. The DiI solution was injected into the optic radiation which is next to the dLGN using a glass micropipette (shown in red).

dLGN, dorsal lateral geniculate nucleus; GP, globus pallidus; IC, internal capsule; MG, medial geniculate nucleus; NRT, nucleus reticularis thalami; OT, optic tract; ST, striatum; Thal, main field of the thalamus; vLGN, ventral lateral geniculate nucleus.

2.4.3.1.2 Retrograde Labelling of LGN

A group of glaucoma rats aged at 16 weeks was used for retrograde labelling of LGN cells. Neurons in the dLGN were stained by injecting the fluorescent dye into the visual cortex *in vivo*. The visual cortex labelling was performed to be compared with the injection labelling in order to confirm the results.

Animals were anesthetized by Isoflurane inhalation (Merial Animal Health Ltd, Harlow, Essex, UK) followed by intraperitoneal injections of ketamine solution containing Ketaset (37.5%, Fort Dodge Animal Health Ltd., Southampton, UK), Domitor (25%, Pfizer Animal Health, Pfizer limited, Kent, UK) and Sterile water (37.5%, Pfizer Animal Health, Exton, PA) at 0.2 ml / 100 g body weight for deep anesthetization. The local anaesthetic agent, Linol containing (w/v) Lidocaine Hydrochloride 2%; Adrenaline 0.001%; Chlorocresol 0.1%; and Sodium Metabisulphite 0.1%, (Arnolds Veterinary Products Ltd, UK) was injected in the animals' scalp at a dose of 0.05ml before making an incision in their skull.

The anesthetized animal was placed in a stereotaxic apparatus during the surgery (Kopf 957, David Kopf Instruments, California, USA) (Fig 2.8). Generally, the rat was mounted onto the stereotaxic apparatus with a heating mat placed underneath the rat to maintain body temperature (Paxinos and Watson, 1998; Athos and Storm, 2001; Geiger et al., 2008).

When performing the surgery, firstly the head skin and muscles were cut and spread apart carefully to expose the dorsal surface of the skull. In the following, two skull holes were made (1 mm from bregma suture and 2.5 mm from the interaural

line) on each brain half using a drill (Fine Science Tools Inc., Heidelberg, Germany). The small area of visual cortex which is underneath the skull was exposed. The crystals of DiI (DiI crystalline, Invitrogen, USA) were then placed in either side of the visual cortex gently using forceps (Fig. 2.9). The holes were then filled with absorbable gelatine film, gelfoam (Gelfilm, The Upjohn Company, Michigan, USA). The skin wounds were sutured using Ethicon absorbable / Coated VICRYL suture (Johnson & Johnson Intl, Belgium) immediately.

Rimadyl (50 mg/ml, Animal Health, Pfizer Ltd., Kent, UK) was administered as pain relief by subcutaneous injection at 0.1mg / 100g body weight. The antibiotic Baytril solution (2.5%, Bayer Healthcare, UK) was applied orally in the drinking water at a dose of 0.4 ml / 100ml for 5 days after surgery. The animals were woken up immediately after the surgery. The recovery drug antipamezole consisting of 20% Antisedan, 80% sterile water (Animal Health, Pfizer Ltd., Kent, UK) was administered at a dose of 0.1mg/ 100g body weight by intraperitoneal injection. The animals were then placed in the recovery room with a heat mat underneath the cage. Softened food pellets and drinking water were provided as well.

The animals were kept alive for four weeks to leave the dye to fully diffuse before being sacrificed. The brains were removed and fixed in 4% PFA for fixation. The sagittal brain slices (400µm, approximately 3.9mm lateral to the midline) were prepared using a Vibratome as described before.

2.4.4 Mounting, Blind Analysis and Confocal Imaging

The brain slices were mounted on the SuperFrost slides (VWR international, Leuven, Belgium) using the glycerol-based mounting medium Citifluor (Citifluor, Kent, UK) as described previously. The blind analysis was also performed before confocal imaging and morphological measurements.

All images were taken using a Zeiss 510 confocal laser scanning microscope (CLSM 510 META, Zeiss, Gottingen, Germany) equipped with LSM software. The microscope was focused on the dorsal lateral geniculate nucleus. The image of single neuron was taken under 16 x oil-immersion lenses as described previously. The serial stack images were collected and projected to reconstruct three dimensional images for analysis.

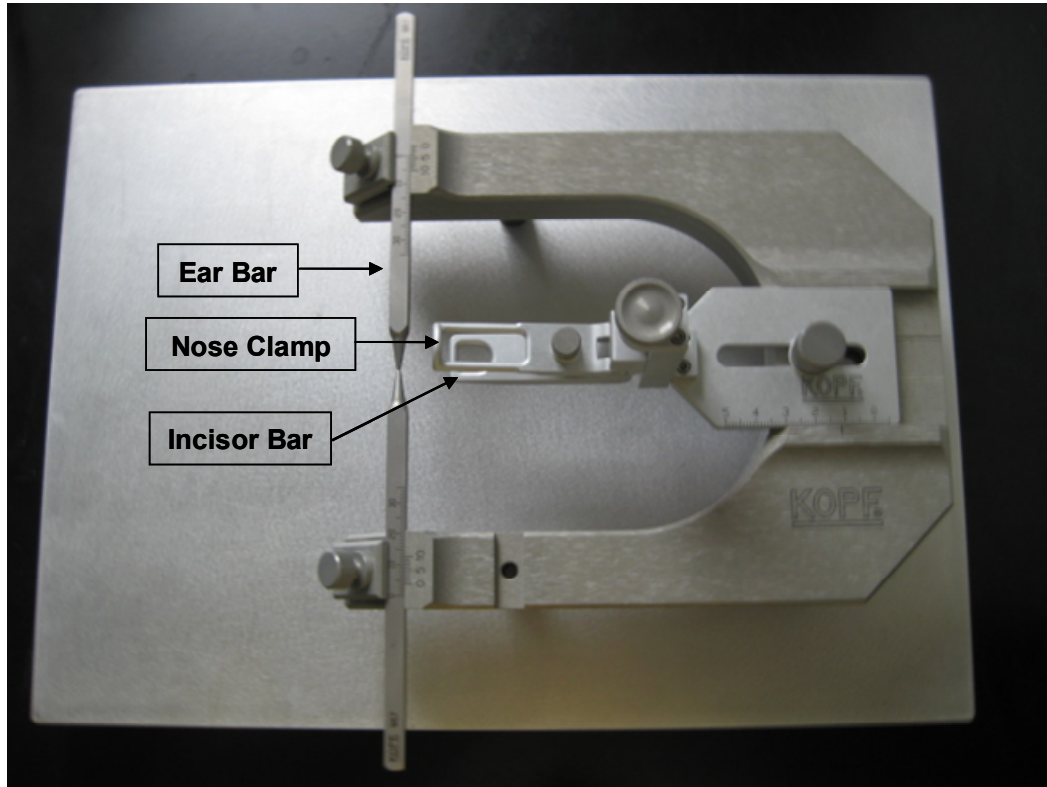


Figure 2.8: The Kopf Stereotaxic Apparatus (Kopf 957, David Kopf Instruments, California, USA).

The stereotaxic apparatus is a versatile and easy-to-use instrument that facilitates proper alignment of small animals (Kopf 957, David Kopf Instruments, California, USA). The anesthetized rats are placed on this stereotaxic apparatus. The ear bars were mounted into the external auditory meatus carefully and tightened. The incisor bar was inserted into the mouth and adjusted to make the lambda and bregma level. The nose clamp was positioned correctly and tightened firmly (Paxinos and Watson, 1998; Athos and Storm, 2001; Geiger et al., 2008)

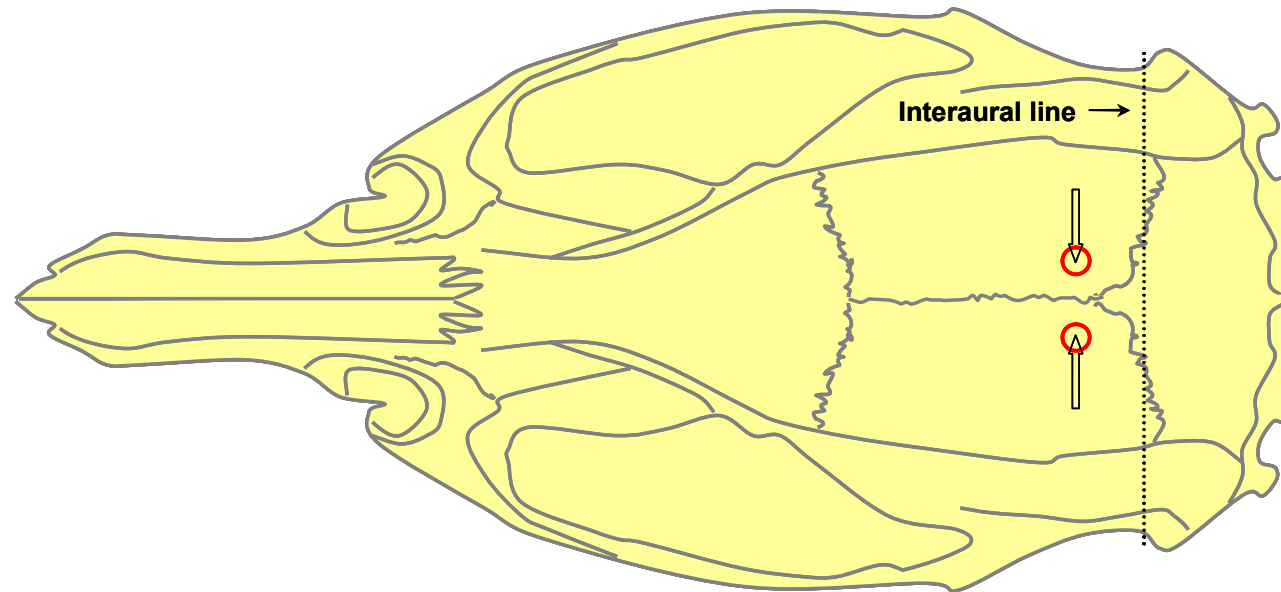


Figure 2.9: The in vivo retrograde labeling method.

The diagram shows the injection sites of DiI crystals. On the dorsal surface of the skull, two holes were drilled (approximately 1 mm from midline and 2.5 mm from the interaural line) on each brain half. Crystals of DiI were placed in either side of the visual cortex to label LGN neurons.

2.4.5 Morphological Analysis of Cells in the Lateral Geniculate

Nucleus

2.4.5.1 Groups of Cells in the LGN

There were in total 37 animals analyzed, which were divided into ten groups: (1) 0 weeks OHT, (2) 4 weeks OHT, (3) 4 weeks CTL, (4) 8 weeks OHT, (5) 8 weeks CTL and (6) 16 weeks OHT, (7) 16 weeks OHT – 2, (8) 16 weeks CTL, (9) 32 weeks OHT and (10) 32 weeks CTL. There were 300 neurons (n=30 neurons for each group, as this is the maximum amount of cells that could be observed) which were analyzed in the study of dendritic changes in the dorsal lateral geniculate nucleus (n=30 per group) (Table 2.4).

2.4.5.2 Classification of Cells in the LGN

The neurons were further classified into two types as relay neuron type I (LG1) and relay neuron type II (LG2) according to their soma size and their dendritic characteristics (Kriebel, 1975) (Fig. 1.10). The type I neurons have multipolar perikarya with mean diameters of 25 μm , giving off four to eight primary dendrites. The type II neurons have smaller soma (mean diameter of 20 μm), with dendrites parallel to the optic fibres but less numerous and shorter compared to type 1 cells. However, primary dendrites of type 2 cells extend further than those of type 1, prior to branching into secondary dendrites. In this study, we did not analyze the type 3 cells that were described in Kriebel's study, due to this type of cell not being

observed frequently. The dendritic parameters of each type of neuron were analyzed respectively.

Brain				Neuron
Group	Fixation	Slicing	Number of neurons	
1	Baseline CTL	4% PFA <i>P</i> -P.S. 400µm	30	
2	4 weeks OHT	4% PFA <i>P</i> -P.S. 400µm	30	
3	4 weeks CTL	4% PFA <i>P</i> -P.S. 400µm	30	
4	8 weeks OHT	4% PFA <i>P</i> -P.S. 400µm	30	
5	8 weeks CTL	4% PFA <i>P</i> -P.S. 400µm	30	
6	16 weeks OHT	4% PFA <i>P</i> -P.S. 400µm	30	
7	16 weeks OHT-2	4% PFA P.S. 400µm	30	
8	16 weeks CTL	4% PFA <i>P</i> -P.S. 400µm	30	
9	32 weeks OHT	4% PFA <i>P</i> -P.S. 400µm	30	
10	32 weeks CTL	4% PFA <i>P</i> -P.S. 400µm	30	

Table 2.4: Summary of brain slices and neurons analyzed in the study of dendritic changes in the dorsal lateral geniculate nucleus.

PFA: paraformaldehyde; P.S. : parasagittal; *P*-P.S. : Pseudo parasagittal; CTL: control; OHT: ocular hypertension; os: left eye.

2.4.5.3 Morphological Analysis

In this study, the morphological characteristics of neurons from 37 animals were analyzed using ImageJ v3.91 software (<http://rsb.info.nih.gov/ij>) as described before. The dendrites were counted and mean dendritic lengths were measured.

2.4.6 Statistical Analysis

Statistical analysis was performed by SPSS 14.0 (Chicago, IL). One-way ANOVA was applied to compare the dendritic parameters among control groups and those in glaucoma groups at different ages. The difference in dendritic parameters between glaucoma animals and age-matched controls was also analyzed. The results from two different labelling methods were also compared ($P < 0.05$ was considered to be significant).

2.5 Dendritic changes in the Retina

2.5.1 Animal Preparation

2.5.1.1 Animals

19 animals were used for studying the dendritic changes of retinal ganglion cells (RGC) in the retina. The animals were sacrificed at 1 (n=3 rats), 4 (n=3 rats), 8 (n=4 rats), 16 (n=3 rats) and 32 (n=3 rats) weeks after ocular hypertension (OHT). A baseline group (n=3 rats), termed as 0 week group, was included in this study as well. The ocular hypertension was induced in the left eye, and the right eye was used as control (Table 2.5).

In this study, the opposite eye rather than different animal was used as control due to the right eye not being affected by the IOP being elevated in the left eye.

2.5.1.2 Animal Sacrifice and Eye Enucleation

The rats were sacrificed by carbon dioxide (CO₂) asphyxiation (Vet Tech Solutions LTD, UK) as described before.

The eyes were enucleated immediately after the animals were sacrificed. The first incision was made in the conjunctiva by inserting fine scissors carefully. The eye ball was then detached from the eye socket by cutting along the conjunctiva using a fine scissor using a blunt dissection technique. The optic nerve was cut at least 5mm distal to the globe to completely enucleate the eye. The fat tissue and muscle was cut away if there was any left on the eye ball. The fresh eye ball with optic nerve was then kept in freshly made Krebs' solution containing (mM) NaCl,

124; KCl, 2; KH₂PO₄, 1.25; MgSO₄, 1; CaCl₂, 2; NaHCO₃, 26 and glucose, 10 (BDH laboratory supplies, Poole, England) to keep the cells alive.

Retina			
Group	OHT week	Age week	Number of Rats
Baseline/ 0 OHT	N/A	7-8	3
1 OHT os	1	8-9	3
1 CTL od	N/A	8-9	3
4 OHT os	4	11-12	3
4 CTL od	N/A	11-12	3
8 OHT os	8	15-16	4
8 CTL od	N/A	15-16	4
16 OHT os	16	22-24	3
16 CTL od	N/A	22-24	3
32 OHT os	32	39-40	3
32 CTL od	N/A	39-40	3

Table 2.5: Animals used for studying dendritic changes in the retinal ganglion cells.

The 0 week group is the baseline group. Animals in this group were sacrificed at the age of 7-8 weeks when the glaucoma surgery was usually performed for the OHT groups. OHT: Ocular Hypertension; CTL: Control animals; os: left eye; od: right eye.

2.5.1.3 Retina Dissection

The eyes were placed in a Petri dish filled with PBS (Oxoid Ltd., Hampshire, England) under a dissection microscope (Leica, Wetzlar, Germany) for retina dissection. During the procedure, the eye ball was held by fixing the part of the optic nerve on the posterior side of the eye using fine forceps (Titanium forceps straight 1 into 2 teeth, Altomed Ltd. Tyne/Wear, UK). A sharp scalpel blade was used to make a small incision at the equator of the eye. The anterior part of the eye was then removed by cutting along the equator with curved 3mm scissors (Vannas curved small, John Weiss International, Milton Keynes, UK). The remaining eye cup contains choroid, scleral and the retina. The retina was then floated out by placing the scissors in between the retina and the sclera gently, and finally detached by cutting the optic nerve head.

2.5.1.4 Retina Flat-mounting

The retina was placed into a new Petri dish filled with fresh PBS. Four incisions were made on the retina at 3, 6, 9 and 12 o'clock. The retina was then flat mounted like a four-leaf clover (Fig. 2.10).

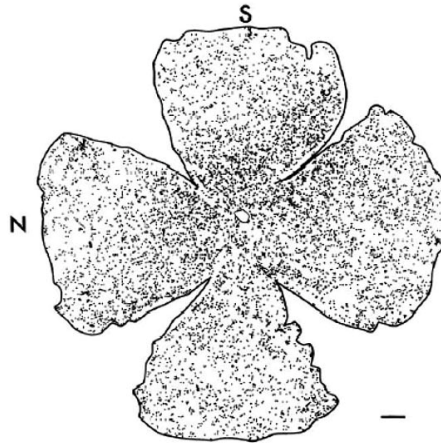


Figure 2.10: The flat-mount retina (Vidal-Sanz et al., 1987).

S: superior; N: nasal

2.5.1.5 Removal of Vitreous and Inner Limiting Membrane

The remaining vitreous and inner limiting membrane (ILM) needed to be completely removed from the retina for optimal staining. In order to make the transparent vitreous and ILM visible, a cyanine dye indocyanine green (ICG) (PULSION Medical Systems AG, Munich, Germany) was used. The retina was transferred into a Petri dish, one or two drops of ICG was placed on top of the tissue. The extra dye was washed off using PBS. The vitreous and ILM were peeled off gradually from peripheral edges to the centre of the retina gently using the fine forceps and paintbrush. The accumulated ILM with vitreous at the optic nerve head were then removed. In order to confirm whether the residual vitreous and ILM were removed completely, a wiper was used to gently dab the retinal surface to check if the surface was still sticky. After the removal of the vitreous and ILM, the retina was transferred onto a small round cover slip (Borosilicate glass, VWR International,

Leuven, Belgium). A drop of PBS was placed on the tissue to keep it moist before gene gun labelling.

2.5.2 DiI Labelling

In this study, the fluorescent dye DiI was applied to label retinal ganglion cells (RGCs) in the retina by biolistic staining.

Biolistic staining is a rapid labelling of cells in various neuronal tissues which has been used increasingly recently (Lo et al., 1994; Gan et al., 2000; Pearson et al., 2005; Becker et al., 2007). Neurons in living or fixed tissue can be labelled by means of particle-mediated ballistic delivery of lipophilic dyes with a gene gun. As the lipophilic dye DiI, DiO or DiD are commonly used in this method, it is also known as DiOListic staining.

2.5.2.1 Preparation of Shooting Bullets

2.5.2.1.1 Pre-coating Tubing with PVP

The tubing was pre-coated with polyvinyl pyrrolidone (PVP) (Sigma Aldrich, UK). The stock solution of PVP (100mg/ml) was dissolved in 100% Ethanol and kept at room temperature. The fresh PVP solution was made by diluting the stock solution as 1/1000 in 100% Ethanol before use.

A length of tubing which fits into the tubing rack (Bio-Rad Laboratories, Inc, UK) was cut using a razorblade. The tubing was then filled with dilute PVP solution

carefully. The PVP was aspirated from tubing slowly to minimize the number of droplets left behind in the tube. The tubing was then left to dry, and the excess PVP was purged with dry nitrogen gas on the tubing rack (Lo et al., 1994; Gan et al., 2000; Pearson et al., 2005; Becker et al., 2007).

2.5.2.1.2 Coating Particles with Dye

DiI (2mg) was placed in the bottom of a tube with a locking snap cap. Every 0.5mg of the dye was suspended in 400 μ l of Dichloromethane (Methylene Chloride, Sigma Diagnostics, UK) by vortexing. The tungsten particles (50mg) (Sigma Aldrich, UK) were then placed on a clean glass slide as a small pile, and four of these slides were prepared in total. The dissolved dye was added to the tungsten particles, and the mixture of them was spread rapidly across the surface of the glass slide to form a thin film. The particles were left to dry for several minutes until they turn grey. In the following, the particles were gently scraped from the slide one layer at a time using a clean razorblade. The fine powders collected in a weighing boat are then ready for being loaded onto the bullets (Lo et al., 1994; Gan et al., 2000; Pearson et al., 2005; Becker et al., 2007).

2.5.2.1.3 Loading the Bullets

One end of the pre-dried tubing was sealed with parafilm (VWR international, Leuven, Belgium). The other end of the tubing was connected with the end of a 5ml pipette tip acting as a funnel. The fine powders were poured into the tubing via the

pipette tip. The open end of the tubing was then sealed before shaking it to make the powder to stick evenly across the whole tubing. The excess powder was tipped out and the tubing was left to dry for 10-20 minutes.

The tubing was cut into appropriate lengths using the tube cutter (Bio-Rad Laboratories, Inc, UK). The bullets were then ready for use in the gene gun. These bullets were stored in a covered or tinted vial with a desiccant pellet at 4 °C (Lo et al., 1994; Gan et al., 2000; Pearson et al., 2005; Becker et al., 2007).

2.5.2.2 Gene Gun Labelling

A Helios gene gun was used for shooting the retinae (Bio-Rad Laboratories, Inc, UK) (Fig. 2.11). It is a convenient, hand-held device that provides rapid and direct transfection into targets *in vivo*.

The whole mount retinae are mounted onto pieces of gridded Millipore filter paper before shooting. The retina/filter paper was then placed on top of a vial cap and the excess medium was blotted off. A tissue culture insert (Falcon) was used as a filter to break up any clumps of particles. The gene gun was positioned over the tissue vertically as close to the culture insert as possible, with the gas pressure adjusted at or above 40 psi. The retina was shot twice with one bullet (Lo et al., 1994; Gan et al., 2000; Pearson et al., 2005; Becker et al., 2007) (Fig. 2.12).

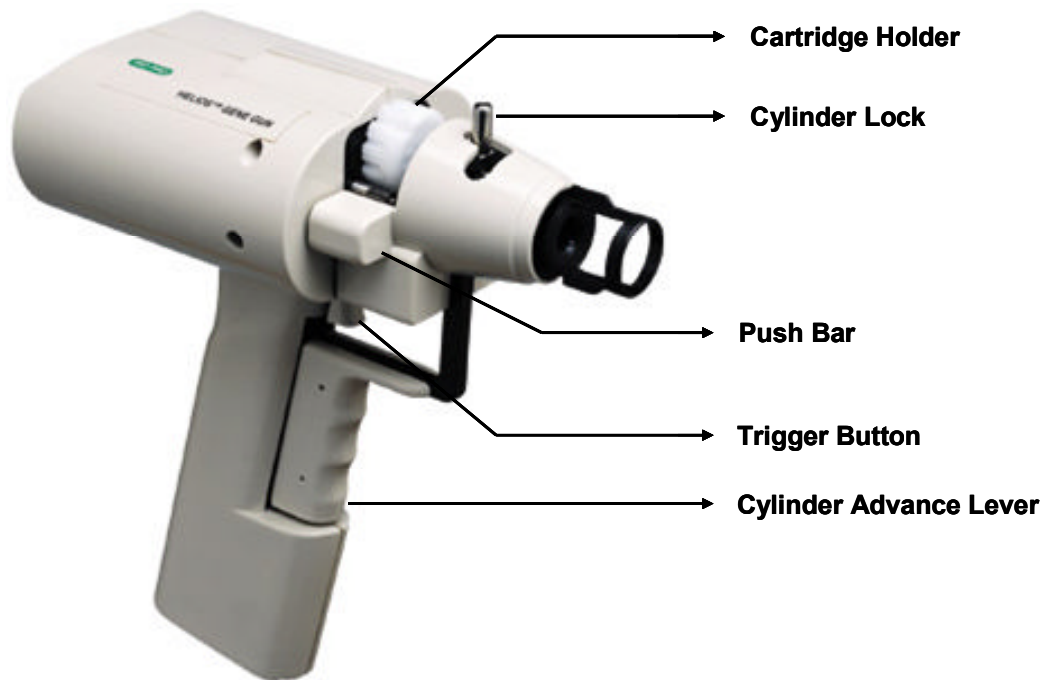


Figure 2.11: The Helios Gene Gun (Bio-Rad Laboratories, Inc, UK).

The Helios gene gun is a convenient handheld device that provides rapid and direct transfection into a range of targets *in vivo*. It uses an adjustable low-pressure helium pulse to drive dye coated particles from the inner wall of a small plastic cartridge directly into target cells (Rio-Rad Laboratories, Inc, UK).

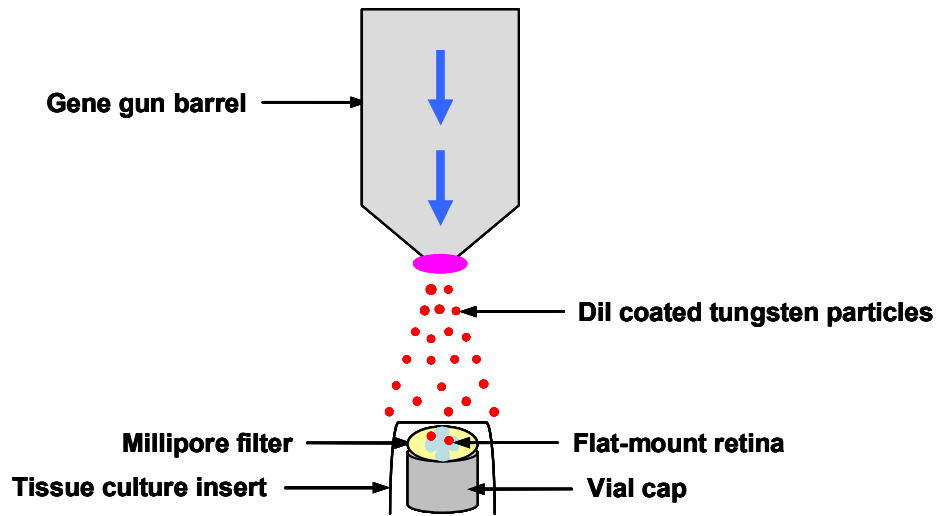


Figure 2.12: Electroporation set up.

This diagram illustrates the set up of electroporation performed using the Helio gene gun (Bio-Rad Laboratories, Inc, UK) (Becker et al., 2007). The flat-mount retina is mounted onto a piece of Millipore filter paper before shooting. The retina/filter paper was then placed on top of a vial cap and the excess medium was blotted off. A tissue culture insert (Falcon) was used as a filter to break up any clumps of particles. The DiI coated tungsten particles were shot into the retina using the gene gun.

2.5.3 Mounting, Blind analysis and Confocal Imaging

The stained retina was kept in PBS for 20 minutes before being put into 4% PFA for fixation. The tissue was washed using PBS three times before being mounted on the SuperFrost slides (VWR international, Leuven, Belgium) using the glycerol-based mounting medium Citifluor (Citifluor, Kent, UK). The slides were

then labelled, wrapped in the kitchen foil to avoid light and stored in the fridge at 4°C.

Blind analysis was also performed as described previously to prevent outcomes from being influenced during the imaging and morphological measurement.

All images were taken using Zeiss 510 confocal laser scanning microscope (CLSM 510 META, Zeiss, Gottingen, Germany) equipped with LSM software. The microscope was focused on the central retina. The image of a single retinal ganglion cell was taken under 16 x oil-immersion lenses as described previously. The serial stack images were collected and projected to reconstruct three dimensional images for analysis.

2.5.4 Morphological Analysis

2.5.4.1 Groups of Retinal Ganglion Cells

In this study, 35 retinae were divided into eleven groups: (1) 0 week CTL, (2) 1 week CTL, (3) 1 week OHT, (4) 4 weeks CTL, (5) 4 weeks OHT, (6) 8 weeks CTL, (7) 8 weeks OHT, (8) 16 weeks CTL, (9) 16 weeks OHT, (10) 32 weeks CTL and (11) 32 weeks OHT. There were 495 neurons (n=45 neurons per group, as this was the maximum amount of cells could that be observed) were analyzed in the study of dendritic changes of retinal ganglion cells (Table 2.6).

Retina		Neruo		
Group	Retina Preparation	Fixation	Number of neurons	
1	Baseline CTL (od)	Flat mount	4% PFA	45
2	1 week OHT (os)	Flat mount	4% PFA	45
3	1 week CTL (od)	Flat mount	4% PFA	45
4	4 weeks OHT (os)	Flat mount	4% PFA	45
5	4 weeks CTL (od)	Flat mount	4% PFA	45
6	8 weeks OHT (os)	Flat mount	4% PFA	45
7	8 weeks CTL (od)	Flat mount	4% PFA	45
8	16 weeks OHT (os)	Flat mount	4% PFA	45
9	16 weeks CTL (od)	Flat mount	4% PFA	45
10	32 weeks OHT (os)	Flat mount	4% PFA	45
11	32 weeks CTL (od)	Flat mount	4% PFA	45

Table 2.6: Summary of retinae and neurons analyzed in the study of dendritic changes in the retinal ganglion cells.

PFA: paraformaldehyde; CTL: control; OHT: ocular hypertension; os: left eye; od: right eye.

2.5.4.2 Classification of Retinal Ganglion Cells

All the retinal ganglion cells were further classified into three types as retinal ganglion cell type I (RI) , type II (RII) and type III (RIII) based on the sizes of their cell bodies and dendritic fields (Perry, 1979). Type I cells have a large soma and a large dendritic field. Type II cells have a small soma and a small dendritic field.

Type III cells have small-to-medium soma, but a large dendritic field. The dendritic changes were analyzed for each type of cell respectively.

2.5.5 Statistical Analysis

Statistical analysis was performed using SPSS 14.0 (Chicago, IL). One-way ANOVA was applied to compare the dendritic parameters among control groups and glaucoma groups at different ages. The dendritic parameters from glaucoma animals and age-matched controls were also compared ($p < 0.05$ was considered to be significant)

Chapter 3: Results

3.1 IOP Measurements

In this study, a well-established rat model of chronic glaucoma is used (Morrison et al., 1997; Cordeiro et al., 2004; Guo et al., 2005a; Guo et al., 2005b; Guo et al., 2006; Guo et al., 2007; Guo and Cordeiro, 2008; Cordeiro et al., 2010; Guo et al., 2010). Ocular hypertension was induced in the left eye of each rat by injection of hypertonic saline solutions into the episcleral vein as previously described. The IOP profiles for both eyes of the rats are shown in Fig. 3.1. The error bar represents the standard deviation (SD) of the mean.

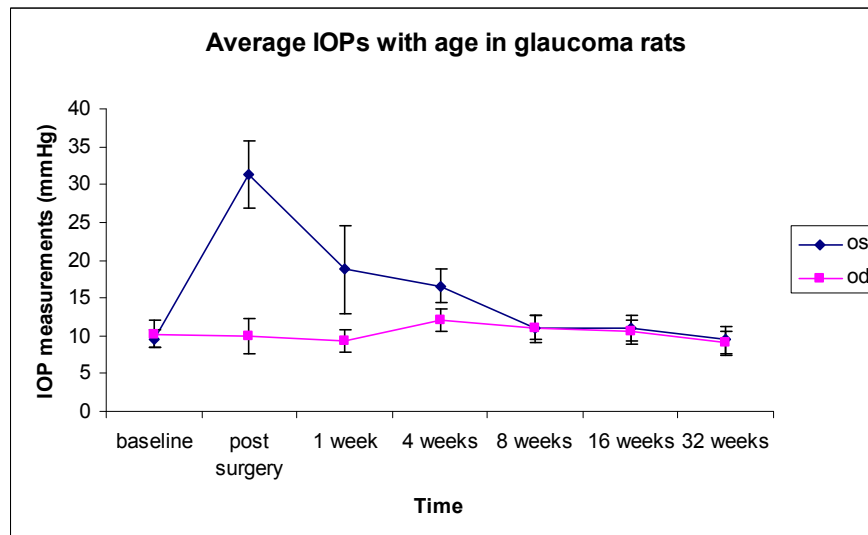


Figure 3.1: Average IOPs with age in the operated eyes (os) and unoperated controls (od).

In the baseline group, the average IOP values were 9.6 ± 1.2 (os) and 10.2 ± 1.8 (od) mmHg, showing no significant difference ($p > 0.05$). The comparison of IOP measurements in control groups at different ages did not show significant differences either. At 1 hour after glaucoma surgery, the IOPs in the left eye were increased substantially (31.3 ± 4.4 mmHg) compared to those in the right eye (9.9 ± 2.3 mmHg) ($p < 0.001$). At 1 week after glaucoma surgery, the IOPs in the operated eye (18.8 ± 5.8 mmHg) were also significantly elevated compared to the unoperated eye (9.3 ± 1.5 mmHg) ($p < 0.001$), although the IOP value was lower than that at 1 hour after surgery. The elevated IOPs were also shown in the operated eye (16.6 ± 2.3 mmHg) at 4 weeks after surgery compared to the unoperated eye (12 ± 1.5 mmHg), reaching statistical significance ($p < 0.001$). However, the comparison of IOP values in the operated and unoperated eyes at 8 (os: 11.1 ± 1.5 mmHg; od: 10.9 ± 1.7 mmHg), 16 (os: 11 ± 1.7 mmHg; od: 10.5 ± 1.6 mmHg), and 32 (os: 9.5 ± 1.8 mmHg; od: 9 ± 1.6 mmHg) weeks after surgery did not show significant differences ($p > 0.05$ at all time points).

3.2 Dendritic Changes in the Superior Colliculus

3.2.1 DiI Labelling Method

3.2.1.1 Immersion Labelling and Injection Labelling

The fluorescent dye DiI was trialled on $100\mu\text{m}$, $200\mu\text{m}$ and $400\mu\text{m}$ brain slices to label neurons in the superior colliculus. DiI was applied onto the slices using two methods: immersion labelling and injection labelling. Using immersion labelling, there were no neurons found in the slices of different thicknesses under the

Zeiss laser confocal microscope. However, positively labelled cell bodies with their dendrites were observed in 400 μ m slices stained by the injection method. It was obvious that the dye was delivered more quickly and with better penetration by injection labelling than by immersion labelling.

3.2.1.2 Comparison of Different DiI Dilutions

In order to find out the optimal concentration of DiI for injection labelling, a series of Vybrant DiI dilutions were applied to brain slices and compared. 400 μ m thick slices were used for assessing the optimal dilution. There were four concentrations of DiI including 0.1% (Fig. 3.2a, e), 0.01% (Fig. 3.2b, f), 0.001% (Fig. 3.2c, g) and 0.0001% (Fig. 3.2d, h) (w/v) which were used for injection labelling.

The superior colliculus slices (SC) were imaged under a x5 lens as shown in Fig. 3.2a-d. In image Fig. 3.2a, the injection sites are clearly shown in red in the rostral and middle sites in the superficial layer of the SC. The selected regions in the superior colliculus indicated using white squares in Fig. 3.2a-d, were also imaged under a x16 oil immersion lens as shown in Fig. 3.2e-h. There is clear labelling of a neuron containing a cell body and its neurites shown in Fig. 3.2e, suggesting that 0.1% (w/v) DiI solution is the optimal concentration for cell labelling.

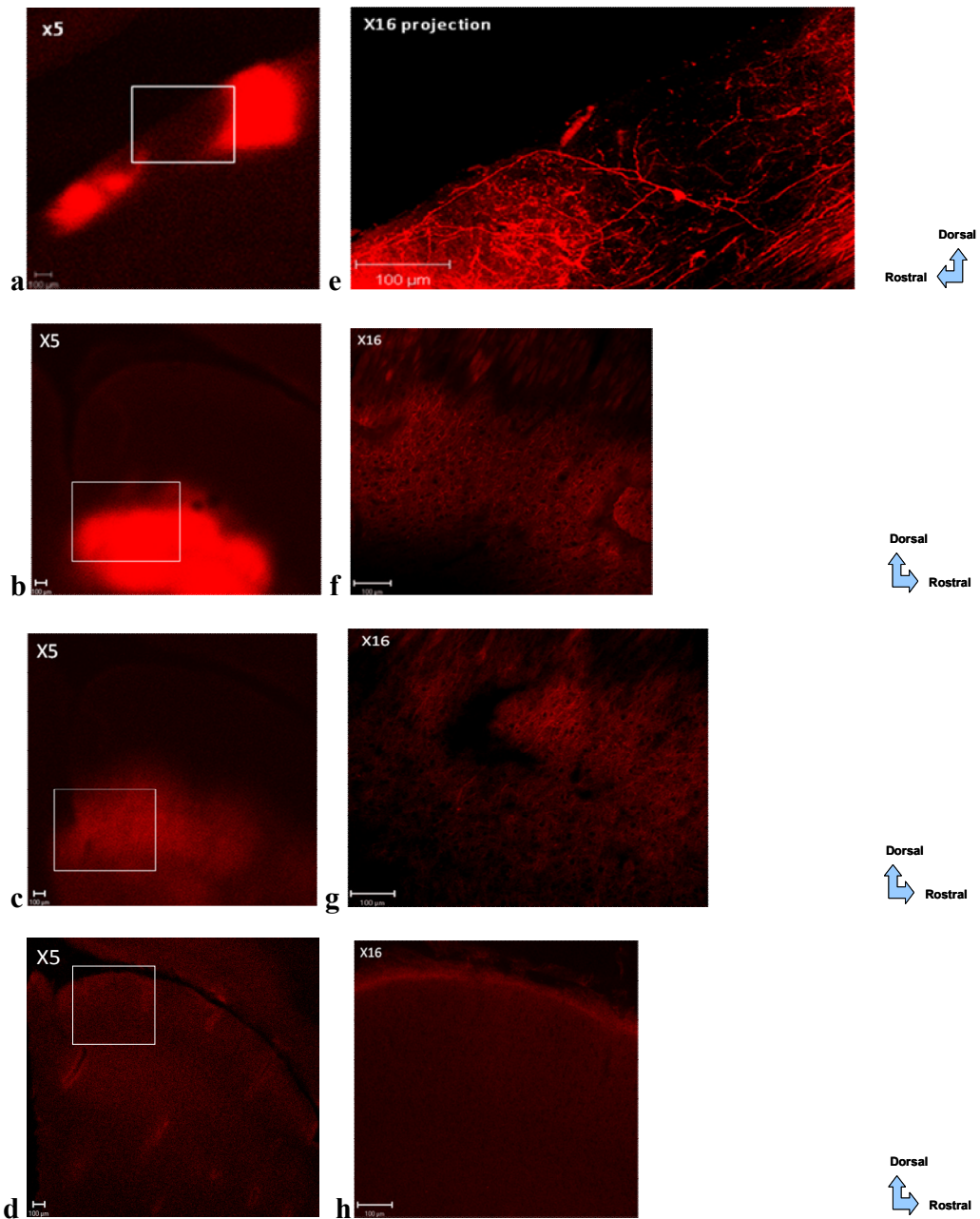


Figure 3.2a-h: Comparison of VyDiI dilutions for labelling neurons in the superior colliculus.

This group of images shows the labelled superior colliculus from rat brain slices stained using injection labelling of DiI. Different dilutions of DiI including 0.1% (**a, e**), 0.01% (**b, f**), 0.001% (**c, g**) and 0.0001% (**d, h**) (w/v) were used for staining. The white square box in images a-d indicates the magnified area shown in images e-h. Images a-d were taken under a x5 lens and e-h were taken under a x16 oil-immersion lens. Scale bar = 100 μ m.

Thus, the method of labelling cells in the superior colliculus was set up based on the above results. In the following studies of dendritic changes in the superior colliculus, the fixed rat brains were sectioned into 400 μ m thick parasagittal slices, which was followed by the injection labelling of 0.1% (w/v) DiI, which was applied at the rostral and middle sites in the superficial layer of the SC.

3.2.2 Comparison of Different Fixation Methods for Rat Brains

Fixation is a crucial process in the preparation of tissue for anatomical study. It can stabilize the structure of the tissue for preservation and harden the tissue for convenient handling such as slicing. The most widely used fixative is 4% paraformaldehyde (PFA) dissolved in Phosphate Buffered Saline (PBS) buffer.

In this study, there were two fixation methods using 4% PFA for brain tissues which were compared. The first method (method I) involved the immersion of the brain blocks in tubes filled with 4% PFA. The second method (method II) involved fixing the brain using cardiac perfusion. Both methods were trialled on at least three animals. The fixed brains were then sectioned, stained and observed under a Zeiss laser confocal microscope. The slices from brain blocks fixed using different methods were imaged under a x16 lens. Fig. 3.3a, b shows the comparison of the two fixation methods. There were several cell bodies with their processes observed in the SC fixed using method I (Fig. 3.3a), whereas a lot of holes were seen in the SC fixed using method II (Fig. 3.3b). Furthermore, complete neuron staining was limited with cardiac perfusion. The results indicated that it is better to use the immersion method

for fixing brain blocks in this study. Thus, all brain tissues were immersed in tubes filled with 4% PFA for at least 1 week before the subsequent sectioning in the following studies.

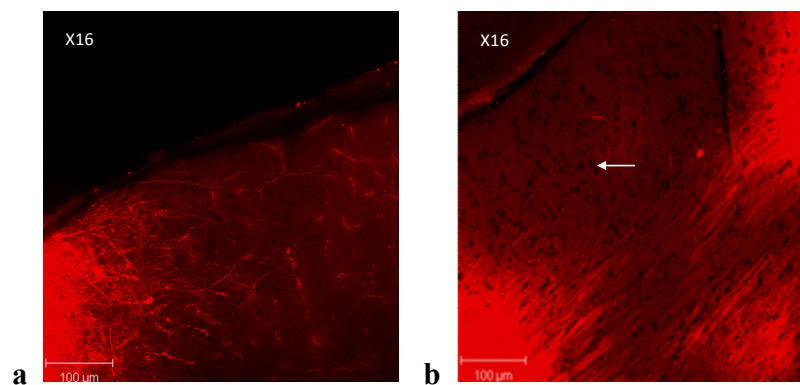


Figure 3.3a, b: Comparison of the fixation methods for rat brains.

These figures show slices from rats with fixation by method I (immersion) **(a)** and by method II (cardiac perfusion) **(b)** which were stained with 0.1% VyDiI. Images were taken under a x16 oil-immersion lens. The arrow in image **b** indicates holes shown in a slice from rat with cardiac perfusion. No completely labelled neurons could be observed in image **b**. Scale bar = 100μm

3.2.3 Classification of Cells in the Rodent Superior Colliculus

In the study of dendritic changes in the superior colliculus, a total of 675 neurons were imaged and analyzed. These cells were from nine animals groups including 4, 8, 16 and 32 weeks glaucoma animals and their age-matched controls, as

well as the baseline group (0 week CTL group). There were 75 cells analyzed for each group, which were further classified into five types as shown in Fig. 3.4a-e. The five types of cells included horizontal cell (H) (a); wide field vertical cell (W) (b); narrow field vertical cell (V) (c); pyriform cell (P) (d) and stellate cell (S) (e), which were classified according to the shape and size of their soma and the orientation of their dendrites (Table 3.1).

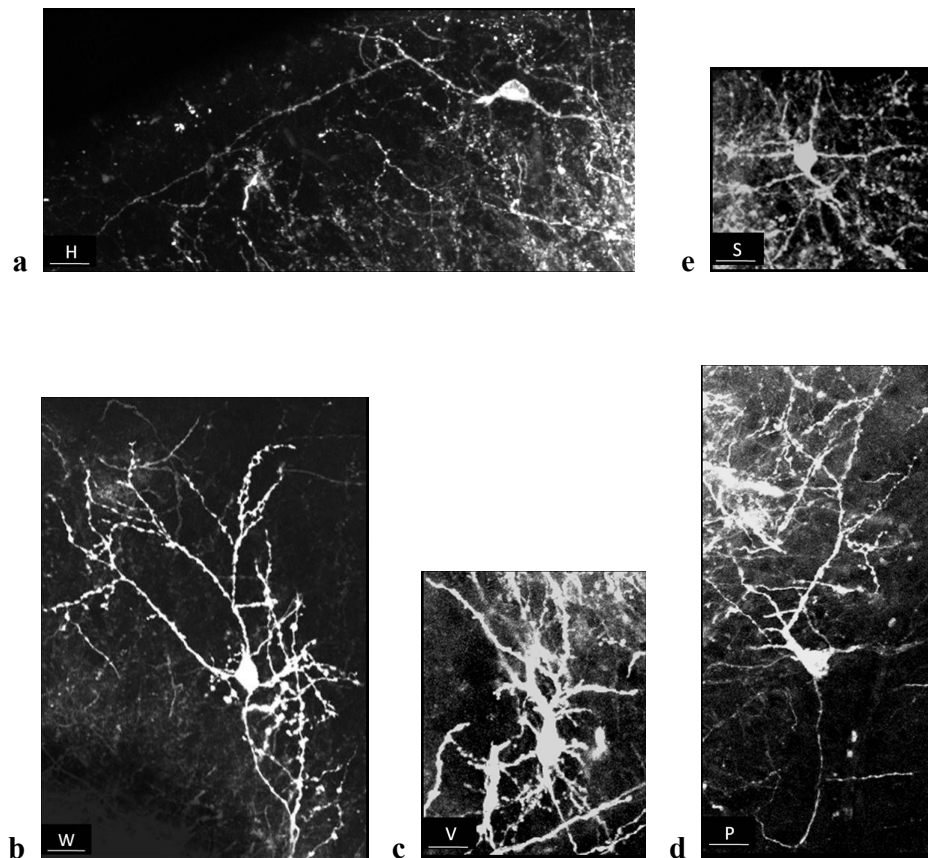


Figure 3.4a-e: Classification of cell types in the rat superior colliculus.

These figures show five types of cells that were identified in the SC: (a), H (Horizontal cells); (b), W (Wide field vertical cells); (c), V (Narrow field vertical cells); (d), P (Piriform cells) and (e) S (Stellate cells). The images were taken under a x16 oil-immersion lens. Scale bar = 20 μ m.

Cell type	Soma shape	Soma size (mean diameter)	Dendritic characteristics
H cells	fusiform	10 μ m	Dendrites are tangential to or parallel with the surface of the colliculus
W cells	horizontal fusiform	15 μ m to 25 μ m	Dendritic fields are large and vertically orientated; Most dendrites extend above the cell body
V cells	narrow, vertical fusiform	10 μ m to 20 μ m	Dendritic fields are narrow and vertically orientated; Dendrites extend both above and below the cell body
P cells	ovoid or cup-shape	10 μ m to 15 μ m	Dendritic fields are vertically orientated; Dendrites are either ascending or descending; The ascending dendrites branch more frequently as they approach the surface
S cells	irregular shape	10 μ m to 25 μ m	Dendrites arise from the cell body symmetrically

Table 3.1: Characteristics of different types of SC cells analyzed in this thesis.

3.2.4 Morphological Changes of Dendrites in the Superior Colliculus

3.2.4.1 Dendritic Changes in Control Animals

3.2.4.1.1 Changes in Mean Dendritic Length

In this study, dendritic parameters in control animals were analyzed to investigate whether there were ageing effects on dendritic morphology. Five groups of control animals were analyzed including 0, 4, 8, 16 and 32 weeks control (CTL) groups. The 0 week CTL group consisted of the baseline group with animals sacrificed at the age when ocular hypertension was induced in the glaucoma groups. The 4, 8, 16 and 32 weeks control groups were age-matched controls for 4, 8, 16 and 32 weeks glaucoma groups respectively.

Cells located in the SC from normal control animals were grouped into five types as H, W, V, P and S cells. The changes in mean dendritic length and dendritic number were analyzed for each type of cell individually. The mean dendritic length of cells in different age groups were analyzed and compared using one-way ANOVA and the post hoc Bonferroni test as shown in Fig. 3.5a-e. The error bar represents the SD of the mean.

Fig. 3.5a shows a significant reduction in the mean dendritic length of H cells from 4 ($72.6 \pm 13 \mu\text{m}$) to 8 weeks ($42 \pm 3.1 \mu\text{m}$), reaching statistical significance ($p < 0.001$). There was another significant reduction shown from 16 ($39.6 \pm 2.2 \mu\text{m}$) to 32 weeks ($26.1 \pm 2.3 \mu\text{m}$) ($p < 0.001$). However, no differences in the mean dendritic length were shown between 0 ($75.3 \pm 9.5 \mu\text{m}$) and 4 weeks ($p = 1.0$), or 8 and 16 weeks ($p = 1.0$).

Fig. 3.5b shows a significant reduction in the mean dendritic length of W cells from 4 ($57.5 \pm 8.7 \mu\text{m}$) to 8 weeks ($41.9 \pm 5.8 \mu\text{m}$) ($p < 0.001$). The dendritic shrinkage was further shown at 32 weeks ($27.7 \pm 2 \mu\text{m}$) compared to that at 8 weeks ($p < 0.001$).

However, the mean dendritic length did not change from 0 ($60.4 \pm 7.4 \mu\text{m}$) to 4 weeks ($p=1.0$), 8 to 16 weeks ($35.6 \pm 12.8 \mu\text{m}$) ($p=0.374$) or 16 to 32 weeks ($p=0.095$).

V cells showed the greatest reduction in mean dendritic length from 4 ($40.2 \pm 4.2 \mu\text{m}$) to 8 weeks ($26.2 \pm 2 \mu\text{m}$) ($p < 0.001$) (Fig. 3.5c). Significant dendritic shrinkage was also observed from 8 to 16 weeks ($19.6 \pm 1.6 \mu\text{m}$) ($p < 0.001$), and 16 to 32 weeks ($14.7 \pm 1.1 \mu\text{m}$) ($p=0.001$). The comparison of mean dendritic length between 0 ($43.4 \pm 4.7 \mu\text{m}$) and 4 weeks did not show any differences ($p=0.057$).

P cells also showed significant dendritic shrinkage from 4 ($51.5 \pm 7.5 \mu\text{m}$) to 8 weeks ($29.6 \pm 2.7 \mu\text{m}$) ($p < 0.001$) (Fig. 3.5d). The mean dendritic length was further decreased from 16 ($26 \pm 1.6 \mu\text{m}$) to 32 weeks ($15.1 \pm 0.7 \mu\text{m}$), reaching statistical significance ($p < 0.001$). However, the mean dendritic length did not change from 0 ($54.5 \pm 6.5 \mu\text{m}$) to 4 weeks ($p=0.776$), or 8 to 16 weeks ($p=0.394$).

Fig. 3.5e shows a significant reduction in the mean dendritic length of S cells at 8 weeks ($25.2 \pm 1.8 \mu\text{m}$) ($p < 0.001$). Significant dendritic shrinkage was also shown from 8 to 16 weeks ($20.9 \pm 1.8 \mu\text{m}$) ($p=0.017$) and 16 to 32 weeks ($15.7 \pm 1.4 \mu\text{m}$) ($p=0.002$). Similar to H, W, V and P cells, the mean dendritic length of S cells did not change from 0 ($52.5 \pm 4.6 \mu\text{m}$) to 4 weeks ($49.7 \pm 5.8 \mu\text{m}$) either ($p=0.371$).

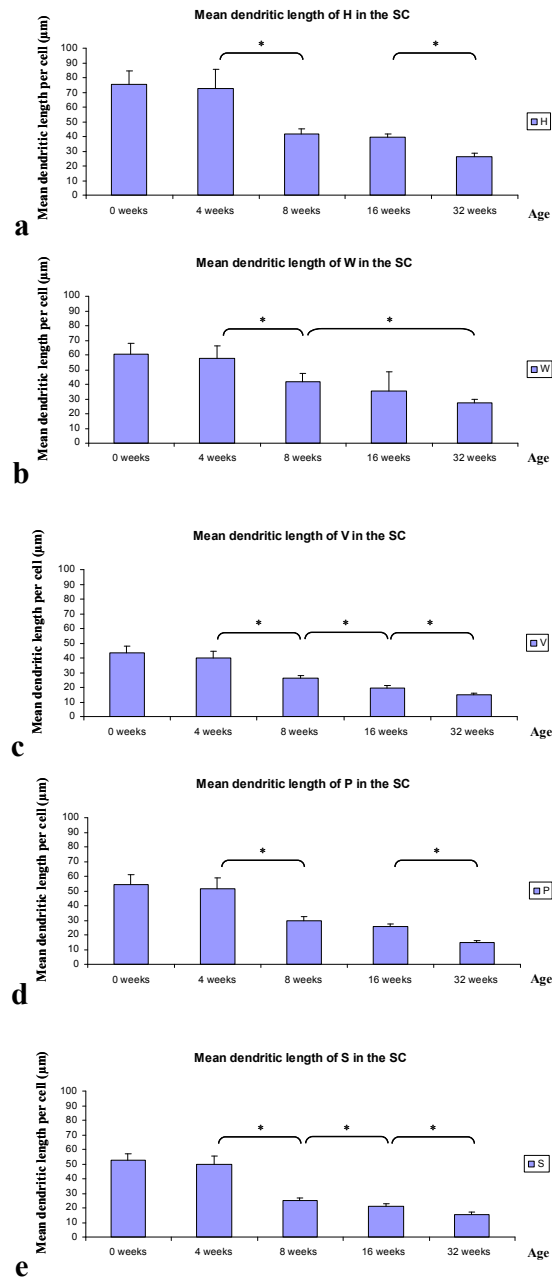


Figure 3.5a-e: Comparison of the mean dendritic length of SC cells between control groups at different time points.

These figures show the mean dendritic length of cells in the SC in control animals. There were five types of cells including H (a); W (b); V (c); P (d) and S (e) that were studied respectively (* $p < 0.05$). The error bar represents the SD of the mean.

For each type of cell, a percentage reduction in the mean dendritic length per cell was calculated, using the formula below:

$$\text{Percentage reduction in mean dendritic length per cell (\%)} = \frac{(\text{Mean dendritic length}_{\text{Baseline group}} - \text{Mean dendritic length}_{\text{n weeks CTL group}}) * 100}{\text{Mean dendritic length}_{\text{Baseline group}}}$$

Fig. 3.6a-e shows percentage reductions in the mean dendritic length increase from the baseline (0% for all cells), 4 weeks (H: 3.59%; W: 4.8%; V: 7.37%; P: 5.5%; S: 5.33%), 8 weeks (H: 44.22%; W: 30.63%; V: 39.63%; P: 45.69%; S: 52%), 16 weeks (H: 47.41%; W: 41.06%; V: 54.84%; P: 52.29%; S: 60.19%) until 32 weeks (H: 65.34%; W: 54.14%; V: 66.13%; P: 72.29%; S: 70.1%).

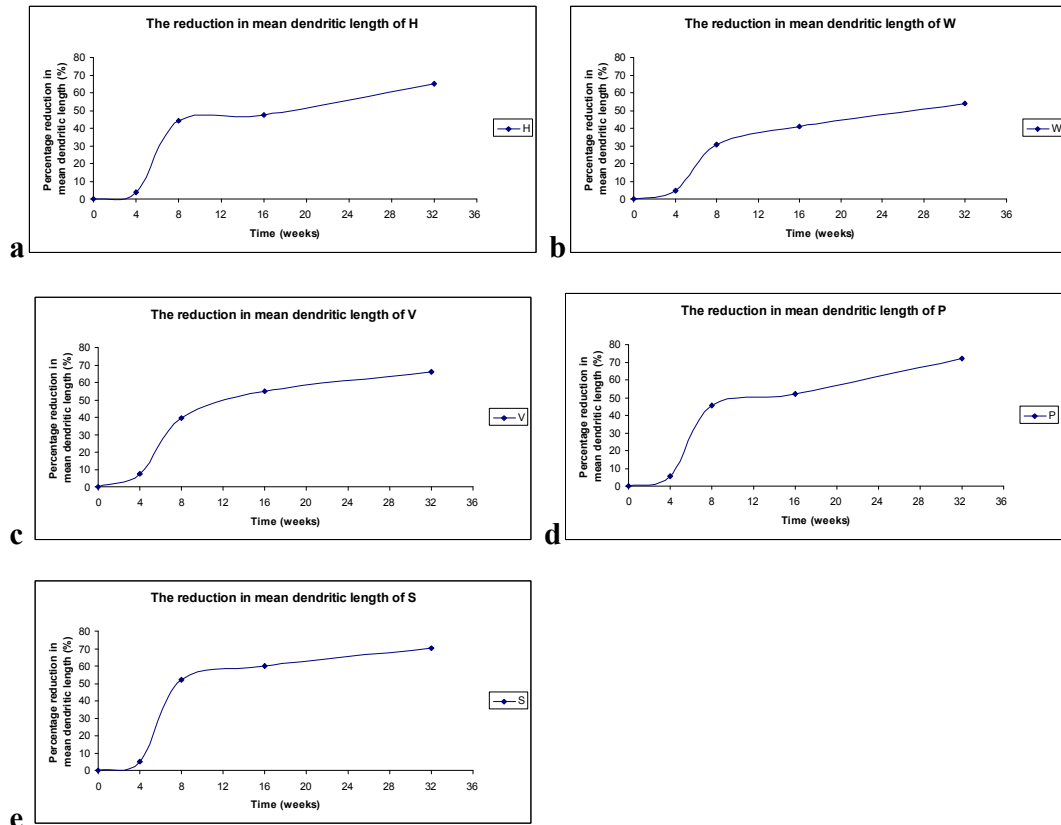


Figure 3.6a-e: Scatter plots of percentage reductions in the mean dendritic length of SC cells in control groups.

These graphs show the dendritic shrinkage in the SC in control animals: (a) H; (b) W; (c) V; (d) P; (e) S.

All of the above results showed that there were significant reductions in the mean dendritic length in the SC from 0 to 32 weeks over time, indicating that there was an age-dependent dendritic shrinkage in control animals.

To determine if there was a relationship between ageing and the mean dendritic length of cells in the SC, an exponential decay analysis was next performed using SigmaPlot 10.0 (Systat Software Inc.) as shown in Fig. 3.7a-e. The results were also confirmed by analyzing data using Origin Pro 8.1 (Silverdale Scientific Ltd.).

The strong regression coefficients (r^2) suggested that changes in the mean dendritic length of SC cells were age-related (H: $r^2=0.86$; W: $r^2=0.91$; V: $r^2=0.92$; P: $r^2=0.90$; S: $r^2=0.85$). The Spearman's correlation test was also performed with a correlation coefficient of -1 ($p<0.001$) for each type of cell, indicating a high probability of a negative correlation between ageing and the mean length of dendrites in the SC.

To characterize the longitudinal profile of dendritic changes, the relationship between the mean dendritic length and the effect of ageing was modelled with exponential decay equations ($y = a \cdot e^{bx}$) and exponential regression analysis. As the decline of mean dendritic length with age fitted well with an exponential decay curve, the rate of dendritic shrinkage was approximated based on the exponential regression equation as shown below:

$$\text{Rate of dendritic shrinkage} = e^b - 1 \text{ (\% / week)}$$

Thus, in control groups, dendrites in the superior colliculus shrunk at a rate of 3.88% (H); 2.77% (W); 4.2% (V); 4.63% (P) and 5.19% (S) per week during ageing.

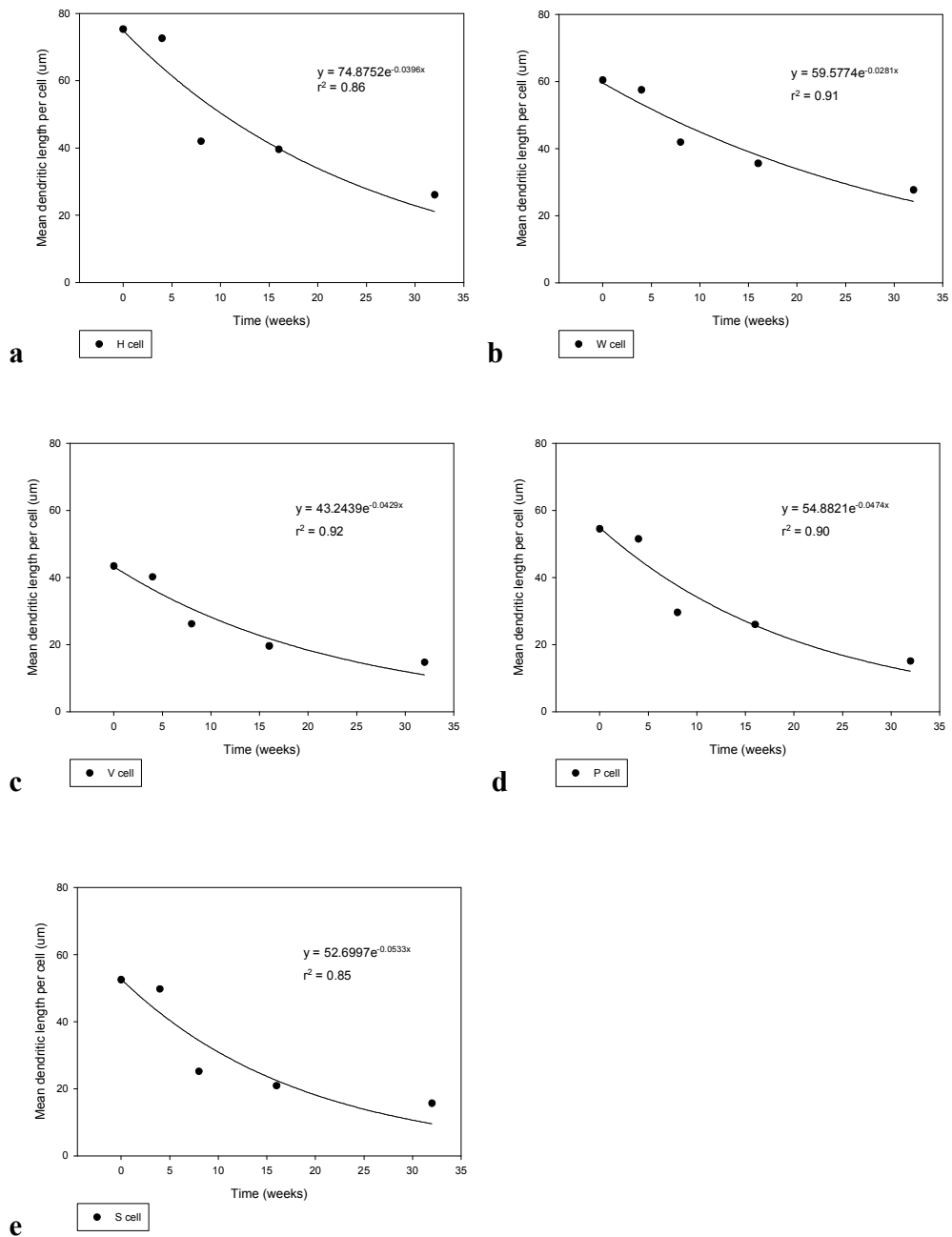


Figure 3.7a-e: The exponential decay of the mean dendritic length of SC cells in control rats.

These graphs show the exponential regression analysis of the mean dendritic length of cells in the SC from control animals: (a) H; (b) W; (c) V; (d) P; (e) S.

3.2.4.1.2 Changes in Dendritic Number

The number of dendrites per neuron were also counted and averaged for each type of cell from control animals at different time points. The dendritic number of cells from 0, 4, 8, 16 and 32 weeks control groups were compared and analyzed using one-way ANOVA and the post hoc Bonferroni test (Fig. 3.8a-e). The error bar represents the SD of the mean.

Fig. 3.8a shows that the dendritic number of H cells was significantly reduced from 4 (9.6 ± 2) to 8 weeks (7 ± 1.1) ($p < 0.001$). There was a greater dendritic loss shown at 16 weeks (4.1 ± 0.6) compared to that at 8 weeks ($p < 0.001$). However, the dendritic number did not further decrease at 32 weeks (3.1 ± 0.5) compared to that at 16 weeks ($p = 0.586$). No differences in the dendritic number between 0 (9.9 ± 2.1) and 4 weeks groups were shown ($p = 1.0$).

W cells initially showed a significant reduction in the dendritic number at 8 weeks (9.1 ± 1.5) compared to that at 4 weeks (12 ± 2.5) ($p < 0.001$) (Fig. 3.8b). The dendritic number was further significantly decreased from 8 to 16 weeks (5.8 ± 0.8) ($p < 0.001$), and 16 to 32 weeks (3.9 ± 0.6) ($p = 0.026$). The dendritic number did not change from the baseline to 4 weeks ($p = 1.0$).

V cells showed an initial reduction in the dendritic number at 8 weeks (7.6 ± 1.7) compared to 4 weeks (12 ± 1.6), reaching statistical significance ($p < 0.001$) (Fig. 3.8c). Significant dendritic losses were also shown from 8 to 16 weeks (5.1 ± 0.5) ($p < 0.001$) and 16 to 32 weeks (3.5 ± 0.5) ($p = 0.008$). Similar to H and W cells, V cells did not show significant dendritic loss from the baseline (12.2 ± 1.5) to 4 weeks ($p = 1.0$).

Fig. 3.8d shows significant dendritic loss in P cells at 8 weeks (7.4 ± 1.4) compared to that at 4 weeks (9.5 ± 1.3) ($p < 0.001$). A significant reduction in the dendritic number was also shown from 8 to 16 weeks (4.2 ± 0.8) ($p < 0.001$). However, the dendritic number did not change either from the baseline (9.7 ± 1.3) to 4 weeks ($p = 1.0$).

S cells also showed initial reduction in the dendritic number at 8 weeks (8.1 ± 1.2) compared to that at 4 weeks (11.9 ± 1.3) ($p < 0.001$), which is similar to H, W, V and P cells (Fig. 3.8e). Significant dendritic loss was also shown at 32 weeks (4.1 ± 0.7) compared to that at 16 weeks (7.9 ± 0.7) ($p < 0.001$). No differences in the dendritic number were shown either from 0 (12.4 ± 1.6) to 4 weeks ($p = 1.0$), or 8 to 16 weeks ($p = 1.0$).

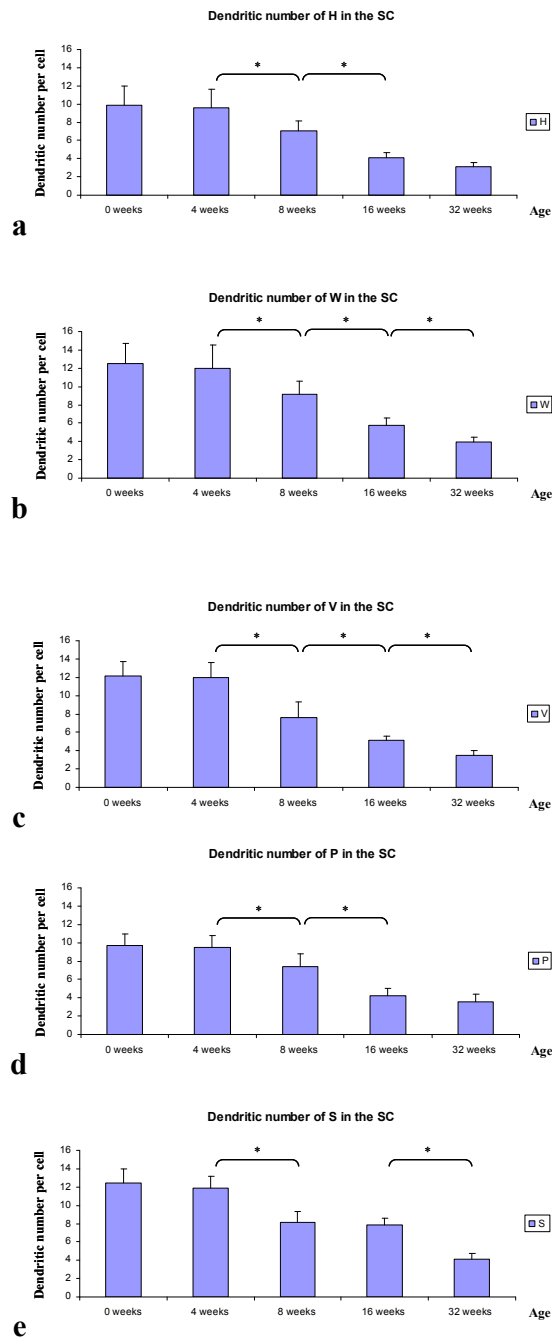


Figure 3.8a-e: Comparison of the dendritic number of SC cells between control groups at different time points.

These graphs show the dendritic number of cells in the SC in control animals. There were five types of cells including H (a); W (b); V (c); P (d) and S (e) that were studied respectively (* $p < 0.05$). The error bar represents the SD of the mean.

For each type of cell, a percentage reduction in the number of dendrites per cell was next calculated, using the formula below:

$$\text{Percentage reduction in dendritic number per cell (\%)} = \frac{(\text{Dendritic number}_{\text{Baseline group}} - \text{Dendritic number}_{\text{n weeks CTL group}}) * 100}{\text{Dendritic number}_{\text{Baseline group}}}$$

Fig. 3.9a-e show an increasing percentage reduction in the dendritic number from the baseline (0% for all cells), 4 weeks (H: 3.03%; W: 4%; V: 1.64%; P: 2.06%; S: 4.03%), 8 weeks (H: 29.29%; W: 27.2%; V: 37.7%; P: 23.71%; S: 34.68%), 16 weeks (H: 58.59%; W: 53.6%; V: 58.2%; P: 56.7%; S: 36.29%) until 32 weeks (H: 68.69%; W: 68.8%; V: 71.31%; P: 62.89%; S: 66.94%).

All of the above results showed that there were significant reductions in the dendritic number in the SC from 0 to 32 weeks over time, indicating that there was an age-dependent dendritic loss in control animals.

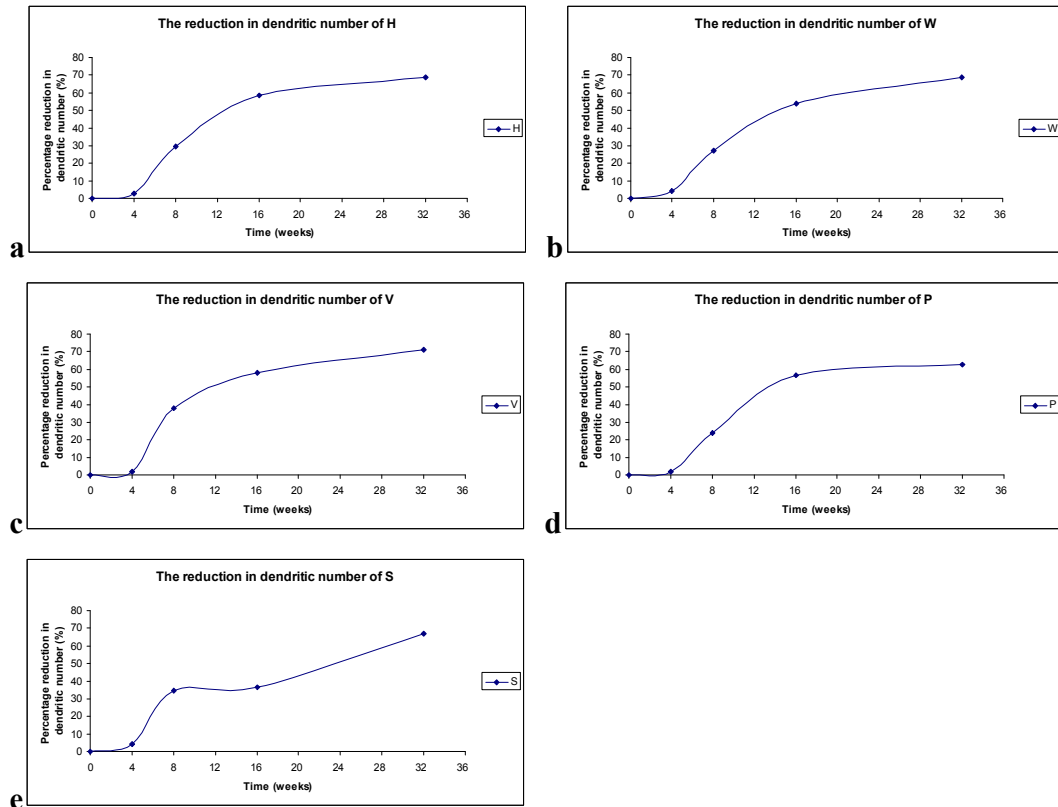


Figure 3.9a-e: Scatter plots of percentage reductions in the dendritic number of SC cells in control groups.

These graphs show the dendritic loss in the SC in control animals: (a) H; (b) W; (c) V; (d) P; (e) S.

To determine if there was a relationship between ageing and the dendritic number of cells in the SC, an exponential decay analysis was next performed using SigmaPlot 10.0 (Systat Software Inc.), as shown in Fig. 3.10a-e. The results were also confirmed by analyzing data using Origin Pro 8.1 (Silverdale Scientific Ltd.). The strong regression coefficients (r^2) suggested that changes in the dendritic number of SC cells were age-related (H: $r^2=0.94$; W: $r^2=0.96$; V: $r^2=0.92$; P: $r^2=0.91$; S: $r^2=0.93$). The Spearman's correlation test was also performed with a correlation coefficient of -1 ($p<0.001$) for each type of cell, indicating a high

probability of a negative correlation between ageing and the number of dendrites in the SC.

To characterize the longitudinal profile of dendritic changes, the relationship between the dendritic number and the effect of ageing was modelled with exponential decay equations ($y = a \cdot e^{bx}$) and exponential regression analysis. As the decline of dendritic number with age also fitted with an exponential decay curve well, the rate of dendritic loss was approximated based on the exponential regression equation as shown below:

$$\text{Rate of dendritic loss} = e^b - 1 \text{ (\% / week)}$$

Thus, in control groups, dendrites in the superior colliculus were lost at a rate of 4.39% (H); 4.1% (W); 4.73% (V); 3.85% (P) and 3.37% (S) per week during ageing.

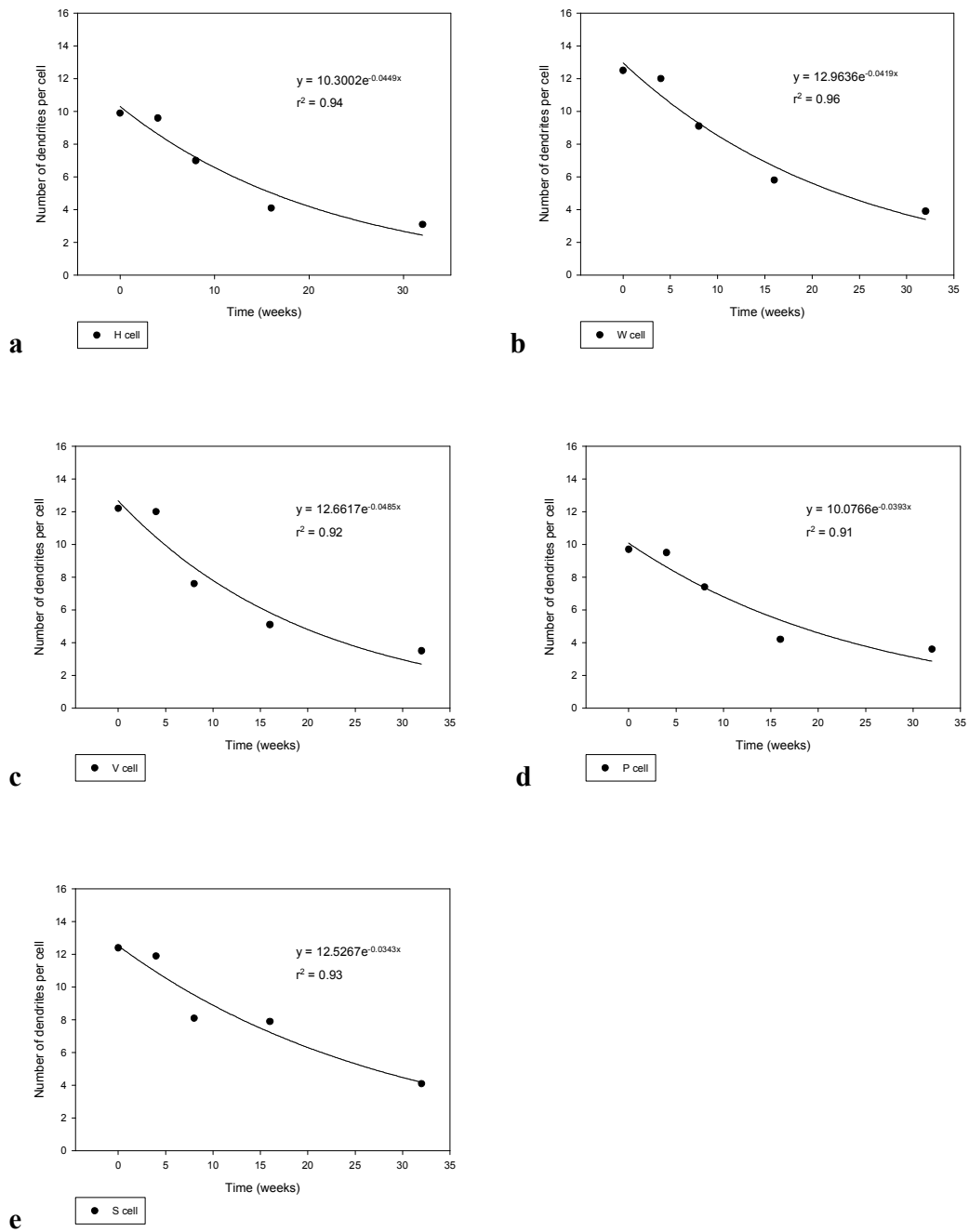


Figure 3.10a-e: The exponential decay of the dendritic number of SC cells in control groups.

These graphs show the exponential regression analysis of the dendritic number of SC cells from control animals: **(a)** H; **(b)** W; **(c)** V; **(d)** P; **(e)** S.

3.2.4.2 Dendritic Changes in Glaucoma Animals

3.2.4.2.1 Changes in Mean Dendritic Length

Two dendritic parameters, the mean dendritic length and dendritic number per cell, were also analyzed in glaucoma groups to investigate effects of the elevated IOP on dendritic morphology in the SC.

The mean dendritic length of cells from the baseline group and 4, 8, 16 and 32 weeks glaucoma animals were compared. The comparison between mean dendritic lengths of each type of cell at different time points was performed using one-way ANOVA and the post hoc Bonferroni test (Fig. 3.11a-e). The error bar represents the SD of the mean.

Fig. 3.11a shows that the mean dendritic length of H cells was significantly decreased from the baseline ($75.3\pm 9.5\mu\text{m}$) to 4 weeks ($34.2\pm 1.4\mu\text{m}$) after OHT induction ($p<0.001$). Significant reductions were also shown from 4 to 8 weeks ($28.8\pm 2.8\mu\text{m}$) ($p<0.05$), and 16 ($27.7\pm 1.9\mu\text{m}$) to 32 weeks ($15.3\pm 1.4\mu\text{m}$) after OHT induction ($p<0.001$). However, there was no difference in the mean dendritic length shown between 8 and 16 weeks after OHT induction ($p=1.0$).

W cells showed a significant reduction in the mean dendritic length at 4 weeks ($31.7\pm 1.9\mu\text{m}$) after OHT induction compared to that of the baseline group ($60.4\pm 7.4\mu\text{m}$) ($p<0.001$) (Fig. 3.11b). It also showed a significant reduction from 16 ($26.8\pm 2.3\mu\text{m}$) to 32 weeks ($17.7\pm 1.5\mu\text{m}$) after OHT induction ($p<0.001$). However, the mean dendritic length did not change from 4 to 8 weeks ($28.2\pm 2.3\mu\text{m}$) ($p=0.115$), and 8 to 16 weeks after OHT induction ($p=1.0$).

V cells also showed a significant reduction in the mean dendritic length at 4 weeks ($20.5 \pm 1.5 \mu\text{m}$) after OHT induction compared to that of the baseline group ($43.4 \pm 4.7 \mu\text{m}$) ($p < 0.001$) (Fig. 3.11c). Similar to H and W cells, V cells also showed significant dendritic shrinkage from 16 ($17 \pm 3.2 \mu\text{m}$) to 32 weeks ($12.1 \pm 1.5 \mu\text{m}$) after OHT induction ($p < 0.001$). The comparison of mean dendritic lengths between 4 and 8 weeks ($18.9 \pm 2.4 \mu\text{m}$) after OHT induction did not show any differences ($p = 1.0$). The mean dendritic length did not change either from 8 to 16 weeks after OHT induction ($p = 0.785$).

Fig. 3.11d shows a significant dendritic shrinkage of P cells at 4 weeks ($27 \pm 1.9 \mu\text{m}$) after OHT induction compared to that of the baseline group ($54.5 \pm 6.5 \mu\text{m}$) ($p < 0.001$). Significant reductions were also observed from 4 to 8 weeks ($20.4 \pm 2 \mu\text{m}$) ($p < 0.001$), and 16 ($17.6 \pm 2.2 \mu\text{m}$) to 32 weeks ($9.8 \pm 0.6 \mu\text{m}$) after OHT induction ($p < 0.001$). The mean dendritic length did not change either from 8 to 16 weeks after OHT induction ($p = 0.221$).

Fig. 3.11e shows a significant reduction in the mean dendritic length of S cells at 4 weeks ($23.6 \pm 1.6 \mu\text{m}$) after OHT induction compared to that of the baseline group ($52.5 \pm 4.6 \mu\text{m}$) ($p < 0.001$). Significant dendritic shrinkage in S cells was also observed from 4 to 8 weeks ($18.6 \pm 2.7 \mu\text{m}$) ($p < 0.001$), 8 to 16 weeks ($15.5 \pm 2.1 \mu\text{m}$) ($p < 0.05$), and 16 to 32 weeks ($9.3 \pm 0.9 \mu\text{m}$) after OHT induction ($p < 0.001$).

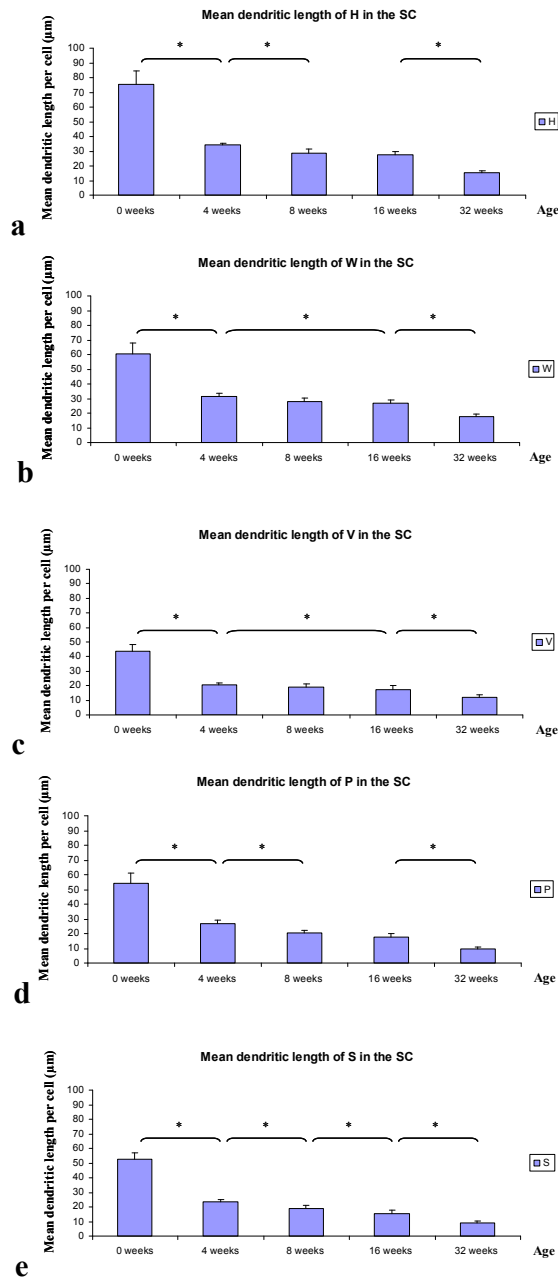


Figure 3.11a-e: Comparison of the mean dendritic length of SC cells between glaucoma groups at different time points.

These graphs show the mean dendritic length of cells in the SC in glaucoma animals at 0, 4, 8, 16 and 32 weeks after OHT induction. There were five types of cells including H (a); W (b); V (c); P (d) and S (e) that were studied respectively (* $p < 0.05$). The error bar represents the SD of the mean.

For each type of cell, furthermore, a percentage reduction in the mean dendritic length per cell in glaucoma animals was calculated, using the formula below:

$$\text{Percentage reduction in mean dendritic length per cell (\%)} = \frac{(\text{Mean dendritic length}_{\text{Baseline group}} - \text{Mean dendritic length}_{\text{n weeks OHT group}}) * 100}{\text{Mean dendritic length}_{\text{Baseline group}}}$$

Fig. 3.12a-e shows an increasing percentage reduction in the mean dendritic length from the baseline (0% for all cells), 4 weeks (H: 54.58%; W: 47.52%; V: 52.76%; P: 50.46%; S: 55.05%), 8 weeks (H: 61.75%; W: 53.31%; V: 56.45%; P: 62.57%; S: 64.57%), 16 weeks (H: 63.21%; W: 55.63%; V: 60.83%; P: 67.71%; S: 70.48%) until 32 weeks (H: 79.68%; W: 70.7%; V: 72.12%; P: 82.02%; S: 82.29%).

The above results showed that there were significant reductions in the mean dendritic length in the SC from the baseline to 32 weeks over time, indicating that there was an age-dependent dendritic shrinkage in glaucoma animals.

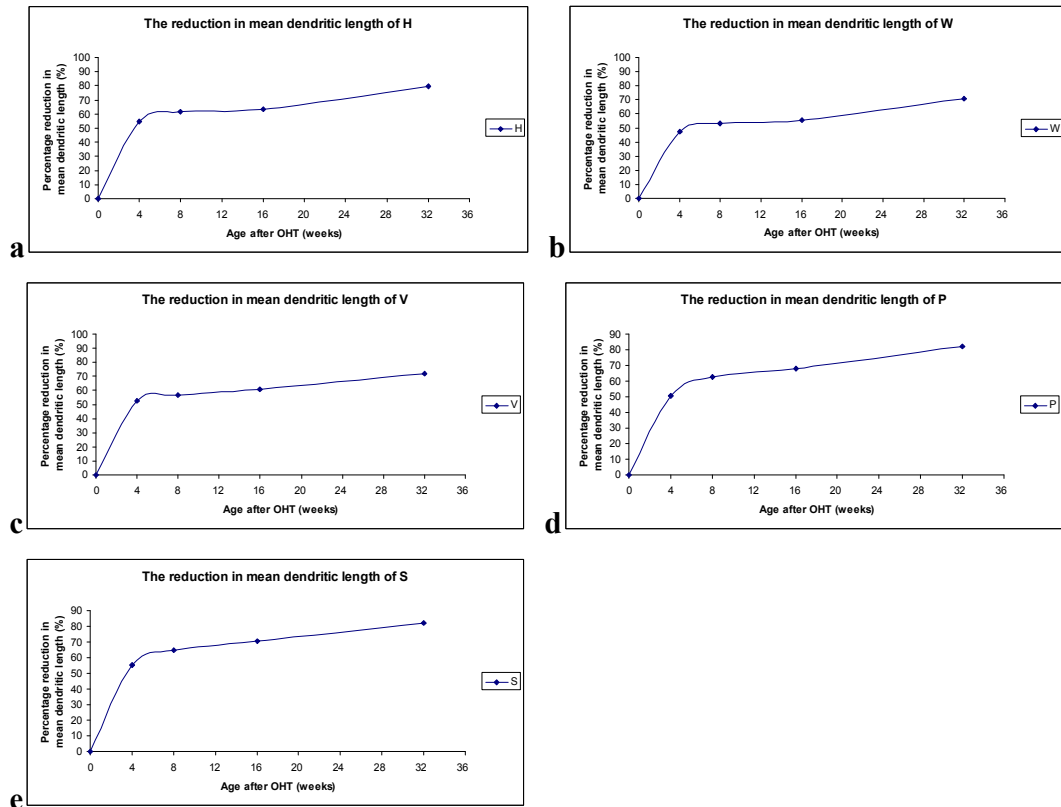


Figure 3.12a-e: Scatter plots of percentage reductions in the mean dendritic length of SC cells in glaucoma animals.

These graphs show the dendritic shrinkage in the SC in glaucoma animals: (a) H; (b) W; (c) V; (d) P; (e) S.

To determine if there was a relationship between ageing and the mean dendritic length of cells in the SC in glaucoma animals, an exponential decay analysis was next performed using SigmaPlot 10.0 (Systat Software Inc.), as shown in Fig. 3.13a-e. The results were also confirmed by analyzing data using Origin Pro 8.1 (Silverdale Scientific Ltd.). The regression coefficients (r^2) suggested that changes in the mean dendritic lengths of SC cells were age-related (H: $r^2=0.76$;

W: $r^2=0.72$; V: $r^2=0.69$; P: $r^2=0.85$; S: $r^2=0.83$). The Spearman's correlation test was also performed with a correlation coefficient of -1 ($p<0.001$) for each type of cell, indicating a high probability of a negative correlation between ageing and the length of dendrites in the SC in glaucoma animals.

To characterize the longitudinal profile of dendritic changes, the relationship between the mean dendritic length and the effect of ageing was modelled with exponential decay equations ($y = a * e^{bx}$) and exponential regression analysis.

As the decline of mean dendritic length with age fitted an exponential decay curve well, the rate of dendritic shrinkage was approximated based on the exponential regression equation as previously described. The results showed that dendrites in the SC in glaucoma animals shrunk at a rate of 7.46% (H); 4.59% (W); 5.47% (V); 8.59% (P) and 9.94% (S) per week during ageing, which were much faster than those in control animals. Especially in H, W, P and S cells, the rates of dendritic shrinkage in glaucoma animals were almost twice as much as those in control animals. The rates of dendritic shrinkage in glaucoma groups and those in control groups were summarised as shown in Table 3.2.

Groups	Rates of dendritic shrinkage (weekly)				
	H	W	V	P	S
Control	3.88%	2.77%	4.2%	4.63%	5.19%
Glaucoma	7.46%	4.59%	5.47%	8.59%	9.94%

Table 3.2: Summary of the rates of dendritic shrinkage in glaucoma and control animals.

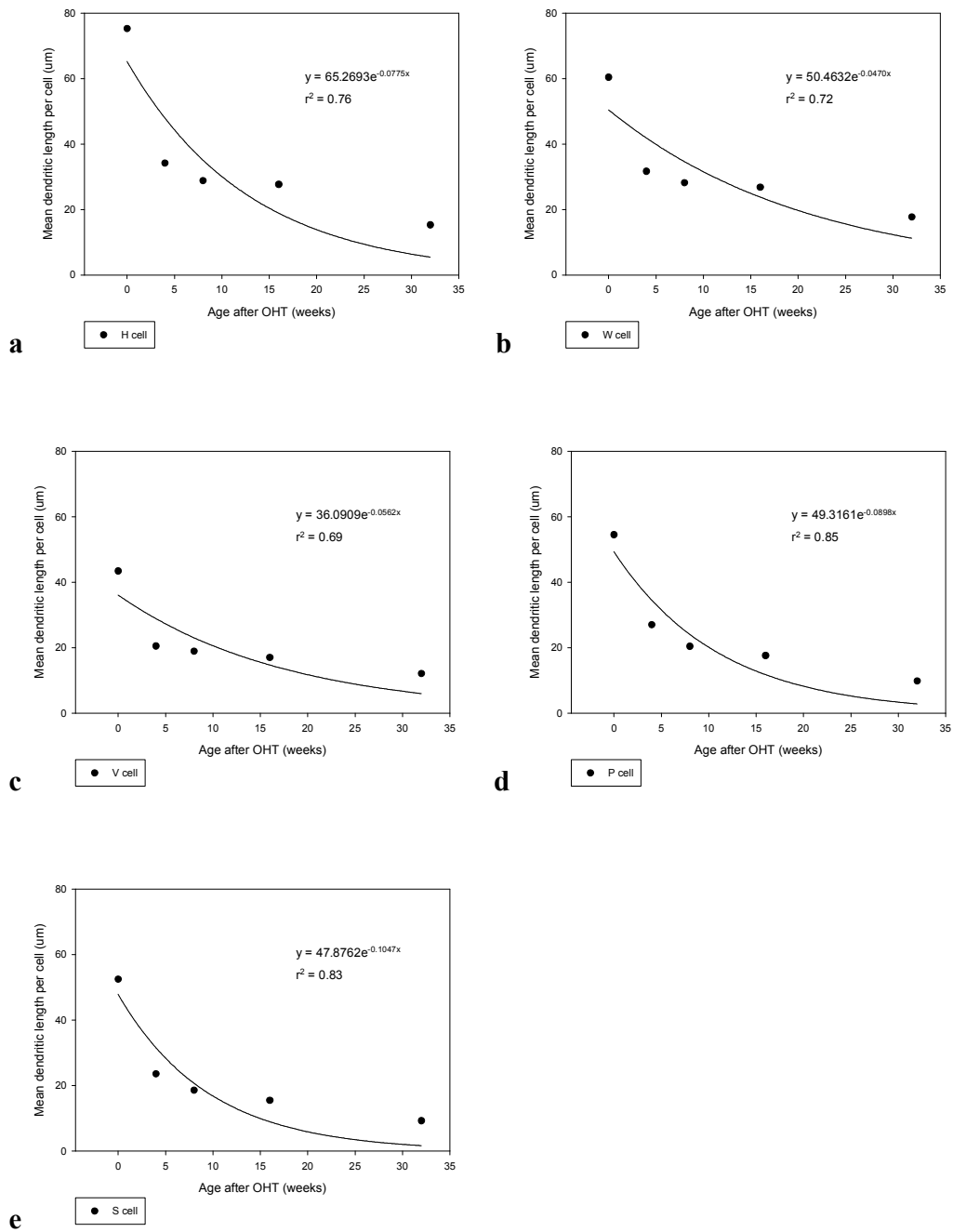


Figure 3.13a-e: The exponential decay of the mean dendritic length of SC cells in glaucoma groups.

These graphs show the exponential regression analysis of the mean dendritic length of cells in the SC from glaucoma animals at the ages of 0, 4, 8, 16 and 32 weeks after OHT induction:

(a) H; (b) W; (c) V; (d) P; (e) S.

3.2.4.2.2 Changes in Dendritic Number

The second dendritic parameter, dendritic number per cell, was also counted and averaged for each type of cell at different time points. The dendritic number of the baseline group, and 4, 8, 16 and 32 weeks glaucoma groups were compared and analyzed using one-way ANOVA and the post hoc Bonferroni test. The changes of dendritic number in each type of cell were studied individually as shown in Fig. 3.14a-e. The error bar represents the SD of the mean.

H cells showed the greatest reduction in dendritic number from 4 weeks (5.1 ± 0.6) after OHT induction compared to that of the baseline group (9.9 ± 2.1) ($p < 0.001$) (Fig. 3.14a). The dendritic number was also significantly decreased from 8 (4.9 ± 0.9) to 16 weeks (3.3 ± 0.7) after OHT induction ($p < 0.05$). However, no differences in the dendritic number were shown between 4 and 8 weeks after OHT induction ($p = 1.0$), and 16 and 32 weeks (2.5 ± 0.5) after OHT induction ($p = 0.251$).

W cells initially showed a significant reduction in the dendritic number at 4 weeks (6.1 ± 0.8) after OHT induction compared to that of the baseline group (12.5 ± 2.2) ($p < 0.001$) (Fig. 3.14b). A significant dendritic loss was also shown from 16 (4.9 ± 0.9) to 32 weeks (3 ± 0.7) after OHT induction as well ($p < 0.05$). However, the dendritic number did not change from 4 to 8 weeks (5.5 ± 1.2) ($p = 1.0$), and 8 to 16 weeks after OHT induction ($p = 1.0$).

V cells also showed the initial reduction in the dendritic number at 4 weeks (5.1 ± 0.7) after OHT induction compared to that of the baseline group (12.2 ± 1.5) ($p < 0.001$) (Fig. 3.14c). Similar to W cells, V cells also showed a significant reduction in the dendritic number at 32 weeks (2.6 ± 0.7) compared to 16 weeks

(4.1 ± 1.1) after OHT induction ($p=0.001$). However, the dendritic number did not change from 4 to 8 weeks (4.7 ± 1) after OHT induction ($p=1.0$), or 8 to 16 weeks after OHT induction ($p=1.0$).

Fig. 3.14d shows significant dendritic loss in P cells at 4 weeks (4.8 ± 0.8) after OHT induction compared to the baseline group (9.7 ± 1.3) ($p < 0.001$). A significant reduction in the dendritic number was also shown from 8 (4.5 ± 0.9) to 16 weeks (3.1 ± 0.9) after OHT induction ($p=0.001$). However, the dendritic number did not change either from 4 to 8 weeks ($p=1.0$) or from 16 to 32 weeks (2.7 ± 0.6) after OHT induction ($p=1.0$).

S cells showed an initial reduction in the dendritic number at 4 weeks (4.7 ± 0.7) after OHT induction compared to the baseline group (12.4 ± 1.6) ($p < 0.001$) (Fig. 3.14e). Significant dendritic loss was also shown from 8 (4.3 ± 0.7) to 32 weeks (3.2 ± 0.7) ($p < 0.05$). However, no differences in the dendritic number were shown between 4 and 8 weeks ($p < 0.001$), 8 and 16 weeks (3.7 ± 0.6) ($p < 0.001$), and 16 and 32 weeks ($p < 0.001$) after OHT induction.

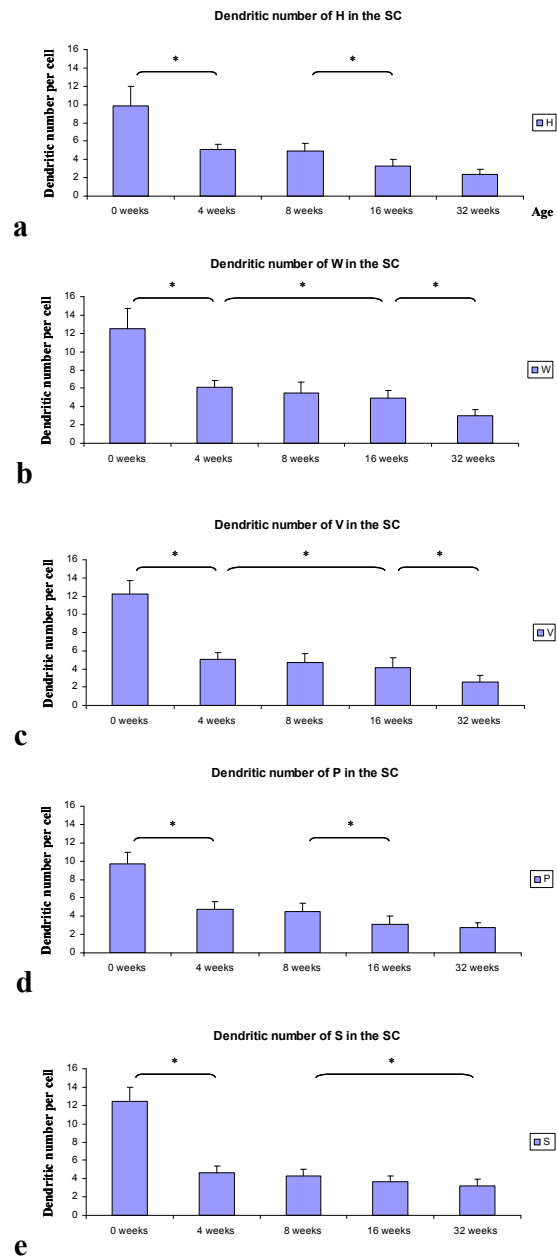


Figure 3.14a-e: Comparison of the dendritic number of SC cells between glaucoma groups at different time points.

These graphs show the dendritic number of SC cells in glaucoma animals at the age of 0, 4, 8, 16 and 32 weeks after OHT induction. There were five types of cells including H (a); W (b); V (c); P (d) and S (e) that were studied respectively (* $p < 0.05$). The error bar represents the SD of the mean.

For each type of cell, a percentage reduction in the number of dendrites per cell was calculated, using the formula below:

$$\text{Percentage reduction in dendritic number per cell (\%)} = \frac{(\text{Dendritic number}_{\text{Baseline group}} - \text{Dendritic number}_{\text{n weeks OHT group}}) * 100}{\text{Dendritic number}_{\text{Baseline group}}}$$

Fig. 3.15a-e show an increasing percentage reduction in the dendritic number from the baseline (0% for all cells), 4 weeks (H: 48.48%; W: 51.2%; V: 58.2%; P: 50.52%; S: 62.1%), 8 weeks (H: 50.51%; W: 56%; V: 61.48%; P: 53.61%; S: 65.32%), 16 weeks (H: 66.67%; W: 60.8%; V: 66.39%; P: 68.04%; S: 70.16%) until 32 weeks (H: 75.76%; W: 76%; V: 78.69%; P: 72.16%; S: 74.19%).

The above results showed that there were significant reductions in the dendritic number from the baseline to 32 weeks OHT group over time in all five types of cells, indicating there was an age-dependent dendritic loss in glaucoma animals.

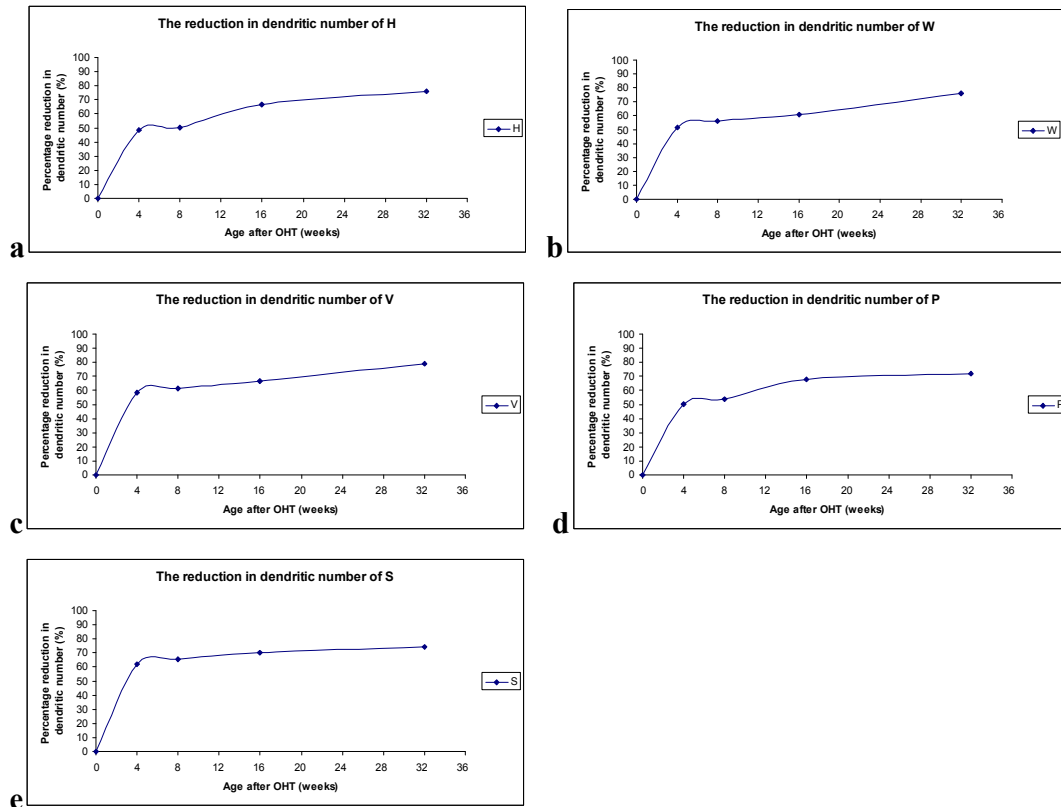


Figure 3.15a-e: Scatter plots of percentage reductions in the dendritic number of SC cells in glaucoma animals.

These graphs show the dendritic loss in the SC in glaucoma animals: **(a)** H; **(b)** W; **(c)** V; **(d)** P; **(e)** S.

To determine if there was a relationship between ageing and the dendritic number of cells in the SC in glaucoma animals, an exponential decay analysis was performed using SigmaPlot 10.0 (Systat Software Inc.), as shown in Fig. 3.16a-e. The results were also confirmed by analyzing data using Origin Pro 8.1 (Silverdale Scientific Ltd.). The regression coefficients (r^2) suggested that changes in the dendritic numbers of SC cells were age-related (H: $r^2=0.83$; W: $r^2=0.76$; V: $r^2=0.74$; P: $r^2=0.76$; S: $r^2=0.67$). The Spearman's correlation test was also performed

with a correlation coefficient of -1 ($p < 0.001$) for each type of cell, indicating a high probability of a negative correlation between ageing and the number of dendrites in the SC in glaucoma animals.

To characterize the longitudinal profile of dendritic changes, the relationship between the dendritic number and the effect of ageing was modelled with exponential decay equations ($y = a \cdot e^{bx}$) and exponential regression analysis. As the decline of dendritic number with age fitted an exponential decay curve best, the rate of dendritic loss was approximated based on the exponential regression equation as previously described. The results showed that dendrites in the SC in glaucoma animals were lost at a rate of 6.26% (H); 5.93% (W); 8.15% (V); 6.31% (P) and 10% (S) per week during ageing, which were much faster than those in control animals. The rates of dendritic loss in glaucoma groups and those in control groups were summarised as shown in Table 3.3.

Groups	Rates of dendritic loss (weekly)				
	H	W	V	P	S
Control	4.39%	4.1%	4.73%	3.85%	3.37%
Glaucoma	6.26%	5.93%	8.15%	6.31%	10%

Table 3.3: Summary of the rates of dendritic in glaucoma and control animals.

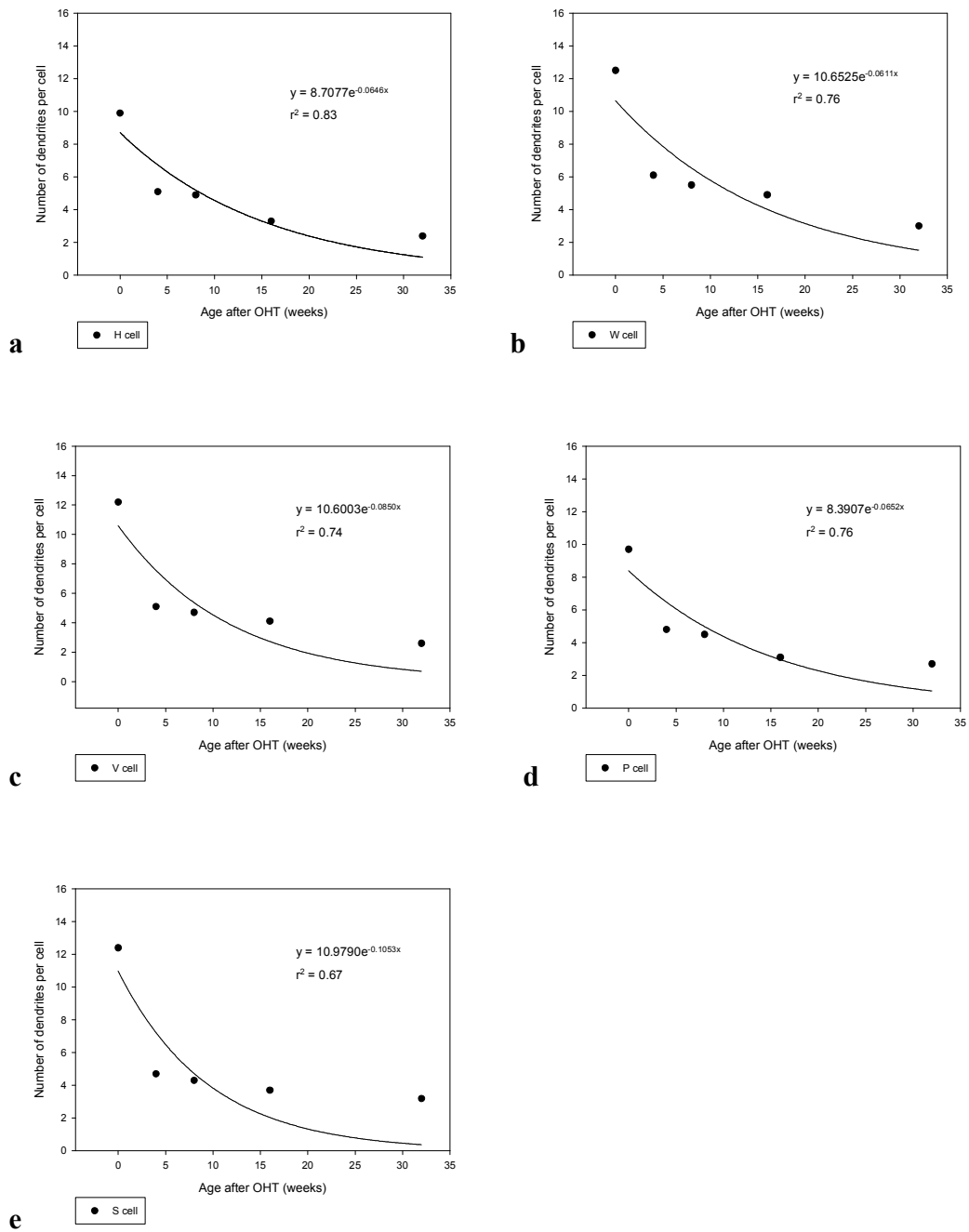


Figure 3.16a-e: The exponential decay of the dendritic number of SC cells in glaucoma groups.

These graphs show the exponential regression analysis of the dendritic number of SC cells from glaucoma animals at the age of 0, 4, 8, 16 and 32 weeks after OHT induction: (a) H; (b) W; (c) V; (d) P; (e) S.

3.2.4.3 Comparison of Dendritic Parameters between Glaucoma and Control Animals

3.2.4.3.1 Comparison of Mean Dendritic Length

In order to delineate the effects of ocular hypertension on dendritic morphology in the central visual target, dendritic parameters of neurons in the superior colliculus were compared between glaucoma rats and age-matched controls. The mean dendritic lengths of H, W, V, P and S cells were studied at 4, 8, 16 and 32 weeks respectively. The comparison of the mean dendritic length between glaucoma groups and age-matched controls were performed using the student T-test. As shown in Fig. 3.17a-e, there were significant reductions in the mean dendritic length at all time points. The error bar represents the SD of the mean.

Fig. 3.17a shows that the mean dendritic length of H cells was significantly reduced at 4, 8, 16 and 32 weeks after glaucoma surgery compared to age-matched controls, indicating that the dendritic shrinkage was also related to elevated IOP ($p < 0.001$ at all time points).

Fig. 3.17b shows that the mean dendritic length of W cells was also significantly decreased at 4, 8, 16 and 32 weeks after glaucoma surgery compared to age-matched controls ($p < 0.001$ at 4, 8 and 32 weeks; $p = 0.014$ at 16 weeks).

Fig. 3.17c shows that significant dendritic shrinkage in V cells was shown at 4, 8, 16 and 32 weeks after glaucoma surgery ($p < 0.001$ at 4, 8 and 32 weeks; $p = 0.008$ at 16 weeks).

Fig. 3.17d shows significant reductions in the mean dendritic length of P cells at 4, 8, 16 and 32 weeks after glaucoma surgery ($p < 0.001$ at all time points).

Fig. 3.17e shows significant dendritic shrinkage in S cells at 4, 8, 16 and 32 weeks, similar to what was shown in the H, W, V and P cells ($p < 0.001$ at all time points).

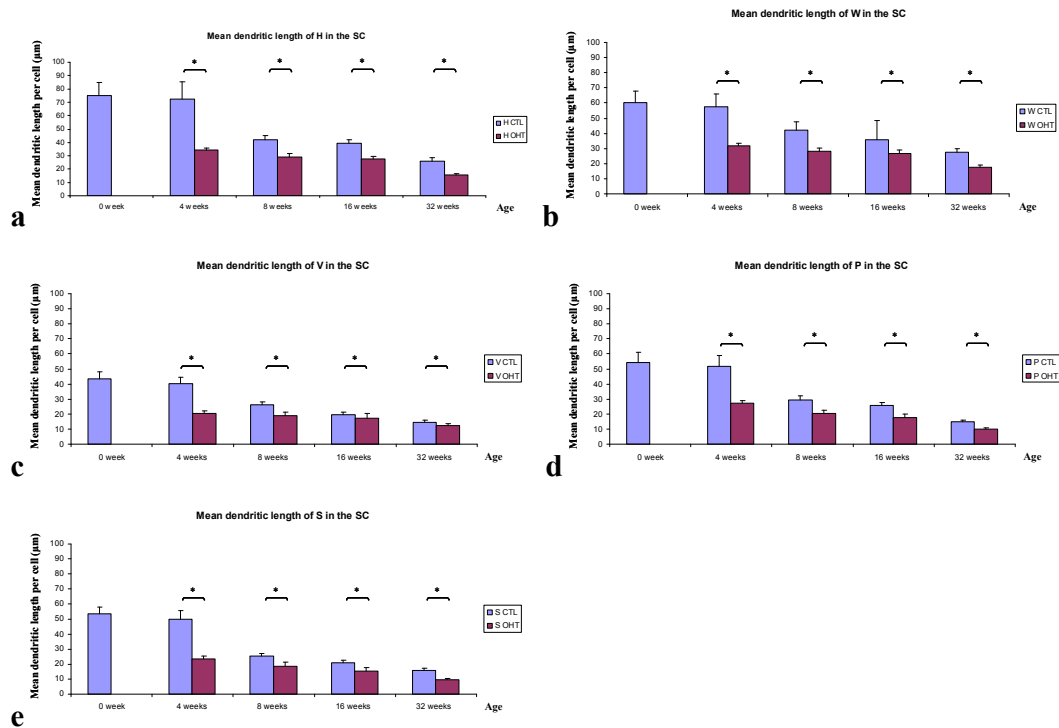


Figure 3.17a-e: Comparison of the mean dendritic length of SC cells between glaucoma and control animals.

These graphs show changes in the mean dendritic length of SC cells at 4, 8, 16 and 32 weeks after glaucoma surgery. Five types of cells including H (a); W (b); V (c); P (d) and S (e) were studied respectively ($*p < 0.05$). The error bar represents the SD of the mean.

For each type of cell, a percentage reduction in the mean dendritic length per cell at 4, 8, 16 and 32 weeks after glaucoma surgery was calculated, using the formula below:

$$\text{Percentage reduction in mean dendritic length per cell (\%)} = \frac{(\text{Mean dendritic length}_{\text{Age-matched CTL group}} - \text{Mean dendritic length}_{\text{OHT group}}) * 100}{\text{Mean dendritic length}_{\text{Age-matched CTL group}}}$$

Fig. 3.18a-e show that the earliest dendritic shrinkage of all types of cells could be observed at 4 weeks after glaucoma surgery (H: 52.89 %; W: 44.87%; V: 49%; P: 47.57%; S: 52.52%). The peaks of percentage reduction in the mean dendritic length were also shown at 4 weeks after OHT induction in all five types of cells. The dendritic shrinkage in cells continued from 8 weeks (H: 31.43%; W: 32.7%; V: 27.86%; P: 31.08%; S: 26.19%), 16 weeks (H: 30.05%; W: 24.72%; V: 13.27%; P: 32.31%; S: 25.84 %) until 32 weeks (H: 41.38%; W: 36.1%; V: 17.69%; P: 35.1%; S: 40.76 %) after OHT induction.

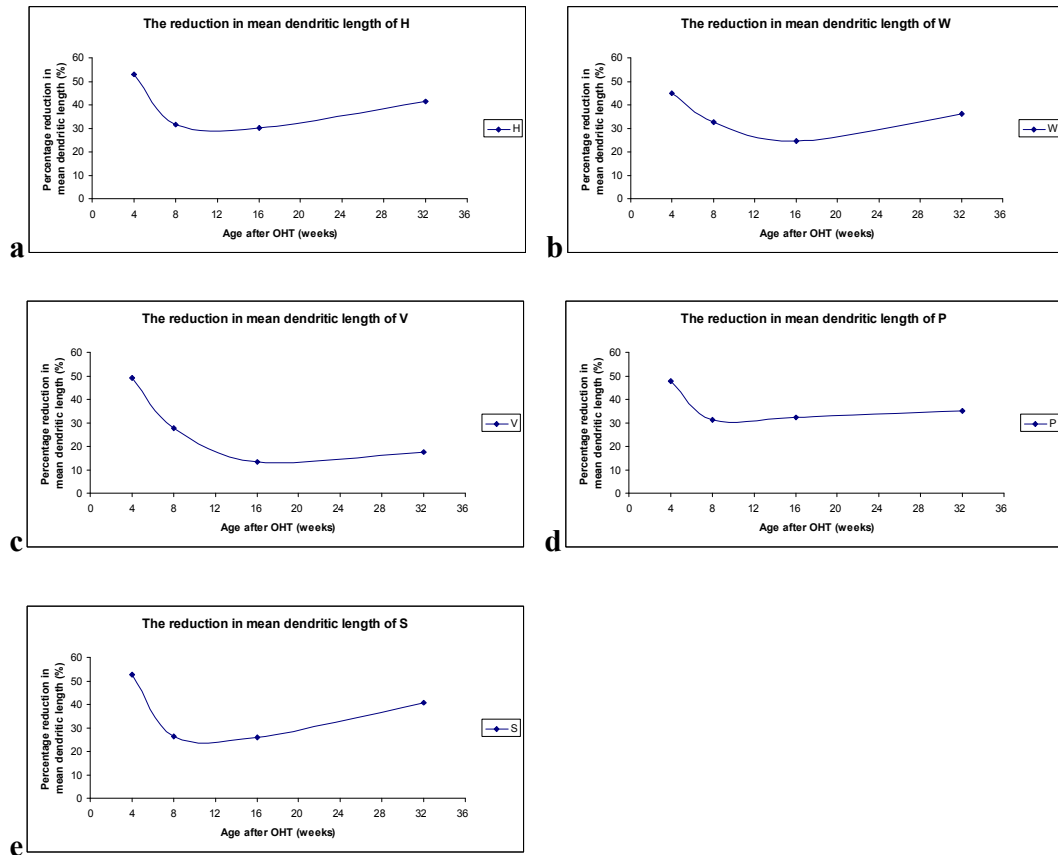


Figure 3.18a-e: Scatter plots of percentage reductions in the mean dendritic length of SC cells after glaucoma surgery.

These graphs show the dendritic shrinkage in the SC after OHT induction: (a) H; (b) W; (c) V; (d) P; (e) S.

3.2.4.3.2 Comparison of Dendritic Number

The effects of ocular hypertension on the dendritic number of H, W, V, P and S cells were also investigated at 4, 8, 16 and 32 weeks respectively. The comparison of the dendritic number in control groups and that in glaucoma groups was performed using the student T-test.

Fig. 3.19a-e show that there were significant reductions in the dendritic number at all time points including 4, 8, 16 and 32 weeks after OHT induction. The error bar represents the SD of the mean.

Fig. 3.19a shows that the dendritic number of H cells was significantly reduced at 4, 8, 16 and 32 weeks after glaucoma surgery compared to age-matched controls, indicating that the dendritic loss was also related to elevated IOP ($p < 0.001$ at 4 and 8 weeks; $p = 0.005$ at 16 weeks; $p = 0.001$ at 32 weeks).

Fig. 3.19b shows that the dendritic number of W cells was also significantly decreased at 4, 8, 16 and 32 weeks after glaucoma surgery compared to age-matched controls ($p < 0.001$ at 4 and 8 weeks; $p = 0.005$ at 16 weeks; $p = 0.001$ at 32 weeks).

Fig. 3.19c shows significant dendritic loss in V cells at 4, 8, 16 and 32 weeks after glaucoma surgery ($p < 0.001$ at 4 and 8 weeks; $p = 0.003$ at 16 weeks; $p = 0.001$ at 32 weeks).

P cells showed significant reductions in the dendritic number at 4, 8, 16 and 32 weeks after glaucoma surgery ($p < 0.001$ at 4 and 8 weeks; $p = 0.001$ at 16 weeks; $p = 0.002$ at 32 weeks) (Fig. 3.19d).

Similar to H, W, V and P cells, S cells also showed significant dendritic loss at 4, 8, 16 and 32 weeks ($p < 0.001$ at 4, 8 and 16 weeks; $p = 0.002$ at 32 weeks) (Fig. 3.19e).

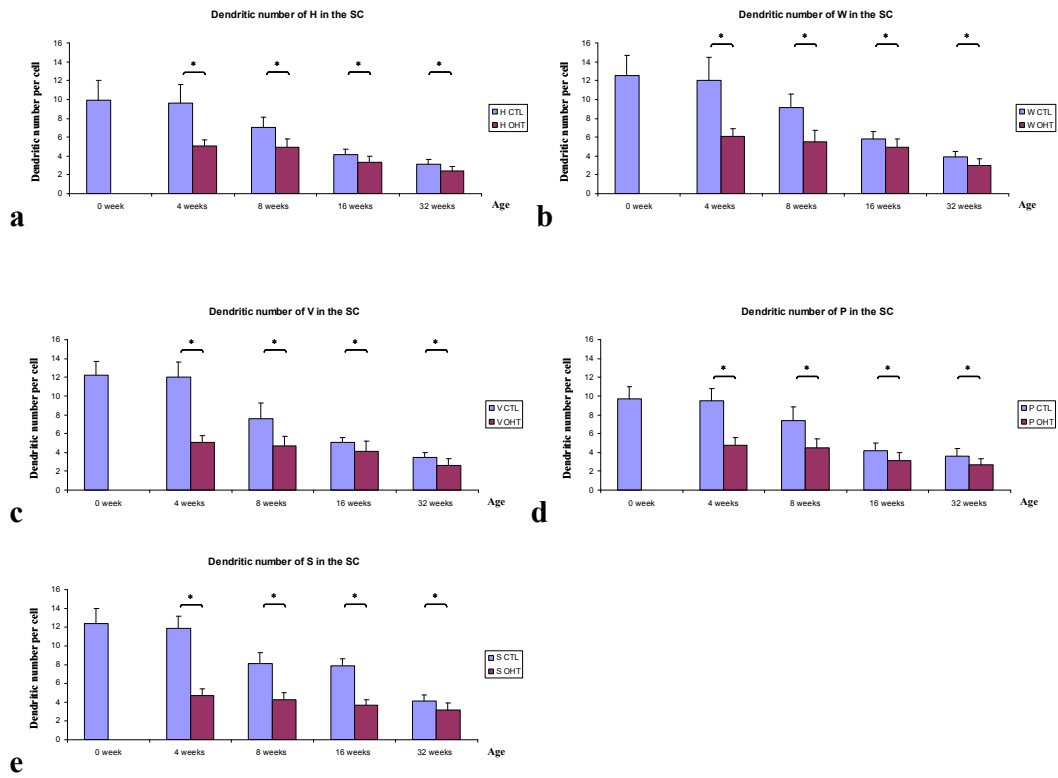


Figure 3.19a-e: Comparison of the dendritic number of SC cells between glaucoma and control animals.

These graphs show changes in the dendritic number of SC cells at 4, 8, 16 and 32 weeks after glaucoma surgery. Five types of cells including H (a); W (b); V (c); P (d) and S (e) were studied respectively (* $p < 0.05$). The error bar represents the SD of the mean.

For each type of cell, furthermore, a percentage reduction in the dendritic number per cell at 4, 8, 16 and 32 weeks after glaucoma surgery was calculated, using the formula below:

$$\text{Percentage reduction in dendritic number per cell (\%)} = \frac{(\text{Dendritic number}_{\text{Age-matched CTL group}} - \text{Dendritic number}_{\text{OHT group}}) * 100}{\text{Dendritic number}_{\text{Age-matched CTL group}}}$$

Fig. 3.20a-e show that the earliest dendritic loss could be observed at 4 weeks after glaucoma surgery (H: 46.88%; W: 49.17%; V: 57.5%; P: 49.47%; S: 60.5%). The peaks of percentage reduction in the dendritic number were also shown at 4 weeks after OHT induction in all five types of cells. The dendritic loss in cells continued from 8 weeks (H: 30%; W: 39.56%; V: 38.16%; P: 39.19%; S: 46.91%), 16 weeks (H: 19.51%; W: 15.52%; V: 19.61%; P: 26.19%; S: 53.16 %) until 32 weeks (H: 22.58 %; W: 23.08%; V: 25.71%; P: 25%; S: 21.95%) after OHT induction.

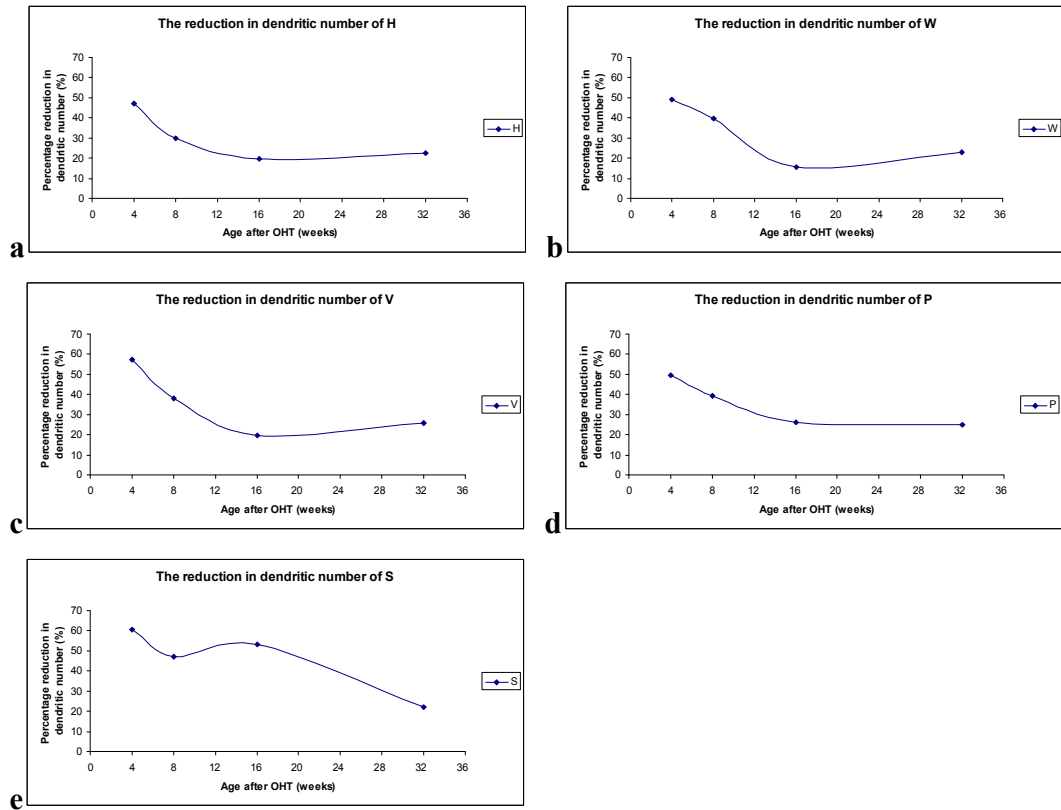


Figure 3.20a-e: Scatter plots of percentage reductions in the dendritic number of SC cells after glaucoma surgery.

These graphs show the dendritic loss in the SC after OHT induction: **(a)** H; **(b)** W; **(c)** V; **(d)** P; **(e)** S.

3.3 Dendritic Changes in the Lateral Geniculate Nucleus

3.3.1 DiI Labelling Methods

Dendritic labelling in the dLGN was achieved by two methods: the injection labelling (Method I) and the retrograde labelling (Method II), which were both assessed on brain slices from 16 weeks glaucoma rats to compare the effects of staining.

Neurons in the dLGN were grouped as LG1 and LG2, and dendritic parameters in each type of cell were analyzed individually. The mean dendritic length and dendritic number of LGN cells labelled by two different methods were compared using the student T-test (Fig. 3.21a, b). Fig. 3.21a shows that there is no significant difference in the mean dendritic length of neurons stained by the Method I and II ($p=0.885$ for LG1; $p=0.633$ for LG2). Fig. 3.21b shows that the dendritic number of neurons stained by two different methods were not significantly different either ($p=0.432$ for LG1; $p=0.271$ for LG2).

The Method I (injection labelling) was employed in the study of dendritic changes in the LGN due to its advantages described as below. Firstly, this *in vitro* method is easier to perform compared with the *in vivo* retrograde labelling. Secondly, The Method I has a shorter period of dye diffusion (1 week) than the Method II does (4 weeks). Thirdly, there would be more risks during both the course of surgery and the dye diffusion period in the Method II, considering that the brain surgery may result in more injuries and the animals need to be kept alive for a long time (4 weeks) after the surgery. Fourthly, the Method I was demonstrated to be equally effective as

the method II. Therefore, the Method I, which is more convenience to perform and less invasive compared with the Method II, was chosen to label LGN neurons in the following study.

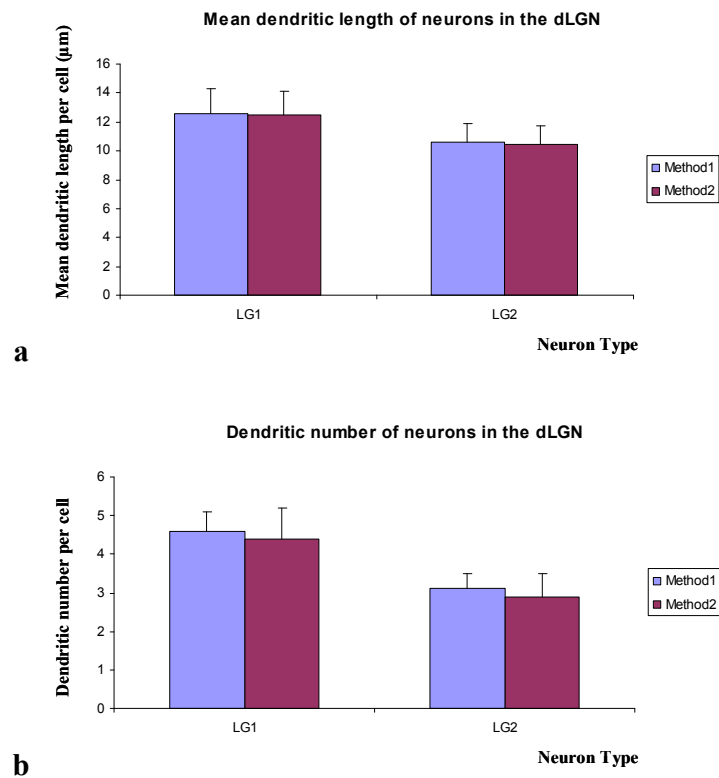


Figure 3.21a, b: Comparison of different methods for labelling cells in the dLGN: (a) Method I; (b) Method II.

These graphs show the comparison of Method I (injection labelling) and II (retrograde labelling). Both mean dendritic length (a) and dendritic number (b) of LG1 and LG2 labelled by two different methods were analyzed.

3.3.2 Classification of Cells in the Rat LGN

In the study of dendritic changes in the dLGN, a total of 270 neurons were imaged and analyzed. These cells were from nine animal groups including 4, 8, 16 and 32 weeks glaucoma animals and their age-matched controls, as well as the baseline group (0 week group). There were 30 cells analyzed for each group, which were further classified into two types as LG1 and LG2, based on the shape and size of their soma and the morphology of their dendrites (Kriebel, 1975) (Fig. 3.22a, b; Table 3.4).

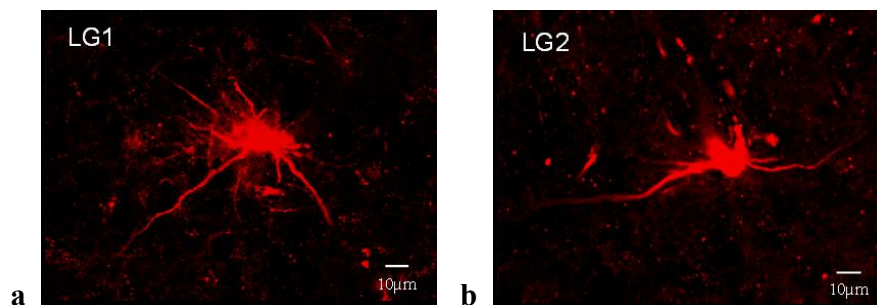


Figure 3.22a, b: Classification of cell types in the rat dorsal lateral geniculate nucleus.

These figures show different types of cells found in the dLGN. There were two types of cells named as: (a), LG1 (Relay neuron type 1) and (b), LG2 (Relay neuron type 2). The images were taken under a x40 oil-immersion lens. Scale bar = 10µm.

Cell type	Soma size (average diameter)	Cell location	Dendritic characteristics
LG1	25 μm	Cells are distributed throughout the dLGN	Cells have 4 to 8 primary dendrites; Dendrites are relatively straight and mostly orientated perpendicular to the optic fibres passing through the dLGN
LG2	20 μm	Cells are only within the superficial zone of the middle third of the dLGN	Dendrites are parallel to the optic fibres, less numerous and shorter

Table 3.4: Characteristics of different types of LGN cells analyzed in this thesis.

3.3.3 Morphological Changes of Dendrites in the Lateral Geniculate

Nucleus

3.3.3.1 Dendritic Changes in Control Animals

3.3.3.1.1 Changes in Mean Dendritic Length

In this study, dendritic parameters in controls animals were analyzed to investigate whether there were ageing effects on dendritic morphology in the LGN. Five groups of control animals including 0, 4, 8, 16 and 32 weeks CTL groups were studied. The 0 week CTL group was baseline group. The 4, 8, 16 and 32 weeks CTL groups were age-matched controls for 4, 8, 16 and 32 weeks glaucoma groups.

The mean dendritic length in different age groups were analyzed and compared using one-way ANOVA and the post hoc Bonferroni test as shown in Fig. 3.23a, b. The error bar represents the SD of the mean.

Fig. 3.23a shows a significant reduction in the mean dendritic length of LG1 from 4 ($28.4 \pm 4.3 \mu\text{m}$) to 8 weeks ($22.9 \pm 1.2 \mu\text{m}$), reaching statistical significance ($p=0.003$). The mean dendritic length was also significantly reduced from 16 ($19.4 \pm 2.7 \mu\text{m}$) to 32 weeks ($14 \pm 2 \mu\text{m}$) ($p=0.004$). However, no significant differences in the mean dendritic length were observed from 0 ($31 \pm 6.8 \mu\text{m}$) to 4 weeks ($p=0.697$) and 8 to 16 weeks ($p=0.153$).

Fig. 3.23b shows that the earliest dendritic shrinkage in LG2 was also at 8 weeks ($19 \pm 2.7 \mu\text{m}$). Significant reductions in the mean dendritic length were observed from 4 ($25.7 \pm 2.7 \mu\text{m}$) to 8 weeks and 16 ($17.2 \pm 2.8 \mu\text{m}$) to 32 weeks ($9.8 \pm 1.5 \mu\text{m}$) ($p < 0.001$ at all time points). However, the mean dendritic length did not change from 0 ($27.7 \pm 2.5 \mu\text{m}$) to 4 weeks ($p=0.304$), or 8 to 16 weeks ($p=0.46$).

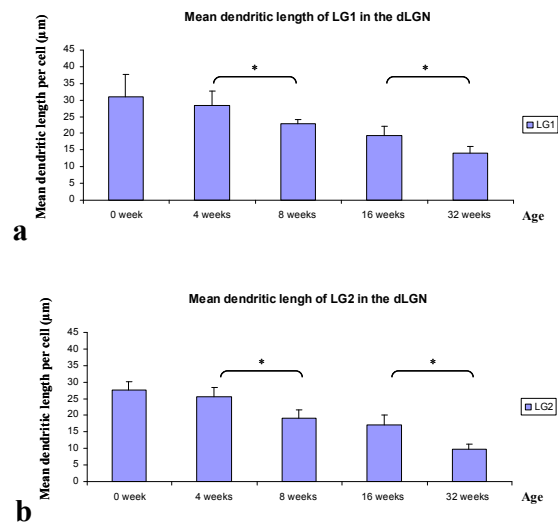


Figure 3.23a, b: Comparison of the mean dendritic length of LGN cells between control groups at different time points.

These figures show the mean dendritic length of cells in the dLGN in control animals. Two types of cells including LG1 (**a**) and LG2 (**b**) were studied individually (* $p < 0.05$). The error bar represents the SD of the mean.

For each type of cell, a percentage reduction in the mean dendritic length per cell was calculated as previously described. Fig. 3.24a, b show an increasing percentage reduction in the mean dendritic length from the baseline (0% for all cells), 4 weeks (LG1: 8.39%; LG2: 7.22%), 8 weeks (LG1: 26.13%; LG2: 31.41%), 16 weeks (LG1: 37.42%; LG2: 37.91%), until 32 weeks (LG1: 54.84%; LG2: 64.62%).

The above results showed that there were significant reductions in the mean dendritic length in the LGN from 0 to 32 weeks over time, indicating that there was an age-dependent dendritic shrinkage in the central visual target in control animals.

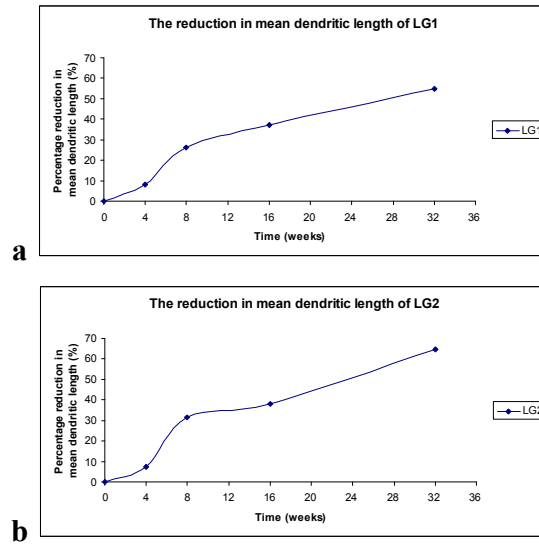


Figure 3.24a-e: Scatter plots of percentage reductions in the mean dendritic length of LGN cells in control groups.

These graphs show the dendritic shrinkage in the LGN in control animals: (a) LG1; (b) LG2.

To determine if there was a relationship between ageing and the mean dendritic length of cells in the LGN, an exponential decay analysis was next performed using SigmaPlot 10.0 (Systat Software Inc.), as shown in Fig. 3.25a, b. The results were also confirmed by analyzing data using Origin Pro 8.1 (Silverdale Scientific Ltd.). The strong regression coefficients (r squared, r^2) suggested that changes in the mean dendritic length of LGN cells were age-related (LG1: $r^2=0.97$; LG2: $r^2=0.96$). The Spearman's correlation test was also performed with a correlation coefficient of -1 ($p<0.001$) for each type of cell, indicating a high

probability of a negative correlation between ageing and the length of dendrites in the LGN.

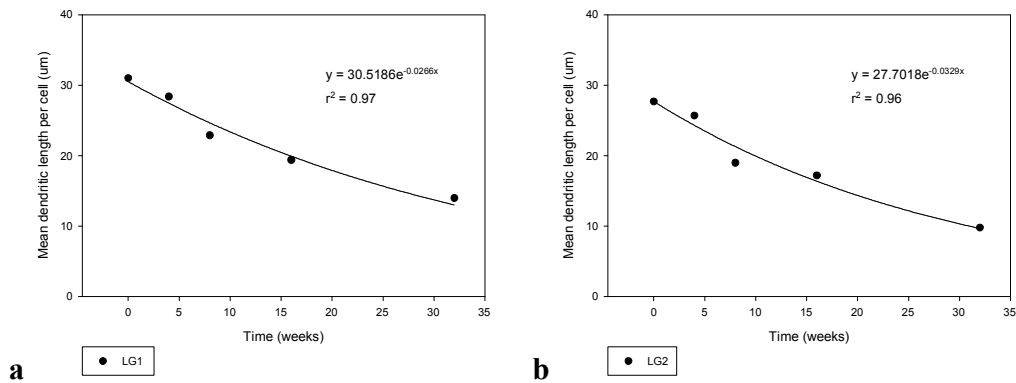


Figure 3.25a, b: The exponential decay of the mean dendritic length of LGN cells in control groups.

These graphs show the exponential regression analysis of the mean dendritic length of LGN cells from control animals: **(a)** LG1; **(b)** LG2.

To characterize the longitudinal profile of dendritic changes, the relationship between the mean dendritic length and the effect of ageing was modelled with exponential decay equations ($y = a \cdot e^{bx}$) and exponential regression analysis. As the decline of mean dendritic length with age fitted well an exponential decay curve, the rate of dendritic shrinkage was approximated based on the exponential regression equation as previously described. Dendrites of LG1 and LG2 from control groups shrunk at a rate of 2.63% (LG1) and 3.24% (LG2) per week during ageing.

3.3.3.1.2 Changes in Dendritic Number

The dendritic number of LGN cells in control animals at different time points were also analyzed and compared using one-way ANOVA and the post hoc Bonferroni test, as shown in Fig 3.26a, b. The error bar represents the SD of the mean.

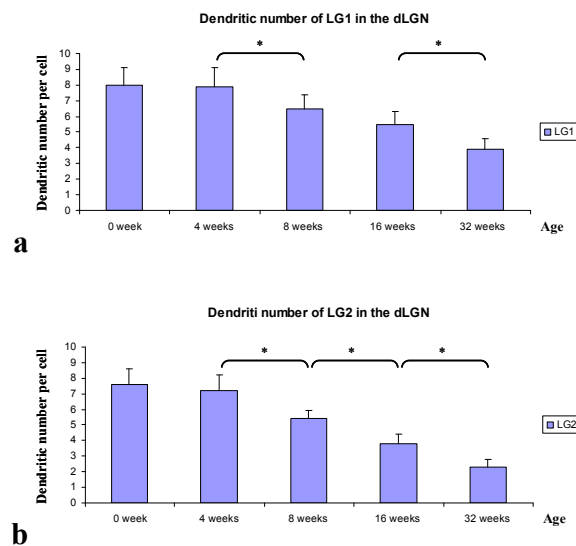


Figure 3.26a, b: Comparison of the dendritic number of LGN cells between control groups at different time points.

These figures show the LGN dendritic number in control animals. Two types of cells including LG1 (a) and LG2 (b) were studied respectively (* $p < 0.05$). The error bar represents the SD of the mean.

LG1 showed the initial dendritic loss from 4 (7.9 ± 1.2) to 8 weeks (6.5 ± 0.9) ($p < 0.001$), reaching statistical significance (Fig. 3.26a). A significant reduction in the dendritic number was also observed from 16 (5.5 ± 0.8) to 32 weeks (3.9 ± 0.7)

($p < 0.001$). However, the dendritic number did not change from 0 (8 ± 1.1) to 4 weeks ($p = 1.0$), and 8 to 16 weeks ($p = 0.074$).

LG2 also showed the earliest dendritic loss at 8 weeks (Fig. 3.26b). The dendritic number significantly decreased from 4 (7.2 ± 1) to 8 weeks (5.4 ± 0.5), 8 to 16 weeks (3.8 ± 0.6), and 16 to 32 weeks (2.3 ± 0.5) ($p < 0.001$ at all time points). However, similar to LG1, LG2 did not show significant dendritic loss from 0 to 4 weeks ($p = 1.0$) either.

A percentage reduction in the dendritic number per cell was next calculated as previously described. Fig. 3.27a, b show an increasing percentage reduction in the dendritic number from the baseline (0% for all cells), 4 weeks (LG1: 1.25%; LG2: 5.26%), 8 weeks (LG1: 18.75%; LG2: 28.95%), 16 weeks (LG1: 31.25%; LG2: 50%), until 32 weeks (LG1: 51.25%; LG2: 69.74%).

All of the above results showed that there were significant reductions in the dendritic number in the LGN from 0 to 32 weeks over time, indicating there was an age-dependent dendritic loss in the central visual targets in control animals.

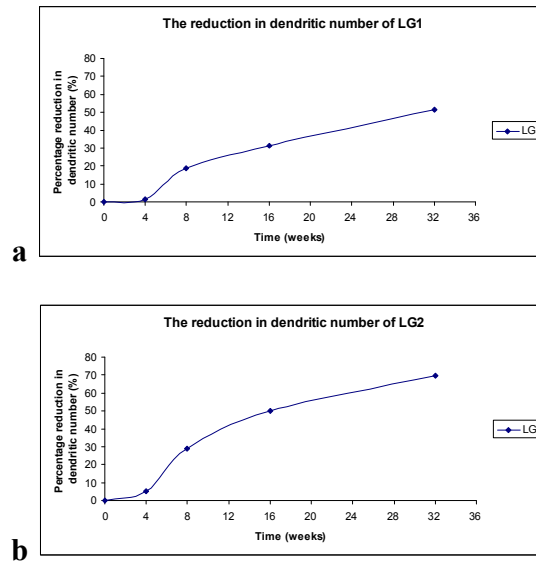


Figure 3.27a-e: Scatter plots of percentage reductions in the dendritic number of LGN cells in control groups.

These graphs show the dendritic loss in the LGN in control animals: **(a)** LG1; **(b)** LG2.

To determine if there was a relationship between ageing and the dendritic number of cells in the LGN, an exponential decay analysis was next performed using SigmaPlot 10.0 (Systat Software Inc.), as shown in Fig. 3.28a, b. The results were also confirmed by analyzing data using Origin Pro 8.1 (Silverdale Scientific Ltd.). The strong regression coefficients (r^2) suggested that changes in the dendritic number of LGN cells were age-related (LG1: $r^2=0.97$; LG2: $r^2=0.97$). The Spearman's correlation test was also performed with a correlation coefficient of -1 ($p<0.001$) for each type of cell, indicating a high probability of a negative correlation between ageing and the number of dendrites in the LGN.

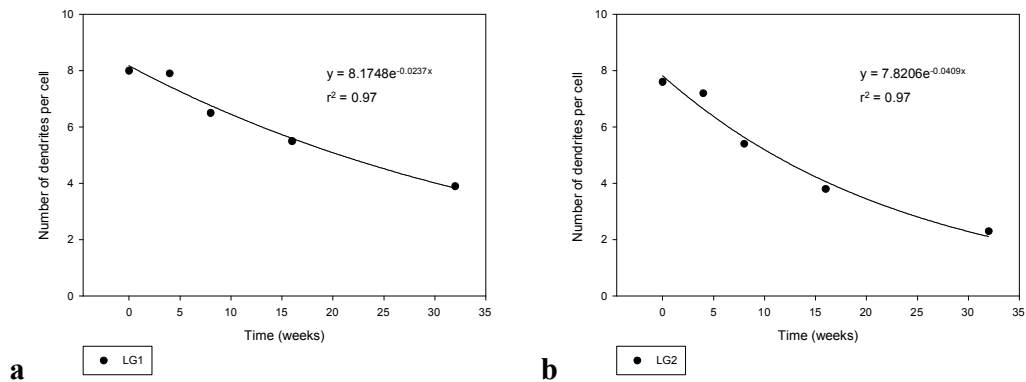


Figure 3.28a, b: The exponential decay of the dendritic number of LGN cells in control groups.

These graphs show the exponential regression analysis of the dendritic number of LGN cells from control animals: **(a)** LG1; **(b)** LG2.

To characterize the longitudinal profile of dendritic changes, the relationship between the dendritic number and the effect of ageing was modelled with exponential decay equations ($y = a \cdot e^{bx}$) and exponential regression analysis. As the decline of dendritic number with age fitted well an exponential decay curve, the rate of dendritic loss was approximated based on the exponential regression equation as previously described. Dendrites of LG1 and LG2 from control groups were lost at a rate of 2.34% (LG1) and 4.01% (LG2) per week during ageing.

3.3.3.2 Dendritic Changes in Glaucoma Animals

3.3.3.2.1 Changes in Mean Dendritic Length

Dendritic parameters, the mean dendritic length and dendritic number, were also analyzed in the study of dendritic changes in the dLGN in glaucoma animals.

The mean dendritic length of each type of cell from the baseline group (0 week), and 4, 8, 16 and 32 weeks glaucoma groups were analyzed and compared. The comparison of mean dendritic length of cells from different groups was performed using one-way ANOVA and the post hoc Bonferroni test. Changes in the mean dendritic length of LG1 and LG2 were studied respectively, as shown in Fig. 3.29a, b. The error bar represents the SD of the mean.

Dendritic shrinkage in LG1 was observed from 4 ($27.9 \pm 5.7 \mu\text{m}$) to 8 weeks ($15.9 \pm 2.1 \mu\text{m}$), reaching statistical significance ($p < 0.001$) (Fig. 3.29a). The mean dendritic length was further reduced significantly from 8 to 32 weeks ($9.1 \pm 1.5 \mu\text{m}$) ($p < 0.001$). However, no significant reductions in the mean dendritic length were observed from 0 ($31 \pm 6.8 \mu\text{m}$) to 4 weeks ($p = 0.445$), 8 to 16 weeks ($12.6 \pm 1.7 \mu\text{m}$) ($p = 0.311$), and 16 to 32 weeks ($p = 0.279$) after OHT induction.

LG2 showed the earliest reduction in the mean dendritic length at 4 weeks ($24 \pm 2.2 \mu\text{m}$) after OHT induction compared to that at 0 week ($27.7 \pm 2.5 \mu\text{m}$) ($p < 0.001$), reaching statistical significance (Fig. 3.29b). Significant dendritic shrinkage were also observed from 4 to 8 weeks ($13.4 \pm 1 \mu\text{m}$), 8 to 16 weeks ($10.6 \pm 1.3 \mu\text{m}$), and 16 to 32 weeks ($7.7 \pm 1.2 \mu\text{m}$) after OHT induction ($P < 0.001$ at all time points).

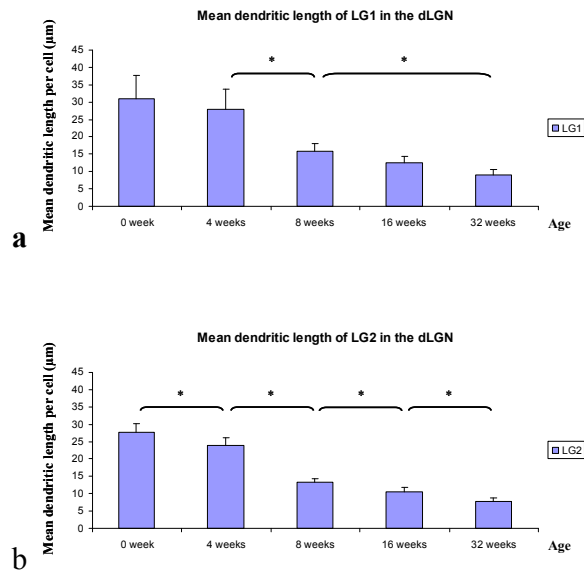


Figure 3.29a, b: Comparison of the mean dendritic length of LGN cells between glaucoma groups at different time points.

These figures show the mean dendritic length of cells in the dLGN from the baseline and glaucoma animals. Two types of cells including LG1 (a) and LG2 (b) were studied respectively (* $p < 0.05$). The error bar represents the SD of the mean.

A percentage reduction in the mean dendritic length per cell was also calculated as previously described. Fig. 3.30a, b show an increasing percentage reduction in mean dendritic length from the baseline (0% for all cells), 4 weeks (LG1: 10%; LG2: 13.36%), 8 weeks (LG1: 48.71%; LG2: 51.62%), 16 weeks (LG1: 59.35%; LG2: 61.73%), until 32 weeks (LG1: 70.65%; LG2: 72.2%).

The above results showed that there were significant reductions in the mean dendritic length in the LGN from 4 to 32 weeks over time, indicating there was an age-dependent dendritic shrinkage in the central visual target in glaucoma animals.

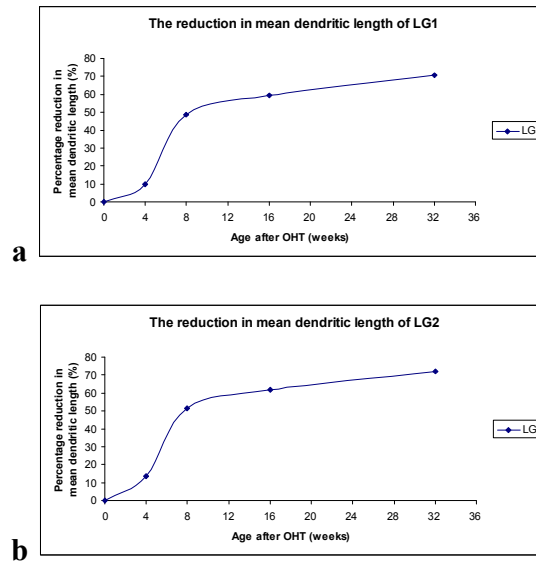


Figure 3.30a, b: Scatter plots of percentage reductions in the mean dendritic length of LGN cells in glaucoma groups.

These graphs show the dendritic shrinkage in the LGN in glaucoma animals: (a) LG1; (b) LG2.

To determine if there was a relationship between ageing and the mean dendritic length of cells in the LGN in glaucoma animals, an exponential decay analysis was performed using SigmaPlot 10.0 (Systat Software Inc.), as shown in Fig. 3.31a, b. The results were also confirmed by analyzing data using Origin Pro 8.1 (Silverdale Scientific Ltd.). The strong regression coefficients (r^2) suggested that changes in the mean dendritic length of LGN cells were age-related (LG1: $r^2=0.89$; LG2: $r^2=0.86$). The Spearman's correlation test was also performed with a correlation coefficient of -1 ($p<0.001$) for each type of cell, indicating a high probability of a negative correlation between ageing and the length of dendrites in the LGN in glaucoma animals.

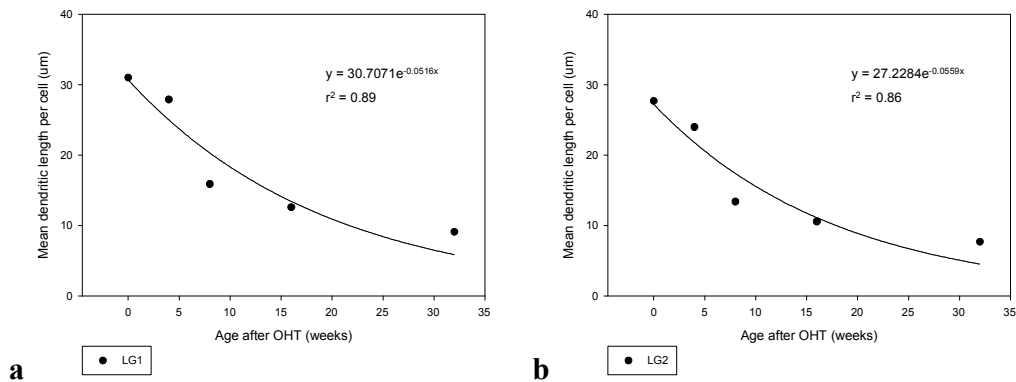


Figure 3.31a, b: The exponential decay of the mean dendritic length of LGN cells in glaucoma groups.

These graphs show the exponential regression analysis of the mean dendritic length of LGN cells in glaucoma animals: (a) LG1; (b) LG2.

To characterize the longitudinal profile of dendritic changes, the relationship between the mean dendritic length and the effect of ageing was modelled with exponential decay equations ($y = a \cdot e^{bx}$) and exponential regression analysis. As the decline of mean dendritic length with age fitted well an exponential decay curve, the rate of dendritic shrinkage was approximated based on the exponential regression equation as previously described. Dendrites of LG1 and LG2 from glaucoma groups shrunk at a rate of 5.03% (LG1) and 5.44% (LG2) per week. The rates of dendritic shrinkage in glaucoma groups and those in control groups were summarised as shown in Table 3.5.

Groups	Rates of dendritic shrinkage (weekly)	
	LG1	LG2
Control	2.63%	3.24%
Glaucoma	5.03%	5.44%

Table 3.5: Summary of the rates of dendritic shrinkage in glaucoma and control animals.

3.3.3.2.2 Changes in Dendritic Number

The dendritic number of LGN cells from the baseline group and 4, 8, 16 and 32 weeks glaucoma groups were analyzed and compared using one-way ANOVA and the post hoc Bonferroni test (Fig 3.32a, b). The error bar represents SD of the mean.

LG1 initially showed significant dendritic loss at 8 weeks after OHT induction (5.4 ± 0.9) ($p < 0.001$) (Fig. 3.32a). A significant reduction in the dendritic number was also shown from 16 (4.6 ± 0.5) to 32 weeks (3.1 ± 0.5) ($p < 0.001$) after OHT induction. However, no significant dendritic losses were shown from the baseline (8 ± 1.1) to 4 week (7.8 ± 1.1) ($p = 1.0$), and 8 to 16 weeks after OHT induction ($p = 0.144$).

LG2 showed the earliest dendritic loss at 4 weeks after OHT induction (6.6 ± 1.2) compared to the baseline (7.6 ± 1) ($p < 0.05$) (Fig. 3.32b). The dendritic number was also significantly decreased from 4 to 8 weeks (3.7 ± 0.5) ($p < 0.001$), and 16 (3.1 ± 0.4) to 32 weeks (2 ± 0.7) ($p < 0.05$) after OHT induction. However, the dendritic number did not change from 8 to 16 weeks after OHT induction ($p = 0.462$).

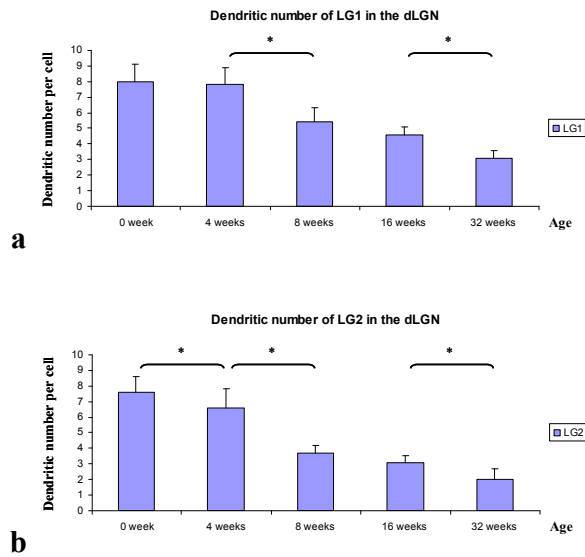


Figure 3.32a, b: Comparison of the dendritic number of LGN cells between glaucoma groups at different time points.

These figures show the dendritic number of cells in the dLGN from glaucoma groups. Two types of cells including LG (a) and LG2 (b) were studied respectively (* $p < 0.05$). The error bar represents the SD of the mean.

A percentage reduction in the dendritic number per cell was calculated as described before. Fig. 3.33a, b show an increasing percentage reduction in the dendritic number from the baseline (0% for all cells), 4 weeks (LG1: 2.5%; LG2: 13.16%), 8 weeks (LG1: 32.5%; LG2: 51.32%), 16 weeks (LG1: 42.5%; LG2: 59.21%), until 32 weeks (LG1: 61.25%; LG2: 73.68%).

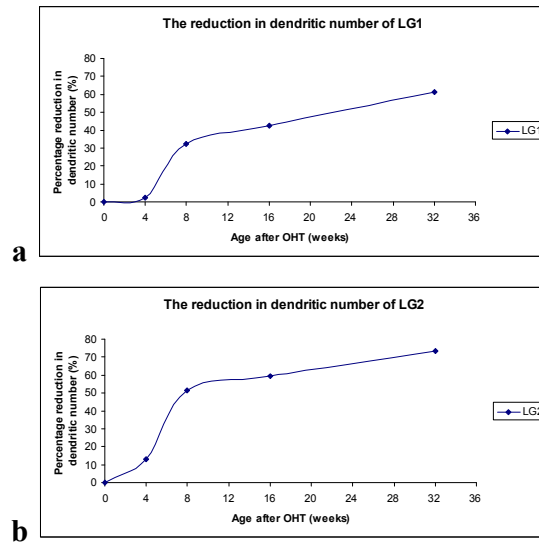


Figure 3.33a-e: Scatter plots of percentage reductions in the dendritic number of LGN cells in glaucoma groups.

These graphs show the dendritic loss in the LGN in glaucoma animals: **(a)** LG1; **(b)** LG2.

The above results showed that there were significant reductions in the dendritic number of LGN cells from 4 to 32 weeks over time, indicating there was an age-dependent dendritic loss in the central visual target in glaucoma animals.

To determine if there was a relationship between ageing and the dendritic number of cells in the LGN in glaucoma animals, an exponential decay analysis was next performed, as shown in Fig. 3.34a, b. The strong regression coefficients (r^2) suggested that changes in the dendritic numbers of LGN cells were age-related (LG1: $r^2=0.93$; LG2: $r^2=0.91$). The Spearman's correlation test was also performed with a correlation coefficient of -1 ($p<0.001$) for each type of cell, indicating a high probability of a negative correlation between ageing and the number of dendrites in the LGN in glaucoma animals.

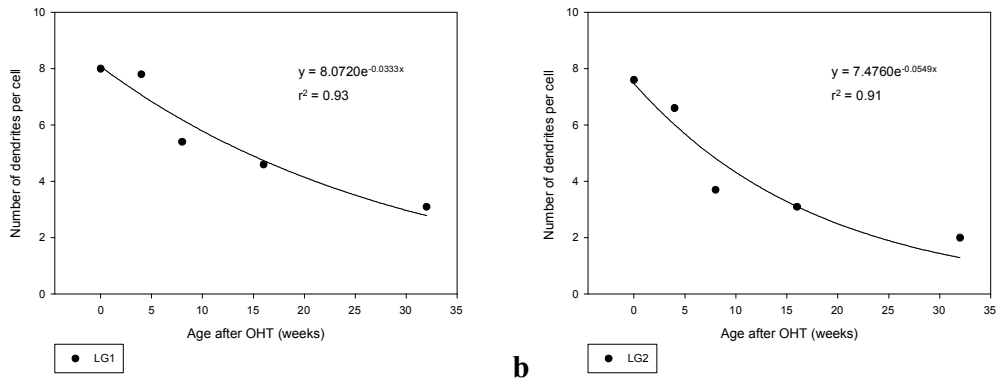


Figure 3.34a, b: The exponential decay of the dendritic number of LGN cells in glaucoma groups.

These graphs show the exponential regression analysis of the dendritic number of LGN cells from glaucoma animals: **(a)** LG1; **(b)** LG2.

To characterize the longitudinal profile of dendritic changes, the relationship between the dendritic number and the effect of ageing was modelled with exponential decay equations ($y = a \cdot e^{bx}$) and exponential regression analysis. As the decline of dendritic number with age fitted well an exponential decay curve, the rate of dendritic loss was approximated based on the exponential regression equation as previously described. Dendrites of LG1 and LG2 from glaucoma groups were lost at a rate of 3.28% (LG1) and 5.34% (LG2) per week. The rates of dendritic loss in glaucoma groups and those in control groups were summarised as shown in Table 3.6.

Groups	Rates of dendritic loss (weekly)	
	LG1	LG2
Control	2.34%	4.01%
Glaucoma	3.28%	5.34%

Table 3.6: Summary of the rates of dendritic loss in glaucoma and control animals.

3.3.3.3 Comparison of Dendritic Parameters between Glaucoma and Control Animals

3.3.3.3.1 Comparison of Mean Dendritic Length

The effects of elevated IOP on dendritic morphology in the dLGN were also investigated by comparing dendritic parameters between glaucoma rats and age matched controls. The mean dendritic lengths of LG1 and LG2 were studied at 4, 8, 16 and 32 weeks respectively. The comparison of the mean dendritic length between glaucoma groups and age-matched controls were performed using the student T-test. Fig. 3.35a, b show that there were significant reductions in the mean dendritic length in glaucoma animals at 8, 16 and 32 weeks after OHT induction. The error bar represents the SD of the mean.

Fig. 3.35a shows that the mean dendritic length of LG1 was significantly reduced at 8, 16 and 32 weeks after glaucoma surgery compared to age-matched controls, indicating that the dendritic shrinkage was also related to elevated IOP ($p < 0.001$ at all time points). The graph clearly shows that the initial dendritic

shrinkage occurred at 8 weeks after OHT induction. However, no dendritic shrinkage was observed at 4 weeks after glaucoma surgery ($p=0.793$).

Fig. 3.35b shows that the mean dendritic length of LG2 was also significantly reduced at 8, 16 and 32 weeks after glaucoma surgery compared to age-matched controls ($p<0.001$ at all time points). LG2 also showed the earliest dendritic shrinkage at 8 weeks after OHT induction, but no dendritic shrinkage at 4 weeks ($p=0.068$).

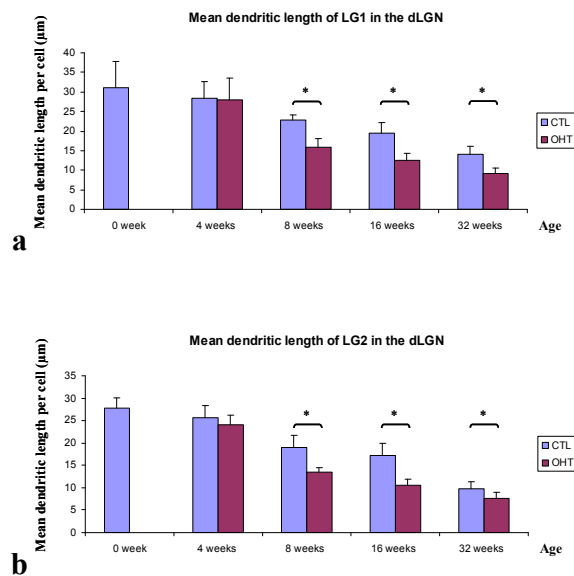


Figure 3.35a, b: Comparison of the mean dendritic length of LGN cells between glaucoma and control groups.

These figures show changes in the mean dendritic length of LGN cells at 4, 8, 16 and 32 weeks after glaucoma surgery. Two types of cells including LG1 (**a**) and LG2 (**b**) were studied respectively ($*p<0.05$). The error bar represents the SD of the mean.

For each type of cell, a percentage reduction in the mean dendritic length of cells at 4, 8, 16 and 32 weeks after glaucoma surgery was calculated as previously described (Fig. 3.36a, b).

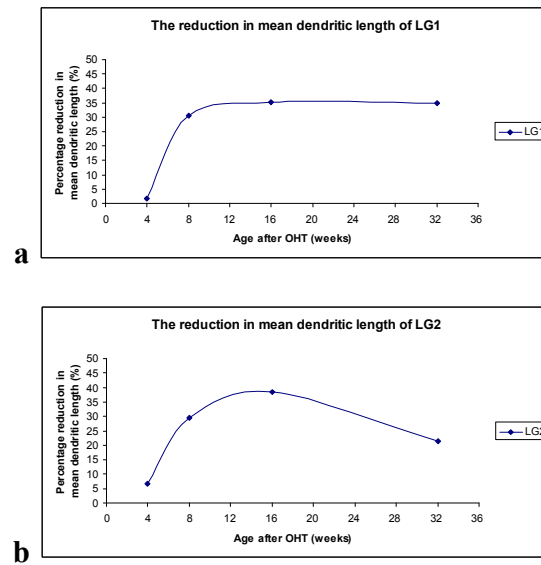


Figure 3.36a, b: Scatter plots of percentage reductions in the mean dendritic length of LGN cells after glaucoma surgery.

These graphs show the dendritic shrinkage in the LGN after glaucoma surgery: (a) LG1; (b) LG2.

Fig. 3.36a shows percentage reductions in the mean dendritic length in LG1 were 1.76% (4 weeks), 30.57% (8 weeks), 35.05% (16 weeks) and 35% (32 weeks). It was from 8 weeks after OHT induction that significant dendritic shrinkage could be observed. A similar amount of dendritic shrinkage was shown at 16 and 32 weeks.

Fig. 3.36b shows percentage reductions in the mean dendritic length in LG2 were 6.61% (4 weeks), 29.47% (8 weeks), 38.37% (16 weeks) and 21.43% (32 weeks). The peak time point of dendritic shrinkage in LG2 was at 16 weeks after OHT induction. A lesser amount of dendritic shrinkage was shown at 32 weeks after OHT induction than that at 16 weeks.

3.3.3.3.2 Comparison of Dendritic Number

The effects of OHT on dendritic number of LG1 and LG2 were also investigated at 4, 8, 16 and 32 weeks after OHT induction (Fig. 3.37a, b). The comparison of the dendritic number between glaucoma groups and age-matched controls was performed using the student T-test. The error bar represents the SD of the mean.

Fig. 3.37a shows that the dendritic number of LG1 was significantly reduced at 8, 16 and 32 weeks after glaucoma surgery compared to age-matched controls, indicating that the dendritic loss was also related to elevated IOP ($p=0.003$ at 8 weeks; $p=0.002$ at 16 weeks; $p=0.004$ at 32 weeks). This graph also shows the earliest dendritic loss in LG1 at 8 weeks OHT. However, no changes in the dendritic number were shown at 4 weeks after glaucoma surgery compared to controls ($p=0.877$).

Fig. 3.37b shows that the dendritic number of LG2 was significantly reduced at 8 and 16 weeks after glaucoma surgery ($p<0.001$ at 8 weeks; $p=0.001$ at 16 weeks). The earliest dendritic loss in LG2 also occurred at 8 weeks after OHT induction. The

number of dendrites did not change at 4 and 32 weeks after glaucoma surgery compared to age-matched controls ($p=0.158$ at 4 weeks; $p=0.125$ at 32 weeks).

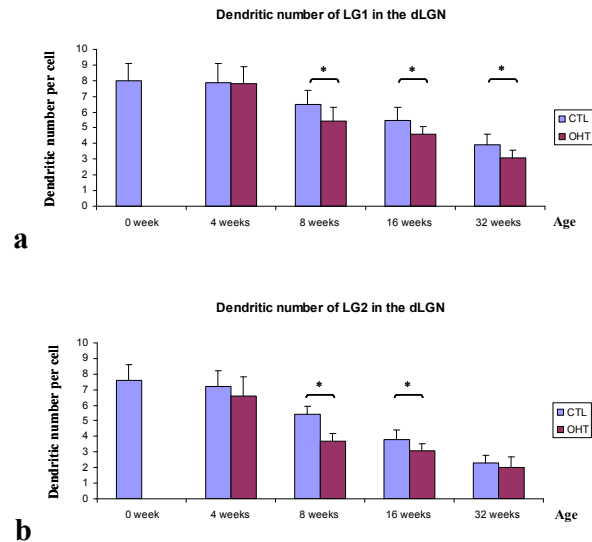


Figure 3.37a, b: Comparison of the dendritic number of LGN cells between glaucoma and control groups.

These figures show changes in the dendritic number of LGN cells at 4, 8, 16 and 32 weeks after glaucoma surgery. Two types of cells including LG1 (a) and LG2 (b) were studied respectively ($*p<0.05$). The error bar represents the SD of the mean.

For each type of cell, a percentage reduction in the dendritic number of cells at 4, 8, 16 and 32 weeks after glaucoma surgery was also calculated as previously described (Fig. 3.38a, b).

Fig. 3.38a shows percentage reductions in the dendritic number in LG1 were 1.27% (4 weeks), 16.92% (8 weeks), 16.36% (16 weeks) and 20.51% (32 weeks). It

was from 8 weeks after OHT induction that significant dendritic loss could be observed. There was a similar amount of dendritic loss shown at 8 and 16 weeks, however, a greater dendritic loss was observed at 32 weeks after OHT induction.

Fig. 3.38b shows percentage reductions in the dendritic number in LG2 were 8.33% (4 weeks), 31.48% (8 weeks), 18.42% (16 weeks) and 13.04% (32 weeks). The peak time point of dendritic loss in LG2 was at 8 weeks after OHT induction. However, the amount of dendritic loss was decreased at 16 and 32 weeks.

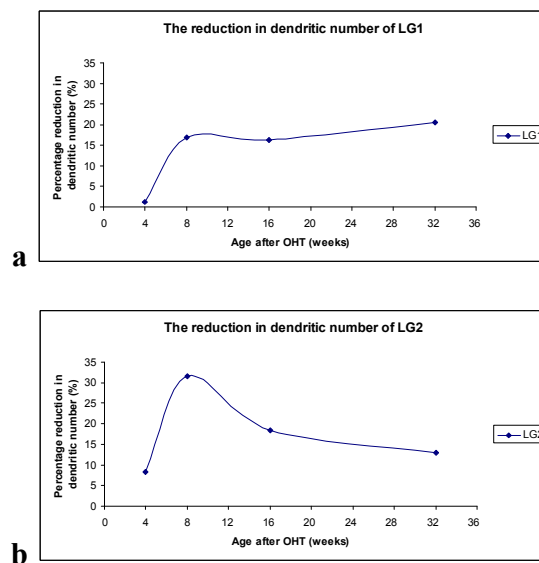


Figure 3.38a, b: Scatter plots of percentage reductions in the dendritic number of LGN cells after glaucoma surgery.

These graphs show the dendritic loss in the LGN after glaucoma surgery: (a) LG1; (b) LG2.

3.4 Dendritic Changes in the Retina

3.4.1 DiI Labelling Method

In this study, dendritic labelling in RGCs in the retina was achieved by the biolistic staining using fluorescent dye DiI. The biolistic staining method was demonstrated as an effective and efficient technique for RGC labelling. RGCs were successfully labelled using DiI by a Helios gene gun, showing complete structures of cells.

3.4.2 Classification of Retinal Ganglion Cells in the Retina

In the study of dendritic changes in RGCs in the retina, 11 groups of retinas were analyzed including 1, 4, 8, 16 and 32 weeks glaucoma groups and their age-matched controls, as well as the baseline group (0 week group). The retinas in 0 week group were at the age when the glaucoma surgery was performed for OHT groups. A total of 495 RGCs were imaged using the Zeiss confocal microscope under a x16 oil-immersion lens, with 45 cells analyzed for each group. The RGCs were further classified into three types as RI, RII and RIII according to their soma size and dendritic morphology (Perry, 1979) (Fig. 3.39a-c; Table 3.7).

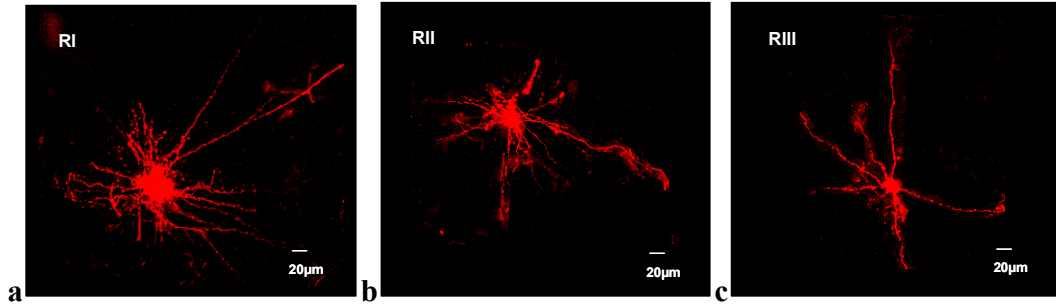


Figure 3.39a-c: Classification of RGC types in the rat retina: (a) RI; (b) RII; (c) RIII.

These figures show images of RGCs taken under a x16 oil-immersion lens. RGCs were classified into three types as: **(a)**, RI (RGC type I); **(b)**, RII (RGC type II); **(c)**, RIII (RGC type III); Scale bar = 20µm.

Cell type	Soma size (average diameter)	Dendritic characteristics
RI	Large (20.4µm)	Large dendritic field (average diameter of 312µm)
RII	Small (13.5µm)	Small dendritic field (average diameter of 150µm)
RIII	Small to medium (12.1µm)	Large dendritic field (average diameter of 339 µm)

Table 3.7: Characteristics of different types of RGCs analyzed in this thesis.

3.4.3 Morphological Changes of Dendrites in the Retina

3.4.3.1 Dendritic Changes in Control Animals

3.4.3.1.1 Changes in Mean Dendritic Length

In this study, dendritic parameters in control animals were analyzed to investigate the effects of ageing on dendritic morphology in RGCs. Six groups of control animals including 0, 1, 4, 8, 16 and 32 weeks CTL groups were studied. The mean dendritic lengths of RGCs in different age groups were analyzed and compared using one-way ANOVA and the post hoc Bonferroni test. Fig. 3.40a-c show that there were significant reductions in the mean dendritic length in all types of cells during ageing. The error bar represents the SD of the mean.

Fig. 3.40a shows that the mean dendritic length of RI was initially reduced at 8 weeks ($56 \pm 7.1 \mu\text{m}$) compared to that at 4 weeks ($74.3 \pm 8.1 \mu\text{m}$), reaching statistical significance ($p < 0.001$). A significant reduction in the mean dendritic length was also observed from 8 to 16 weeks ($35.3 \pm 5.5 \mu\text{m}$) ($p < 0.001$). However, it did not show significant dendritic shrinkage from 0 ($83.2 \pm 11.6 \mu\text{m}$) to 1 week ($80.9 \pm 11.3 \mu\text{m}$) ($p = 1.0$), 1 to 4 weeks ($p = 0.56$), or 16 to 32 weeks ($27.9 \pm 4.3 \mu\text{m}$) ($p = 0.3$).

Fig. 3.40b shows that the initial dendritic shrinkage in RII occurred at 4 weeks ($43.9 \pm 6.7 \mu\text{m}$) compared to that at 1 week ($49 \pm 5.7 \mu\text{m}$), reaching statistical significance ($p = 0.045$). The mean dendritic length was further reduced significantly from 4 to 8 weeks ($30.7 \pm 5.3 \mu\text{m}$) ($p < 0.001$), and 8 to 16 weeks ($19.5 \pm 1.6 \mu\text{m}$) ($p < 0.001$). However, it did not show significant dendritic shrinkage from 0 ($51.9 \pm 3.8 \mu\text{m}$) to 1 week ($p = 1.0$), or 16 to 32 weeks ($15.4 \pm 1.8 \mu\text{m}$) ($p = 0.266$).

Fig. 3.40c shows that the initial dendritic shrinkage in RIII was also shown at 8 weeks ($51.9 \pm 7.8 \mu\text{m}$) compared to that at 4 weeks ($68 \pm 7.4 \mu\text{m}$), reaching statistical significance ($p < 0.001$). Significant dendritic shrinkage was also shown from 8 to 16 weeks ($30.2 \pm 3.6 \mu\text{m}$) ($p < 0.001$). However, the mean dendritic length did not change from 0 ($75.7 \pm 9.4 \mu\text{m}$) to 1 week ($75 \pm 8.2 \mu\text{m}$) ($p = 1.0$), 1 to 4 weeks ($p = 0.134$), or 16 to 32 weeks ($26.2 \pm 4.3 \mu\text{m}$) ($p = 1.0$).

For each type of cell, a percentage reduction in the mean dendritic length per cell was calculated as previously described. Fig. 3.41a-c show an increasing percentage reductions in the mean dendritic length of RGCs from the baseline (0% for all cells), 1 week (RI: 2.76%; RII: 5.59%; RIII: 0.92%), 4 weeks (RI: 10.7%; RII: 15.41%; RIII: 10.17%), 8 weeks (RI: 32.69%; RII: 40.85%; RIII: 31.44%), 16 weeks (RI: 57.57%; RII: 62.43%; RIII: 60.11%), until 32 weeks (RI: 66.47%; RII: 70.33%; RIII: 65.39%).

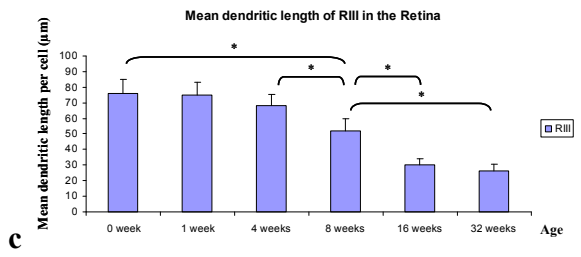
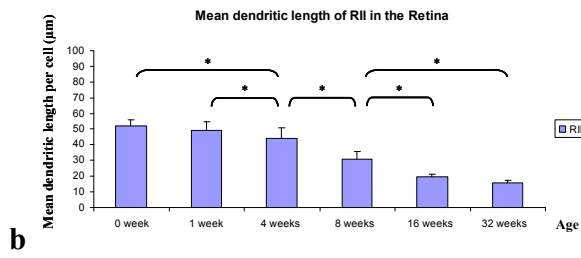
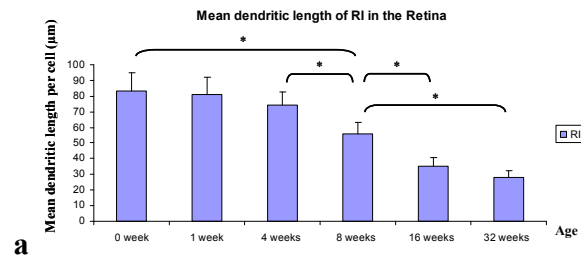


Figure 3.40a-c: Comparison of the mean dendritic length of RGCs between control groups at different time points.

These figures show the mean dendritic length of RGCs in control animals. Three types of cells including RI (a), RII (b) and RIII (c) were studied respectively (* $p < 0.05$). The error bar represents the SD of the mean.

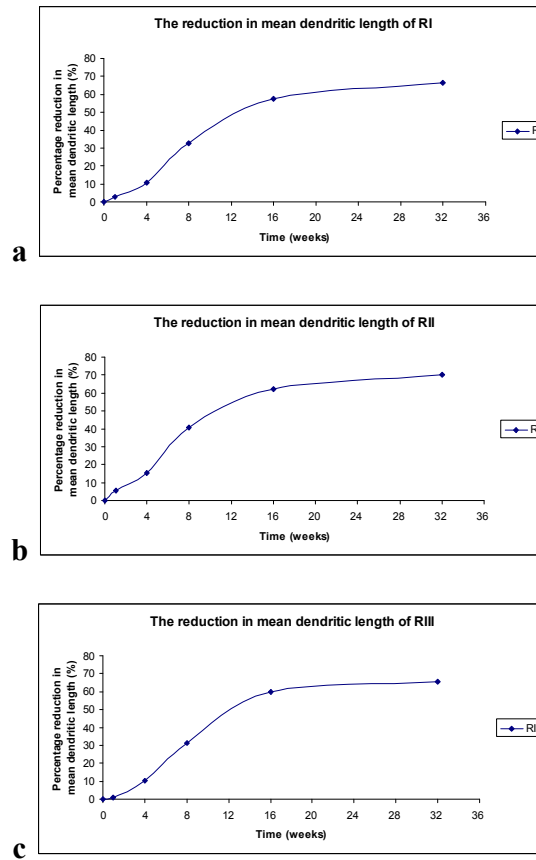


Figure 3.41a-c: Scatter plots of percentage reductions in the mean dendritic length of RGCs in control groups.

These graphs show the dendritic shrinkage in RGCs from control animals: (a) RI; (b) RII; (c) RIII.

To determine if there was a relationship between ageing and the mean dendritic length of RGCs in control animals, an exponential decay analysis was performed, as shown in Fig. 3.42a-c. The strong regression coefficients (r^2) suggested that changes in the mean dendritic length of RGCs was age-related (RI: $r^2=0.96$; RII: $r^2=0.95$; RIII: $r^2=0.94$). The Spearman's correlation test was also performed with a correlation coefficient of -1 ($p<0.001$) for each type of cell,

indicating a high probability of a negative correlation between ageing and the mean dendritic length of RGCs in control animals.

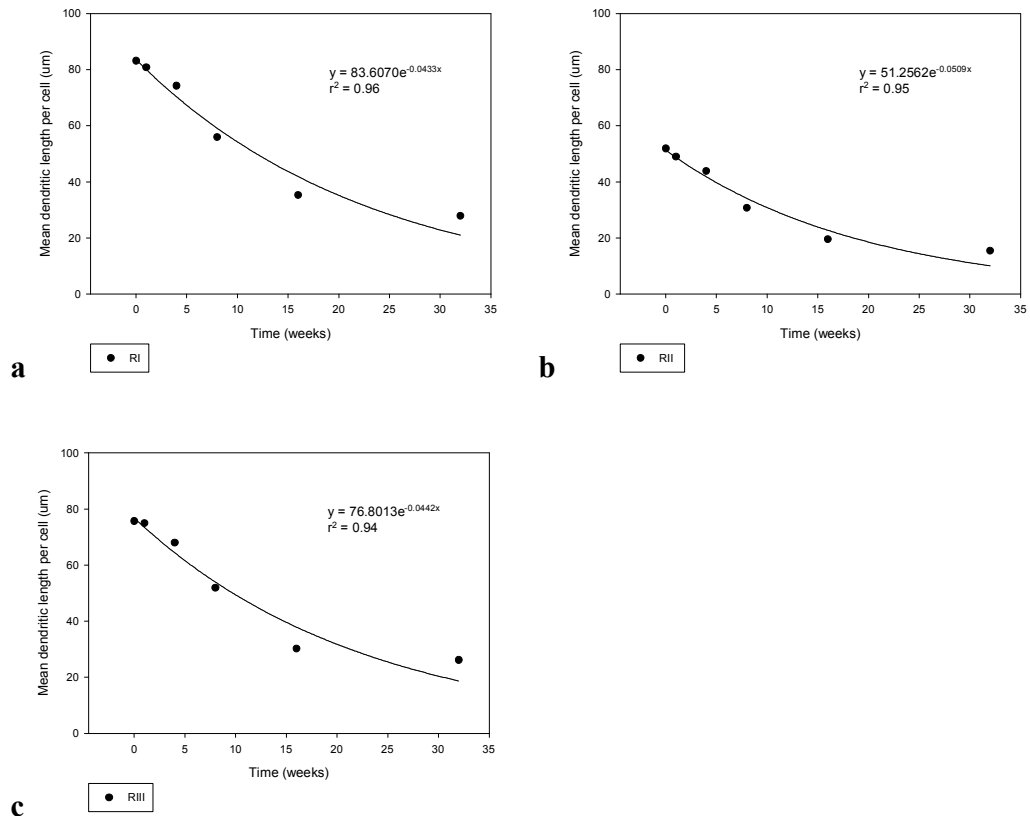


Figure 3.42a-c: The exponential decay of the mean dendritic length of RGCs in control groups.

These graphs show the exponential regression analysis of the mean dendritic length of RGCs from control animals: (a) RI; (b) RII; (c) RIII.

To characterize the longitudinal profile of dendritic changes, the relationship between the mean dendritic length and the effect of ageing was modelled with

exponential decay equations ($y = a \cdot e^{bx}$) and exponential regression analysis. As the decline of mean dendritic length with age fitted well an exponential decay curve, the rate of dendritic shrinkage was approximated based on the exponential regression equation as previously described. Dendrites of RI, RII and RIII from control groups shrunk at a rate of 4.24% (RI); 4.96% (RII) and 4.32% (RIII) per week during ageing.

3.4.3.1.2 Changes in Dendritic Number

The dendritic number of RGCs from control animals was also counted and compared between different age groups using one way ANOVA and the post hoc Bonferroni test. Fig 3.43a-c show that there was significant dendritic loss in all types of cells during ageing. The error bar represents the SD of the mean.

RI showed the earliest dendritic loss at 4 weeks (15.3 ± 5.2) (Fig. 3.43a). Significant reductions in the dendritic number were shown from 1 (20.9 ± 6) to 4 weeks ($p=0.029$), and 4 to 32 weeks (6.6 ± 1.9) ($p<0.001$). However, no differences in the dendritic number were shown between the baseline (21.6 ± 6.8) and 1 week ($p=1.0$), 4 and 8 weeks (15.3 ± 5.2) ($p=1.0$), 8 and 16 weeks (8.4 ± 1.7) ($p=0.091$), or 16 and 32 weeks groups ($p=1.0$).

RII showed the initial dendritic loss at 8 weeks (6.7 ± 2.1) (Fig. 3.43b). Significant dendritic loss was shown from 4 (10.9 ± 3.1) to 8 weeks ($p<0.001$), and 4 to 32 weeks (4.8 ± 1.1) ($p<0.001$). However, the dendritic number was not significantly decreased from 0 (13.3 ± 3.5) to 1 week (12.2 ± 3) ($p=1.0$), 1 to 4 weeks ($p=1.0$), 8 to 16 weeks (5.5 ± 1.4) ($p=1.0$), or 16 to 32 weeks ($p=1.0$).

The initial dendritic loss in RIII was shown at 4 weeks (9.1 ± 1.6) ($p=0.001$) (Fig. 3.43c). Significant reductions in the dendritic number were also observed from 8 (8.9 ± 2.4) to 16 weeks (5.2 ± 1.2) and 8 to 32 weeks (4.5 ± 0.8) ($p < 0.001$ at all time points). However, the comparison of dendritic number did not show significant difference between the baseline (12.3 ± 3.5) and 1 week (11.1 ± 2.5) ($p=1.0$), 1 and 4 weeks ($p=0.171$), 4 and 8 weeks ($p=1.0$), or 16 and 32 weeks groups ($p=1.0$).

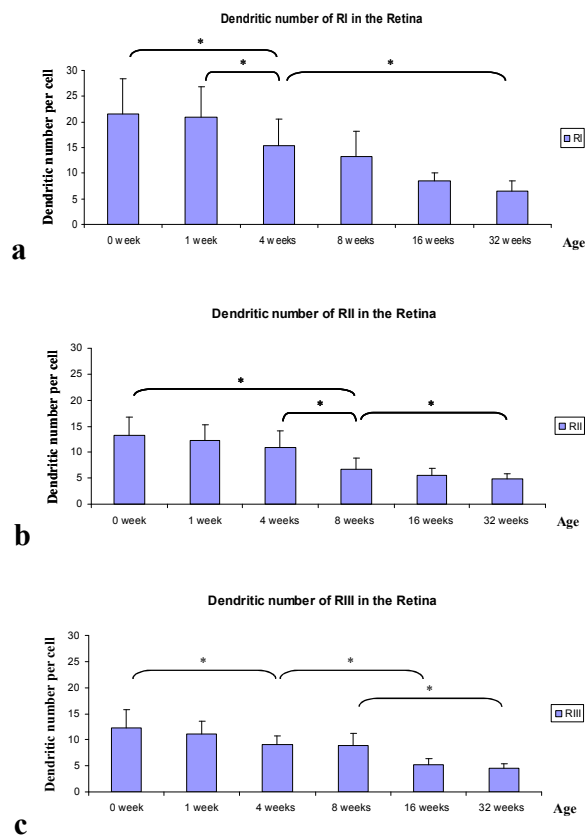


Figure 3.43a-c: Comparison of the dendritic number of RGCs between control groups at different time points.

These figures show the dendritic number of RGCs from control animals. Three types of cells including RI (a), RII (b) and RIII (c) were studied respectively ($*p < 0.05$). The error bar represents the SD of the mean.

For each type of cell, a percentage reduction in the number of dendrites per cell was calculated as previously described. Fig. 3.44a-c show an increasing percentage reduction in the number of dendrites per cell from the baseline (0% for all cells), 1 week (RI: 3.24%; RII: 8.27%; RIII: 9.76%), 4 weeks (RI: 29.17%; RII: 18.05%; RIII: 26.02%), 8 weeks (RI: 38.43%; RII: 49.62%; RIII: 27.64%), 16 weeks (RI: 61.11%; RII: 58.65%; RIII: 57.72%), until 32 weeks (RI: 69.44%; RII: 63.91%; RIII: 63.41%).

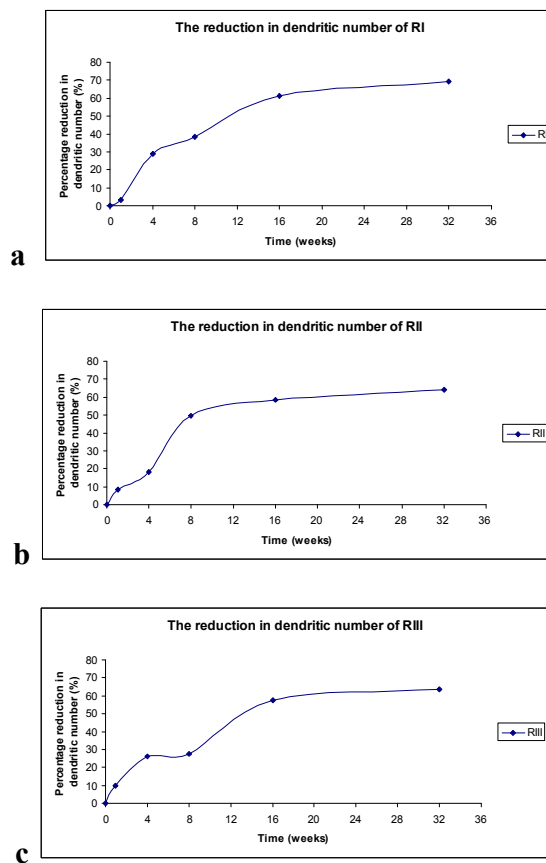


Figure 3.44a-c: Scatter plots of percentage reductions in the dendritic number of RGCs in control groups.

These graphs show the dendritic loss in RGCs in control animals: (a) RI; (b) RII; (c) RIII.

To determine if there was a relationship between ageing and the dendritic number of RGCs in control animals, an exponential decay analysis was performed, as shown in Fig. 3.45a-c. The strong regression coefficients (r^2) suggested that changes in the dendritic number of RGCs were age-related (RI: $r^2=0.94$; RII: $r^2=0.87$; RIII: $r^2=0.92$). The Spearman's correlation test was also performed with a correlation coefficient of -1 ($p<0.001$) for each type of cell, indicating a high probability of a negative correlation between ageing and the dendritic number of RGCs in control animals.

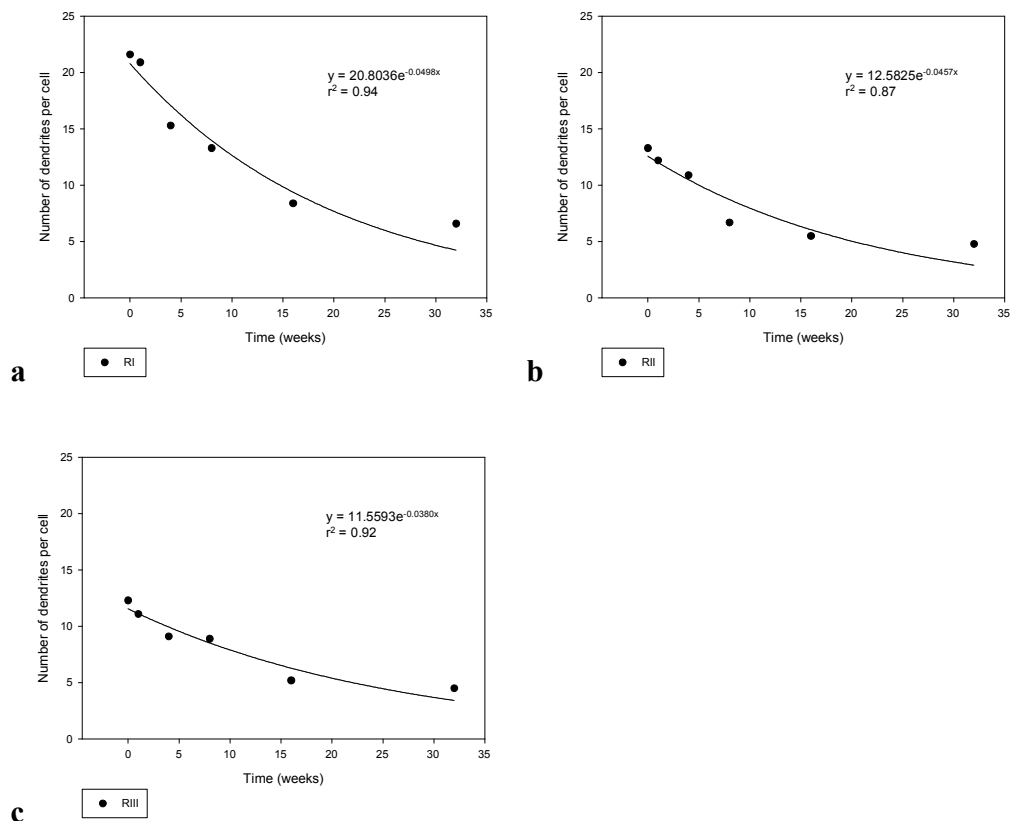


Figure 3.45a-c: The exponential decay of the dendritic number of RGCs in control groups.

These graphs show the exponential regression analysis of the dendritic number of RGCs from control animals: (a) RI; (b) RII; (c) RIII.

To characterize the longitudinal profile of dendritic changes, the relationship between the dendritic number and the effect of ageing was modelled with exponential decay equations ($y = a \cdot e^{bx}$) and exponential regression analysis. As the decline of dendritic number with age fitted well an exponential decay curve, the rate of dendritic loss was approximated based on the exponential regression equation as previously described. Dendrites of RI, RII and RIII from control groups were lost at a rate of 5.11% (RI); 4.47% (RII) and 3.73% (RIII) per week during ageing.

3.4.3.2 Dendritic Changes in Glaucoma Animals

3.4.3.2.1 Changes in Mean Dendritic Length

In the study of dendritic changes in RGCs in glaucoma animals, both mean dendritic length and dendritic number were analyzed for each type of cell respectively. The mean dendritic length of RI, RII and RIII was calculated and compared at the age of 1, 4, 8, 16 and 32 weeks after OHT induction using one-way ANOVA and the post hoc Bonferroni test, in order to find out whether there was an age-related dendritic change in glaucoma animals. Fig. 3.46a-c show that there were significant reductions in the mean dendritic length in RGCs from 0 to 32 weeks over time, indicating there was an age-dependent dendritic shrinkage in the retina in glaucoma animals. The error bar represents the SD of the mean.

RI showed the earliest reduction in the mean dendritic length at 1 week ($63.7 \pm 13.6 \mu\text{m}$) after OHT induction compared to that in baseline group ($83.2 \pm 11.6 \mu\text{m}$) ($p < 0.001$) (Fig. 3.46a). The mean dendritic length was further

reduced significantly from 1 to 4 weeks ($50.3 \pm 10.2 \mu\text{m}$) ($p < 0.05$), 8 ($44.4 \pm 6.9 \mu\text{m}$) to 16 weeks ($31.7 \pm 4.2 \mu\text{m}$) ($p < 0.05$), and 16 to 32 weeks ($21.5 \pm 3.5 \mu\text{m}$) ($p < 0.05$) after OHT induction. However, no significant dendritic shrinkage was observed from 4 to 8 weeks after OHT induction ($p = 1.0$).

RII also showed the initial reduction in the mean dendritic length at 1 week after OHT induction ($35.6 \pm 5.4 \mu\text{m}$) compared with that in the baseline group ($51.9 \pm 3.8 \mu\text{m}$), reaching statistical significance ($p < 0.001$) (Fig. 3.46b). The mean dendritic length was further reduced significantly from 1 to 4 weeks ($24.6 \pm 2.7 \mu\text{m}$) ($p < 0.001$), 4 to 8 weeks ($19.9 \pm 2.5 \mu\text{m}$) ($p < 0.05$), and 16 ($16.8 \pm 2.4 \mu\text{m}$) to 32 weeks ($12.9 \pm 2.2 \mu\text{m}$) ($p < 0.05$) after OHT induction. However, it did not show significant dendritic shrinkage from 8 to 16 weeks after OHT induction ($p = 0.201$).

The mean dendritic length of RIII was significantly reduced from baseline to 1 week ($58 \pm 11.2 \mu\text{m}$) after OHT induction ($p < 0.001$), similar to what were in RI and RII (Fig. 3.46c). Significant dendritic shrinkage was also observed from 1 to 4 weeks ($34.6 \pm 3.9 \mu\text{m}$) ($P < 0.001$), 4 to 16 weeks ($25.3 \pm 2.6 \mu\text{m}$) ($p < 0.05$), and 8 to 32 weeks ($20.5 \pm 3.6 \mu\text{m}$) ($p < 0.001$) after OHT induction. However, no dendritic shrinkage was observed from 4 to 8 weeks ($31.5 \pm 3.5 \mu\text{m}$) ($p = 1.0$), 8 to 16 weeks ($p = 0.178$), and 16 to 32 weeks ($p = 0.74$) after OHT induction.

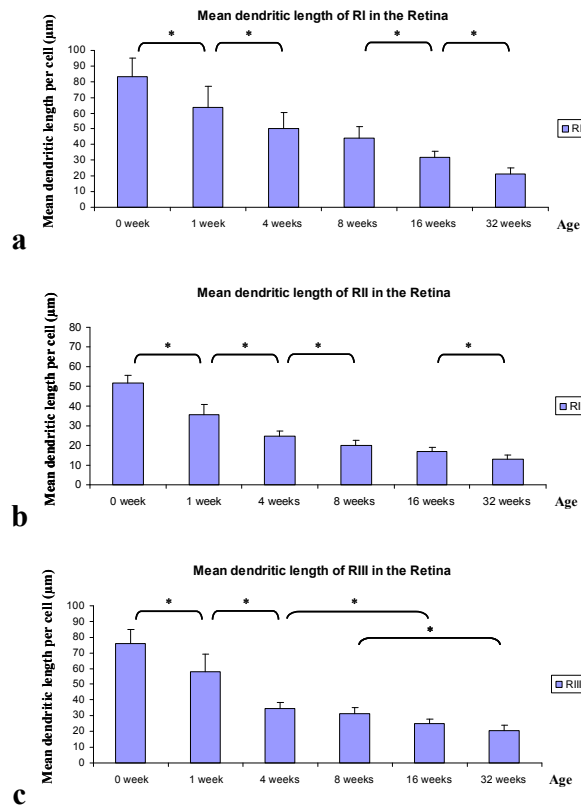


Figure 3.46a-c: Comparison of the mean dendritic length of RGCs between glaucoma groups at different time points.

This figure shows the mean dendritic length of RGCs from glaucoma groups. Three types of cells including RI (a), RII (b) and RIII (c) were studied respectively (* $p < 0.05$). The error bar represents the SD of the mean.

For each type of cell, a percentage reduction in mean dendritic length per cell was calculated as previously described. Fig. 3.47a-c show an increasing percentage reduction in the mean dendritic length from the baseline (0% for all cells), 1 week (RI: 23.44%; RII: 31.41%; RIII: 23.38%), 4 weeks (RI: 39.54%; RII: 52.6%; RIII: 54.29%), 8 weeks (RI: 46.63%; RII: 61.66%; RIII: 58.39%), 16 weeks (RI: 61.9%; RII: 67.63%; RIII: 66.58%), until 32 weeks (RI: 74.16%; RII: 75.14%; RIII: 72.92%).

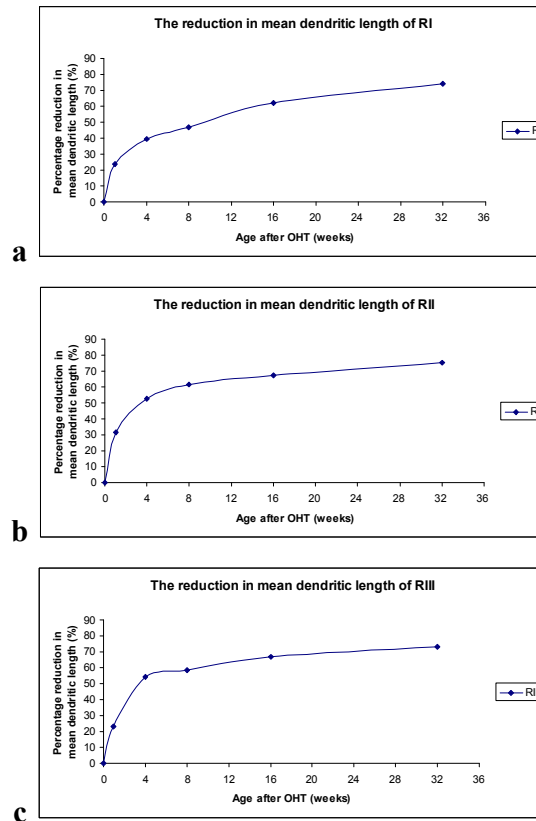


Figure 3.47a-c: Scatter plots of percentage reductions in the mean dendritic length of RGCs in glaucoma groups.

These graphs show the dendritic shrinkage in RGCs from glaucoma animals: (a) RI; (b) RII; (c) RIII.

To determine if there was a relationship between ageing and the mean dendritic length of RGCs in glaucoma animals, an exponential decay analysis was performed, as shown in Fig. 3.48a-c. The strong regression coefficients (r^2) suggested that changes in the mean dendritic length of RGCs were age-related (RI: $r^2=0.88$; RII: $r^2=0.75$; RIII: $r^2=0.76$). The Spearman's correlation test was also performed with a correlation coefficient of -1 ($p<0.001$) for each type of cell,

indicating a high probability of a negative correlation between ageing and the mean dendritic length of RGCs in glaucoma animals.

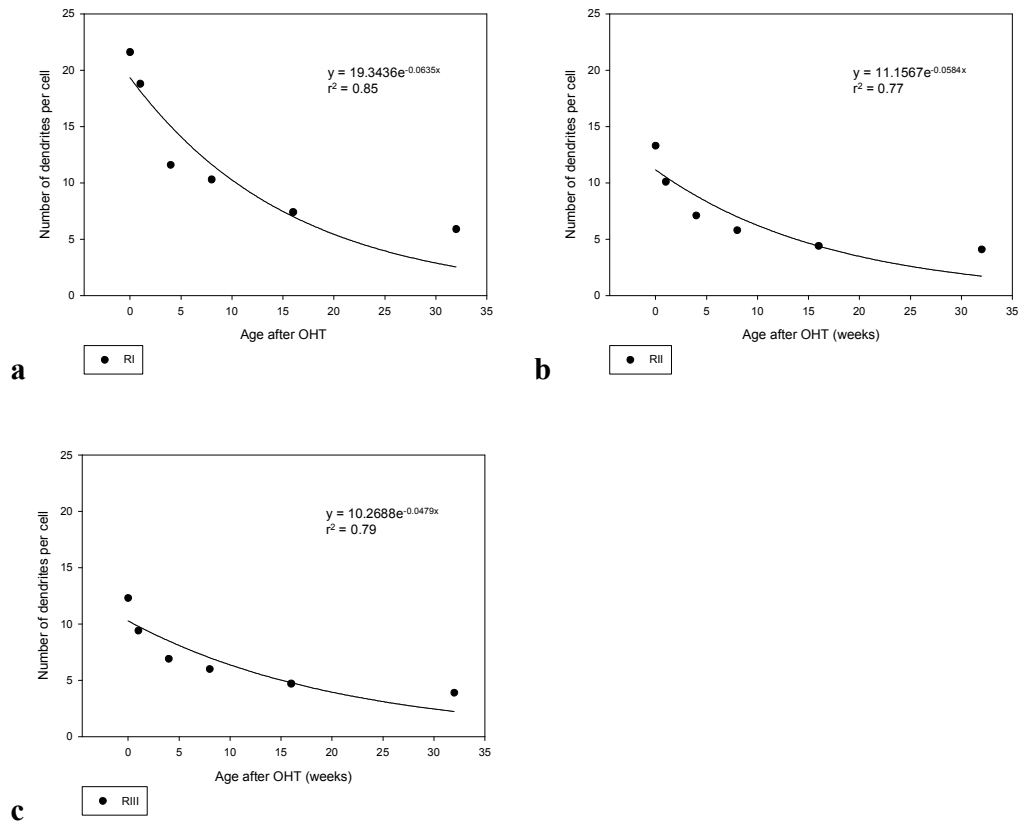


Figure 3.48a-c: The exponential decay of the mean dendritic length of RGCs in glaucoma groups.

These graphs show the exponential regression analysis of the mean dendritic length of RGCs from glaucoma animals: **(a)** RI; **(b)** RII; **(c)** RIII.

To characterize the longitudinal profile of dendritic changes, the relationship between the mean dendritic length and the effect of ageing was modelled with exponential decay equations ($y = a \cdot e^{bx}$) and exponential regression analysis. As the

decline of mean dendritic length with age fitted well an exponential decay curve, the rate of dendritic shrinkage was approximated based on the exponential regression equation as previously described. Dendrites of RI, RII and RIII from glaucoma groups shrunk at a rate of 4.99% (RI); 6.83% (RII) and 6.54% (RIII) per week. The rates of dendritic shrinkage in glaucoma groups and those in control groups were summarised as shown in Table 3.8.

Groups	Rates of dendritic shrinkage (weekly)		
	RI	RII	RIII
Control	4.24%	4.96%	4.32%
Glaucoma	4.99%	6.83%	6.54%

Table 3.8: Summary of the rates of dendritic shrinkage in glaucoma and control animals.

3.4.3.2.2 Changes in Dendritic Number

The dendritic numbers of RGCs in glaucoma groups at different time points were also compared and analyzed using one-way ANOVA and the post hoc Bonferroni test. Fig 3.49a-c show that there were significant reductions in the number of dendrites in RGCs during ageing. The error bar represents the SD of the mean.

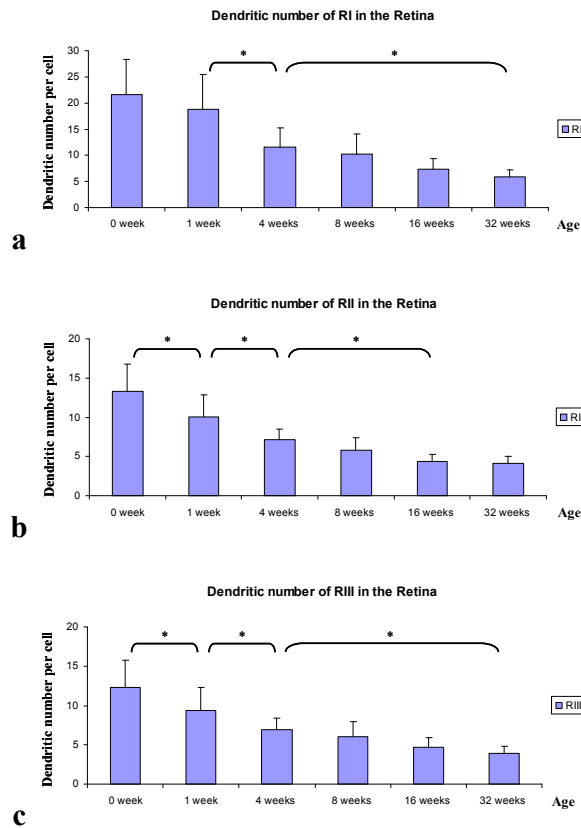


Figure 3.49a-c: Comparison of the dendritic number of RGCs in glaucoma groups at different time point.

These figures show the dendritic number of RGCs from glaucoma groups. Three types of cells including RI (a), RII (b) and RIII (c) were studied respectively (* $p < 0.05$). The error bar represents the SD of the mean.

RI showed the earliest dendritic loss at 4 weeks (11.6 ± 3.6) compared to that at 1 week (18.8 ± 6.6) after OHT induction ($p = 0.001$) (Fig. 3.49a). Significant dendritic loss was also shown at 32 weeks (5.9 ± 1.3) compared to that at 4 weeks after OHT induction ($p < 0.05$). However, the dendritic number did not change from the baseline (21.6 ± 6.8) to 1 week ($p = 1.0$), 4 to 8 weeks (10.3 ± 3.7) ($p = 1.0$), 8 to 16 weeks (7.4 ± 2) ($p = 1.0$), or 16 to 32 weeks OHT groups ($p = 1.0$).

RII also showed the initial dendritic loss at 1 week after OHT induction compared to that in the baseline group (13.3 ± 3.5) ($P=0.001$) (Fig. 3.49b). The number of dendrites was also significantly decreased from 1 (10.1 ± 2.7) to 4 weeks (7.1 ± 1.4) ($p=0.001$), 4 to 32 weeks (4.1 ± 0.9) ($p<0.05$) after OHT induction. However, the dendritic number did not change from 4 to 8 weeks (5.8 ± 1.6) ($p=1.0$), 8 to 16 weeks (4.4 ± 0.8) ($p=0.967$), and 16 to 32 weeks ($p=1.0$) after OHT induction.

The dendritic number of RIII was also initially decreased from the baseline (12.3 ± 3.5) to 1 week after OHT induction (9.4 ± 2.9) ($p<0.05$) (Fig. 3.49c). Significant reductions in the number of dendrites was also observed from 1 to 4 weeks (6.9 ± 1.5) ($p<0.05$), 4 to 32 weeks (3.9 ± 0.9) ($p<0.05$) after OHT induction. However, no dendritic loss was observed from 4 to 8 weeks (6 ± 1.9) ($p=1.0$), 8 to 16 weeks (4.7 ± 1.2) ($p=1.0$), and 16 to 32 weeks after OHT induction ($p=1.0$).

For each type of cell, a percentage reduction in the number of dendrites per cell was calculated as previously described. Fig. 3.50a-c show an increasing percentage reduction in the number of dendrites per cell from the baseline (0% for all cells), 1 week (RI: 12.96%; RII: 24.06%; RIII: 23.58%), 4 weeks (RI: 46.3%; RII: 46.62%; RIII: 43.9%), 8 weeks (RI: 52.31%; RII: 56.39%; RIII: 51.22%), 16 weeks (RI: 65.74%; RII: 66.92%; RIII: 61.79%), until 32 weeks (RI: 72.69%; RII: 69.17%; RIII: 68.29%).

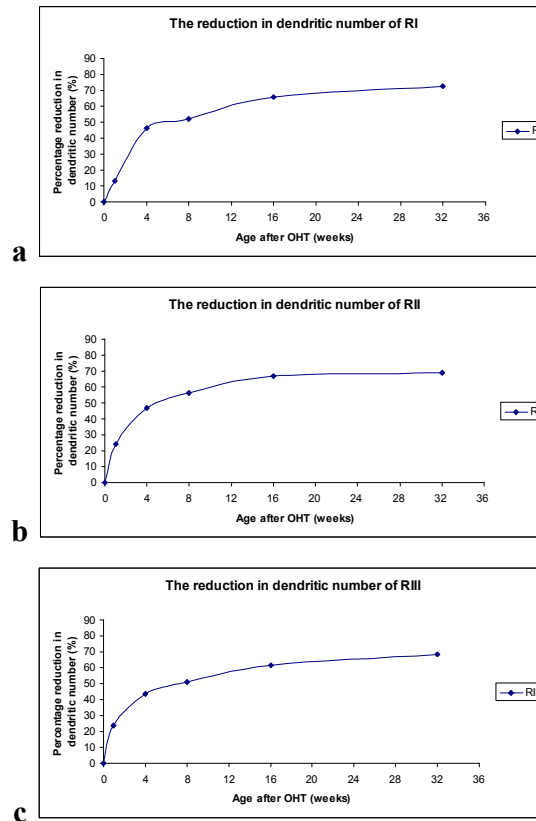


Figure 3.50a-c: Scatter plots of percentage reductions in the dendritic number of RGCs in glaucoma groups.

These graphs show the dendritic loss in RGCs from glaucoma animals: (a) RI; (b) RII; (c) RIII.

To determine if there was a relationship between ageing and the dendritic number of RGCs in glaucoma animals, an exponential decay analysis was performed, as shown in Fig. 3.51a-c. The strong regression coefficients (r^2) suggested that changes in the dendritic number of RGCs were age-related (RI: $r^2=0.85$; RII: $r^2=0.77$; RIII: $r^2=0.79$). The Spearman's correlation test was also performed with a correlation coefficient of -1 ($p<0.001$) for each type of cell, indicating a high

probability of a negative correlation between ageing and the dendritic number of RGCs in glaucoma animals.

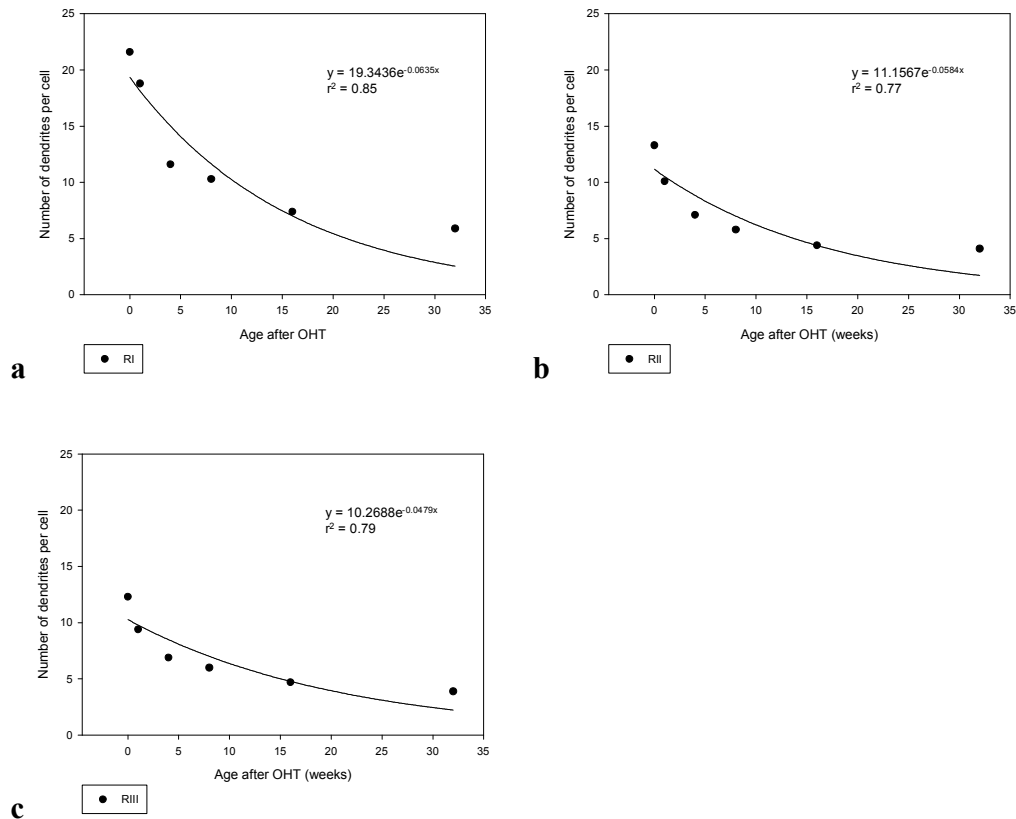


Figure 3.51a-c: The exponential decay of the dendritic number of RGCs in glaucoma groups.

These graphs show the exponential regression analysis of the dendritic number of RGCs from glaucoma animals: **(a)** RI; **(b)** RII; **(c)** RIII.

To characterize the longitudinal profile of dendritic changes, the relationship between the dendritic number and the effect of ageing was modelled with

exponential decay equations ($y = a \cdot e^{bx}$) and exponential regression analysis. The rate of dendritic loss was then approximated based on the exponential regression equation as previously described. Dendrites of RI, RII and RIII from glaucoma groups were lost at a rate of 6.15% (RI); 5.67% (RII) and 4.68% (RIII) per week. The rates of dendritic loss in glaucoma groups and those in control groups were summarised as shown in Table 3.9.

Groups	Rate of dendritic shrinkage (weekly)		
	RI	RII	RIII
Control	5.11%	4.47%	3.73%
Glaucoma	6.15%	5.67%	4.68%

Table 3.9: Summary of the rates of dendritic loss in glaucoma and control animals.

3.4.3.3 Comparison of Dendritic Parameters between Glaucoma and Control Animals

3.4.3.3.1 Comparison of Mean Dendritic Length

The effects of elevated IOP on dendritic morphology in RGCs were also investigated by comparing dendritic parameters between glaucoma rats and age-matched controls. The mean dendritic lengths of RI, RII and RIII were studied at different time points of 1, 4, 8, 16 and 32 weeks respectively. The comparison of mean dendritic length in RGCs from control groups and those from glaucoma groups were performed using the student T-test. Fig. 3.52a-c show that there were

significant reductions in the mean dendritic length of RGCs at 1, 4, 8 and 32 weeks after OHT induction. The error bar represents the SD of the mean.

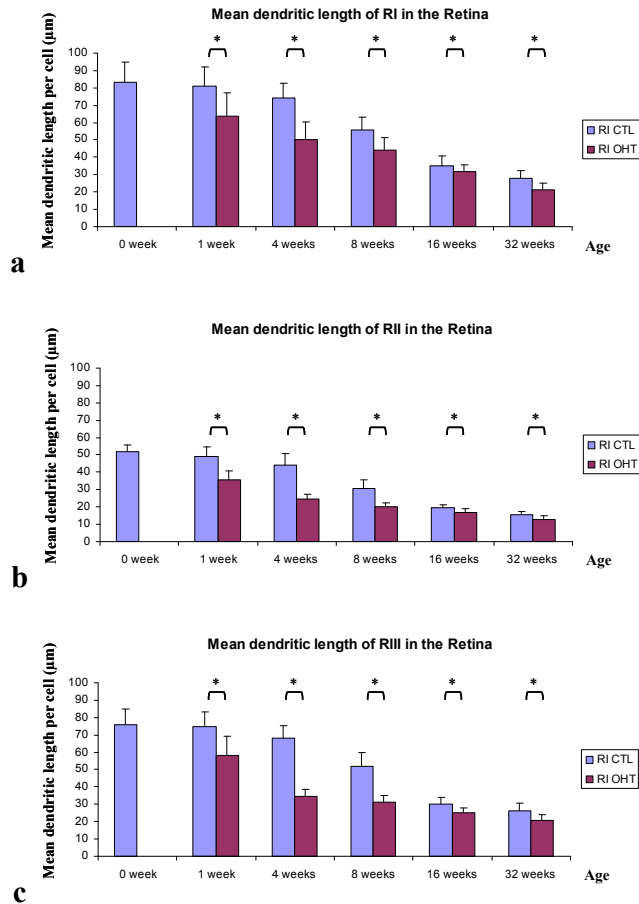


Figure 3.52a-c: Comparison of the mean dendritic length of RGCs between glaucoma and control animals.

These figures show changes in the mean dendritic length of RGCs at 4, 8, 16 and 32 weeks after glaucoma surgery. Three types of cells including RI (a), RII (b) and RIII (c) were studied respectively (* $p < 0.05$). The error bar represents the SD of the mean.

Fig. 3.52a shows that the mean dendritic length of RI was significantly reduced at 1, 4, 8 and 32 weeks after glaucoma surgery compared to age-matched

controls, indicating that the dendritic shrinkage was also related to elevated IOP ($p=0.001$ at 1 week; $P<0.001$ at 4, 8 and 32 weeks). However, no significant dendritic shrinkage was shown at 16 weeks after OHT induction ($p=0.057$).

Fig. 3.52b shows that the mean dendritic length of RII was significantly reduced after glaucoma surgery at all time points ($p<0.001$ at 1, 4 and 8 week; $p=0.001$ at 16 weeks; $p=0.002$ at 32 weeks).

Fig. 3.52c also shows significant reductions in the mean dendritic length of RIII at all time points after OHT induction ($p<0.001$ at all time points).

For each type of cell, a percentage reduction in mean dendritic length of RGCs 1, 4, 8, 16 and 32 weeks after glaucoma surgery was also analyzed as previously described (Fig. 3.53a-c).

Fig. 3.53a-c shows that the earliest dendritic shrinkage in all types of RGCs could be observed at 1 week after glaucoma surgery (RI: 21.26%; RII: 27.35%; RIII: 22.67%).

Significant dendritic shrinkage in RI was shown continually from 4 (32.3%), 8 (20.71%), 16 (10.2%), until 32 weeks (22.94%) (Fig. 3.52a). The peak time point of dendritic shrinkage in RI was at 4 weeks after OHT induction.

RII also showed significant reductions in the mean dendritic length from 4 (43.96%), 8 (35.18%), 16 (13.85%), until 32 weeks (16.23%) (Fig. 3.53b). The maximum dendritic shrinkage in RII was also shown at 4 weeks after OHT induction.

Significant dendritic shrinkage in RIII was also observed from 4 (49.12%), 8 (39.31%), 16 (16.23%), until 32 weeks (21.76%), with the maximum shrinkage shown at 4 weeks after OHT induction (Fig. 3.53c).

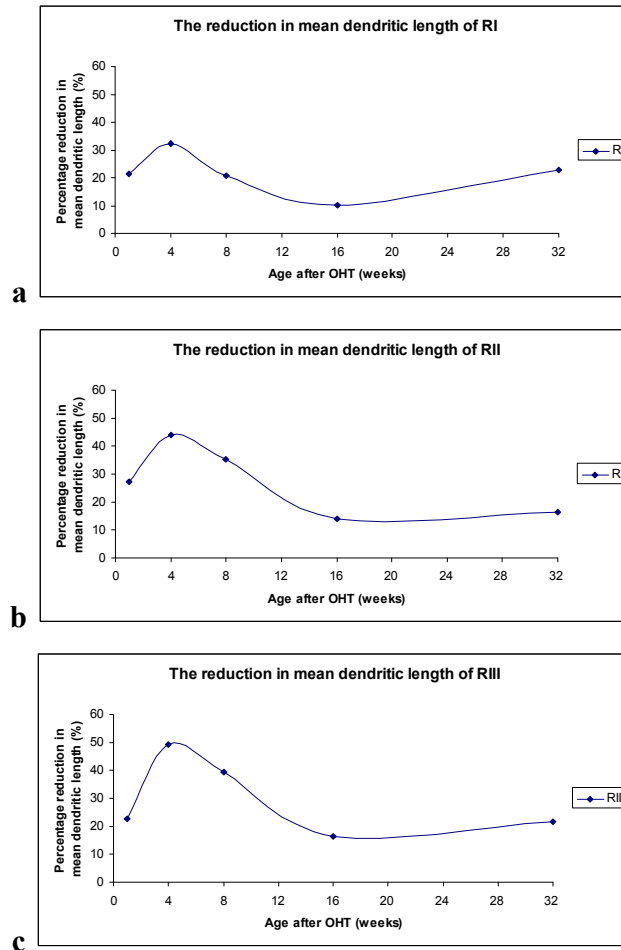


Figure 3.53a-c: Scatter plots of percentage reductions in mean dendritic length of RGCs after glaucoma surgery.

These graphs show the dendritic shrinkage in RGCs after OHT induction: (a) RI; (b) RII; (c) RIII.

3.4.3.3.2 Comparison of Dendritic Number

The effects of elevated IOP on dendritic number of RI, RII and RIII were also investigated at 1, 4, 8, 16 and 32 weeks respectively (Fig. 3.54a-c). The comparison of the dendritic number between glaucoma and control groups was performed using the student T-test. The error bar represents the SD of the mean.

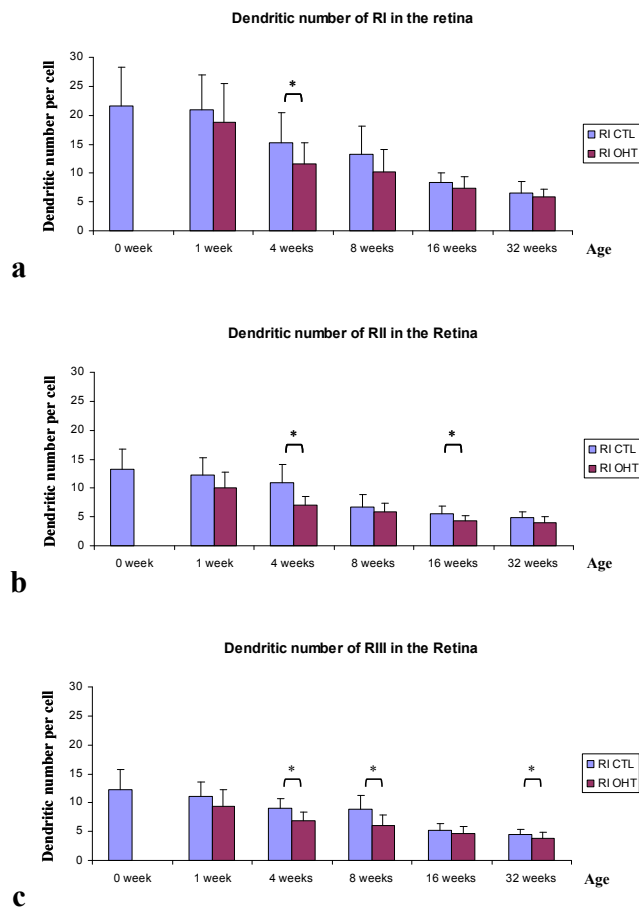


Figure 3.54a-c: Comparison of the dendritic number of RGCs between glaucoma and control animals.

These figures show changes in the dendritic number of RGCs at 4, 8, 16 and 32 weeks after glaucoma surgery. Three types of cells including RI (a), RII (b) and RIII (c) were studied respectively (* $p < 0.05$). The error bar represents the SD of the mean.

Fig. 3.54a shows that the only significant dendritic loss in RI was shown at 4 weeks after OHT induction ($p=0.029$). The dendritic number of RI did not change at 1 ($p=0.361$), 8 ($p=0.066$), 16 ($p=0.157$) and 32 weeks ($p=0.273$) after glaucoma surgery.

Fig. 3.54b shows that the dendritic number of RII was significantly reduced at 4 and 16 weeks after glaucoma surgery ($p<0.001$ at 4 weeks; $p=0.015$ at 16 weeks). The earliest dendritic loss in RII also occurred at 4 weeks after OHT induction. However, no significant changes in the dendritic number were observed at 1 ($p=0.055$), 8 ($p=0.177$) and 32 weeks ($p=0.089$) after OHT induction.

Fig. 3.54c shows significant reductions in the dendritic number of RIII at 4, 8 and 32 weeks after glaucoma surgery ($p<0.001$ at 4 weeks; $p=0.001$ at 8 weeks; $p=0.046$ at 32 weeks). Similar to that in RI and RII, the earliest dendritic loss in RIII also occurred at 4 weeks after OHT induction. However, no significant dendritic loss was shown at 1 ($p=0.089$) and 16 weeks ($p=0.29$) after glaucoma surgery.

For each type of cell, a percentage of reduction in the dendritic number of RGCs at 1, 4, 8, 16 and 32 weeks after glaucoma surgery was also analyzed as previously described (Fig. 3.55a-c).

Fig. 3.55a shows that the percentage dendritic loss in RI was 10.05% (1 week); 24.18% (4 weeks); 22.56% (8 weeks); 11.9% (16 weeks) and 10.61% (32 weeks). The peak dendritic loss in RI was shown at 4 weeks after OHT induction.

Fig. 3.55b shows that the percentage dendritic loss in RII was 17.21% (1 week); 34.86% (4 weeks); 13.43% (8 weeks); 20% (16 weeks) and 14.58% (32 weeks).

weeks). The peak time point of dendritic loss in RII was at 4 weeks after OHT induction as well.

Fig. 3.55c shows that the percentage dendritic loss in RIII was 15.32% (1 week); 24.16% (4 weeks); 32.58% (8 weeks), 9.62% (16 weeks) and 13.33% (32 weeks). Unlike that in RI and RII, the maximum dendritic loss in RIII was shown at 8 weeks after OHT induction.

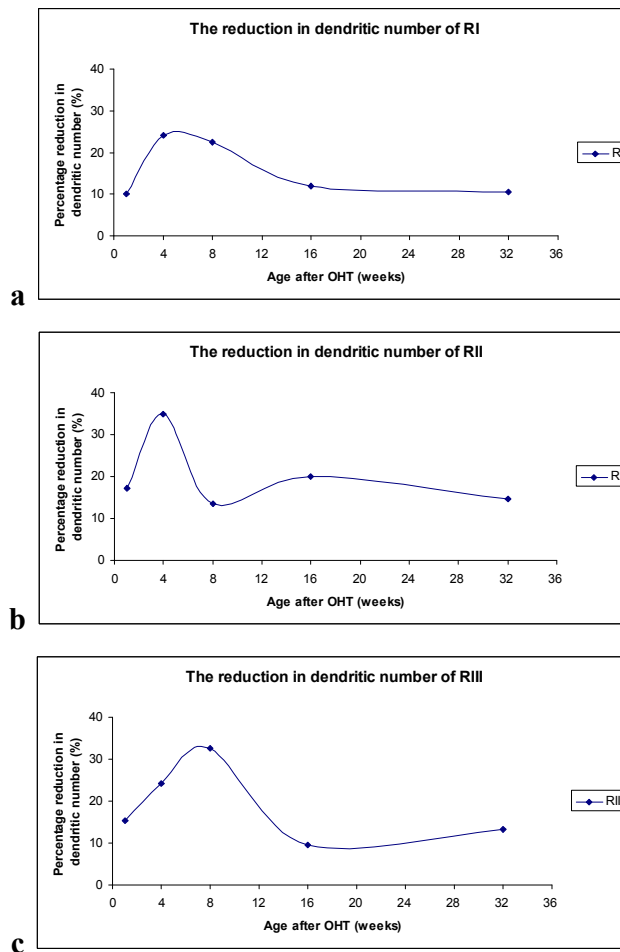


Figure 3.55a-c: Scatter plots of percentage reductions in the dendritic number of RGCs after glaucoma surgery.

These graphs show the dendritic loss in RGCs after OHT induction: (a) RI; (b) RII; (c) RIII.

3.5 Comparison of Dendritic Changes in RGCs, SC cells and LGN cells

In addition to studying dendritic morphology in RGCs, SC cells and LGN cells separately, we also analyzed dendritic parameters of all RGCs, SC cells and LGN cells, and compared dendritic changes in these three sites.

3.5.1 Dendritic Changes in Control Animals

3.5.1.1 Changes in Mean Dendritic Length

The mean dendritic length of all RGCs, SC cells and LGN cells were compared between different age groups using one way ANOVA and the post hoc Bonferroni test. Fig. 3.56 shows significant reductions in the mean dendritic length of RGCs from the baseline ($70.3 \pm 16 \mu\text{m}$) to 4 ($62.1 \pm 15.1 \mu\text{m}$) weeks ($p < 0.05$), 4 to 8 ($46.2 \pm 13 \mu\text{m}$) weeks ($p < 0.001$), and 8 to 16 ($28.3 \pm 7.7 \mu\text{m}$) weeks ($p < 0.001$). The mean dendritic length of RGCs did not differ between the baseline and 1 week ($68.3 \pm 16.4 \mu\text{m}$) ($p = 1.0$), 1 and 4 weeks ($p = 0.379$), or 16 and 32 weeks ($23.2 \pm 6.6 \mu\text{m}$) ($p = 0.959$) control groups.

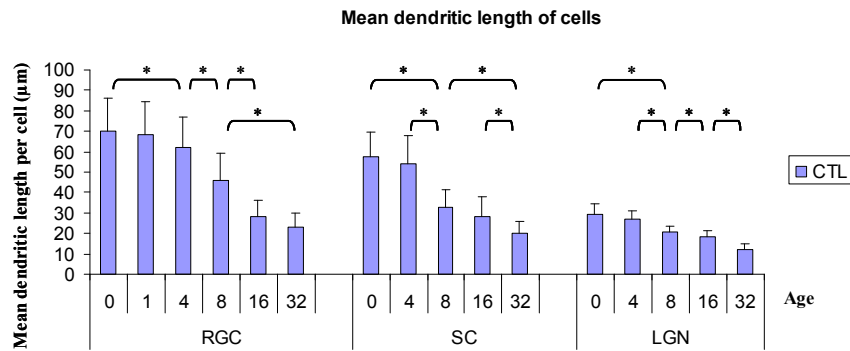


Figure 3.56: Comparison of the mean dendritic length of RGCs, SC cells and LGN cells in control groups.

This figure shows a comparison of the mean dendritic length of all RGCs, SC cells and LGN cells in control animals at different time points. The error bar represents the SD of the mean. * $p < 0.05$

The mean dendritic length of SC cells showed the earliest reduction at 8 weeks ($33 \pm 8.2 \mu\text{m}$) compared to that at 4 weeks ($54.3 \pm 13.5 \mu\text{m}$), reaching statistical significance ($p < 0.001$). A significant reduction in the mean dendritic length was also shown from 16 ($28.3 \pm 9.9 \mu\text{m}$) to 32 weeks ($19.9 \pm 6 \mu\text{m}$) ($p < 0.001$). However, no significant dendritic shrinkage was shown from the baseline ($57.2 \pm 12.5 \mu\text{m}$) to 4 weeks ($p = 0.846$), and 8 to 16 weeks ($p = 0.068$).

The mean dendritic length of LGN cells also showed the earliest reduction at 8 weeks ($20.9 \pm 2.9 \mu\text{m}$). Significant dendritic shrinkage was observed from 4 ($27 \pm 3.8 \mu\text{m}$) to 8 weeks ($p < 0.001$), 8 to 16 weeks ($18.3 \pm 2.9 \mu\text{m}$) ($p = 0.048$) and 16 to 32 weeks ($11.9 \pm 2.8 \mu\text{m}$) ($p < 0.001$). However, no significant dendritic shrinkage was observed from the baseline ($29.4 \pm 5.3 \mu\text{m}$) to 4 weeks ($p = 0.151$).

Although both SC and LGN did not show dendritic shrinkage at 4 weeks, RGCs had a significant reduction in the mean dendritic length from the baseline to 4 weeks ($p < 0.05$). Therefore, this study also investigated dendritic parameters in the 1 week RGC group and found no significant differences in the mean dendritic length between the baseline and 1 week ($p = 1.0$), or 1 and 4 weeks group ($p = 0.379$).

Furthermore, a percentage reduction in the mean dendritic length was calculated as previously described (Fig. 3.57). Fig. 3.57 shows an increasing percentage reduction in the mean dendritic length from the baseline (0%), 1 week (RGC: 2.84%), 4 weeks (RGC: 11.66%; SC: 5.07%; LGN: 8.16%), 8 weeks (RGC: 34.28%; SC: 42.31%; LGN: 28.91%), 16 weeks (RGC: 59.74%; SC: 50.52%; LGN: 37.76%), until 32 weeks (RGC: 67%; SC: 65.21%; LGN: 59.52%).

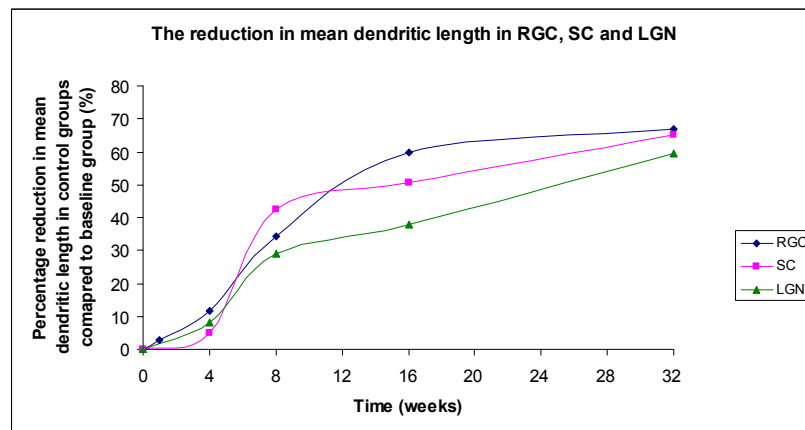


Figure 3.57: Scatter plot of percentage reductions in the mean dendritic length of RGCs, SC cells and LGN cells in control groups.

This graph shows the dendritic shrinkage in RGCs, SC cells and LGN cells in control animals.

To determine if there was a relationship between ageing and the mean dendritic length of RGCs, SC cells and LGN cells, an exponential decay analysis was performed, as shown in Fig. 3.58a-c. The strong regression coefficients (r^2) suggested that changes in the mean dendritic length of cells were age-related (RGC: $r^2=0.95$; SC: $r^2=0.89$; LGN: $r^2=0.97$). The Spearman's correlation test was also performed with a correlation coefficient of -1 ($p<0.001$), indicating a high probability of a negative correlation between ageing and the mean dendritic length of RGCs, SC cells and LGN cells in control animals.

To characterize the longitudinal profile of dendritic changes, the relationship between the mean dendritic length and the effect of ageing was modelled with exponential decay equations ($y = a \cdot e^{bx}$) and exponential regression analysis. The rate of dendritic shrinkage was approximated based on the exponential regression equation as previously described. Dendrites of RGC in the retina and those in the SC and LGN from control groups shrunk at a rate of 4.43% (RGC); 3.98% (SC) and 2.92% (LGN) per week during ageing.

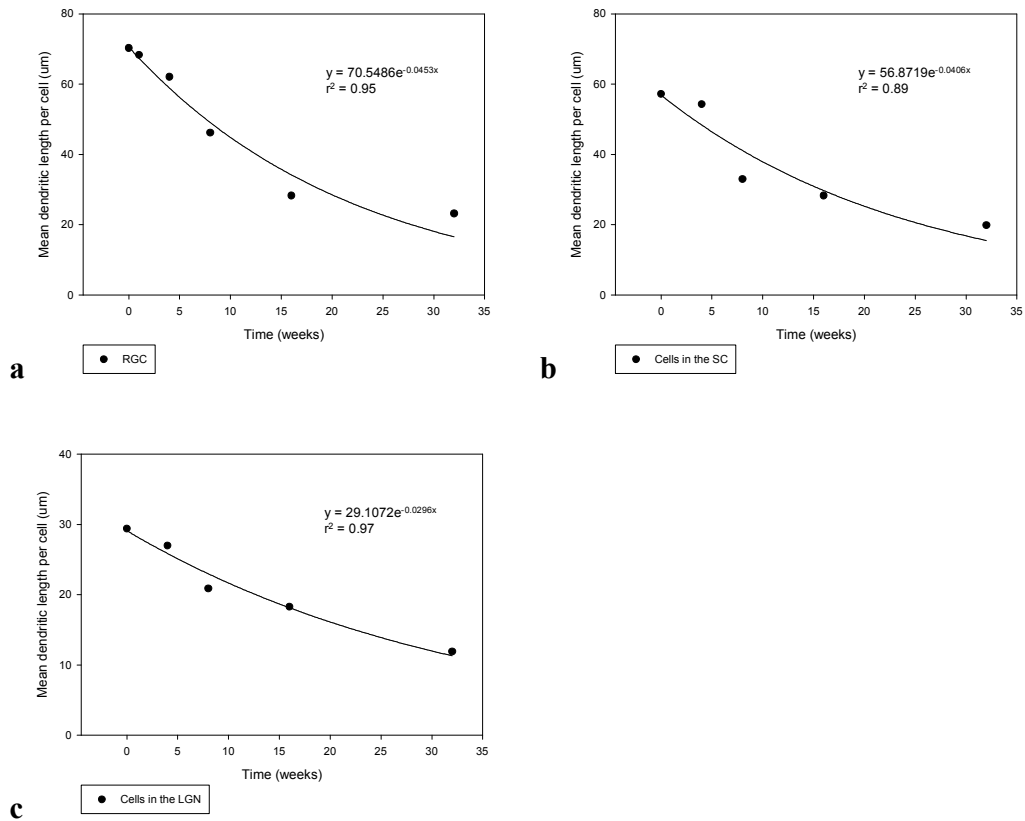


Figure 3.58a-c: The exponential decay of the mean dendritic length of RGCs, SC cells and LGN cells in control groups.

These graphs show the exponential regression analysis of the mean dendritic length of RGCs, SC cells and LGN cells in control animals: (a) RGC; (b) SC; (c) LGN.

3.5.1.2 Changes in Dendritic Number

The dendritic number of all RGCs, SC cells and LGN cells were also compared between control groups at different time points using one way ANOVA and the post hoc Bonferroni test.

Fig. 3.59 shows that the dendritic number of RGCs was significantly reduced from 1 (14.8 ± 6) to 4 weeks (11.8 ± 4.4) ($p=0.025$), and 8 (9.6 ± 4.3) to 16 weeks (6.4 ± 2) ($p=0.009$). However, no significant dendritic loss was shown from 0 (15.8 ± 6.3) to 1 week ($p=1.0$), 4 to 8 weeks ($p=0.392$), or 16 to 32 weeks (5.3 ± 1.6) ($p=1.0$).

Significant reductions in the dendritic number of SC cells was shown from 4 (10.99 ± 2.1) to 8 weeks (7.9 ± 2.5), 8 to 16 weeks (5.4 ± 1.5) and 16 to 32 weeks (3.6 ± 0.7) ($p < 0.001$ at all time points). However, no significant dendritic loss was observed from 0 (11.3 ± 2.2) to 4 weeks ($p=1.0$).

LGN cells also showed significant reductions in the dendritic number from 4 (7.5 ± 1.2) to 8 weeks (5.9 ± 0.9), 8 to 16 weeks (4.6 ± 1.1) and 16 to 32 weeks (3.1 ± 1) ($p < 0.001$ at all time points), but not from 0 (7.8 ± 1.1) to 4 weeks ($p=1.0$).

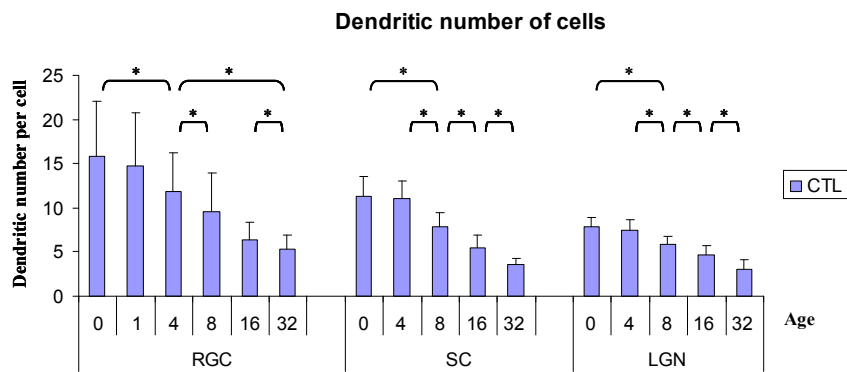


Figure 3.59: Comparison of the dendritic number of RGCs, SC cells and LGN cells in control groups.

This graph shows a comparison of the dendritic number of RGCs, SC cells and LGN cells in control animals at different time points. The error bar represents the SD of the mean.
* $p < 0.05$

Furthermore, a percentage reduction in the number of dendrites was calculated as previously described. Fig. 3.60 shows an increasing percentage reduction in dendritic number from the baseline (0%), 1 week (RGC: 6.33%), 4 weeks (RGC: 25.32%; SC: 2.74%; LGN: 3.85%), 8 weeks (RGC: 39.24%; SC: 30.09%; LGN: 24.36%), 16 weeks (RGC: 59.49%; SC: 52.21%; LGN: 41.03%), until 32 weeks (RGC: 66.46%; SC: 68.14%; LGN: 60.26%).

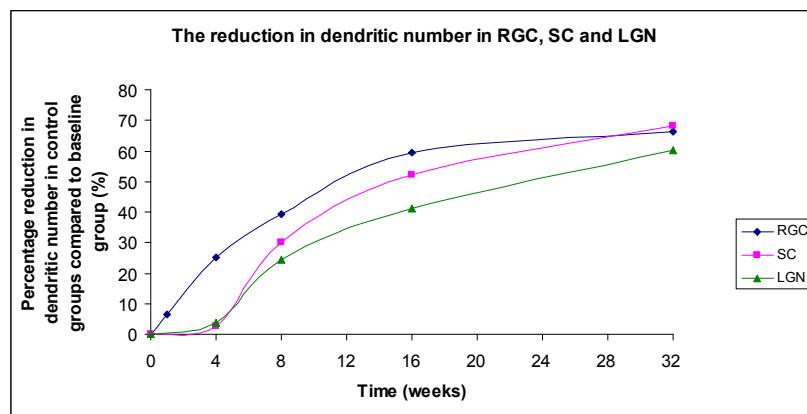


Figure 3.60: Scatter plot of percentage reductions in the dendritic number of RGCs, SC cells and LGN cells in control groups.

This graph shows the dendritic loss in RGCs, SC cells and LGN cells in control animals.

To determine if there was a relationship between ageing and dendritic number per cell in RGCs, SC cells and LGN cells, an exponential decay analysis was performed, as shown in Fig. 3.61a-c. The strong regression coefficients (r^2) suggested that changes in the dendritic number of cells were age-related (RGC: $r^2=0.94$; SC: $r^2=0.95$; LGN: $r^2=0.97$). The Spearman's correlation test was also

performed with a correlation coefficient of -1 ($p < 0.001$), indicating a high probability of a negative correlation between ageing and dendritic number of RGCs, SC cells and LGN cells in control animals.

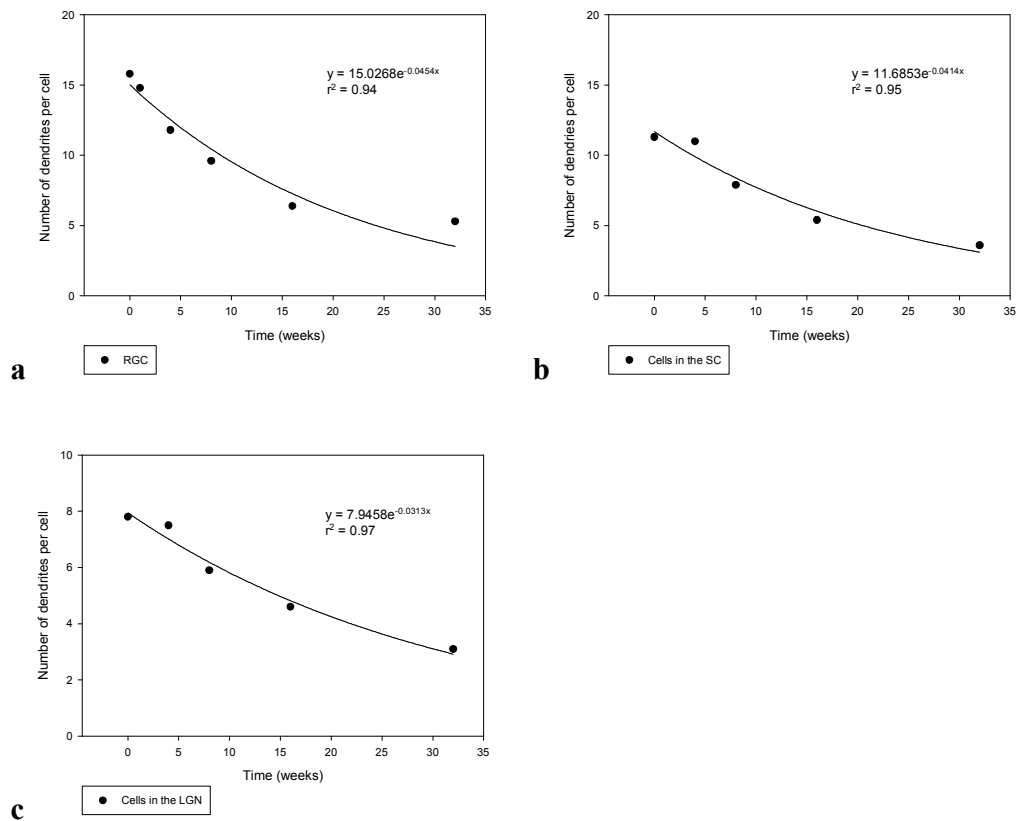


Figure 3.61a-c: The exponential decay of the dendritic number of RGCs, SC cells and LGN cells in control groups.

These graphs show the exponential regression analysis of the dendritic number of RGCs, SC cells and LGN cells from control animals: **(a)** RGC; **(b)** SC; **(c)** LGN.

To characterize the longitudinal profile of dendritic changes, the relationship between the dendritic number of cells and the effect of ageing was modelled with exponential decay equations ($y = a \cdot e^{bx}$) and exponential regression analysis. The rate of dendritic loss was approximated based on the exponential regression equation as

previously described. Dendrites of RGCs and those in the SC and LGN from control groups were lost at a rate of 4.44% (RGC); 4.06% (SC) and 3.08% (LGN) per week during ageing.

3.5.2 Dendritic Changes in Glaucoma Animals

3.5.2.1 Changes in Mean Dendritic Length

The mean dendritic length of RGCs, SC cells and LGN cells were compared between glaucoma groups at different time points using one way ANOVA and the post hoc Bonferroni test.

Fig. 3.62 shows that the mean dendritic length of all RGCs was significantly reduced from the baseline ($70.3\pm 16\mu\text{m}$) to 1 week ($52.4\pm 16.1\mu\text{m}$) after OHT induction ($p<0.001$). Significant dendritic shrinkage was also observed from 1 to 4 weeks ($36.5\pm 12.5\mu\text{m}$) ($p<0.001$), 4 to 16 weeks ($24.6\pm 6.9\mu\text{m}$) ($p<0.001$), and 8 ($31.9\pm 11.1\mu\text{m}$) to 32 weeks ($18.3\pm 5\mu\text{m}$) ($p<0.001$) after OHT induction. The comparison of the mean dendritic length of RGCs did not show any differences between 4 and 8 weeks ($p=1.0$), 8 and 16 weeks ($p=0.063$) or 16 and 32 weeks ($p=0.197$) glaucoma groups.

SC cells showed significant reductions in the mean dendritic length from the baseline ($57.2\pm 12.5\mu\text{m}$) to 4 weeks ($27.4\pm 5.3\mu\text{m}$) ($p<0.001$), 4 to 8 weeks ($23\pm 5.2\mu\text{m}$) ($p<0.05$) and 16 ($20.9\pm 5.7\mu\text{m}$) to 32 weeks ($12.8\pm 3.5\mu\text{m}$) ($p<0.001$) after OHT induction. However, no significant dendritic shrinkage was observed from 8 to 16 weeks after OHT induction ($p=0.761$).

LGN cells had significant dendritic shrinkage from the baseline to 4 weeks ($25.9 \pm 4.7 \mu\text{m}$) ($p < 0.05$), 4 to 8 weeks ($14.7 \pm 2 \mu\text{m}$) ($p < 0.001$), 8 to 16 weeks ($11.6 \pm 1.8 \mu\text{m}$) ($p < 0.05$) and 16 to 32 weeks ($8.5 \pm 1.5 \mu\text{m}$) ($p < 0.05$) after OHT induction.

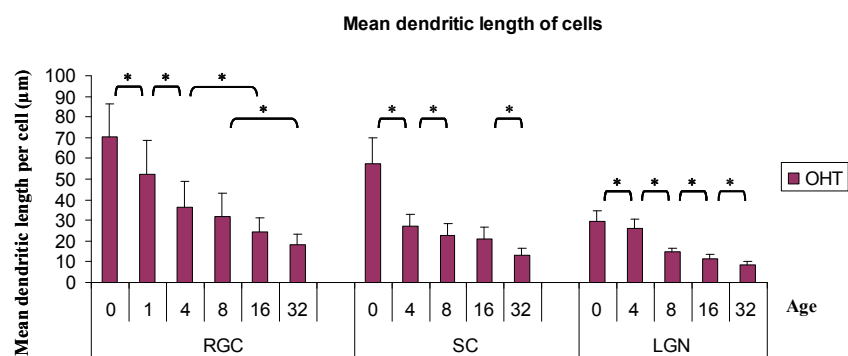


Figure 3.62: Comparison of the mean dendritic length of RGCs, SC cells and LGN cells in glaucoma groups.

This graph shows a comparison of the mean dendritic length of RGC cells, SC cells and LGN cells at different time points after glaucoma surgery. The error bar represents the SD of the mean. * $p < 0.05$

Furthermore, a percentage reduction in the mean dendritic length was calculated as previously described. Fig. 3.63 shows an increasing percentage reduction in mean dendritic length from the baseline (0%), 1 week (RGC: 25.46%), 4 weeks (RGC: 48.08%; SC: 52.1%; LGN: 11.9%), 8 weeks (RGC: 54.62%; SC: 59.79%; LGN: 50%), 16 weeks (RGC: 65.01%; SC: 63.46%; LGN: 60.54%), until 32 weeks (RGC: 73.97%; SC: 77.62%; LGN: 71.09%).

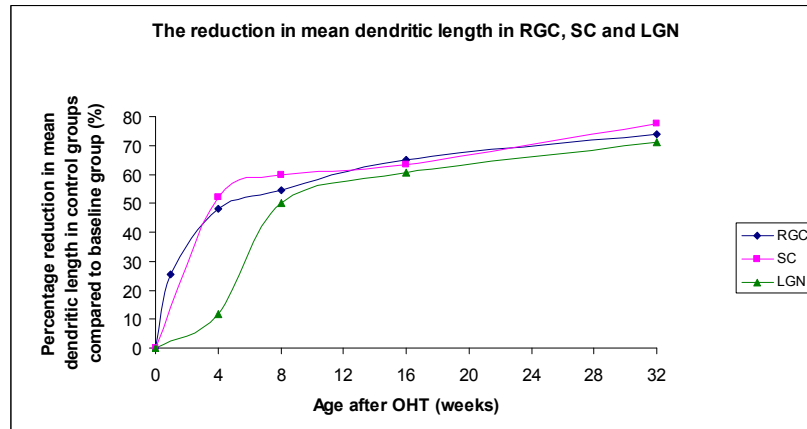


Figure 3.63: Scatter plot of percentage reductions in the mean dendritic length of RGCs, SC cells and LGN cells in glaucoma groups.

This graph shows the dendritic shrinkage in RGCs, SC cells and LGN cells in glaucoma animals.

To determine if there was a relationship between ageing and the mean dendritic length of RGCs, SC cells and LGN cells in glaucoma animals, an exponential decay analysis was performed, as shown in Fig. 3.64a-c. The strong regression coefficients (r^2) suggested that changes in the mean dendritic length of cells were age-related (RGC: $r^2=0.81$; SC: $r^2=0.77$; LGN: $r^2=0.89$). The Spearman's correlation test was also performed with a correlation coefficient of -1 ($p<0.001$), indicating a high probability of a negative correlation between ageing and the mean dendritic length of RGCs, SC cells and LGN cells in glaucoma animals.

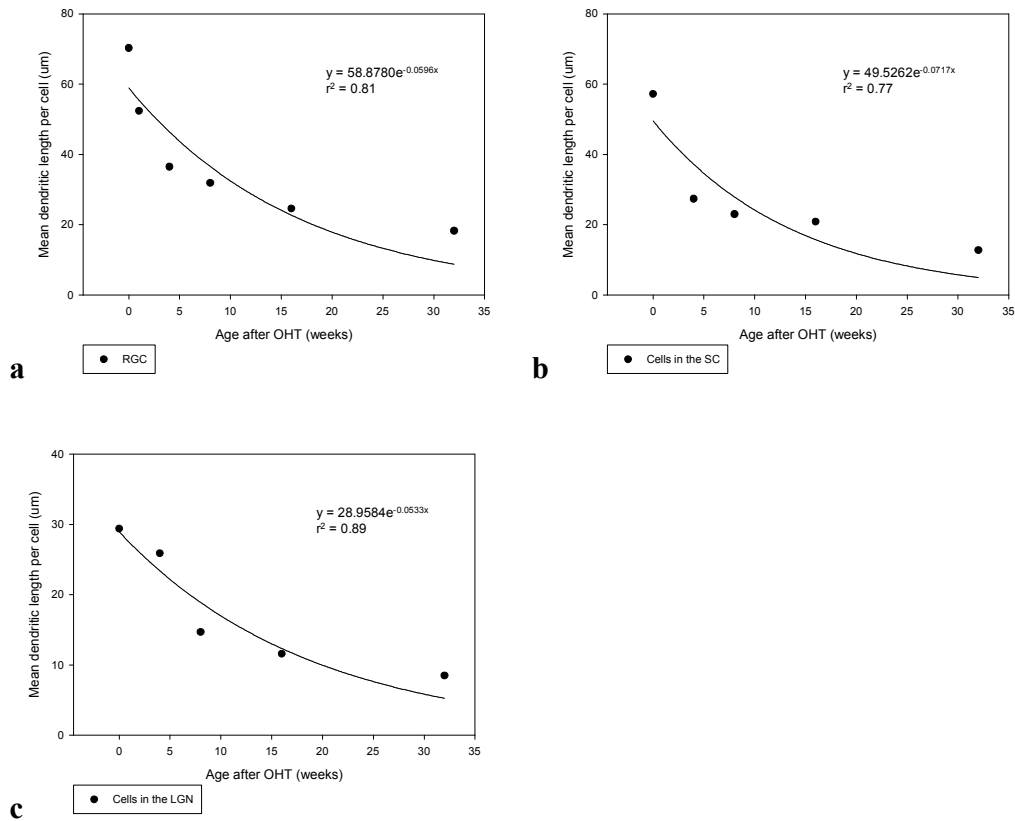


Figure 3.64a-c: The exponential decay of the mean dendritic length of RGCs, SC cells and LGN cells in glaucoma groups.

These graphs show the exponential regression analysis of the mean dendritic length of RGCs, SC cells and LGN cells from glaucoma animals: **(a)** RGC; **(b)** SC; **(c)** LGN.

To characterize the longitudinal profile of dendritic changes, the relationship between the mean dendritic length and the effect of ageing was modelled with exponential decay equations ($y = a \cdot e^{bx}$) and exponential regression analysis. The rate of dendritic shrinkage was approximated based on the exponential regression equation as previously described. Dendrites of RGCs and those in the SC and LGN from glaucoma groups shrank at a rate of 5.79% (RGC); 6.92% (SC) and 5.19%

(LGN) per week during ageing. To characterize the longitudinal profile of dendritic changes, the relationship between the dendritic number and the effect of ageing was modelled with exponential decay equations ($y = a \cdot e^{bx}$) and exponential regression analysis. The rate of dendritic loss was then approximated based on the exponential regression equation as previously described. The rates of dendritic shrinkage in glaucoma groups and those in control groups were summarised as shown in Table 3.10.

Groups	Rates of dendritic shrinkage (weekly)		
	RGCs	SC cells	LGN cells
Control	4.43%	3.98%	2.92%
Glaucoma	5.79%	6.92%	5.19%

Table 3.10: Comparison of the rates of dendritic shrinkage in glaucoma and control animals.

3.5.2.2 Changes in Dendritic Number

The dendritic number of all RGCs, SC cells and LGN cells were also compared between glaucoma groups at different time points, using one way ANOVA and the post hoc Bonferroni test.

Fig. 3.65 shows that the dendritic number of all RGCs from glaucoma groups was significantly decreased at 1 week (12.8 ± 6.1) after OHT induction compared to the baseline (15.8 ± 6.3) ($p < 0.05$). Significant dendritic loss was also observed from 1 to 4 (8.5 ± 3.2) weeks ($p < 0.001$), 4 to 16 weeks (5.5 ± 1.9) ($p < 0.05$) and 8 (7.4 ± 3.3) to

32 weeks (4.6 ± 1.4) ($p < 0.05$) after OHT induction. However, no significant dendritic loss was shown from 4 to 8 weeks ($p = 1.0$), 8 to 16 weeks ($p = 0.518$), or 16 to 32 weeks ($p = 1.0$) after OHT induction.

SC cells showed significant reductions in the dendritic number from the baseline (11.3 ± 2.2) to 4 weeks (5.2 ± 0.9) ($p < 0.001$), 8 (4.8 ± 1) to 16 weeks (3.8 ± 1) ($p < 0.001$) and 16 to 32 weeks (2.8 ± 0.7) ($p < 0.001$) after OHT induction, but not from 4 to 8 weeks after OHT induction ($p = 0.628$).

LGN cells showed significant dendritic loss from 4 ($7.2 \pm 1.3 \mu\text{m}$) to 8 weeks (4.6 ± 1.1) ($p < 0.001$), and 16 (3.9 ± 0.9) to 32 weeks (2.6 ± 0.8) ($p < 0.001$) after OHT induction. However, no significant dendritic loss was shown from the baseline (7.8 ± 1.1) to 4 weeks ($p = 0.275$) and 8 to 16 weeks after OHT induction ($p = 0.103$).

The earliest dendritic loss was observed in RGCs at 1 week, in SC cells at 4 weeks and in LGN cells at 8 weeks after OHT induction. Significant dendritic loss in the RGC, SC and LGN were shown until 32 weeks after OHT induction. The graph indicated that there was an age-related dendritic loss of RGCs, SC cells and LGN cells in glaucoma groups.

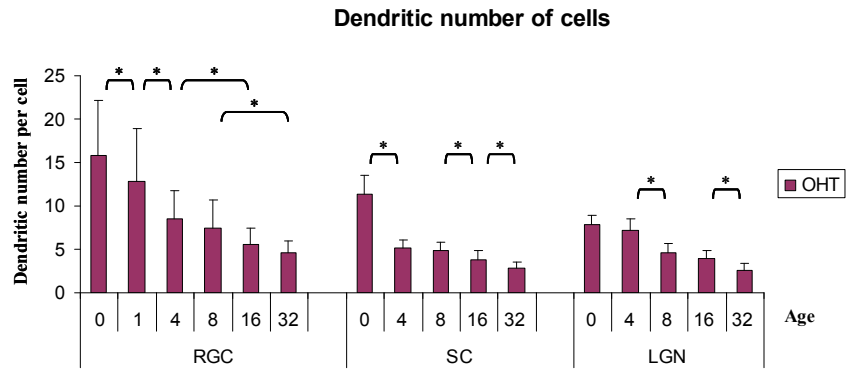


Figure 3.65: Comparison of the dendritic number of RGCs, SC cells and LGN cells in glaucoma groups.

This graph shows a comparison of the dendritic number of RGCs, SC cells and LGN cells at different time points after glaucoma surgery. The error bar represents the SD of the mean.

*p<0.05

Furthermore, a percentage reduction in the number of dendrites was calculated as previously described. Fig. 3.66 shows an increasing percentage reduction in the dendritic number from the baseline (0%), 1 week (RGC: 18.99%), 4 weeks (RGC: 46.2%; SC: 54%; LGN: 7.69%), 8 weeks (RGC: 53.16%; SC: 57.52%; LGN: 41.03%), 16 weeks (RGC: 65.19%; SC: 66.37%; LGN: 50%), until 32 weeks (RGC: 70.89%; SC: 75.22%; LGN: 66.67%).

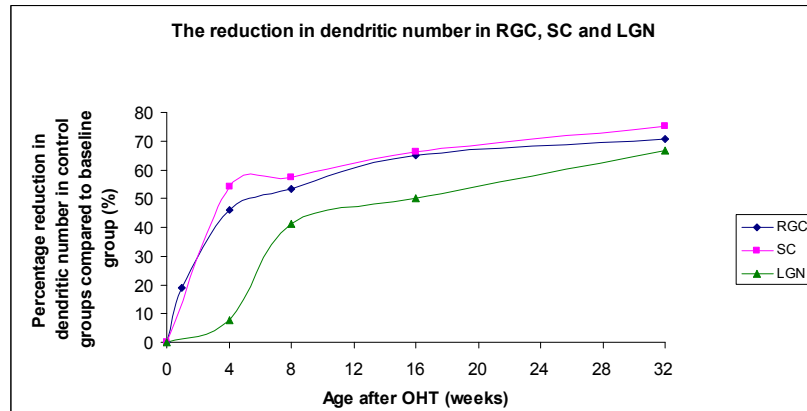


Figure 3.66: Scatter plot of percentage reductions in the dendritic number of RGCs, SC cells and LGN cells in glaucoma groups.

This graph shows the dendritic loss in RGCs, SC cells and LGN cells in glaucoma animals.

To determine if there was a relationship between ageing and dendritic number of RGCs, SC cells and LGN cells in glaucoma animals, an exponential decay analysis was performed, as shown in Fig. 3.67a-c. The strong regression coefficients (r^2) suggested that changes in the dendritic number of cells were age-related (RGC: $r^2=0.77$; SC: $r^2=0.75$; LGN: $r^2=0.92$). The Spearman's correlation test was also performed with a correlation coefficient of -1 ($p<0.001$), indicating a high probability of a negative correlation between ageing and the dendritic number of RGCs, SC cells and LGN cells in glaucoma animals.

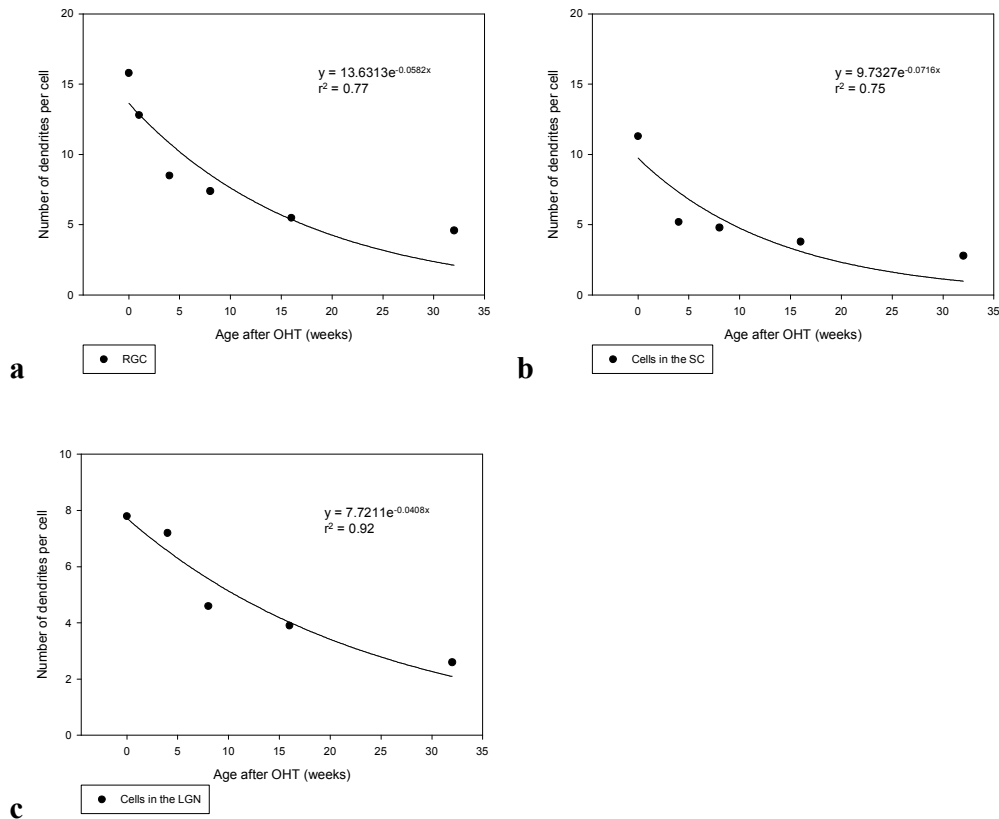


Figure 3.67a-c: The exponential decay of the dendritic number of RGCs, SC cells and LGN cells in glaucoma groups.

These graphs show the exponential regression analysis of the dendritic number of RGCs, SC cells and LGN cells from glaucoma animals: (a) RGC; (b) SC; (c) LGN.

To characterize the longitudinal profile of dendritic changes, the relationship between the dendritic number and the effect of ageing was modelled with exponential decay equations ($y = a \cdot e^{bx}$) and exponential regression analysis. The rate of dendritic loss was approximated based on the exponential regression equation as previously described. Dendrites of RGC and those in the SC and LGN from glaucoma groups were lost at a rate of 5.65% (RGC); 6.91% (SC) and 4.00% (LGN)

per week during ageing. The rates of dendritic shrinkage in glaucoma groups and those in control groups were summarised as shown in Table 3.11.

Groups	Rates of dendritic loss (weekly)		
	RGCs	SC cells	LGN cells
Control	4.44%	4.06%	3.08%
Glaucoma	5.65%	6.91%	4.00%

Table 3.11: Comparison of the rates of dendritic loss in glaucoma and control animals.

3.5.3 Comparison of Dendritic Parameters between Glaucoma and Control Animals

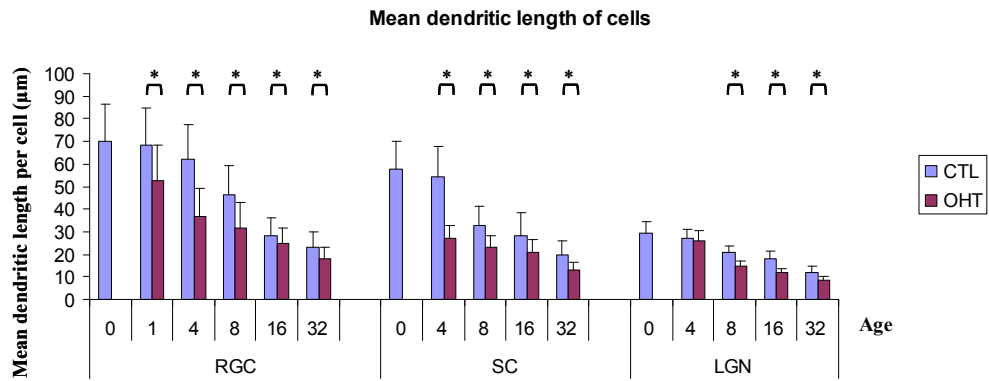
3.5.3.1 Comparison of Mean Dendritic Length

The mean dendritic lengths of all RGCs, SC cells and LGN cells were also compared between glaucoma and age-matched control animals using the student T-test (Fig. 3.68a, b).

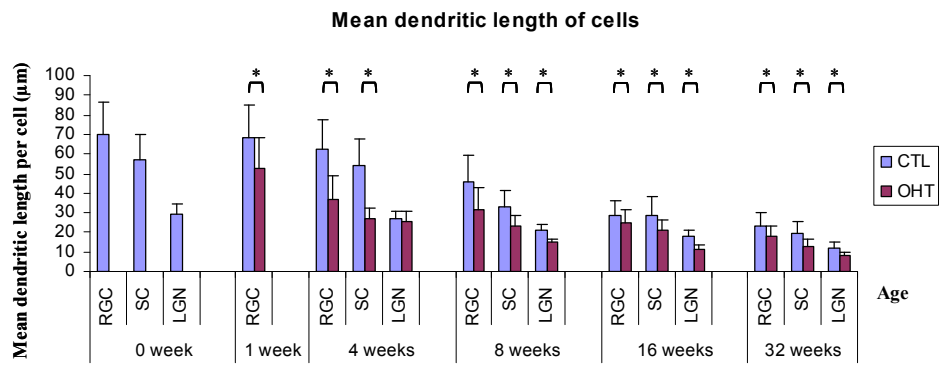
Firstly, Fig. 3.68a shows a glaucoma-related reduction in the mean dendritic length of RGCs, SC cells and LGN cells. The mean dendritic length of RGCs was significantly reduced after OHT induction at all time points ($p < 0.001$ at 1, 4, 8 and 32 weeks; $p = 0.018$ at 16 weeks). The mean dendritic length of SC cells was also significantly decreased at all time points after glaucoma surgery ($p < 0.001$ at all time points). LGN cells had significant dendritic shrinkage at 8, 16 and 32 weeks after

glaucoma surgery ($p < 0.001$ at all time points), but not at 4 weeks after OHT induction ($p = 0.321$).

Secondly, glaucoma-related dendritic shrinkage in RGCs, SC cells and LGN cells was compared, as shown in Fig. 3.68b. Significant dendritic shrinkage in RGCs was observed at 1 week after OHT induction. At 4 weeks after OHT induction, both RGCs and SC cells showed significant dendritic shrinkage. At 8, 16 and 32 weeks after OHT induction, significant reductions in the mean dendritic length were observed in all groups: RGCs, SC cells and LGN cells.



a



b

Figure 3.68a, b: Comparison of the mean dendritic length of RGCs, SC cells and LGN cells between glaucoma and control groups.

These figures show changes in the mean dendritic length of RGCs, SC cells and LGN cells after glaucoma surgery (a), and a comparison of dendritic changes in these three sites at different time points (b). The error bar represents the SD of the mean. *p<0.05

Furthermore, percentage reductions in the mean dendritic length in RGCs, SC cells and LGN cells after glaucoma surgery were also analyzed as previously described (Fig. 3.69).

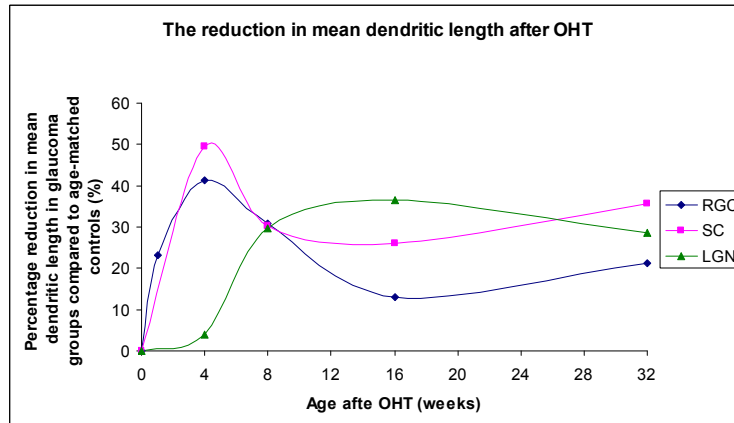


Figure 3.69: Scatter plot of percentage reductions in the mean dendritic length of RGCs, SC cells and LGN cells after glaucoma surgery.

This graph shows the dendritic shrinkage in RGCs, SC cells and LGN cells after OHT induction.

Fig. 3.69 shows that significant dendritic shrinkage in RGCs was observed as early as 1 week after OHT induction (23.28%) and was continually shown until 32 weeks. From 4 weeks after OHT induction, significant reductions in the mean dendritic length were shown in the RGCs (41.22%) and SC cells (49.54%), but not in the LGN cells, with the greatest shrinkage shown in the SC. At 8 weeks after OHT induction, there was a similar amount of dendritic shrinkage shown in RGCs (30.95%), SC (30.3%), and LGN (29.67%). From 16 weeks after OHT induction, LGN cells had greater dendritic shrinkage (36.61%) than RGCs (13.07%) and SC cells (26.15%). At 32 weeks after OHT induction, the greatest dendritic shrinkage was shown in SC cells (35.68%) again, and LGN cells (28.57%) showed greater shrinkage than RGCs (21.12%).

This figure also shows that the initial dendritic shrinkage in RGCs was observed at 1 week after OHT induction, and the peak time point of dendritic shrinkage was at 4 weeks after OHT induction. Significant dendritic shrinkage in the SC and LGN were observed from 4 and 8 weeks after OHT induction. The SC and LGN also showed the maximum dendritic shrinkage 4 and 16 weeks after OHT induction respectively.

3.5.3.2 Comparison of Dendritic Number

The dendritic numbers of RGCs, SC cells and LGN cells were also compared between glaucoma animals and age-matched controls using the student T-test (Fig. 3.70a, b).

Firstly, Fig. 3.70a shows glaucoma-related reductions in dendritic number in the RGC, SC and LGN. The dendritic number of all RGCs was significantly decreased at 4, 8, 16 and 32 weeks after elevated IOP ($p < 0.001$ at 4 weeks; $p = 0.006$ at 8 weeks; $p = 0.048$ at 16 weeks; $p = 0.04$ at 32 weeks), but not at 1 week after OHT induction ($p = 0.125$). The SC showed significant dendritic loss at all time points after glaucoma surgery ($p < 0.001$ at all time points). The LGN showed significant reductions in the dendritic number at 8, 16 and 32 weeks after glaucoma surgery ($p < 0.001$ at 8 weeks; $p = 0.004$ at 16 weeks; $p = 0.027$ at 32 weeks), but not at 4 weeks after OHT induction ($p = 0.3$).

Secondly, glaucoma-related dendritic loss in RGCs, SC cells and LGN cells was also compared as shown in Fig. 3.70b. There was significant dendritic loss

shown in the RGC at 1 week after OHT induction. At 4 weeks after OHT induction, both RGCs and SC cells showed significant reductions in the dendritic number. At 8, 16 and 32 weeks after OHT induction, significant dendritic loss was observed in all sites including the RGC, SC and LGN.

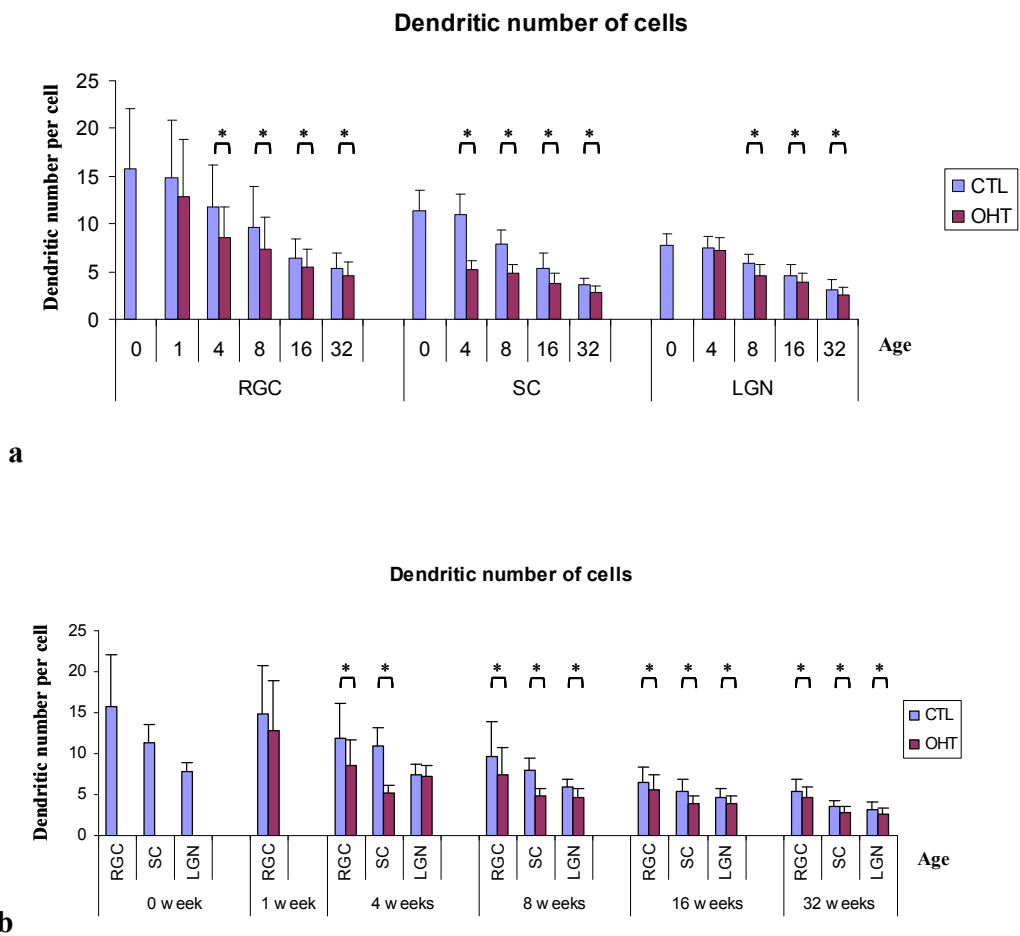


Figure 3.70a, b: Comparison of the dendritic number of RGCs, SC cells and LGN cells between glaucoma and control groups.

These figures show changes in the dendritic number of RGCs, SC cells and LGN cells after glaucoma surgery (a), and a comparison of dendritic changes in these three sites at different time points (b). The error bar represents the SD of the mean. *p<0.05

Furthermore, percentage reductions in the dendritic number of RGCs, SC cells and LGN cells after glaucoma surgery were also analyzed as previously described (Fig. 3.71).

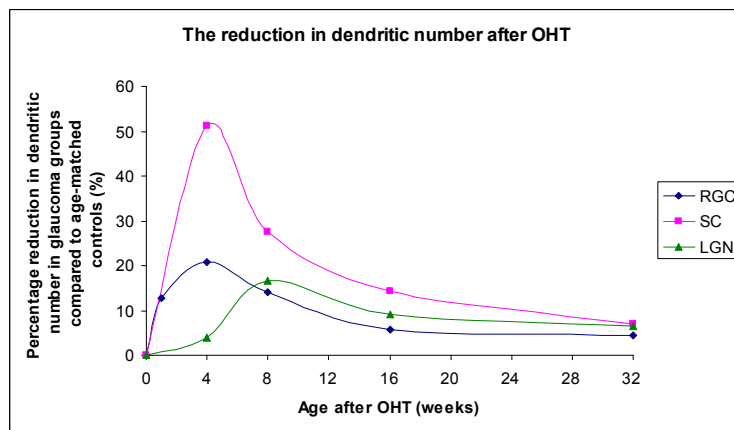


Figure 3.71: Scatter plot of percentage reductions in the dendritic number of RGCs, SC cells and LGN cells after glaucoma surgery.

This graph shows the dendritic loss in RGCs, SC cells and LGN cells after OHT induction.

Fig. 3.71 shows that there was 13.51% dendritic loss in the RGCs at 1 week after OHT induction, but not reaching statistical significance ($p=0.125$). At 4 weeks after OHT induction, significant dendritic loss was observed in the RGCs (27.97%) and SC cells (52.68%), but not in the LGN cells, with the greatest loss shown in the SC. From 8 weeks after OHT induction, a greater amount of dendritic loss was shown in SC cells (39.24%) than those in RGCs (22.92%) and LGN cells (22.03%). At 16 weeks after OHT induction, SC cells still showed greater dendritic loss

(29.63%) compared to RGCs (14.06%) and LGN cells (15.22%). At 32 weeks after OHT induction, LGN cells showed a greater amount of dendritic loss (16.13%) than RGCs (13.21%), although the greatest dendritic loss was shown in SC cells (22.2%).

This figure also shows that the peak time point of dendritic loss in RGCs was at 4 weeks after OHT induction. Significant dendritic losses in SC cells and LGN cells were observed from 4 and 8 weeks after OHT induction. The SC cells and LGN cells also showed maximum dendritic loss at 4 and 8 weeks respectively.

Chapter 4: Discussion

In this thesis, dendritic changes in the RGCs and neurons in the SC and LGN were characterized using a rat model with chronic glaucoma. Dendritic labelling in the SC cells, LGN cells and RGCs was achieved using DiI with *in vivo* and *in vitro* techniques, followed by confocal microscopy and morphological analysis. The mean dendritic length and dendritic number per cell in the baseline group, glaucoma animals and age-matched controls were analyzed. Five types of SC cells (H, W, V, P and S cells) (Fig. 3.4), two types of LGN cells (LG 1 and LG 2) (Fig. 3.22) and three types of RGCs (RI, RII and RIII) (Fig. 3.39) were studied individually (Langer and Lund, 1974; Kriebel, 1975; Perry, 1979). Additionally, dendritic parameters of all SC cells, LGN cells and RGCs in the retina were analyzed to compare dendritic changes in these three different sites.

This study demonstrated both age-related and glaucoma-related dendritic shrinkage and dendritic loss in the retina and central visual targets in this rat model of experimental glaucoma.

In normal animals, the SC cells, LGN cells and RGCs showed significant reductions in the mean dendritic length and dendritic number from the baseline to 32 weeks (actual age: 40 weeks) over time. The earliest dendritic shrinkage and loss in SC cells (Fig. 3.5, 3.8), LGN cells (Fig. 3.23, 3.26) and most RGCs (Fig. 3.40, 3.43) could be observed at 8 weeks (actual age: 16 weeks).

In glaucoma animals, significant dendritic shrinkage and loss was also observed from the baseline to 32 weeks after OHT induction. The earliest dendritic changes in SC cells (Fig. 3.11 and 3.14), LGN cells (Fig. 3.29 and 3.32) and RGCs (Fig. 3.46 and 3.49) were observed at 4 weeks, 4 to 8 weeks, and 1 week after glaucoma surgery respectively, which were shown earlier than those in normal animals. Additionally, dendritic shrinkage and loss in glaucoma animals also had faster rates than those in normal animals (Table 3.2, 3.3, 3.5, 3.6, 3.8 and 3.9).

A significant decrease in the mean dendritic length and dendritic number in the SC cells (Fig. 3.17 and 3.19), LGN cells (Fig. 3.35 and 3.37) and RGCs (Fig. 3.52 and 3.54) were also observed in glaucoma animals compared to age-matched controls. The SC cells had significant dendritic shrinkage and loss at 4, 8, 16 and 32 weeks after OHT induction; the LGN cells had significant reductions in the mean dendritic length and dendritic number at almost all time points from 4 to 32 weeks after OHT induction; RGCs showed significant dendritic shrinkage from 1 to 32 weeks after OHT induction, and dendritic loss at most time points.

Furthermore, the comparison of average dendritic parameters of all SC cells, all LGN cells and all RGCs in glaucoma animals suggested that the RGC was the first site to show dendritic changes after IOP surgery (Fig. 3.62 and 3.65). Both dendritic shrinkage and loss were observed in RGCs at as early as 1 week after OHT induction, whereas the initial dendritic changes in the SC and LGN were observed at 4 weeks after OHT induction. The most prominent dendritic changes after OHT induction were observed in SC cells. In addition, both RGCs and SC cells showed the maximum dendritic changes at 4 weeks after OHT induction, whilst the peak

time point of dendritic changes in LGN cells was at 8 (dendritic loss) and 16 weeks (dendritic shrinkage) after OHT induction.

In summary, dendritic morphology in the RGCs, SC cells and LGN cells were demonstrated to be affected by both ageing and elevated IOP. Dendritic shrinkage and loss observed in glaucoma animals had greater amounts and faster rates than those observed during ageing. Additionally, the RGC was demonstrated as the first site to show dendritic degeneration, and the SC cells had the most pronounced dendritic changes following elevated IOP. Dendritic changes in the RGCs and SC cells were faster than those in the LGN cells. The peak of dendritic changes in the RGCs and SC cells were both observed at 4 weeks after glaucoma surgery, which were earlier and greater than those shown in the LGN cells.

4.1 The Methodologies of Dendritic Labelling and Analysis

4.1.1 Dendritic Labelling

Dendrites are fine processes that extend out from the nerve cell body, receiving signals from other neurons (Purves et al., 2001). Successful dendritic labelling was essential to enable the study of dendritic morphology in RGCs and nerve cells in the SC and LGN.

Various labelling methods have been applied in the staining of dendrites including the Golgi technique, intracellular labelling, retrograde injection labelling, immunochemical staining, immersion staining and biolistic staining. The Golgi impregnation staining which was introduced by Camillo Golgi a century ago, is a

traditional method for the visualization of neuronal processes in fixed brain tissue. This method has been widely used to study dendritic morphology in different species (Machado-Salas et al., 1977; Mervis, 1978; Cupp and Uemura, 1980; Nakamura et al., 1985; Jacobs et al., 1997; De Brabander et al., 1998). Retrograde injection labelling is another technique applied in the study of neuronal morphology. Kabaso et al., performed intracortical injection of 4% Fast Blue to label long and local projection neurons in monkeys (Kabaso et al., 2009). Nimchinsky et al., used 4% Fast Blue and 4% Diamidino Yellow to retrogradely label cortical projection neurons in monkeys which were then kept alive for about 3 weeks for optimal retrograde transport (Nimchinsky et al., 1996). An immunostaining method using MAP2 as a sensitive marker was also employed to identify dendritic structure in the CNS (Kitagawa et al., 1989; Li et al., 1995; Lewen et al., 1996; Li et al., 2000; Gupta et al., 2007).

Recently, fluorescent dye DiI has been increasingly used to label neurons either *in vivo* or in fixed tissue by immersion labelling, injection labelling and biolistic staining (Elberger and Honig, 1990; Buhl and Dann, 1991; Lo et al., 1994; Hofmann and Bleckmann, 1999; Lavdas et al., 1999; Gan et al., 2000; Molnar et al., 2002; Pearson et al., 2005; Becker et al., 2007). DiI is a lipophilic carbocyanine dye, which was introduced as a neuronal tracer in fixed tissue by Godement et al. twenty years ago (Godement et al., 1987). Compared with the Golgi technique, the DiI staining method is more simple and rapid. This fluorescent labelling combined with confocal microscopy produces images with better resolution and allows a larger sampling size (Kim et al., 2007). Since DiI has been proved as a convenient and effective cell marker, it has been employed to label the structure of cells including

dendritic arborisation and spine structures extensively (Ragnarson et al., 1992; Hosokawa et al., 1995; Hofmann and Bleckmann, 1999; Kirov and Harris, 1999; Gan et al., 2000; Kim et al., 2007).

In this thesis, DiI was used for labelling dendrites in the RGCs, SC and LGN due to its advantages stated above. 0.1% DiI solution was applied to label cells in the SC and LGN in brain slices fixed by 4% PFA. The labelled brain slices were kept at 37°C for 7 days for optimal diffusion of the dye. In addition, DiI crystals were injected in the visual cortex for retrograde labelling of neurons in the LGN. Animals were sacrificed after a survival time of 4 weeks to permit optimal retrograde transport. Dendritic labelling in RGCs has been previously achieved using DiI by biolistic staining, which was also termed as Diolistic staining in other studies (Gan et al., 2000; Sun et al., 2002a, b; Morgan et al., 2006; O'Brien and Lummis, 2006).

Kim et al., have compared three DiI labelling methods to establish optimal staining protocols in cortical slices (200 µm thickness) from female Sprague-Dawley rats (Kim et al., 2007). They found that fixation of cortical slices with 1.5% PFA could improve the quality of neuronal staining and preserve the structural integrity of dendrites and dendritic spines better than those slices without fixation. The labelling of live slices using DiI crystals showed similar results as that in lightly fixed slices, but the dye diffusion was completed more quickly within one hour. However, the fixation of brain slices with 4% PFA kept at room temperature for 24 hours before confocal microscopy, showed very limited diffusion of DiI.

This present study differs from the previous studies in several ways. Firstly, brain blocks from male DA rats were sliced into thicker (400 µm) slices which were

then fixed in 4% PFA. Secondly, liquid DiI solution rather than DiI crystals was applied on brain slices for cell labelling. Thirdly, the slices were maintained at a higher temperature (37°C) for 7 days, which is a lot longer than the dye diffusion period (24 hours) in Kim's study. The complete structure of neurons consisting of the cell body and dendritic processes was clearly labelled in this study.

In order to further determine the reliability of the results from *in vitro* injection labelling, the *in vivo* retrograde labelling method was also employed to stain LGN neurons in this thesis. The comparison showed no difference between these two methods, confirming that the data from the *in vitro* injection labelling method is reliable. Also, 400 µm was demonstrated to be the optimal thickness of the brain slices to preserve the structural integrity of dendritic processes. Hence, the higher temperature, longer diffusion period for the dye, thicker brain slices and liquid dye solution used in the present study may have contributed to produce better dendritic labelling using DiI.

4.1.2 Analysis of Dendritic Parameters

The Sholl analysis, which was initially introduced to study dendritic organization in cat cortical neurons stained using the Golgi method, is a quantitative method being widely used in studies of dendritic morphology (Sholl, 1953; Cupp and Uemura, 1980; Nakamura et al., 1985; Larkman, 1991; Neale et al., 1993; Duan et al., 2003; Gupta et al., 2007). It creates a series of concentric circles with increasing radii that are centred in the perikaryon. The cumulative intersections, number of dendritic

segments and the relative length of the dendrites were then calculated.

In this thesis, the actual length of dendrites was measured and the number of dendrites per cell was counted. The tracing and the quantitative analysis of dendrites were performed using Neuron J plugin in the ImageJ programme, which was designed by the National Institutes of Health and is being increasingly used for morphometric neuronal analysis (Collins, 2007). Neuron J is a programme specifically designed to facilitate the tracing and quantification of elongated structures, in particular neuritis in fluorescence microscopy images (Abramoff et al., 2004; Meijering et al., 2004). Compared to the traditionally used Sholl analysis, the recently designed Neuron J programme is a simpler and direct method for quantifying dendrites. Hence, all the measurements of dendritic length and number in the present study were performed using the Neuron J programme, revealing the more accurate tracing of the labelled dendrites. In addition, a comparison of the Neuron J programme to Sholl analysis was also performed by analyzing a sample neuron, as shown in the appendix.

4.2 Classification of the SC cells, LGN cells and RGCs

4.2.1 Classification of Neurons in the SC

In the present study, SC cells were stained using fluorescent dye DiI with the *in vitro* technique, and the labelled dendrites were traced and quantified using the Neuron J programme. The five types of cells, including H; W; V; P and S cells, analyzed in this thesis were defined according to their dendritic orientation and the shape and size of the cell body as described in Langer and Lund's study (Table 3.1)

(Langer and Lund, 1974).

The H cells in this study have fusiform cell bodies with an average diameter of 10 μ m. Their dendrites are tangential to or parallel with the surface of the colliculus. There were three types of vertical cells analyzed in the present study, including the W, V and P cells which have their dendritic fields vertically orientated. The P cells have ovoid or cup-shaped cell bodies with a diameter of 10 μ m to 15 μ m. These cells usually have 2-5 primary dendrites which are either ascending or descending. The ascending dendrites branch more frequently as they approach the surface. The V cells have narrow, fusiform cell bodies ranging from 10 μ m to 20 μ m in diameter, and the dendrites extend both above and below the cell body. The W cells refer to those which have horizontal fusiform cell bodies in a diameter of 15 μ m to 25 μ m, 3-7 primary dendrites and large dendritic fields. Unlike that in Langer and Lund's study, the W cells were not further classified into subtypes in this thesis. The S cells have multipolar cell bodies with dendrites arising from the cell body symmetrically. The mean dendritic lengths of SC cells in DA rats aged at 7 to 8 weeks are 75.3 \pm 9.5 μ m (H); 60.4 \pm 7.4 μ m (W); 43.4 \pm 4.7 μ m (V); 54.5 \pm 6.5 μ m (P); 52.5 \pm 4.6 μ m (S).

In Langer and Lund's study, Golgi methods were used to label cells in adult white rats at the age of 3-6 months. They found the higher order dendrites of horizontal cells may run over 300 μ m and dendrites of piriform cells could extend for about 150 μ m to 350 μ m in width and slightly less than 200 μ m in depth. The dendritic fields of narrow field vertical cells are about 100 μ m to 200 μ m in width and dendritic fields of wide field vertical cells may be over 400 μ m in diameter. However, there was little quantitative data shown in their study and the actual dendritic length in

different types of cells was never measured. Langer and Lund additionally assessed another cell type called marginal cells characterized by a small ovoid cell body with a diameter of 5-8 μ m. As the most superficially located soma in the SC, marginal cells are within or just beneath the anteroposterior coursing fibres of the stratum zonale. However, the marginal cells were not analyzed in this present study due to this type of cell not being observed frequently.

Compared with dendrites of SC cells recorded in this thesis, the labelled dendrites in Langer and Lund's study appeared longer. This is may be due to the different staining methods or different species of rats used in this study. Although the true neuronal structure may not be completely shown due to the technical limitations in the present study, the relative difference between neurons are essentially consistent through the entire study as that stated in Cupp and Uemura's, and Coleman and Riesen's studies (Coleman and Riesen, 1968; Cupp and Uemura, 1980).

4.2.2 Classification of Neurons in the LGN

The LGN, another central target of retinal axons in rodents, was also investigated for changes in this study. As far as I am aware, this is the first time that dendritic changes during ageing have been investigated in rat LGN.

In this present study, LGN cells were classified into two types as LG1 and LG2, based on their dendritic morphology as described by Kriebel (Table 3.2) (Kriebel, 1975). Dendritic parameters of LG1 and LG2 were analyzed individually. The type 3 cell was not analyzed in this study due to it is not being observed frequently. The LG1 cell in this thesis was defined according to the soma size (about

25 μm) and the number of primary dendrites (4 to 8 dendrites). The LG2 cell was defined by the soma size (about 20 μm), the dendritic morphology (dendrites are less numerous and shorter) and the location of cells (superficial zone of the middle third of the dLGN).

In Kriebel's original study, neurons in the dLGN were stained using the Golgi method and three neuronal types were described, although the type 3 neuron was observed less often than type 1 and 2 neurons. The type 1 neuron is the predominant cell type which may correspond to the class 1 cells in feline and the type I neurons in primate (Guillery, 1966; Wong-Riley, 1972). This type of cell has multipolar perikarya with a mean diameter of 25 μm , giving off four to eight primary dendrites. The type 2 neuron is observed less often than the type 1 neuron. They have smaller somas with a diameter of 20 μm , and are located only within the superficial zone of the middle third of the dLGN. Their dendrites are less numerous and shorter compared to type 1 cells, however, the primary dendrites of type 2 cells extend further than those of type 1, prior to branching into secondary dendrites.

In the present study, the mean dendritic lengths of labelled LG1 and LG2 in rats aged at 7-8 weeks were $31 \pm 6.8 \mu\text{m}$ and $27.7 \pm 2.5 \mu\text{m}$ respectively. In Kriebel's paper, dendrites of type 1 neurons could extend for 108 to 120 μm , but the dendritic length in type 2 neurons was not mentioned. Although the labelled dendrites in the present study appeared shorter, the comparison of *in vitro* labelling and the *in vivo* retrograde labelling using DiI showed no difference in the length and number of dendrites, indicating that the data analyzed from the *in vitro* labelled dendrites are reliable.

4.2.3 Classification of the RGCs

Dendritic changes in the RGCs, which project to the SC and LGN in the brain, were also examined in this thesis. RGCs were labelled by the biolistic staining technique, which is being increasingly used in labelling various live tissues and has been proven as an efficient and effective labelling method (Lo et al., 1994; Gan et al., 2000; Pearson et al., 2005; Becker et al., 2007).

In the present study, RGCs were classified into three types as RI, RII and RIII according to their soma size and dendritic morphology (Table 3.3) (Perry, 1979). Dendritic parameters were then analyzed for each type of cell respectively. The mean dendritic length of cells from rats aged between 7 to 8 weeks are $83.2 \pm 11.6 \mu\text{m}$ (RI), $51.9 \pm 3.8 \mu\text{m}$ (RII) and $75.7 \pm 9.4 \mu\text{m}$ (RIII). The number of dendrites per cell was 21.6 ± 6.8 (RI); 13.3 ± 3.5 (RII) and 12.3 ± 3.5 (RIII).

In Perry's original paper, rat RGCs were stained using the Golgi method and three main types of ganglion cells were described. The type I cells have a large soma (average diameter of $20.4 \mu\text{m}$) and a large dendritic field (average diameter of $312 \mu\text{m}$). The type II cells have a small soma (average diameter of $13.5 \mu\text{m}$) and a small dendritic field (average diameter of $150 \mu\text{m}$). The type III cells have small-to-medium soma (average diameter of $12.1 \mu\text{m}$), but a large dendritic field (average diameter of $339 \mu\text{m}$). These three types of cells were also observed in other studies and termed as RG_A , RG_B and RG_C (Huxlin and Goodchild, 1997), or Class I, II and III (Dreher et al., 1985). Sun et al., further divided rodent RG_A , RG_B and RG_C cells into subtypes using the DiOlistic staining method and analyzed dendritic morphology using Sholl analysis (Sun et al., 2002b, a). In Sun et al.'s paper, more quantitative data were provided for different types of RGCs including the soma size, the mean

value and the range of dendritic field sizes. RG_A cells were subdivided into RG_{A1} and RG_{A2} with mean soma diameters of $24\mu\text{m}$ and $23\mu\text{m}$, and dendritic field sizes ranging from $120\mu\text{m}$ to $430\mu\text{m}$; RG_B cells were subdivided into RG_{B1} , RG_{B2} , RG_{B3} and RG_{B4} , with mean soma diameters ranging from $14\mu\text{m}$ to $17\mu\text{m}$ and dendritic field sizes ranging from $66\mu\text{m}$ to $284\mu\text{m}$; RG_C were subdivided into six types as RG_{C1} to RG_{C6} , with mean soma diameters ranging from $15\mu\text{m}$ to $17\mu\text{m}$ and dendritic field sizes ranging from $127\mu\text{m}$ to $467\mu\text{m}$ (Sun et al., 2002b). Although the actual dendritic field size was not measured in the present study, dendritic field size of RGCs could be approximately estimated by doubling the mean dendritic length per cell. Thus, the approximate dendritic field size in the present study is $166\mu\text{m}$ (RI), $104\mu\text{m}$ (RII) and $151\mu\text{m}$ (RIII), which could fit in the range of dendritic field size described in Sun et al.'s study (Sun et al., 2002b).

4.3 Age-related Dendritic Changes in Normal Animals

In this thesis, dendritic morphologies of neurons in the SC and LGN from normal DA rats aged from 8 to 40 weeks were studied in order to delineate the relationship between dendritic alteration and ageing in the CNS. Consistent with published literature which found age-related dendritic changes in the brain (Feldman, 1977; Mervis, 1978; Cupp and Uemura, 1980; Leuba, 1983; Nakamura et al., 1985; Jacobs et al., 1993; Jacobs and Scheibel, 1993; Jacobs et al., 1997; De Brabander et al., 1998; Jacobs et al., 2001; Peters et al., 2001; Kabaso et al., 2009), results in this thesis also demonstrated an age-dependent reduction in dendritic length and arborisation in the CNS of DA rats.

4.3.1 Dendritic Changes in the Superior Colliculus

To study dendritic changes in the SC, which is the major target of retinal axons in rodents, the mean dendritic length and dendritic number of neurons in the upper layer of the SC was analyzed. As far as I am aware, this is the first time that dendritic changes during the progression of adulthood have been investigated in the rodent SC. Furthermore, as dendritic morphology varies in different types of neurons, cells in the SC were grouped into five types following which dendritic parameters for each type of cell were analyzed respectively to study dendritic changes in depth. A comparison of percentage changes of dendrites in the SC cells is shown in Table 4.1.

Dendritic Changes	Time point / Actual age	H	W	V	P	S	Average
Dendritic shrinkage (%)	4 / 12 weeks	NS	NS	NS	NS	NS	NS
	8 / 16 weeks	44.22	30.63	39.63	45.69	52	42.31
	16 / 24 weeks	47.41	41.06	54.84	52.29	60.19	50.52
	32 / 40 weeks	65.34	54.14	66.13	72.29	70.1	65.21
Dendritic loss (%)	4 / 12 weeks	NS	NS	NS	NS	NS	NS
	8 / 16 weeks	29.29	27.2	37.7	23.71	34.68	30.09
	16 / 24 weeks	58.59	53.6	58.2	56.7	36.29	52.21
	32 / 40 weeks	68.69	68.8	71.31	62.89	66.94	68.14

Table 4.1: Comparison of percentage dendritic changes in the SC cells from normal animals at different time points.

NS: No significant changes

Table 4.1 shows that the earliest dendritic shrinkage and loss in all five types of cells in the SC were observed in the 8 weeks group (actual age: 16 weeks), reaching statistical significance ($p < 0.05$). Further dendritic shrinkage and loss were observed in the 16 weeks group (actual age: 24 weeks). In the 32 weeks group (actual age: 40 weeks), more than 50% dendritic shrinkage and 60% dendritic loss were shown in all types of SC cells.

SC cells showed various patterns of dendritic changes during ageing. Comparison of reductions in dendritic length and dendritic number showed that at 8 weeks (actual age: 16 weeks) all types of cells showed greater dendritic shrinkage than dendritic loss, suggesting that the degeneration of dendrites during ageing starts with shrinkage and then progresses to dendritic loss. At 16 weeks (actual age: 24 weeks), most cells showed slightly more dendritic loss than dendritic shrinkage, apart from the S cells where there was still greater reduction in the mean dendritic length. Changes in dendritic length and number at 16 weeks (actual age: 24 weeks) were greater than those at 8 weeks (actual age: 16 weeks). The results indicated that at this time point, most cells further degenerated by losing more dendrites. At 32 weeks (actual age: 40 weeks), the H, W and V cells showed a greater decrease in dendritic number, whilst the P and S cells still showed a greater reduction in dendritic length. These findings indicated that the H, W and V cells in rats aged at about 40 weeks continued to degenerate by losing the entire dendritic tree. The P cells showed the greatest dendritic shrinkage at 8 weeks (actual age: 16 weeks), whereas the peak time point of dendritic loss occurred at 16 weeks (actual age: 24 weeks). The S cells showed significant reductions in the mean dendritic length at all time points until 32 weeks (actual age: 40 weeks). Unlike the other four types of cells,

the S cells had a greater amount of dendritic shrinkage than dendritic loss at all time points.

4.3.2 Dendritic Changes in the Lateral Geniculate Nucleus

In the LGN of normal rats, the mean dendritic length and number of dendrites significantly decreased over time from 0 week (actual age: 8 weeks) to 32 weeks (actual age: 40 weeks), indicating an age-related dendritic shrinkage and loss in rat LGN. A comparison of percentage changes of dendrites in the LGN cells is shown in Table 4.2.

Dendritic Changes	Time point / Actual age	LG1	LG2	Average
Dendritic shrinkage (%)	4 / 12 weeks	NS	NS	NS
	8 / 16 weeks	26.13	31.41	28.91
	16 / 24 weeks	37.42	37.91	37.76
	32 / 40 weeks	54.84	64.62	59.52
Dendritic loss (%)	4 / 12 weeks	NS	NS	NS
	8 / 16 weeks	18.75	28.95	24.36
	16 / 24 weeks	31.25	50	41.03
	32 / 40 weeks	51.25	69.74	60.26

Table 4.2: Comparison of percentage dendritic changes in the LGN cells from normal animals at different time points.

NS: No significant changes

Table 4.2 shows that both the LG1 and LG2 had significant dendritic shrinkage and loss from 8 weeks (actual age: 16 weeks). An increased level of dendritic shrinkage and loss were observed in the 16 weeks group (actual age: 24 weeks). By the time of 32 weeks (actual age: 40 weeks), more than 50% reduction in the dendritic length and number was observed, which is similar to what was seen in the SC cells.

LGN cells also showed different patterns of dendritic changes during ageing. Comparison of reductions in dendritic length and dendritic number showed that both LG1 and LG2 showed greater dendritic shrinkage than dendritic loss at 8 weeks (actual age: 16 weeks), indicating that the degeneration of dendrites in aged LGN also starts with shrinkage and then progresses to loss of the dendritic tree. At 16 weeks (actual age: 24 weeks), the LG1 cells showed slightly greater dendritic shrinkage than dendritic loss. The LG2 cells showed a similar amount of dendritic shrinkage as that in the LG1 cells, but of about 50% dendritic loss. The results indicated that the LG2 cells may degenerate faster during ageing than the LG1 cells. At 32 weeks (actual age: 40 weeks), the LG2 cells still showed a greater reduction in dendritic number, whilst the LG1 cells continually showed a greater reduction in dendritic length, similar to the stellate cells in the SC.

The above results showing dendritic shrinkage and loss in the LGN during the progression of adulthood are similar to what we have found in the SC. Hence, in the present study, both the length and number of dendrites of neurons are demonstrated to be associated with age in the central visual targets of DA rats.

4.3.3 Dendritic Changes in the Brain

Over the past four decades, age-related morphological changes of neurons in the brain have been recorded in different species such as primates, dogs and rodents. Irregularities in dendritic morphology, including changes in dendritic complexity and dendritic length have been identified in aged animals (Dickstein et al., 2007). Cupp and Uemura found significant shrinkage and loss of apical and basal dendrites in the prefrontal region in aged rhesus monkeys (Cupp and Uemura, 1980). Nakamura et al. reported a decline in the number of dendrites in pyramidal cells with age in human motor cortex (Nakamura et al., 1985). In human dentate gyrus, 43% dendritic shrinkage was observed in the very old adults, although an increase in dendritic length was found in old compared to middle aged adults (Flood et al., 1985). Jacobs and Scheibel demonstrated an inverse relationship between age and dendritic length of the basilar dendrites of supragranular pyramidal cells in human superior temporal gyrus (Jacobs and Scheibel, 1993). Similarly, Anderson and Rutledge also reported age-related dendritic shrinkage in supragranular pyramidal cells in humans (Anderson and Rutledge, 1996). De Brabander et al. revealed an age-related decrease in the total dendritic length, total number of dendritic segments, and terminal dendritic length in pyramidal cells in human prefrontal cortex (De Brabander et al., 1998). Recently, Kabaso et al. investigated dendritic changes in pyramidal neurons in monkey prefrontal cortex and found a significant reduction in dendritic length and branching complexity in long projection neurons (Kabaso et al., 2009). Dendritic shrinkage was also demonstrated in the neocortex in aged dogs (Mervis, 1978).

In rodents, significant decreases in the dendritic extent and complexity have also been recorded in different types and locations of cells in the brain. Machado-

Salas et al. have described the morphological changes of dendrites including the shortening of dendrites and a reduction in dendritic arborisation in the hypothalamus in old mice (Machado-Salas et al., 1977). In aged mice, Leuba demonstrated significant loss of dendritic branches around the soma of pyramidal neurons in the visual cortex (Leuba, 1983). In aged rats, significant dendritic shrinkage and loss were also observed in pyramidal cells in the cortex (Feldman, 1977). In the medial frontal cortex of aged rats, significant shrinkage of basal dendrites in layer 2/3 pyramidal neurons was demonstrated, although no significant dendritic loss was shown (Grill and Riddle, 2002). The shortening and loss of basal dendrites in layer V pyramidal neurons was shown in aged rats (Wong et al., 2000). Recently, Xu et al, have demonstrated an age-related decrease in the dendritic length in rat visual cortex (Xu et al., 2007). At a functional level, however, visual abilities were found to decline during ageing, and these declines have been found to be associated with the structural changes of neurons prior to cell loss in the retina and brain (Ahmad and Spear, 1993; Spear, 1993; Grill and Riddle, 2002). This suggests that investigation of dendritic changes with age in the visual pathway could facilitate early detection of visual impairment and therapeutic strategies.

Although these previous studies have shown dendritic shrinkage and loss with age in the CNS, no previous studies have investigated dendritic changes with age in the SC and LGN in rats. In this thesis, dendritic alterations of neurons in the SC and LGN were investigated in normal DA rats aged from 8 to 40 weeks. The mean dendritic length and number of dendrites of neurons in the SC and LGN were significantly decreased over time, indicating an age-dependent dendritic shrinkage

and loss in rat SC and LGN (Table 4.1, 4.2). The results in the present study support the previous findings of age-dependent reductions in dendritic length and complexity in humans and animals. However, unlike the previous studies which mostly reported dendritic alterations in old animals, this thesis demonstrated age-related dendritic changes during the progression of adulthood. A comparison of results in this thesis and those in published literature is shown in Table 4.3a, b.

Compared with the age-related dendritic shrinkage that was shown in the cortex of rodents, reductions in the dendritic extent in the SC and LGN were greater (Feldman, 1977; Leuba, 1983; Wong et al., 2000; Grill and Riddle, 2002; Xu et al., 2007) (Table 4.3a). In the present study, 65.2% and 59.5% dendritic shrinkage were shown in the SC and LGN cells aged at 10 months compared to baseline controls. In the visual cortex, 40% dendritic shrinkage was shown in pyramidal neurons from aged Long-Evans hooded rats (22-24 months) compared to young rats (2-3 months) (Xu et al., 2007). There was a 23.6% shortening of basal dendrites shown in layer V pyramidal neurons in aged BN rats (28-37 months) compared to young ones (1-2 months) (Wong et al., 2000). In the medial frontal cortex of BN rats, 20% to 26% shrinkage of basal dendrites in pyramidal neurons was also shown from 18 to 28 months, although a 37% increase of dendritic extent was found from 2 to 18 months (Grill and Riddle, 2002).

Apart from age-related dendritic shrinkage, dendritic loss in the central visual target of DA rats was also found to be associated with age (Table 4.3b). There were 68.1% and 60.3% decreases in dendritic numbers shown in the SC cells and LGN cells aged at 10 months, which were greater than those shown in the cortex of rodents. In the cortex, about 28% and 34% loss of dendritic branches around the

soma were shown in pyramidal neurons of aged mice (18 month) compared to adult ones (6 months) (Leuba, 1983). In the rat parietal cortex, a 34.5% loss of basal dendrites was shown in layer V pyramidal neurons aged at 28-37 months (Wong et al., 2000).

Although various patterns of age-related dendritic changes in the brain have been observed, depending on the species, cells types, cell locations in the brain, labelling techniques, sample size or even the environmental factors, regressive changes in dendritic extent and arborisation generally occur in the CNS of humans and other animals during ageing. Accordingly, the interpretation of data in studies of age-dependent dendritic changes is appropriate as long as the youngest controls are mature (Flood, 1993; Anderson and Rutledge, 1996). In the present study, significant reductions in dendritic length and number in the SC cells and LGN cells were shown from about 4 to 6 months until 10 months; of those ages the rats were all indeed mature. Hence, this thesis demonstrated age-related dendritic changes during the progression of adulthood in rats. In addition, multiple age groups including rats aged at 8, 12, 16, 24 and 40 weeks were studied in this thesis. The temporal profile of dendritic changes in the SC and LGN was presented, which helped to evaluate whether age-related dendritic changes were constant and allowed the delineation of nonlinear changes (Coleman et al., 1990). Another advantage of this present study is that dendritic changes with age was studied in different types of cells individually, and thus various patterns of age-dependent changes of dendrites were shown in the SC cells and LGN cells, as described earlier in chapters **4.3.1** and **4.3.2**.

Dendritic parameters of neurons from DA rats aged from about 2 to 10 months were shown in this present study. However, dendritic morphologies of cells

in middle-aged or old animals are still unclear. Although the definitions of middle-aged or old rats in published literature are varied, rats that were 2 to 3 months, 12 to 15 months, and above 18 months of age were generally considered as young adults, middle-aged rats, and old rats respectively (Leuba, 1983; Flood, 1993; Lu et al., 1998; Wong et al., 2000; Grill and Riddle, 2002; Xu et al., 2007; Kinoshita et al., 2009). Hence, the dendritic parameters of cells in the SC and LGN in middle-aged (12 months) and old rats (18 months) could be estimated based on the exponential regression equations that have been shown in this thesis. In fact, the dendritic parameters estimated using the exponential equations would never be zero. Using the equations, the mean dendritic lengths of SC cells and LGN cells in 12 month old rats are estimated as 11.2 μ m and 8.9 μ m, and those of SC cells and LGN cells in 18 month old rats are estimated as 4.23 μ m and 4.38 μ m. Likewise, the dendritic numbers of SC cells and LGN cells in 12 month old rats are estimated as 2, and those of SC cells and LGN cells in 18 month old rats are estimated as 1. Compared to the dendritic parameters of pyramidal neurons that have been studied in the cortex of middle-aged or aged rats, the estimated dendritic extents and arborizations of SC cells and LGN cells in middle-aged and old DA rats appeared shorter and lesser (Leuba, 1983; Wong et al., 2000; Grill and Riddle, 2002; Xu et al., 2007). This could be due to limitations of the estimation and the staining technique, different types and locations of cells or different species of rats that were analyzed in this thesis. Therefore, it would be worth investigating the actual dendritic parameters of SC cells and LGN cells in middle-aged or old animals in the future for better delineation of dendritic morphologies.

Species	(a) Dendritic Shrinkage with Age in the CNS		References
Rats	SC	<ul style="list-style-type: none"> • Up to 65.21% dendritic shrinkage • <i>Average 3.98% /week shrinkage</i> 	This thesis
	LGN	<ul style="list-style-type: none"> • Up to 59.52 % dendritic shrinkage • <i>Average 2.92% /week shrinkage</i> 	
Rats	Cortex	29% and 50% shrinkage of layer III and V basal dendrites in pyramidal neurons	(Feldman, 1977)
Rats	Visual cortex	40% dendritic shrinkage in pyramidal neurons	(Xu et al., 2007)
Rats	Medial frontal cortex	20% to 26% shrinkage of basal dendrites in layer 2/3 pyramidal neurons	(Grill and Riddle, 2002)
Rats	Parietal cortex	23.6% shrinkage of basal dendrites in layer V pyramidal neurons	(Wong et al., 2000)
Monkeys	Prefrontal cortex	33% and 24% shrinkage of apical and basal dendrites in pyramidal neurons	(Cupp and Uemura, 1980)
Monkeys	Prefrontal cortex	31% shrinkage of apical dendrites in pyramidal neurons	(Kabaso et al., 2009)
Humans	Superior temporal gyrus	13% to 16% shrinkage of the basilar dendrites in supragranular pyramidal cells	(Jacobs and Scheibel, 1993)
Humans	Posterior superior temporal gyrus	Over 65% dendritic shrinkage in supragranular pyramidal neurons	(Anderson and Rutledge, 1996)
Species	(b) Dendritic Loss with Age in the CNS		References
Rats	SC	<ul style="list-style-type: none"> • Up to 68.14% dendritic loss • <i>Average 4.06% /week loss</i> 	This thesis
	LGN	<ul style="list-style-type: none"> • Up to 60.26 % dendritic loss • <i>Average 3.08% /week loss</i> 	
Monkeys	Prefrontal cortex	39% and 18% loss of apical and basal dendrites in pyramidal neurons	(Cupp and Uemura, 1980)
Humans	Motor cortex	Up to 50% and 66% loss of layer III and V basal dendrites in pyramidal neurons	(Nakamura et al., 1985)
Mice	Cortex	28% and 34% loss of dendritic branches around the soma of the pyramidal neurons	(Leuba, 1983)
Rats	Parietal cortex	34.5% loss of basal dendrites in layer V pyramidal neurons	(Wong et al., 2000)

Table 4.3: Comparison of age-related dendritic changes found in this thesis and in published literature: (a) dendritic shrinkage; (b) dendritic loss.

4.3.4 Functional Changes in the SC and LGN during Ageing

The functional consequences of dendritic loss and shrinkage in the SC and LGN during ageing are still unclear. Spear et al. investigated the effects of ageing on neural functions in the LGN of rhesus monkeys aged either 5-16 years or 25-28 years by single cell recording (Spear et al., 1994), but showed few statistical changes in either parvocellular or magnocellular neurons of the LGN during ageing. However, Potheary et al. found an age-related decline in the contribution of NMDA receptors to fEPSP (field excitatory post-synaptic potentials) responses in the superficial superior colliculus of 8-12 month old royal college of surgeon non-dystrophic rats compared to those aged 1-2 months (Potheary et al., 2005). As NMDA receptors were suggested to be associated with neuronal plasticity, their findings of declined NMDA receptor-mediated retinocollicular transmission may indicate an age-related decline in neuroplasticity. In addition, Lacey et al. also demonstrated age-dependent changes in the functions of Group III receptors, which are involved in visual processing, in the SC of pigmented Lister hooded rats (Lacey et al., 2005). Group III receptor mediated modulation of retinocollicular transmission was found to decline with age during development and adulthood. These findings are also in accordance with the age-dependent reductions in dendritic extents and arborization in the SC and LGN that have been shown in this thesis. Neuronal dendrites are essential targets for synapses, functioning in the formation and maintenance of neural networks, the regulation of synaptic plasticity and the integration of electrical inputs (Purves et al., 2001). It has been hypothesized that the abnormalities in dendritic morphology with age may alter the neuron's response to synaptic input, which ultimately results in detrimental effects in the absence of neuronal degeneration (Duan et al., 2003;

Nguyen et al., 2004; Dickstein et al., 2007). Hence, dendritic abnormalities found in the central visual targets may contribute to visual impairment in aged rats, but this needs further investigation for validation.

4.3.5 Dendritic Changes in the Retinal Ganglion Cells

In this thesis, the mean dendritic length and dendritic number of RGCs were found to significantly decrease over time from 0 week (actual age: 8 weeks) to 32 weeks (actual age: 40 weeks) over time, suggesting that age-related dendritic shrinkage and loss occurred in RGCs in rats. Table 4.4 shows a comparison of percentage changes of dendrites in the RGCs.

As shown in Table 4.4, the RI and RIII cells had significant dendritic shrinkage from 8 weeks (actual age: 16 weeks). The RII cells showed significant dendritic shrinkage from 4 weeks (actual age: 12 weeks), which was earlier than that was shown in the RI and RIII cells. In the 16 weeks group (actual age: 24 weeks), RGC dendrites have shrunk by more than 50%. However, at the same time point, LGN cells (37%) and most SC cells (40%-60%) had less dendritic shrinkage. In the 32 weeks group (actual age: 40 weeks), dendrites of RGCs were shrunken by more than 65%. At the same time point, SC cells showed a similar amount of dendritic shrinkage, whilst LGN cells had less shrunken dendrites.

The RI, RII and RIII cells also showed significant dendritic loss from 4 (actual age: 12 weeks) and 8 (actual age: 16 weeks) weeks. In the 16 weeks group (actual age: 24 weeks), all RGCs have lost more than 50% of their dendrites. Most SC cells and the LG2 in the LGN also showed more than 50% of dendritic loss at the

same age. By the age of 40 weeks, there was approximately 63-69% reduction in the dendritic number in RGCs.

Dendritic Changes	Time point / Actual age	RI	RII	RIII	Average
Dendritic shrinkage (%)	1 / 9 weeks	NS	NS	NS	NS
	4 / 12 weeks	NS	15.41	NS	11.66
	8 / 16 weeks	32.69	40.85	31.44	34.28
	16 / 24 weeks	57.57	62.43	60.11	59.74
	32 / 40 weeks	66.47	70.33	65.39	67
Dendritic loss (%)	1 / 9 weeks	NS	NS	NS	NS
	4 / 12 weeks	29.17	NS	NS	25.32
	8 / 16 weeks	38.43	49.62	27.64	39.24
	16 / 24 weeks	61.11	58.65	57.72	59.49
	32 / 40 weeks	69.44	63.91	63.41	66.46

Table 4.4: Comparison of percentage dendritic changes in the RGCs from normal animals at different time points.

NS: No significant changes

Although no previous studies have investigated dendritic changes in rat RGCs during ageing, the losses of RGCs and optic nerve axons have been described and quantified in aged rodents (Kawai et al., 2001; Danias et al., 2003; Neufeld and Gachie, 2003; Cepurna et al., 2005). Kawai et al. suggested that ageing is the most significant risk factor for RGC loss in male albino Fischer rats. By comparing the number of RGCs between 2 year old and 2 month old rats and assuming a linear

decrease, the RGC loss with age was approximated as 1.5% RGCs/month. By the age of 24 months, approximately 35% RGCs would have been lost in rats. Danias et al. found that the RGC loss in C57 mice started from the age of 12-15 months, showing a mean reduction of approximately 18% in the number of RGCs. By the age of 18 months, the C57 rats have lost approximately 46% of their RGCs, and this figure seems to be greater than that in aged rats. Neufeld and Gachie also demonstrated that there was an age-dependent RGC loss in albino mice and rats. The rates of RGC loss in the mice and rats were approximated as 2.3% per month and 1.5% per month (Neufeld and Gachie, 2003). In adult brown norway rats, the age-related optic nerve axonal loss was described by an exponential regression curve, showing low values of 0.55 degenerating axons/1000 axons for the 5-month group and 3.03 for the 24-month group and a high of 9 degenerating axons/1000 axons for the 31-month group. Although there was a sharp rise in degenerating axons from 5 to 31 months, there was no significant difference between 5 and 24 months (Cepurna et al., 2005). As all rats used in the present study were less than 12 months of age, the age-related axonal loss would be between 0.05% and 0.3%, which is much lesser than dendritic changes.

In patients, the natural loss of RGCs with age in patients was reported as approximately 0.4%-0.5% yearly (Zeyen, 1999; Harwerth et al., 2008). In agreement with the age-related RGC loss demonstrated in patients, Harwerth et al. also showed an age-dependent loss of axons in the retinal nerve fibre layer (RNFL) with a reduction of 0.46% per year (Harwerth et al., 2008). In a study of neuronal density in the human RGC layer, the cell number was shown to fall throughout the retina with a mean reduction of 0.53% per year (Harman et al., 2000). Jonas et al. also demonstrated an age-dependent reduction in the optic nerve fibre count in humans,

showing a linear loss of approximately 0.3% per year (Jonas et al., 1992).

A comparison of dendritic changes in the RGCs shown in this thesis and the loss of RGCs and optic nerve axons observed in published literature is summarised in Table 4.5.

Species	Age-related changes	Approximate rates of Changes	Reference
DA rats	RGC Dendritic shrinkage	<ul style="list-style-type: none"> • Up to 67% shrinkage of dendrites • Average 4.43% / week (approximately equivalent to 7.66% /year in humans)	This thesis, (Ruth, 1935)
	RGC Dendritic loss	<ul style="list-style-type: none"> • Up to 66.5% loss of dendrites • Average 4.44% /week (approximately equivalent to 7.68% /year in humans)	
Albino rats	RGC loss	1.5% /month	(Kawai et al., 2001; Neufeld and Gachie, 2003)
Albino mice	RGC loss	2.3% /month	(Neufeld and Gachie, 2003)
C57 mice	RGC loss	18% and 46% decrease in RGC number at 12-15 and 18 months	(Danas et al., 2003)
Humans	RGC loss	0.4% to 0.5% /year	(Zeyen, 1999; Harwerth et al., 2008)
	Cell density in RGC layer	0.53% /year	(Harman et al., 2000)
BN rats	RGC axonal loss	0.05%, 0.3% and 0.9% axonal loss at 5, 24 and 31 months	(Cepurna et al., 2005)
Humans	Optic nerve fibre count	0.3% /year	(Jonas et al., 1992)
	Axonal loss in RNFL	0.46% /year	(Harwerth et al., 2008)

Table 4.5: Comparison of RGC age-related changes shown in this thesis and in published literature.

Dendritic changes in the RGCs of DA rats started from the age of about 3 to 4 months, showing 11.66% average reduction in the mean dendritic length and 25.32%

average decrease in the number of dendrites (Table 4.4). Compared with the RGC loss which was observed from 12-15 months in C57 mice (Danas et al., 2003), RGC dendritic changes shown in this thesis occurred much earlier. In the present study, RGCs in DA rats aged at about 10 months showed about 67% dendritic shrinkage and 66.5% dendritic loss. However, smaller amounts of RGC loss were shown in aged Albino rats (35% at 24 months) (Kawai et al., 2001) and in C57 mice (46% at 18 months). Furthermore, in this thesis, the rates of dendritic changes with age were approximated based on the exponential decay curve as it fits better than the linear curve. Similarly, the rate of RGC loss with age was also approximated by a non-linear curve, a second-order polynomial decay curve, in C57 mice. Comparison of the rates of dendritic changes (shrinkage: 4.43%/ week; loss: 4.44%/ week) and that of RGC loss (rats: 1.5% /month) shows that age-related dendritic changes occur faster than the loss of RGCs. In addition, as each rat month is roughly equivalent to 2.5 human years in adulthood (Ruth, 1935), dendritic changes with age in the present study could be approximately equivalent to 7.66% (dendritic shrinkage) and 7.68% (dendritic loss) yearly in humans. Thus, dendritic changes are also much faster than the natural loss of RGCs with age in humans which is approximately 0.4%-0.5% yearly (Zeyen, 1999; Harwerth et al., 2008). These results indicate that dendritic abnormalities in RGCs occurred prior to cell death in aged animals, and the rate of dendritic changes is much faster than cell loss.

The findings of dendritic abnormalities during ageing are not only consistently observed in the RGC, SC and LGN in normal rats in the present study, but also evident in other studies of age-related neuronal changes introduced earlier in this chapter (Feldman, 1977; Mervis, 1978; Cupp and Uemura, 1980; Leuba, 1983;

Nakamura et al., 1985; Jacobs et al., 1993; Jacobs and Scheibel, 1993; Jacobs et al., 1997; De Brabander et al., 1998; Jacobs et al., 2001; Peters et al., 2001; Kabaso et al., 2009).

In addition, dendritic parameters of RGCs in middle-aged and old animals were also estimated based on the exponential regression equations that have been described earlier in this thesis. Rats that were aged 12 months and 18 months were considered as middle-aged and old subjects (Leuba, 1983; Flood, 1993; Lu et al., 1998; Wong et al., 2000; Grill and Riddle, 2002; Xu et al., 2007; Kinoshita et al., 2009). The mean dendritic lengths of RGCs in 12 month and 18 month old rats are estimated as 11.5 μ m and 3.9 μ m. The dendritic numbers of RGCs in 12 month and 18 month old rats are estimated as 2 and 1. In order to better describe dendritic morphologies of RGCs, the actual dendritic parameters of RGCs in middle-aged or old animals are also worth investigating in the future.

In the following section, age-related dendritic changes in the RGCs, and those in the SC cells and LGN cells are also compared and discussed.

4.3.6 Comparison of Dendritic Changes in the RGCs, SC cells and LGN cells

In addition to analyzing dendritic changes in individual types of cell, dendritic parameters of all SC cells, LGN cells and RGCs were analyzed and compared without classifying cells into different types. Table 4.6 shows the comparison of dendritic changes in the RGCs, SC cells and LGN cells, revealing that significant dendritic shrinkage and dendritic loss in RGCs could be observed earlier

than those in the SC cells and LGN cells. The temporal profile of percentage reductions in the dendritic length and number also clearly showed greater dendritic shrinkage and loss in the RGCs and SC cells than those in the LGN cells (Fig. 3.57, 3.60).

	Time point / Actual age	RGCs	SC cells	LGN cells
Dendritic shrinkage (%)	1 / 9 weeks	NS	/	/
	4 / 12 weeks	11.66	NS	NS
	8 / 16 weeks	34.28	42.31	28.91
	16 / 24 weeks	59.74	50.52	37.76
	32 / 40 weeks	67	65.21	59.52
Dendritic loss (%)	1 / 9 weeks	NS	/	/
	4 / 12 weeks	25.32	NS	NS
	8 / 16 weeks	39.24	30.09	24.36
	16 / 24 weeks	59.49	52.21	41.03
	32 / 40 weeks	66.46	68.14	60.26

Table 4.6: Comparison of age-related dendritic changes in the RGCs, SC cells and LGN cells.

NS: No significant changes

The average rates of dendritic changes in all cells from the SC and LGN, and in all RGCs were also calculated for comparison, as shown in Table 4.7. The rates of dendritic changes approximated based on the exponential decay equation also showed that dendritic changes in RGCs were faster than those in cells of the central visual targets. Dendrites in RGCs (4.43% weekly) shrunk faster than those in the SC

cells (3.98% weekly) and LGN cells (2.92% weekly). The loss of dendrites with age also appeared faster in the RGCs (4.44% weekly) than those in the SC cells (4.06% weekly) and LGN cells (3.08% weekly). The above results indicated that there might be a secondary degeneration in the central visual targets following the retinal degeneration. In addition, dendritic changes were found to be more pronounced in the SC than those in the LGN. This may be due to the fact that the SC is the major visual target receiving more retinal projections than the LGN in rodents.

	RGCs	SC cells	LGN cells
Dendritic shrinkage	4.43% /week	3.98% /week	2.92% /week
Dendritic loss	4.44% /week	4.06% /week	3.08% /week

Table 4.7: Comparison of average rates of age-related dendritic changes in the RGCs, SC cells and LGN cells.

4.4 Dendritic Changes in Glaucoma Animals

In this thesis, dendritic morphology in the RGCs, SC and LGN was investigated in a rat model of experimental glaucoma (Morrison et al., 1997; Guo et al., 2005a; Guo et al., 2005b; Morgan et al., 2006). Dendritic parameters were studied at different time points after glaucoma surgery (Chapter 4.4.1), and were compared between glaucoma animals and age-matched controls (Chapter 4.4.2). Average dendritic changes in all RGCs, SC cells and LGN cells were also compared

(Chapter 4.4.3). This present study found that both ageing and elevated IOP have contributed to the dendritic alterations in the RGCs, SC cells and LGN cells in our rat model of experimental glaucoma.

4.4.1 Age-related Dendritic Alteration in Glaucoma Animals

In this thesis, dendritic changes are found to be associated with ageing in the RGCs, SC cells and LGN cells from normal rats, which is in agreement with earlier findings in the nervous system, as discussed in Chapter 4.3. In glaucoma animals, both mean dendritic length and number of dendrites in the RGCs, SC and LGN were also found to be significantly reduced from the baseline to 32 weeks after OHT induction, indicating age-related dendritic shrinkage and loss. Furthermore, these age-related dendritic changes in glaucoma rats were also demonstrated to have a greater amount and faster rate than those in control groups.

4.4.1.1 Dendritic Changes in the Superior colliculus

Dendritic changes in the SC cells from glaucoma animals were compared between different time points, and were also compared with age-matched controls (Table 4.8).

Dendritic Changes (CTL vs BL; OHT vs BL)	Time point (weeks)	H	W	V	P	S	Average
Dendritic shrinkage (%)	4 CTL	NS					
	4 OHT	54.58	47.52	52.76	50.46	55.05	52.1
	8 CTL	44.22	30.63	39.63	45.69	52	42.31
	8 OHT	61.75	53.31	56.45	62.57	64.57	59.79
	16 CTL	47.41	41.06	54.84	52.29	60.19	50.52
	16 OHT	63.21	55.63	60.83	67.71	70.48	63.46
	32 CTL	65.34	54.14	66.13	72.29	70.1	65.21
	32 OHT	79.68	70.7	72.12	82.02	82.29	77.62
Dendritic loss (%)	4 CTL	NS					
	4 OHT	48.4	51.2	58.2	50.52	62.1	54
	8 CTL	29.29	27.2	37.7	23.71	34.68	30.09
	8 OHT	50.51	56	61.48	53.61	65.32	57.52
	16 CTL	58.59	53.6	58.2	56.7	36.29	52.21
	16 OHT	66.67	60.8	66.39	68.04	70.16	66.37
	32 CTL	68.69	68.8	71.31	62.89	66.94	68.14
	32 OHT	75.76	76	78.69	72.16	74.19	75.22

Table 4.8: Comparison of percentage dendritic changes in the SC cells of glaucoma and control animals.

CTL: Control; OHT: Ocular hypertension (blue); BL: Baseline control; NS: No significant changes

Table 4.8 shows that significant dendritic shrinkage in all five types of SC cells was observed from 4 weeks after OHT induction, which was earlier than what was seen in normal rats (8 weeks CTL group with cells aged at 16 weeks). Dendritic

shrinkage observed at 8 weeks after OHT induction was greater (average 59.79%) than at 4 weeks (average 52.1%), and was also greater than that in normal rats (average 42.31%) at the same age. An increased level of dendritic shrinkage was also observed in the 16 weeks OHT group (average 63.46%). At 32 weeks after OHT induction, dendrites in all types of SC cells shrunk by an average of 77.62%, which was also greater than what was seen in age-matched controls (average 65.21%).

All five types of cells also showed significant dendritic loss from 4 weeks after OHT induction, which was also earlier than what was seen in normal rats (8 weeks CTL group with cells aged at 16 weeks). Dendritic loss observed at 8 weeks after OHT induction (average 57.52%) was greater than that in normal rats (average 30.09%) at the same age. In the 16 weeks OHT groups, an average of 66.37% dendritic loss was observed in each type of cell, whilst in normal rats at the same age there was less dendritic loss (average 52.21%). In the 32 weeks OHT group, about 75.22% of dendrites in SC cells have been lost, which was still greater than that seen in age-matched controls (average 68.14%).

In addition, the rates of dendritic changes in the SC cells from glaucoma animals and from control animals were summarised and compared, as shown in Table 4.9. The average rate of dendritic shrinkage in glaucoma animals (6.92%/ week) was almost twice as much as that in control animals (3.98%/ week). The average rate of dendritic loss with age in glaucoma animals (6.91%/ week) was also much faster than that in control groups (4.06%/ week).

Rates of dendritic changes (%/ week)		H	W	V	P	S	Average
Dendritic shrinkage	Control	3.88	2.77	4.2	4.63	5.19	3.98
	Glaucoma	7.46	4.59	5.47	8.59	9.94	6.92
Dendritic loss	Control	4.39	4.1	4.73	3.85	3.37	4.06
	Glaucoma	6.26	5.93	8.15	6.31	10	6.91

Table 4.9: Comparison of the rates of dendritic changes in the SC cells from glaucoma and control animals.

In summary, significant dendritic changes in SC cells from glaucoma animals were observed earlier than those from control animals. The amount of dendritic changes in glaucoma animals was greater than that in age-matched controls. In addition, dendrites in SC cells changed at a faster rate in glaucoma animals than that in control animals.

4.4.1.2 Dendritic Changes in the Lateral Geniculate Nucleus

In the LGN, dendritic changes in cells from glaucoma and control animals at different ages were also compared (Table 4.10).

Table 4.10 shows that the initial dendritic shrinkage in LG2 cells occurred at 4 weeks after OHT induction, which was earlier than that observed in normal rats (8 weeks CTL group with cells aged at 16 weeks). At this time point, dendrites in LG2 cells shrunk by 13.36%. LG1 cells showed the initial dendritic shrinkage at 8 weeks

after OHT induction, with an amount of 48.71%. A greater reduction in the mean dendritic length in LG2 cells was observed at 8 weeks after OHT induction, showing 51.62% dendritic shrinkage. Both LG1 and LG2 cells showed greater dendritic shrinkages at 16 weeks and 32 weeks after OHT induction. Compared with the age-matched controls, the LGN cells of glaucoma animals had a greater amount of dendritic shrinkage at all time points.

Dendritic Changes (CTL vs BL; OHT vs BL)	Time point (weeks)	LG1	LG2	Average
Dendritic shrinkage (%)	4 CTL	NS		
	4 OHT	NS	13.36	11.9
	8 CTL	26.13	31.41	28.91
	8 OHT	48.71	51.62	50
	16 CTL	37.42	37.91	37.76
	16 OHT	59.35	61.73	60.54
	32 CTL	54.84	64.62	59.52
	32 OHT	70.65	72.2	71.09
Dendritic loss (%)	4 CTL	NS		
	4 OHT	NS	13.16	NS
	8 CTL	18.75	28.95	24.36
	8 OHT	32.5	51.32	41.03
	16 CTL	31.25	50	41.03
	16 OHT	42.5	59.21	50
	32 CTL	51.25	69.74	60.26
	32 OHT	61.25	73.68	66.67

Table 4.10: Comparison of percentage dendritic changes in the LGN cells from glaucoma and control animals.

Age-related dendritic loss was also observed in the LGN. LG2 cells showed the earliest dendritic loss at 4 weeks after OHT induction with 13.16% of dendrites being lost, whereas LG2 cells in normal rats showed the initial dendritic loss at 8 weeks. LG2 cells showed an increasing reduction in the dendritic number from 8 weeks, 16 to 32 weeks after OHT induction, with 32.5%, 42.5% and 61.25% dendritic losses respectively. However, LG1 cells still showed the initial dendritic shrinkage at 8 weeks after OHT induction with 32.5% of dendrites lost. A significant reduction in dendritic number of LG1 cells was also observed at 16 and 32 weeks after OHT induction, showing 59.21% and 73.68% dendritic loss. There was also a greater dendritic loss shown in glaucoma animals than that in age-matched controls at all time points.

In addition, the rates of dendritic changes in glaucoma animals and those in control animals were also summarised in Table 4.11. The average rate of dendritic shrinkage in the OHT group (5.19%/ week) was almost twice as much as that in control animals (2.92%/ week) and the rate of dendritic loss with age in glaucoma animals (4%/ week) was also faster than that in controls (3.08%/ week).

Rates of dendritic changes (%/ week)		LG1	LG2	Average
Dendritic shrinkage	Control	2.63	3.98	2.92
	Glaucoma	5.03	6.92	5.19
Dendritic loss (%/ week)	Control	2.34	4.06	3.08
	Glaucoma	3.28	6.91	4

Table 4.11: Comparison of the rates of dendritic changes in the LGN cells from glaucoma and control animals.

In summary, dendritic changes in the LGN in glaucoma animals were initially observed from 4 to 8 weeks after OHT induction. The average dendritic shrinkage in the LGN cells from glaucoma groups were shown earlier and were greater than those in control groups. Although the average dendritic loss in the LGN cells were observed at the same age in glaucoma and control groups, the amount of loss in glaucoma animals was still greater than that in controls. In addition, the rate of dendritic changes in LGN cells in glaucoma animals was faster than that in controls, similar to what was in the SC.

4.4.1.3 Dendritic Changes in the Retinal Ganglion Cell

Dendritic changes in the RGCs from glaucoma animals and controls at different ages were also compared, as shown in Table 4.12.

All types of RGCs showed the initial dendritic shrinkage at 1 week after OHT induction, showing an average of 25.46% reduction in the mean dendritic length, whereas the earliest dendritic shrinkage in RGCs in normal animals was observed from 4 to 8 weeks. A greater amount of dendritic shrinkage was observed at 4 weeks after OHT induction in all types of RGCs (average: 48.08%). At 8 weeks after OHT induction, only the RII showed greater dendritic shrinkage than that at 4 weeks. At 16 weeks after OHT induction, the RI had greater dendritic shrinkage than that at 8 weeks, whereas the RII and RIII had similar amounts of reductions as that at 8 weeks. At 32 weeks after OHT induction, a similar amount of dendritic shrinkage was observed in all three types of RGCs (average: 73.97%).

Dendritic Changes (CTL vs BL; OHT vs BL)	Time point (weeks)	RI	RII	RIII	Average
Dendritic shrinkage (%)	1 CTL	NS			
	1 OHT	23.44	31.41	23.38	25.46
	4 CTL	NS	15.41	NS	11.66
	4 OHT	39.54	52.6	54.29	48.08
	8 CTL	32.69	40.85	31.44	34.28
	8 OHT	46.63	61.66	58.39	54.62
	16 CTL	57.57	62.43	60.11	59.74
	16 OHT	61.9	67.63	66.58	65.01
	32 CTL	66.47	70.33	65.39	67
	32 OHT	74.16	75.14	72.92	73.97
Dendritic loss (%)	1 CTL	NS			
	1 OHT	NS	24.06	23.58	18.99
	4 CTL	29.17	NS	26.02	25.32
	4 OHT	46.3	46.62	43.9	46.2
	8 CTL	38.43	49.62	27.64	39.24
	8 OHT	52.31	56.39	51.22	53.16
	16 CTL	61.11	58.65	57.72	59.49
	16 OHT	65.74	66.92	61.79	65.19
	32 CTL	69.44	63.91	63.41	66.46
	32 OHT	72.69	69.17	68.29	70.89

Table 4.12: Comparison of percentage dendritic changes in the RGCs from glaucoma and control animals.

Apart from the RI, both the RII and RIII showed the initial dendritic loss at 1 week after OHT induction, which was earlier than that in control animals. A similar

amount of dendritic loss was shown in the RII and RIII (RII: 24.06%; RIII: 23.58%). The RI showed the earliest dendritic loss at 4 weeks after OHT induction, which was earlier than that in control groups. At 4 weeks after OHT induction, both the RII and RIII showed greater dendritic loss than that at 1 week. The RI also showed a similar amount of dendritic loss as the RII and RIII at this time point, with 46.3% dendrites being lost. All RGCs continually showed dendritic loss at 8, 16 and 32 weeks after OHT induction. Average dendritic loss at 32 weeks (70.89%) was much greater than that which was seen at 4 weeks (46.2%) after OHT induction, although no significant difference in the amount of dendritic loss was shown from 4 to 8, 8 to 16, and 16 to 32 weeks (Fig 3.65).

In addition, the rates of dendritic shrinkage (5.79%/ week) and loss (5.65%/ week) in the OHT groups were also faster than those in control animals (shrinkage: 4.43%/ week; loss: 4.44%/ week), as shown in Table 4.13.

Rates of dendritic changes (%/ week)		RI	RII	RIII	Average
Dendritic shrinkage	Control	4.24	4.96	4.32	4.43
	Glaucoma	4.99	6.83	6.54	5.79
Dendritic loss	Control	5.11	4.47	3.73	4.44
	Glaucoma	6.15	5.67	4.68	5.65

Table 4.13: Comparison of the rates of dendritic changes in the RGCs from glaucoma and control animals.

As a hallmark of glaucoma disease, RGC loss has been described extensively in previous studies (Sommer, 1989; Zeyen, 1999; Agar et al., 2000; Shou et al., 2003; Cordeiro et al., 2004; Guo et al., 2005a; Guo et al., 2006; Leung et al., 2008) (Table 4.20). In glaucoma patients, the rate of RGC loss has been shown to be approximately 4% yearly, which is much faster than that occurs during normal ageing (Zeyen, 1999). Guo et al., investigated RGC apoptosis in the same rat model of experimental glaucoma as that used in this thesis (Guo et al., 2005a), and found the number of RGCs in glaucomatous eyes significantly reduced by $61.21\% \pm 7.54\%$ compared to that in control eyes at 3 months after elevated IOP. Leung et al. studied the longitudinal profile of RGC loss after the optic nerve crush in mice and suggested a two-phase exponential decay model for describing RGC degeneration (Leung et al., 2008). Their group also studied RGC loss in mouse retina after ischaemic reperfusion injury (Leung et al., 2009). In their study, significant RGC loss was observed at 1 week following acute elevation of IOP for 90 minutes, and the number of RGCs has dropped by 20.5% to 85.5% at 4 weeks after OHT induction. The longitudinal profile of remaining RGCs after elevated IOP fits best a linear regression line. Recently, Cone et al. investigated the RGC layer cell loss in a mouse model of experimental glaucoma which was induced by bead and viscoelastic injections (Cone et al., 2010). The RGC loss in glaucomatous eyes ranged from 4.1% to 20.1% by the age of 12 weeks, corresponding to an approximate rate of glaucoma-related RGC loss of 1.3% to 6.7% per month.

In this thesis, dendritic changes in glaucomatous eyes were also observed at 1 week after chronic elevation of IOP. At 4 weeks after OHT induction, there was a greater amount of dendritic shrinkage (40% to 54%) and loss (46% to 47%) in RGCs

in this study than the amount of RGC loss shown in Leung's study (Leung et al., 2009). Furthermore, the temporal profile of dendritic parameters in RGCs fits best a one-phase exponential decay curve in this present study. Compared with Guo et al.'s study which showed significant RGC loss in the glaucomatous retina at 3 months after OHT induction, RGC dendritic changes in the same rat glaucoma model were demonstrated to occur earlier (1 week after OHT induction) in this study, suggesting that dendritic pathology could be an early indicator of neuronal degeneration. Additionally, dendritic changes in the glaucoma groups in the present study were approximately equivalent to 8.6% to 11.7% (dendritic shrinkage) and 8.1% to 10.6% (dendritic loss) yearly in humans, according to the assumption that each rat month is roughly equivalent to 2.5 human years (Ruth, 1935), indicating again that dendritic changes are faster than RGC loss (4% yearly) (Zeyen, 1999). In this thesis, the glaucoma related dendritic degeneration was found to be greater and faster than the age-related dendritic changes, supporting the finding that an accelerated ageing process accompanies neurodegeneration in glaucomatous eyes (Tezel et al., 2007). A previous study also demonstrated that RGC loss was increased in glaucoma animals (Danas et al., 2003). Danas et al. studied effects of ageing and elevated IOP on RGC loss in mice and found that the RGC loss in C57 mice started between the ages of 12-15 months. By the age of 18 months, the C57 mice lost approximately 46% of their RGCs. In comparison, in the transgenic glaucoma DBA/2N^{Nia} mice, RGC loss commenced at approximately 12 months of age, but occurred at a faster rate and led to an approximate 64% of RGC loss by 15 months. Comparisons of RGC loss between 12 to 15 months of age show an age-related loss of 0.39% and an IOP-related loss of 19.15% per month.

As far as I am aware, this thesis describes for the first time the temporal profile of dendritic changes in RGCs in the glaucomatous retina. Dendritic changes in RGCs from glaucoma groups were demonstrated to occur earlier than those in control animals. Furthermore, dendritic changes in RGCs after OHT induction showed a greater amount and faster rate than that of normal animals. Similar findings were also found in the SC and LGN in glaucoma animals, where dendritic changes were observed earlier with greater amounts and faster rates than those in controls. These results indicate that not only ageing, but also elevated IOP have an affect on dendritic morphology in the retina and the central visual targets in this rat model of experimental glaucoma.

4.4.1.4 Comparison of Dendritic Changes in the RGCs, SC cells and LGN cells

Comparison of dendritic changes in the RGCs, SC cells and LGN cells from glaucoma animals revealed that RGCs had earlier and faster dendritic alterations than neurons in the SC and LGN. As shown in the temporal profile of dendritic changes in glaucoma animals (Fig. 3.63), significant dendritic shrinkage in RGCs was observed at as early as 1 week after OHT induction, whilst those in the SC and LGN occurred at 4 weeks after OHT induction. Dendritic loss in RGCs was also observed earlier (1 week) than those seen in the SC (4 weeks) and LGN (8 weeks).

Table 4.14 shows the average dendritic changes in the RGCs, SC cells and LGN cells at different time points after OHT induction, revealing that both RGCs

and SC cells show greater dendritic shrinkage and loss than LGN cells at all time points.

Dendritic Changes (OHT vs BL)	Time point (weeks after OHT induction)	RGCs	SC cells	LGN cells
Dendritic shrinkage (%)	1	25.46	/	/
	4	48.08	52.1	11.9
	8	54.62	59.79	50
	16	65.01	63.46	60.54
	32	73.97	77.62	71.09
Dendritic loss (%)	1	18.99	/	/
	4	46.2	54	NS
	8	53.16	57.52	41.03
	16	65.19	66.37	50
	32	70.89	75.22	66.67

Table 4.14: Comparison of dendritic changes in the RGCs, SC cells and LGN cells from glaucoma animals at different time points.

Furthermore, dendrites in the SC cells were found to degenerate faster than those in the RGCs and LGN cells in glaucoma animals, showing higher rates of dendritic shrinkage and loss (Table 4.15). Compared with control animals, glaucoma animals showed higher rates of dendritic shrinkage and loss in the RGCs, SC cells and LGN cells.

Rates of dendritic changes (%/ week)		RGCs	SC cells	LGN cells
Dendritic shrinkage	Control	4.43	3.98	2.92
	Glaucoma	5.79	6.92	5.19
Dendritic loss	Control	4.44	4.06	3.08
	Glaucoma	5.65	6.91	4.00

Table 4.15: Comparison of the rates of dendritic changes in the RGCs, SC cells and LGN cells from glaucoma and control animals.

The above results indicate that the RGC is the first site to show dendritic alteration in glaucoma animals, similar to what was found in control animals. Dendritic changes in the SC and LGN occurred later than those in the RGC again indicating that there was secondary degeneration in the central visual targets after the retinal degeneration.

4.4.2 Glaucoma-related Dendritic Changes

Although dendritic changes in the brain during ageing have been reported in different species as described previously, few studies have investigated dendritic changes in the CNS after OHT induction. Recently, Gupta et al. found morphological changes of dendrites in the LGN in an experimental primate model (Gupta et al., 2007). In their study, striking changes with thickened and shortened dendrites in the LGN were observed following chronically elevated IOP. The dendritic field size in glaucoma groups was significantly reduced by approximately 53% (M layer) and

56% (P layer) compared to that in controls. The dendrite complexity was also decreased by 47% and 41% in M and P layers respectively after OHT induction. Recently, reductions in dendrite complexity and length were also demonstrated in LGN relay neurons in a primate model of glaucoma (Ly et al., 2010). Approximately 52% (M layer) and 50% (P layer) dendritic shrinkage and 53% (M layer) and 47% (P layer) dendritic loss were shown in glaucoma monkeys.

Dendritic changes also have been found in CNS injury and other neurodegenerative conditions, apart from glaucoma (Yanagihara et al., 1985; Matsumoto et al., 1987; Kitagawa et al., 1989; Bywood and Johnson, 2000). Dendritic damage in gerbil cerebral ischemia have been demonstrated (Kitagawa et al., 1989). At the early stage of ischemia, only dendritic loss was observed in the ischemic lesions; whilst at the severe stage of ischemia, the loss of nerve cell bodies and dendrites were both detected. Previous studies also found dendrites were more sensitive than the nerve cell bodies in the vulnerable regions (Yanagihara et al., 1985; Matsumoto et al., 1987). Bywood and Johnson demonstrated dendritic loss in degenerated catecholamine (CA) neurons in the substantia nigra (SN) of rat brain (Bywood and Johnson, 2000), and suggested dendritic changes as the early indicator of neurodegeneration. In addition, dendritic pathology of neurons in the brain was also documented in Alzheimer's disease (AD) (De Ruiter and Uylings, 1987; Einstein et al., 1994; Baloyannis et al., 2007; Baloyannis, 2009). The decrease in dendritic length, dendritic diameter, abnormal varicosities, and loss of dendritic spines in dentate granule cells have been reported in AD (De Ruiter and Uylings, 1987; Flood et al., 1987). De Ruiter and Uylings found the total dendritic length reduced by approximately 30% in AD cases, although no significant differences in

dendritic branching was found between AD and controls. Consistent with these findings, Einstein *et al.* also reported that dendrites of granule cells in Alzheimer's cases appeared shorter and less numerous than those in age-matched controls (Einstein *et al.*, 1994), with over 50% reduction in the total dendritic length, 33% fewer dendritic segments and 19% shorter dendritic segment length. Recently, Baloyannis demonstrated a 45% decrease in dendritic branches in acoustic and visual cortices in AD patients (Baloyannis, 2009). In addition, dendritic alteration has also been documented in ALS. Kato *et al.*, found dendrites of anterior horn cells in ALS patients appeared shorter, thinner and less numerous (Kato *et al.*, 1987). Sasaki and Iwata also found the thin and thread-like atrophic proximal dendrites with shorter lengths in anterior horn cells in ALS patients (Sasaki and Iwata, 1996). Karpati *et al.*, suggested that the loss and atrophy of dendrites could precede the death of motor neurons in ALS cases (Karpati *et al.*, 1988). Recently, Sgobio *et al.*, found 37% and 14% reductions in the length of basal dendrites and dendritic branching in PFC neurons in a mouse model of ALS (Sgobio *et al.*, 2008). Until present, only limited data of OHT-related dendritic changes in the central visual targets have been reported.

Since only limited data of dendritic changes in the central visual target in glaucoma has been reported, this present study investigated dendritic alterations in the SC and LGN using a rat model of experimental glaucoma, in order to further characterize the OHT-related dendritic changes in the brain.

4.4.2.1 Dendritic Changes in the Superior Colliculus

To investigate the relationship between elevated IOP and dendritic morphologies in the SC, dendritic parameters of SC cells from glaucoma animals and those from age-matched controls were compared. A comparison of dendritic changes in the SC from glaucoma animals at different time points is shown in Table 4.16.

Dendritic Changes (OHT vs AMT)	Time after OHT induction (weeks)	H	W	V	P	S	Average
Dendritic Shrinkage (%)	4	52.89	44.87	49	47.57	52.52	49.54
	8	31.43	32.7	27.86	31.08	26.19	30.3
	16	30.05	24.72	13.27	32.31	25.84	26.15
	32	41.38	36.1	17.69	35.1	40.76	35.68
Dendritic loss (%)	4	46.88	49.17	57.5	49.47	60.5	52.68
	8	30	39.56	38.16	39.19	46.91	39.24
	16	19.51	15.52	19.61	26.19	53.16	29.63
	32	22.58	23.08	25.71	25	21.95	22.2

Table 4.16: Comparison of dendritic changes in the SC cells after OHT induction.

AMT: Age-matched control

As shown in Table 4.16, in the SC, all five types of cells showed significant reductions in the mean dendritic length in glaucoma groups compared to those in controls. At 4 weeks after OHT induction, the mean dendritic length of SC cells was reduced by an average of 52.52%. Significant dendritic shrinkage was also observed

at 8 (average: 26.19%) and 16 weeks (average: 25.84%) after OHT induction, with a lesser amount of reduction than that at 4 weeks. At 32 weeks after OHT induction, most cells showed greater dendritic shrinkage (average: 40.76%) than that at 8 and 16 weeks, but still less than that at 4 weeks after OHT induction.

All five types of cells also showed significant dendritic loss at 4, 8, 16 and 32 weeks after glaucoma surgery. The peak time point of dendritic loss was at 4 weeks after OHT induction, with the number of dendrites reduced by an average of 60.5%. Significant dendritic loss was also observed at 8 (average: 46.91%), 16 (average: 53.16%), and 32 (average: 21.95%) weeks after OHT induction, with a lower amount of dendritic loss than that at 4 weeks.

In summary, the glaucoma-related dendritic changes in the SC could be observed at 4 weeks after OHT induction. Compared with the age-related dendritic changes which were initially observed in the 8 weeks CTL group (actual age: 16 weeks), the glaucoma-related dendritic changes appeared earlier. In addition, the age-related dendritic changes showed an increasing amount of reduction in the number and length of dendrites from baseline to the 32 weeks group, whereas the glaucoma-related dendritic changes showed the maximum reductions in the length and number at 4 weeks after OHT induction. A lesser amount of dendritic changes in the SC cells was shown at 8, 16 and 32 weeks compared to those at 4 weeks after OHT induction. This could be due to the elevated IOP being maintained for less than 8 weeks after the glaucoma surgery, as shown in Fig. 3.1.

4.4.2.2 Dendritic Changes in the Lateral Geniculate Nucleus

Dendritic changes in the LGN cells from glaucoma animals at different time points after OHT induction were also compared, as shown in Table 4.17.

Dendritic Changes (OHT vs AMT)	Time after OHT induction (weeks)	LG1	LG2	Average
Dendritic Shrinkage (%)	4	NS		
	8	30.57	29.47	29.67
	16	35.05	38.37	36.61
	32	35	21.43	28.57
Dendritic loss (%)	4	NS		
	8	16.92	31.48	22.03
	16	16.36	18.42	15.22
	32	20.51	NS	16.13

Table 4.17: Comparison of dendritic changes in the LGN cells after OHT induction.

In the LGN, both the LG1 and LG2 showed significant reductions in the mean dendritic length from 8 weeks after OHT induction. Unlike that in the SC, no difference in the mean dendritic length was shown in the LGN between 4 weeks glaucoma animals and age-matched controls. At 8 weeks after OHT induction, the mean dendritic lengths of the two types of cells were reduced by an average of 29.67%. An increased level of dendritic shrinkage was observed at 16 weeks (average: 36.61%) after OHT induction. A lesser amount of dendritic shrinkage was

also observed 32 weeks (average: 28.57%) after OHT induction.

All two types of cells also showed significant dendritic loss from 8 weeks after glaucoma surgery. The number of dendrites did not show a difference between the 4 weeks glaucoma animals and age-matched controls. The number of dendrites was significantly reduced at 8 (average: 22.03%) and 16 (average: 15.22%) weeks after OHT induction. The maximum dendritic loss was also shown at 8 weeks after OHT induction. At 32 weeks after OHT induction, only the LG1 showed significant dendritic loss.

In summary, the glaucoma-related dendritic changes were also demonstrated in the LGN in rats with chronic glaucoma. The earliest dendritic changes in the LGN cells were observed at 8 weeks after OHT induction, which is later than those shown in the SC cells (4 weeks after glaucoma surgery). In addition, the LGN cells had a lower amount of dendritic shrinkage and loss than SC cells after OHT induction. Furthermore, the glaucoma-related dendritic changes did not appear earlier than the age-related dendritic changes in the LGN, which was unlike that in the SC.

4.4.2.3 Dendritic Changes in the CNS in Neurodegenerative Conditions

Morphological changes of dendrites in degenerated neurons in the brain have been documented in different neurodegenerative conditions, including glaucoma (Gupta et al., 2007; Ly et al., 2010), CNS injury (Yanagihara et al., 1985; Matsumoto et al., 1987; Kitagawa et al., 1989; Bywood and Johnson, 2000), AD (De Ruiter and Uylings, 1987; Einstein et al., 1994; Baloyannis et al., 2007; Baloyannis, 2009) and ALS (Kato et al., 1987; Sasaki and Iwata, 1996; Sgobio et al., 2008).

In the present study, dendritic morphologies in neurons of the SC and LGN from glaucoma rats and age-matched controls were analyzed and compared. Significant dendritic shrinkage and loss in the SC and LGN were observed in glaucoma animals compared to age-matched controls (chapter 4.5.1, 4.5.2), indicating OHT-related dendritic changes in our rat model of experimental glaucoma.

Compared with previous studies, dendritic labelling and morphological analysis were achieved in a different way in this thesis. Firstly, the *in vitro* DiI labelling was employed rather than the Golgi staining (De Ruiter and Uylings, 1987; Kato et al., 1987; Sgobio et al., 2008; Baloyannis, 2009), immunostaining (Kitagawa et al., 1989; Bywood and Johnson, 2000; Gupta et al., 2007; Ly et al., 2010), or intracellular staining (Einstein et al., 1994) that were used in other studies to label neurons. Secondly, the actual length of dendritic branches rather than the relative length of dendritic segments were recorded. Although a different staining technique and analysis method was employed, results in this thesis also demonstrated dendritic degeneration in the central visual targets in DA rats following chronically elevated IOP. The glaucoma-related morphological changes of dendrites were investigated by comparing the dendritic parameters between glaucoma animals and age matched controls, revealing significant shortening of dendritic length and the loss of dendrites which were observed in the SC and LGN in glaucoma animals.

The findings in this thesis are in agreement with those in other neurodegenerative conditions such as toxin-induced ischemia, AD and ALS described before. Table 4.18 shows the comparison of findings in this thesis and those in published literature.

Species and Disease	(a) Dendritic Shrinkage in the CNS		References
Rats with glaucoma	SC cells	<ul style="list-style-type: none"> ● Up to 49.54% dendritic shrinkage ● <i>Average 6.92% /week shrinkage</i> 	This thesis
	LGN cells	<ul style="list-style-type: none"> ● Up to 36.61% dendritic shrinkage ● <i>Average 5.19% /week shrinkage</i> 	
Primates with glaucoma	LGN cells	Up to 53% and 56% shrinkage in M and P layers after OHT	(Gupta et al., 2007)
Primates with glaucoma	LGN cells	52% and 50% shrinkage in M and P layers after OHT	(Ly et al., 2010)
AD Patients	Fascia dentata granule cells	30% reduction in the dendritic length	(De Ruiter and Uylings, 1987)
AD Patients	Dentate granule cells	50% reduction in the total dendritic length and 19% shorter average dendritic segment length	(Einstein et al., 1994)
ALS patients	Anterior horn cells	Thin and thread-like atrophic proximal dendrites with 23.9% reduction in the mean dendritic length	(Sasaki and Iwata, 1996)
Mice with ALS	PFC neurons	37% reduction in the length the basal dendrites	(Sgobio et al., 2008)
Species and Disease	(b) Dendritic Loss in the CNS		References
Rats with glaucoma	SC cells	<ul style="list-style-type: none"> ● Up to 52.68% dendritic loss ● <i>Average 6.91% /week loss in OHT rats</i> 	This thesis
	LGN cells	<ul style="list-style-type: none"> ● Up to 22.03% dendritic loss ● <i>Average 4% /week loss in OHT rats</i> 	
Primates with glaucoma	LGN cells	Up to 47% and 41% loss in M and P layers after OHT	(Gupta et al., 2007)
Primates with glaucoma	LGN cells	53% and 47% loss in M and P layers after OHT	(Ly et al., 2010)
AD Patients	Dentate granule cells	33% fewer dendritic segments	(Einstein et al., 1994)
AD Patients	Acoustic, visual cortex cells	45% reduction dendritic branches	(Baloyannis, 2009)
Mice with ALS	PFC neurons	14% reduction in branch points	(Sgobio et al., 2008)

Table 4.18: Comparison of dendritic changes in glaucoma and neurodegenerative conditions in this thesis and in published literature: (a) dendritic shrinkage; (b) dendritic loss.

As shown in Table 4.18, this present study demonstrated significant reductions in dendritic length and number in the LGN of glaucoma rats (Table 4.17), which is in agreement with previous findings in a primate model of experimental glaucoma (Gupta et al., 2007; Ly et al., 2010). Over 50% and 40% reductions in dendritic length and complexity were observed in the LGN following elevated IOP in Gupta and Ly's et al. studies, whereas a lower amount of decrease in LGN dendritic extent (up to 36.6%) and complexity (up to 22.03%) was found in glaucoma rats in the present study. This may be due to the fact that the LGN is the major visual target in primates but not in rodents.

Similarly, significant dendritic shrinkage and loss in different types and locations of cells were also shown in AD (De Ruiter and Uylings, 1987; Einstein et al., 1994; Baloyannis, 2009), and ALS (Sasaki and Iwata, 1996; Sgobio et al., 2008) (Table 4.18). Although the amounts and patterns of dendritic changes observed in the degenerated cells are various, regressive changes of dendritic trees in the CNS generally occur in these neurodegenerative conditions.

Accordingly, dendritic changes in different visual targets (the SC and LGN), and different types of neurons (5 types of SC cells and 2 types of LGN cells) in the brain were investigated individually in the present study. Both the SC and LGN showed significant dendritic shrinkage and loss in glaucoma animals, showing different patterns of dendritic changes in the SC cells and LGN cells. The difference in dendritic changes between the SC and LGN after OHT induction might be due to the fact that the SC is the major visual target in rodents, whilst the LGN only receives about 30% of retinal projections (Dreher et al., 1985). Therefore, the elevated IOP in the retina may affect the dendritic morphology in the SC more than

in the LGN. Furthermore, in the present study, multiple age groups were analyzed and average rates of dendritic changes in the SC and LGN after OHT induction were approximated, as shown in Table 4.15 and 4.18. Dendrites in the SC cells were demonstrated to degenerate faster than those in the LGN cells following elevated IOP.

All of the above findings suggest that dendritic pathology could be regarded as an indicator of degeneration in neurodegenerative conditions. The reduced axoplasmic transport was suggested to contribute to the dendritic changes (Anderson and Hendrickson, 1974; Pavlidis et al., 2003; Gupta et al., 2007). Axoplasmic flow consisting of the transport organelles and metabolic substances along the axon could be partially obstructed by moderately elevated IOP in the region of the lamina cribrosa, optic nerve or central visual targets in the brain. This obstruction could lead to dendritic degeneration which would further proceed to cell death. However, the mechanisms involved in the dendritic degeneration are still not clear and further investigation is needed in the future.

4.4.2.4 Functional Changes in the SC and LGN in Glaucoma

Although the SC and LGN are primary targets for retinal projections, few studies have been conducted on the functional changes that occur in these two areas in a rat model of experimental glaucoma. In a monkey model of experimental glaucoma, Vickers et al. have shown changes in neurochemical features in the LGN following OHT (Vickers et al., 1997). Both P- and M-cellular layers of the LGN which received retinal input from the glaucomatous eyes showed decreased levels of

cytochrome oxidase (CO) staining and synaptophysin immunoreactivity. Crawford et al. also demonstrated a glaucoma-related reduction in neural metabolism in the LGN (Crawford et al., 2000), suggesting that both the severity and duration of the experimental glaucoma could affect the P- and M-cellular visual pathways. Recently, Georgiou et al. from our group have shown that there were functional changes in the SC following RGC degeneration in the same rat glaucoma model (Georgiou et al., 2010). In their study, an increase in NMDA receptor contribution to the SC synaptic responses was observed at 32 weeks after OHT induction. Previous work from our laboratory showed that peak RGC apoptosis occurred at 3 weeks after OHT induction in the same rat model of experimental glaucoma, and the number of RGCs in glaucomatous eyes was reduced by 61.21% at 3 months after elevated IOP (Cordeiro et al., 2004; Guo et al., 2005a). Therefore, the functional changes observed in the SC after OHT induction appeared later than the major period of RGC loss, suggesting that early detection and treatment in glaucoma may prevent or slow down the progression to functional changes. Gupta et al. have detected the atrophy of the LGN in glaucoma patients by magnetic resonance imaging (MRI), showing a significant reduction in the LGN height in glaucoma subjects compared to age-matched controls (Gupta et al., 2009). In addition, functional changes in other brain areas have also been shown in glaucoma patients (Duncan et al., 2007b, a; Garaci et al., 2009). Duncan et al. have found correlations between either visual field loss or optic disk damage and functional changes in the primary visual cortex in human POAG (Duncan et al., 2007a, b). Changes in the blood oxygen level dependent signal in the V1 were detected in POAG patients using fMRI and were found to be correlated with the loss of visual functions (Duncan et al., 2007a). The correlation

between fMRI responses to visual stimulation and the damage to optic disc was also observed in POAG patients (Duncan et al., 2007b). Using the high-field-strength diffusion-tensor (DT) magnetic resonance (MR) imaging technique, Garaci et al. also evaluated the axonal architecture of the optic radiation in glaucoma patients and found that the alterations in DT MR imaging-derived parameters were also correlated with glaucoma stages (Garaci et al., 2009). All of the above findings indicated that not only the eyes but also the central visual targets should be considered in glaucoma studies such as the evaluation of functional changes, disease severity or therapeutic responses.

4.4.2.5 Dendritic Changes in the Retinal Ganglion Cells

In the RGCs, significant decreases of dendritic length and number were also observed in glaucoma animals compared to age-matched controls. The comparison of dendritic changes in the RGCs from glaucoma animals at different time points is shown in Table 4.19.

Dendritic Changes (OHT vs AMT)	Time after OHT induction (weeks)	RI	RII	RIII	Average
Dendritic Shrinkage (%)	1	21.26	27.35	22.67	23.28
	4	32.3	43.96	49.12	41.2
	8	20.71	35.18	39.31	30.95
	16	10.2	13.85	16.23	13.07
	32	22.94	16.23	21.76	21.12
Dendritic loss (%)	1	NS			
	4	24.18	34.86	24.16	27.97
	8	NS	NS	33	22.92
	16	NS	20	NS	14.06
	32	NS	NS	13.33	13.21

Table 4.19: Comparison of dendritic changes in the RGCs after OHT induction

All three types of RGCs had significant reductions in the mean dendritic length at 1 week after OHT induction, showing an average of 23.28% dendritic shrinkage. Compared with dendritic changes that were shown in the brain (SC: 4 weeks; LGN: 8 weeks), dendritic abnormalities in the retina appeared earlier following elevated IOP. The peak of dendritic shrinkage was observed at 4 weeks after OHT induction, showing about 41.2% reduction in the dendritic length. Similarly, in the SC, the peak reduction in dendritic length was also observed at 4 weeks after OHT induction. Significant dendritic shrinkage in the RGCs was also shown at 8 (average: 30.95%) and 16 (average: 13.07%) weeks after OHT induction, with a lower amount of shrinkage than that at 4 weeks. A greater amount of reduction in RGC dendritic length was observed at 32 weeks than that at 16 weeks after OHT induction. These findings were similar to those in the SC, showing a

greater dendritic shrinkage at 32 weeks (average: 21.12%) than at 16 weeks after OHT induction. However in the LGN, dendritic changes at 32 weeks were no more than those at 16 weeks after OHT induction.

The RGCs showed significant dendritic loss at 4 weeks after OHT induction, which was observed later than dendritic shrinkage (1 week). At the same time point, a significant reduction in the dendritic number was also shown in the SC. At 4 weeks after OHT induction, the dendritic number in RGCs was reduced by an average of 27.97%. At 8 weeks after OHT induction, the RIII had significant dendritic loss, showing 33% reduction in the dendritic number. The RII had significant dendritic loss at 16 weeks after OHT induction, showing 20% decrease in dendritic number. At 32 weeks after OHT induction, the RIII had 13.33% dendritic loss.

Additionally, the comparison of average dendritic shrinkage and loss in the RGCs shows that a lower amount of reduction in dendritic number than that in dendritic length at 4 (loss: 27.97%; shrinkage: 41.2%), 8 (loss: 22.92%; shrinkage: 30.95%) and 32 (loss: 13.21%; shrinkage: 21.12%) weeks after OHT induction.

Dendritic changes in RGCs have also been described previously in glaucoma patients and animal models of glaucoma (Weber et al., 1998; Pavlidis et al., 2003; Shou et al., 2003; Jakobs et al., 2005), supporting the findings in the present study. A summary of findings in this thesis and other studies is shown in Table 4.20.

Species	Glaucoma-related changes in RGCs	Amount of changes / <i>Approximate rates of Changes</i>	Reference
DA rats with chronic glaucoma	Dendritic shrinkage	<ul style="list-style-type: none"> ● Average 23.28% dendritic shrinkage at 1 week after OHT compared to age-matched CTL ● Average 41.22% dendritic shrinkage at 4 weeks after OHT compared to age-matched CTL ● <i>Average 5.79% /week</i> 	This thesis
Primates with chronic glaucoma	Dendritic shrinkage	Up to 42.4% reduction in the mean dendritic field size of parasol cells	(Weber et al., 1998)
Cats with chronic glaucoma	Dendritic shrinkage	63.4% and 58.6% dendritic shrinkage in α - and β - type RGCs at 1 month after OHT	(Shou et al., 2003)
Norwegian Brown rats with chronic glaucoma	Dendritic shrinkage	25.7% reduction in dendritic tree diameter	(Morgan et al., 2006)
DA rats with chronic glaucoma	Dendritic loss	<ul style="list-style-type: none"> ● Average 27.97% dendritic loss at 4 weeks after OHT compared to age-matched CTL ● <i>Average 5.65% /week</i> 	This thesis
Humans	Dendritic loss	50% (midget cells) and 33% (parasol cells) reductions in the dendritic number in the advance stage of glaucoma	(Pavlidis et al., 2003)
Cats with chronic glaucoma	Dendritic loss	59.5% and 44.2% dendritic loss in α - and β - type RGCs at 1 month after OHT	(Shou et al., 2003)
Humans	RGC loss	<i>4% /year</i>	(Zeyen, 1999)
Cats	RGC loss	49% to 67% RGC loss at 1 month after OHT	(Shou et al., 2003)
DA rats with chronic glaucoma	RGC loss	Significant RGC loss (61.21%) at 3 months after elevated IOP	(Guo et al., 2005a)
Mice with acute glaucoma	RGC loss	20.5% to 85.5% RGC loss at 4 weeks after OHT.	(Leung et al., 2009)
Mice with chronic glaucoma	RGC loss	1.3% to 6.7% /month	(Cone et al., 2010)
Transgenic glaucoma DBA/2NNia mice	RGC loss	64% RGC loss from 12 months to 15 months.	(Danias et al., 2003)

Table 4.20: Comparison of structural changes of RGCs following elevated IOP shown in this thesis and in published literature.

Weber et al. found that the early signs of RGC degeneration involved the structural changes of dendrites in a primate model of glaucoma (Weber et al., 1998). The parasol cells in the glaucomatous eyes showed a significant decrease in the complexity of the dendritic tree compared to controls. The mean dendritic field size of parasol cells significantly reduced up to 42.4% in glaucomatous eyes, although no significant dendritic changes were found in midget cells. Pavlidis et al. also found the number of dendrites in central midget cells and parasol cells significantly dropped by approximately 50% and 33% in the advanced stage of glaucoma in patients (Pavlidis et al., 2003). Shou et al.'s found RGC dendritic shrinkage and loss in cats with experimental chronic glaucoma (Shou et al., 2003). 63.4% and 58.6% dendritic shrinkage occurred in α - and β - type RGCs at 1 month after OHT induction. The number of dendritic branches also significantly decreased by 59.5% and 44.2% in α - and β - type RGCs. The dendritic changes after OHT induction appeared more pronounced in large cells (α - type RGCs) than small cells (β - type RGCs). Jakobs et al. also studied RGC dendritic loss in 1 year old DBA/2J mice, and found that only the cell body and the proximal part of the primary dendrites were visible in some severely affected ganglion cells (Jakobs et al., 2005). In Norwegian Brown rats with chronic glaucoma, 25.7% reduction in the dendritic tree diameter was also demonstrated in the RGCs (Morgan et al., 2006).

In the present study, the RGCs from glaucomatous eyes showed up to 41% shrinkage of dendrites in rats, which is comparable to the amount of dendritic shrinkage (42.4%) which occurred in parasol cells in a primate model of glaucoma (Weber et al., 1998). The significant shrinkage of dendrites in the RGCs was also recorded in cats (59%-63%) and Norwegian Brown rats (25.7%), showing either

greater or lower amounts of decreases (Shou et al., 2003; Morgan et al., 2006). This present study also demonstrated up to 27.97% average dendritic loss in the RGCs at 4 weeks after OHT induction, which was less than what was seen in patients (33% to 50%) and cats (44.2% to 59.5%) (Pavlidis et al., 2003; Shou et al., 2003). Furthermore, some severely degenerated RGCs were also found to only contain a cell body and the primary dendrites, which were consistent with Jakobs' finding.

In addition, the large RGCs (RIII and RI) did not show greater dendritic changes in the glaucomatous retinae in this present study. Although the RIII cells showed greater dendritic shrinkage than the RI and RII cells, they did not show greater dendritic loss. This finding is consistent with studies which showed no selective damage to one particular type of RGC or one specific retinogeniculate pathway in glaucoma (Graham et al., 1996; Morgan et al., 2000; Ansari et al., 2002; Morgan, 2002; Morgan et al., 2006).

Hence, both shrunken dendritic extents and less numerous dendritic branches in the RGCs were generally observed in glaucomatous eyes compared to normal controls in patients, monkeys, cats and rats, although different patterns of dendritic changes have been shown depending on different species and cell types. The findings of glaucoma-related dendritic shrinkage and loss in this thesis are not only evident by published literature (chapters **4.4.1.3**, **4.4.2.3**; Table 4.20), but also in agreement with what was seen in the SC and LGN (chapters **4.4.2.1**, **4.4.2.2**; Table 4.18). In the following sections, the average dendritic changes in the RGCs, SC cells and LGN cells from glaucoma animals were also compared and discussed.

4.4.2.6 Comparison of Dendritic Changes in the RGCs, SC Cells and LGN Cells

The comparison of dendritic parameters in the RGCs, SC cells and LGN cells between glaucoma animals and age-matched controls showed significant reductions in the dendritic length and number after elevated IOP. The average amounts of dendritic changes in the RGCs, SC cells and LGN cells at different time points after OHT induction are summarised in Table 4.21.

Dendritic Changes (OHT vs AMT)	Time after OHT induction (weeks)	RGCs	SC cells	LGN cells
Dendritic shrinkage (%)	1	23.28	/	/
	4	41.2	49.54	NS
	8	30.95	30.3	29.67
	16	13.07	26.15	36.61
	32	21.12	35.68	28.57
Dendritic loss	1	NS	/	/
	4	27.97	52.68	NS
	8	22.92	39.24	22.03
	16	14.06	29.63	15.22
	32	13.21	22.2	16.13

Table 4.21: Comparison of dendritic changes in the RGCs, SC cells and LGN cells after OHT induction.

The first site to show dendritic shrinkage after OHT induction is the RGCs (Fig. 3.69). At 1 week after glaucoma surgery, dendritic length in the RGCs was significantly reduced by 23.28%. The peak dendritic shrinkage in RGCs and SC cells

was at 4 weeks after OHT induction, showing 41.22% and 49.54% dendritic shrinkage. However, the maximum dendritic shrinkage in the LGN cells was observed at 16 weeks after OHT induction, showing 36.61% reduction in the dendritic length.

The initial dendritic loss in the RGCs and SC cells was observed at 4 weeks after OHT induction, showing 27.97% and 52.68% decrease in the number of dendrites. In the LGN cells, significant dendritic loss was observed at 8 weeks after OHT induction, showing 22.03% reduction in the number of dendritic branches. The peak reduction in dendritic number in the RGCs and SC cells was at 4 weeks after glaucoma surgery, whilst the peak of dendritic loss in the LGN cells was at 8 weeks after OHT induction.

Dendritic changes were observed both in the retina and central visual targets after OHT induction. However, the degeneration of dendrites appeared later in the LGN than in the SC. Data in the present study indicated the RGC as the first site to show dendritic degeneration in glaucoma. These findings could also be supported by previous studies in cats with chronic glaucoma (Shou et al., 2003). Shou et al. demonstrated the dendritic shrinkage in RGCs, and the cell loss in the retina and LGN in cats after chronic elevation of IOP. They showed that the effects of elevated IOP on the average cell loss in the LGN is less significant than the RGC loss in the retina. At 1 month after OHT induction, there was 49% to 67% RGC loss in the retina, whilst there was 24% to 35% cell loss in layer A1 of the LGN, suggesting a second-order degeneration on LGN cells after retinal degeneration, which is in agreement with the findings in this thesis. In addition, significant degeneration of LGN cells in cats with chronic glaucoma was observed at 1 month, which is

comparable to the findings in this thesis demonstrating significant dendritic degeneration in the SC at 4 weeks in rats with chronic glaucoma. However, the LGN dendritic degeneration was observed at 8 weeks after OHT induction in rats, which appeared later than the cell degeneration in the LGN shown in cats. This could be due to the fact that the LGN is a primary target of retinal projections in felines, whilst in rats, it is the SC (Guillery, 1970; Paxinos, 2004).

Additionally, the pronounced dendritic changes were seen in the SC in the present study although the first site to show dendritic denegation was the RGC. The results in this thesis suggested that both RGC and SC could be potential sites for early detection of neuronal degeneration. Furthermore, this study demonstrated dendritic degeneration in the RGCs, SC cells and LGN cells in glaucoma animals, implicating that both the retina and the central visual targets should be targeted when considering therapies for glaucoma.

Chapter 5: Summary and Future Perspectives

Glaucoma is a neurodegenerative disease characterized by retinal ganglion cell (RGC) loss, and elevated IOP is regarded as a primary risk factor (Sommer, 1989; Guo et al., 2005a). This thesis characterizes dendritic changes in the RGC, SC and LGN in a rat model of experimental glaucoma.

Firstly, dendritic labelling in the RGCs, SC and LGN was achieved using the fluorescent dye DiI by *in vivo* and *in vitro* techniques. 0.1% (w/v) was demonstrated to be the optimal concentration of Vybrant DiI solution for *in vitro* dendritic labelling. 400µm was shown as the appropriate thickness of brain slices to reserve complete dendritic structures in the SC and LGN. In the study of SC dendritic morphology, fixed brain blocks were sectioned into parasagittal slices containing the SC. 0.1% DiI was next applied to the rostral and middle sites in the superficial layer of the SC by gently poking the slices using a glass micropipette with a sharp tip. The stained slices were kept at 37°C for 7 days in the laboratory incubator to allow the dye to fully diffuse along the dendritic processes. In the study of LGN dendritic morphology, fixed brain blocks were sectioned into *pseudo*-parasagittal slices containing the LGN (Turner and Salt, 1998). 0.1% DiI was applied to the optic radiation using a glass micropipette to retrogradely label neurons in the dLGN. The stained slices were also kept at 37°C for 7 days. Additionally, an *in vivo* labelling method was also employed on a group of rats to be compared with the *in vitro* labelling. The *in vivo* retrograde labelling of dLGN was achieved by injecting the DiI crystals into the visual cortex. Animals were kept alive for 4 weeks before sacrifice,

and the brain blocks were fixed in 4% PFA before being sectioned into 400µm parasagittal slices. No difference was found between data from the two different labelling methods, confirming that results from the *in vitro* labelling technique were reliable. In the study of RGC dendritic morphology, fresh retinas were flat mounted and the vitreous and ILM were completely removed from the retina for optimal staining. RGCs were labelled using the biolistic technique which delivers particle-coated DiI into cells using a gene gun (Lo et al., 1994; Gan et al., 2000; Becker et al., 2007). The stained retina was kept in PBS for 20 minutes before fixation. Confocal microscopy was next performed to image RGCs and cells in the SC and LGN.

Secondly, Neuron J programme from the Image J software was employed to analyze dendritic morphology in this thesis. Neuron J was designed to facilitate the tracing and quantification of elongated structures, in particular processes of neurons in fluorescence microscopy images (Abramoff et al., 2004; Meijering et al., 2004; Collins, 2007). Accordingly, Neuron J programme was an appropriate tool for tracing and quantifying the DiI labelled dendrites in this study. Two dendritic parameters, the mean dendritic length and the number of dendrites per neuron, were quantified in this thesis. The rates of dendritic changes were approximated based on an exponential regression equation.

Thirdly, RGCs and neurons in the SC and LGN were further classified into different types to study dendritic changes in depth, including five types of SC cells (H; W; V; P and S cells) (Langer and Lund, 1974), two types of LGN cells (LG1 and LG2) (Kriebel, 1975) and three types RGCs (RI; RII and RIII) (Perry, 1979).

Dendritic parameters of RGCs and neurons in the SC and LGN were analyzed individually.

This thesis, for the first time, demonstrates age-related and glaucoma-related dendritic changes in RGCs, SC cells and LGN cells in a rat model of experimental glaucoma.

In RGCs and neurons in the SC and LGN, the mean dendritic length and dendritic number of all types of cells were significantly reduced from the baseline to 32 weeks (actual age: 40 weeks) over time. In the SC, the earliest dendritic shrinkage and dendritic losses were both observed in the 8 weeks CTL groups. The rates of dendritic changes were 2.8% to 5.2% (shrinkage) and 3.4% to 4.4% (loss) per week. In the LGN, the earliest dendritic shrinkage and dendritic losses were also observed in the 8 weeks CTL groups. The rates of dendritic changes were 2.6% to 3.2% (shrinkage) and 2.3% to 4% (loss) per week. Most of the RGCs showed the earliest dendritic shrinkage and dendritic losses in the 8 weeks CTL groups. The rates of dendritic changes were 4.2% to 5% (shrinkage) and 3.7% to 5.1% (loss) per week. Hence, both age-related dendritic shrinkage and dendritic losses were shown in the retina and the central visual targets during the progression of adulthood in DA rats.

In this study, age-related dendritic alterations in the SC, LGN and RGCs were also demonstrated in rats with chronic glaucoma. Significant dendritic shrinkage and losses were shown in all types of cells from the baseline to 32 weeks after OHT induction. In the SC, the earliest dendritic shrinkage and dendritic losses were both observed at 4 weeks after OHT induction. The rates of dendritic changes were 4.6% to 9.9% (shrinkage) and 5.9% to 10% (loss) per week. In the LGN, the earliest

dendritic shrinkage and dendritic losses were observed from the 4 to the 8 weeks OHT groups. The rates of dendritic changes were 5% to 5.4% (shrinkage) and 3.3% to 5.3% (loss) per week. Most of the RGCs showed the earliest dendritic shrinkage and dendritic losses at 1 week after OHT induction. The rates of dendritic changes were 5% to 6.8% (shrinkage) and 4.7% to 6.2% (loss) per week. Hence, age-related dendritic changes in the retina and the central visual targets were also demonstrated in glaucoma animals, with a greater amount and faster rate than those that were shown in normal animals.

In addition, dendritic parameters between glaucoma groups and age-matched controls were also compared. In the SC, the mean dendritic length and dendritic number were both significantly decreased at 4, 8, 16 and 32 weeks after OHT induction. The maximum dendritic shrinkage and losses in SC cells were observed at 4 weeks after glaucoma surgery, showing 44.9% to 52.9% reduction in the mean dendritic length and 46.9% to 60.5% decrease in the dendritic number. In the LGN, significant reductions in the mean dendritic length and dendritic number were shown at almost all time points from 4 to 32 weeks after OHT induction. The maximum dendritic changes in LGN cells were shown at 16 weeks (shrinkage), and 8 to 32 weeks (loss) after OHT induction, showing 35.1% to 38.4% dendritic shrinkage and 20.5% to 31.5% dendritic loss. In RGCs, significant dendritic shrinkage was observed at 1, 4, 8, 16 and 32 weeks after OHT induction compared to age-matched controls. Significant reductions in dendritic numbers were observed in all types of cells at 1 week after OHT induction. Some cells also showed significant dendritic loss at 8, 16 or 32 weeks after OHT induction. The maximum dendritic shrinkage in RGCs was shown at 4 weeks after OHT induction, showing 32.3% to 49.1%

reduction in the mean dendritic length. The peak of dendritic loss was observed at 4 weeks to 8 weeks after glaucoma surgery, showing 24.2% to 34.9% decrease in the dendritic number.

In order to compare dendritic changes in RGCs, SC cells and LGN cells, dendritic parameters of all cells were analyzed without classifying cells into different types. The RGC was demonstrated to be the first site to show dendritic shrinkage and dendritic loss. In normal animals during ageing, dendrites in RGCs shrunk at the rate of 4.43% per week, which was faster than those in the SC (3.98% per week) and LGN (2.92% per week). The dendritic loss in RGCs (4.44% per week) was also faster than those in the SC (4.06% per week) and LNG (3.08% per week). Similar findings were also generated from glaucoma animals, but the dendritic changes in glaucoma animals were shown even earlier and faster than those in control animals. In glaucoma animals, dendrites in the SC shrunk at a rate of 6.92% weekly, which was faster than those in the LGN (5.19%) and RGCs (5.79%). The dendritic loss in the SC (6.91% weekly) was also faster than those in and LGN (4.00% weekly) and RGCs (5.65% weekly). Hence, age-related dendritic shrinkage and dendritic loss were firstly shown in RGCs, and both RGCs and SC cells showed greater dendritic changes than LGN cells.

Finally, dendritic changes in RGCs, SC and LGN in glaucoma animals were also compared with age-matched controls. The RGC was demonstrated to be the first site to show dendritic shrinkage, although more prominent changes were shown in the SC. Dendritic changes in RGCs could be observed at 1 week after OHT induction, whereas those in the SC and LGN were seen from 4 and 8 weeks after OHT

induction. The peaks of dendritic shrinkage and dendritic loss in RGCs and SC cells were both observed at 4 weeks after OHT induction, whilst the maximum dendritic changes in LGN cells appeared at 8 (loss) to 16 weeks (shrinkage) after OHT induction. Hence, the RGC was the first site to show glaucoma-related dendritic shrinkage and dendritic loss. Both RGCs and SC cells showed maximum dendritic changes earlier and greater than those in LGN cells.

In conclusion, this thesis, for the first time, characterizes dendritic changes in the RGCs, SC cells and LGN cells in a rat model of experimental glaucoma. Both ageing and elevated IOP were demonstrated to affect the dendritic morphology of the retina and central visual targets. In glaucoma animals, RGCs in the retina were demonstrated as the first site to show dendritic changes, whilst changes in the SC and LGN appeared later, indicating that there was a secondary effect on the central visual targets after retinal degeneration. Although RGCs and SC cells showed the maximum dendritic changes at the same time after elevated IOP, the more pronounced changes were shown in the SC.

Following this study, the investigation of changes in dendritic spines in the same rat model of glaucoma could also contribute to the better understanding of dendritic changes. At a functional level, the consequences of dendritic changes are still not clear and further investigation is needed in the future. Furthermore, the mechanisms involved in dendritic degeneration during ageing and after elevated IOP, and dendritic protection should also be investigated in future studies. In addition, the data generated from this thesis also has implications in diagnosis and therapeutic strategies, suggesting that both RGCs in the retina and the SC could be potential sites

for early detection in glaucoma. This thesis also suggests that not only the retina, but also the visual targets in the brain should be considered in future studies of therapeutic treatments for glaucoma.

References

- Abramoff MD, Magalhaes PJ, Ram SJ (2004) Image processing with imageJ. *Biophotonics international*:36-42.
- Agar A, Yip SS, Hill MA, Coroneo MT (2000) Pressure related apoptosis in neuronal cell lines. *J Neurosci Res* 60:495-503.
- Ahmad A, Spear PD (1993) Effects of aging on the size, density, and number of rhesus monkey lateral geniculate neurons. *J Comp Neurol* 334:631-643.
- Al-Abdulla NA, Portera-Cailliau C, Martin LJ (1998) Occipital cortex ablation in adult rat causes retrograde neuronal death in the lateral geniculate nucleus that resembles apoptosis. *Neuroscience* 86:191-209.
- Anderson B, Rutledge V (1996) Age and hemisphere effects on dendritic structure. *Brain* 119 (Pt 6):1983-1990.
- Anderson DR (1977) The management of elevated intraocular pressure with normal optic discs and visual fields. I. Therapeutic approach based on high risk factors. *Surv Ophthalmol* 21:479-489.
- Anderson DR, Hendrickson A (1974) Effect of intraocular pressure on rapid axoplasmic transport in monkey optic nerve. *Invest Ophthalmol* 13:771-783.
- Anderson MG, Smith RS, Savinova OV, Hawes NL, Chang B, Zabaleta A, Wilpan R, Heckenlively JR, Davisson M, John SW (2001) Genetic modification of glaucoma associated phenotypes between AKXD-28/Ty and DBA/2J mice. *BMC Genet* 2:1.
- Ansari EA, Morgan JE, Snowden RJ (2002) Psychophysical characterisation of early functional loss in glaucoma and ocular hypertension. *Br J Ophthalmol* 86:1131-1135.
- Athos J, Storm DR (2001) High precision stereotaxic surgery in mice. *Curr Protoc Neurosci Appendix 4:Appendix 4A*.
- Azuara-Blanco A, Burr J, Thomas R, MacLennan G, McPherson S (2007) The accuracy of accredited glaucoma optometrists in the diagnosis and treatment recommendation for glaucoma. *Br J Ophthalmol* 91:1639-1643.

- Baloyannis SJ (2006) Mitochondrial alterations in Alzheimer's disease. *J Alzheimers Dis* 9:119-126.
- Baloyannis SJ (2009) Dendritic pathology in Alzheimer's disease. *J Neurol Sci* 283:153-157.
- Baloyannis SJ, Costa V, Mauroudis I, Psaroulis D, Manolides SL, Manolides LS (2007) Dendritic and spinal pathology in the acoustic cortex in Alzheimer's disease: morphological and morphometric estimation by Golgi technique and electron microscopy. *Acta Otolaryngol* 127:351-354.
- Baltmr A, Duggan J, Nizari S, Salt TE, Cordeiro MF (2010) Neuroprotection in glaucoma - Is there a future role? *Exp Eye Res*.
- Becker DL, Webb KF, Thrasivoulou C, Lin CC, Nadershahi R, Tsakiri N, Cook JE (2007) Multiphoton imaging of chick retinal development in relation to gap junctional communication. *J Physiol* 585:711-719.
- Binns KE (1999) The synaptic pharmacology underlying sensory processing in the superior colliculus. *Prog Neurobiol* 59:129-159.
- Bourassa J, Deschenes M (1995) Corticothalamic projections from the primary visual cortex in rats: a single fiber study using biocytin as an anterograde tracer. *Neuroscience* 66:253-263.
- Boycott BB, Wassle H (1974) The morphological types of ganglion cells of the domestic cat's retina. *J Physiol* 240:397-419.
- Buhl EH, Dann JF (1991) Cytoarchitecture, neuronal composition, and entorhinal afferents of the flying fox hippocampus. *Hippocampus* 1:131-152.
- Bunce C, Wormald R (2006) Leading causes of certification for blindness and partial sight in England & Wales. *BMC Public Health* 6:58.
- Bunt AH, Hendrickson AE, Lund JS, Lund RD, Fuchs AF (1975) Monkey retinal ganglion cells: morphometric analysis and tracing of axonal projections, with a consideration of the peroxidase technique. *J Comp Neurol* 164:265-285.
- Bywood PT, Johnson SM (2000) Dendrite loss is a characteristic early indicator of toxin-induced neurodegeneration in rat midbrain slices. *Exp Neurol* 161:306-316.
- Cajal SR (1955) *Histologie du systeme nerveux de l'homme et des vertebres*. Consejo superior de investigaciones cientificas. II.

- Cajal SRY (1911) *Histologie du Système Nerveux de l'Homme et des Vertébrés.*: Paris, A. Maloine.
- Callaway EM (2005) Structure and function of parallel pathways in the primate early visual system. *J Physiol* 566:13-19.
- Casagrande VA (1994) A third parallel visual pathway to primate area V1. *Trends Neurosci* 17:305-310.
- Casagrande VA, Yazar F, Jones KD, Ding Y (2007) The morphology of the koniocellular axon pathway in the macaque monkey. *Cereb Cortex* 17:2334-2345.
- Cepurna WO, Kayton RJ, Johnson EC, Morrison JC (2005) Age related optic nerve axonal loss in adult Brown Norway rats. *Exp Eye Res* 80:877-884.
- Chao MV (2003) Neurotrophins and their receptors: a convergence point for many signalling pathways. *Nat Rev Neurosci* 4:299-309.
- Chauhan BC, Pan J, Archibald ML, LeVatte TL, Kelly ME, Tremblay F (2002) Effect of intraocular pressure on optic disc topography, electroretinography, and axonal loss in a chronic pressure-induced rat model of optic nerve damage. *Invest Ophthalmol Vis Sci* 43:2969-2976.
- Cohen-Cory S, Lom B (2004) Neurotrophic regulation of retinal ganglion cell synaptic connectivity: from axons and dendrites to synapses. *Int J Dev Biol* 48:947-956.
- Coleman AL (1999) Glaucoma. *Lancet* 354:1803-1810.
- Coleman P, Finch C, Joseph J (1990) The need for multiple time points in aging studies. *Neurobiol Aging* 11:1-2.
- Coleman PD, Riesen AH (1968) Environmental effects on cortical dendritic fields. I. Rearing in the dark. *J Anat* 102:363-374.
- Collins TJ (2007) ImageJ for microscopy. *Biotechniques* 43:25-30.
- Cone FE, Gelman SE, Son JL, Pease ME, Quigley HA (2010) Differential susceptibility to experimental glaucoma among 3 mouse strains using bead and viscoelastic injection. *Exp Eye Res* 91:415-424.
- Cordeiro MF, Guo L, Luong V, Harding G, Wang W, Jones HE, Moss SE, Sillito AM, Fitzke FW (2004) Real-time imaging of single nerve cell apoptosis in retinal neurodegeneration. *Proc Natl Acad Sci U S A* 101:13352-13356.

- Cordeiro MF, Guo L, Coxon KM, Duggan J, Nizari S, Normando EM, Sensi SL, Sillito AM, Fitzke FW, Salt TE, Moss SE (2010) Imaging multiple phases of neurodegeneration: a novel approach to assessing cell death in vivo. *Cell Death and Disease* 1,e3; doi:10.1038/cddis.2009.3.
- Crawford ML, Harwerth RS, Smith EL, 3rd, Shen F, Carter-Dawson L (2000) Glaucoma in primates: cytochrome oxidase reactivity in parvo- and magnocellular pathways. *Invest Ophthalmol Vis Sci* 41:1791-1802.
- Crish SD, Sappington RM, Inman DM, Horner PJ, Calkins DJ (2010) Distal axonopathy with structural persistence in glaucomatous neurodegeneration. *Proc Natl Acad Sci U S A* 107:5196-5201.
- Cupp CJ, Uemura E (1980) Age-related changes in prefrontal cortex of *Macaca mulatta*: quantitative analysis of dendritic branching patterns. *Exp Neurol* 69:143-163.
- Danias J, Lee KC, Zamora MF, Chen B, Shen F, Filippopoulos T, Su Y, Goldblum D, Podos SM, Mittag T (2003) Quantitative analysis of retinal ganglion cell (RGC) loss in aging DBA/2Nnia glaucomatous mice: comparison with RGC loss in aging C57/BL6 mice. *Invest Ophthalmol Vis Sci* 44:5151-5162.
- Dann JF, Buhl EH (1987) Retinal ganglion cells projecting to the accessory optic system in the rat. *J Comp Neurol* 262:141-158.
- Dann JF, Buhl EH, Peichl L (1987) Dendritic maturation in cat retinal ganglion cells: a Lucifer yellow study. *Neurosci Lett* 80:21-26.
- Dann JF, Buhl EH, Peichl L (1988) Postnatal dendritic maturation of alpha and beta ganglion cells in cat retina. *J Neurosci* 8:1485-1499.
- De Brabander JM, Kramers RJ, Uylings HB (1998) Layer-specific dendritic regression of pyramidal cells with ageing in the human prefrontal cortex. *Eur J Neurosci* 10:1261-1269.
- De Ruiter JP, Uylings HB (1987) Morphometric and dendritic analysis of fascia dentata granule cells in human aging and senile dementia. *Brain Res* 402:217-229.
- Dickstein DL, Kabaso D, Rocher AB, Luebke JI, Wearne SL, Hof PR (2007) Changes in the structural complexity of the aged brain. *Aging Cell* 6:275-284.

- Donello JE, Padillo EU, Webster ML, Wheeler LA, Gil DW (2001) $\alpha(2)$ -Adrenoceptor agonists inhibit vitreal glutamate and aspartate accumulation and preserve retinal function after transient ischemia. *J Pharmacol Exp Ther* 296:216-223.
- Dreher B, Sefton AJ, Ni SY, Nisbett G (1985) The morphology, number, distribution and central projections of Class I retinal ganglion cells in albino and hooded rats. *Brain Behav Evol* 26:10-48.
- Duan H, Wearne SL, Rocher AB, Macedo A, Morrison JH, Hof PR (2003) Age-related dendritic and spine changes in corticocortically projecting neurons in macaque monkeys. *Cereb Cortex* 13:950-961.
- Dubin MW, Cleland BG (1977) Organization of visual inputs to interneurons of lateral geniculate nucleus of the cat. *J Neurophysiol* 40:410-427.
- Duncan RO, Sample PA, Weinreb RN, Bowd C, Zangwill LM (2007a) Retinotopic organization of primary visual cortex in glaucoma: Comparing fMRI measurements of cortical function with visual field loss. *Prog Retin Eye Res* 26:38-56.
- Duncan RO, Sample PA, Weinreb RN, Bowd C, Zangwill LM (2007b) Retinotopic organization of primary visual cortex in glaucoma: a method for comparing cortical function with damage to the optic disk. *Invest Ophthalmol Vis Sci* 48:733-744.
- Einstein G, Buranosky R, Crain BJ (1994) Dendritic pathology of granule cells in Alzheimer's disease is unrelated to neuritic plaques. *J Neurosci* 14:5077-5088.
- el Hachimi KH, Foncin JF (1990) [Loss of dendritic spines in Alzheimer's disease]. *C R Acad Sci III* 311:397-402.
- Elberger AJ, Honig MG (1990) Double-labeling of tissue containing the carbocyanine dye DiI for immunocytochemistry. *J Histochem Cytochem* 38:735-739.
- Feldman ML (1977) Dendritic changes in aging rat brain: pyramidal cell dendrite length and ultrastructure. In: K Nandy and I Sherwin, Editors, *The Aging Brain and Senile Dementia, Advances in Behavioral Biology* 23:323-337.
- Fiala JC, Spacek J, Harris KM (2002) Dendritic spine pathology: cause or consequence of neurological disorders? *Brain Res Brain Res Rev* 39:29-54.

- Fitzgibbon T, Bittar RG, Dreher B (1999) Projections from striate and extrastriate visual cortices of the cat to the reticular thalamic nucleus. *J Comp Neurol* 410:467-488.
- Flood DG (1993) Critical issues in the analysis of dendritic extent in aging humans, primates, and rodents. *Neurobiol Aging* 14:649-654.
- Flood DG, Buell SJ, Horwitz GJ, Coleman PD (1987) Dendritic extent in human dentate gyrus granule cells in normal aging and senile dementia. *Brain Res* 402:205-216.
- Flood DG, Buell SJ, Defiore CH, Horwitz GJ, Coleman PD (1985) Age-related dendritic growth in dentate gyrus of human brain is followed by regression in the 'oldest old'. *Brain Res* 345:366-368.
- Foster PJ, Buhrmann R, Quigley HA, Johnson GJ (2002) The definition and classification of glaucoma in prevalence surveys. *Br J Ophthalmol* 86:238-242.
- Fu CT, Sretavan D (2009) Laser-induced ocular hypertension in albino CD-1 mice. *Invest Ophthalmol Vis Sci* 51:980-990.
- Fukuda Y, Stone J (1974) Retinal distribution and central projections of Y-, X-, and W-cells of the cat's retina. *J Neurophysiol* 37:749-772.
- Fukuda Y, Stone J (1975) Direct identification of the cell bodies of Y-, X- and W-cells in the cat's retina. *Vision Res* 15:1034-1036.
- Fukuda Y, Hsiao CF, Watanabe M (1985) Morphological correlates of Y, X and W type ganglion cells in the cat's retina. *Vision Res* 25:319-327.
- Gabbott PL, Bacon SJ (1994) Two types of interneuron in the dorsal lateral geniculate nucleus of the rat: a combined NADPH diaphorase histochemical and GABA immunocytochemical study. *J Comp Neurol* 350:281-301.
- Gabbott PL, Somogyi J, Stewart MG, Hamori J (1986) GABA-immunoreactive neurons in the dorsal lateral geniculate nucleus of the rat: characterisation by combined Golgi-impregnation and immunocytochemistry. *Exp Brain Res* 61:311-322.
- Gan WB, Grutzendler J, Wong WT, Wong RO, Lichtman JW (2000) Multicolor "DiOlistic" labeling of the nervous system using lipophilic dye combinations. *Neuron* 27:219-225.

- Garaci FG, Bolacchi F, Cerulli A, Melis M, Spano A, Cedrone C, Floris R, Simonetti G, Nucci C (2009) Optic nerve and optic radiation neurodegeneration in patients with glaucoma: in vivo analysis with 3-T diffusion-tensor MR imaging. *Radiology* 252:496-501.
- Garey LJ, Powell TP (1968) The projection of the retina in the cat. *J Anat* 102:189-222.
- Geiger BM, Frank LE, Caldera-Siu AD, Pothos EN (2008) Survivable stereotaxic surgery in rodents. *J Vis Exp*.
- Georgiou AL, Guo L, Cordeiro MF, Salt TE (2010) Changes in NMDA receptor contribution to synaptic transmission in the brain in a rat model of glaucoma. *Neurobiol Dis* 39:344-351.
- Glaser J (1999) *Neuro-ophthalmology* In. Philadelphia: Lippincott Williams and Wilkins.
- Glovinsky Y, Quigley HA, Dunkelberger GR (1991) Retinal ganglion cell loss is size dependent in experimental glaucoma. *Invest Ophthalmol Vis Sci* 32:484-491.
- Glovinsky Y, Quigley HA, Pease ME (1993) Foveal ganglion cell loss is size dependent in experimental glaucoma. *Invest Ophthalmol Vis Sci* 34:395-400.
- Godement P, Vanselow J, Thanos S, Bonhoeffer F (1987) A study in developing visual systems with a new method of staining neurones and their processes in fixed tissue. *Development* 101:697-713.
- Goldblum D, Mittag T (2002) Prospects for relevant glaucoma models with retinal ganglion cell damage in the rodent eye. *Vision Res* 42:471-478.
- Gonatas NK (1967) Neocortical synapses in a presenile dementia. *J Neuropathol Exp Neurol* 26:150-151.
- Graham SL, Drance SM, Chauhan BC, Swindale NV, Hnik P, Mikelberg FS, Douglas GR (1996) Comparison of psychophysical and electrophysiological testing in early glaucoma. *Invest Ophthalmol Vis Sci* 37:2651-2662.
- Grill JD, Riddle DR (2002) Age-related and laminar-specific dendritic changes in the medial frontal cortex of the rat. *Brain Res* 937:8-21.
- Grozdanic SD, Betts DM, Sakaguchi DS, Allbaugh RA, Kwon YH, Kardon RH (2003) Laser-induced mouse model of chronic ocular hypertension. *Invest Ophthalmol Vis Sci* 44:4337-4346.

- Guerin MB, McKernan DP, O'Brien CJ, Cotter TG (2006) Retinal ganglion cells: dying to survive. *Int J Dev Biol* 50:665-674.
- Guillery RW (1966) A study of Golgi preparations from the dorsal lateral geniculate nucleus of the adult cat. *J Comp Neurol* 128:21-50.
- Guillery RW (1970) The laminar distribution of retinal fibers in the dorsal lateral geniculate nucleus of the cat: a new interpretation. *J Comp Neurol* 138:339-368.
- Guo L, Cordeiro MF (2008) Assessment of neuroprotection in the retina with DARC. *Prog Brain Res* 173:437-450.
- Guo L, Normando EM, Nizari S, Lara D, Cordeiro MF (2010) Tracking Longitudinal Retinal Changes in Experimental Ocular Hypertension Using the cSLO and Spectral Domain-OCT. *Invest Ophthalmol Vis Sci*.
- Guo L, Moss SE, Alexander RA, Ali RR, Fitzke FW, Cordeiro MF (2005a) Retinal ganglion cell apoptosis in glaucoma is related to intraocular pressure and IOP-induced effects on extracellular matrix. *Invest Ophthalmol Vis Sci* 46:175-182.
- Guo L, Tsatourian V, Luong V, Podoleanu AG, Jackson DA, Fitzke FW, Cordeiro MF (2005b) En face optical coherence tomography: a new method to analyse structural changes of the optic nerve head in rat glaucoma. *Br J Ophthalmol* 89:1210-1216.
- Guo L, Salt TE, Maass A, Luong V, Moss SE, Fitzke FW, Cordeiro MF (2006) Assessment of neuroprotective effects of glutamate modulation on glaucoma-related retinal ganglion cell apoptosis in vivo. *Invest Ophthalmol Vis Sci* 47:626-633.
- Guo L, Salt TE, Luong V, Wood N, Cheung W, Maass A, Ferrari G, Russo-Marie F, Sillito AM, Cheetham ME, Moss SE, Fitzke FW, Cordeiro MF (2007) Targeting amyloid-beta in glaucoma treatment. *Proc Natl Acad Sci U S A* 104:13444-13449.
- Gupta N, Ly T, Zhang Q, Kaufman PL, Weinreb RN, Yucel YH (2007) Chronic ocular hypertension induces dendrite pathology in the lateral geniculate nucleus of the brain. *Exp Eye Res* 84:176-184.

- Gupta N, Greenberg G, de Tilly LN, Gray B, Polemidiotis M, Yucel YH (2009) Atrophy of the lateral geniculate nucleus in human glaucoma detected by magnetic resonance imaging. *Br J Ophthalmol* 93:56-60.
- Hajdu F, Somogyi G, Tombol T (1974) Neuronal and synaptic arrangement in the lateralis posterior-pulvinar complex of the thalamus in the cat. *Brain Res* 73:89-104.
- Harman A, Abrahams B, Moore S, Hoskins R (2000) Neuronal density in the human retinal ganglion cell layer from 16-77 years. *Anat Rec* 260:124-131.
- Harwerth RS, Wheat JL, Rangaswamy NV (2008) Age-related losses of retinal ganglion cells and axons. *Invest Ophthalmol Vis Sci* 49:4437-4443.
- Hayreh SS, Weingeist TA (1980) Experimental occlusion of the central artery of the retina. IV: Retinal tolerance time to acute ischaemia. *Br J Ophthalmol* 64:818-825.
- Heijl A, Leske MC, Bengtsson B, Hyman L, Bengtsson B, Hussein M (2002) Reduction of intraocular pressure and glaucoma progression: results from the Early Manifest Glaucoma Trial. *Arch Ophthalmol* 120:1268-1279.
- Hemelt ME, Keller A (2007) Superior sensation: superior colliculus participation in rat vibrissa system. *BMC Neurosci* 8:12.
- Hendry SH, Reid RC (2000) The koniocellular pathway in primate vision. *Annu Rev Neurosci* 23:127-153.
- Hoffmann KP (1972) The retinal input to the superior colliculus in the cat. *Invest Ophthalmol* 11:467-473.
- Hoffmann KP (1973) Conduction velocity in pathways from retina to superior colliculus in the cat: a correlation with receptive-field properties. *J Neurophysiol* 36:409-424.
- Hofmann MH, Bleckmann H (1999) Effect of temperature and calcium on transneuronal diffusion of DiI in fixed brain preparations. *J Neurosci Methods* 88:27-31.
- Honig MG, Hume RI (1986) Fluorescent carbocyanine dyes allow living neurons of identified origin to be studied in long-term cultures. *J Cell Biol* 103:171-187.
- Honjo M, Tanihara H, Kido N, Inatani M, Okazaki K, Honda Y (2000) Expression of ciliary neurotrophic factor activated by retinal Muller cells in eyes with

- NMDA- and kainic acid-induced neuronal death. *Invest Ophthalmol Vis Sci* 41:552-560.
- Hosokawa T, Rusakov DA, Bliss TV, Fine A (1995) Repeated confocal imaging of individual dendritic spines in the living hippocampal slice: evidence for changes in length and orientation associated with chemically induced LTP. *J Neurosci* 15:5560-5573.
- Houser CR, Hendry SH, Jones EG, Vaughn JE (1983) Morphological diversity of immunocytochemically identified GABA neurons in the monkey sensory-motor cortex. *J Neurocytol* 12:617-638.
- Huang EJ, Reichardt LF (2001) Neurotrophins: roles in neuronal development and function. *Annu Rev Neurosci* 24:677-736.
- Hubel DH, Wiesel TN (1977) Ferrier lecture. Functional architecture of macaque monkey visual cortex. *Proc R Soc Lond B Biol Sci* 198:1-59.
- Huber GC, Crosby EC (1933) A Phylogenetic Consideration of the Optic Tectum. *Proc Natl Acad Sci U S A* 19:15-22.
- Huxlin KR, Goodchild AK (1997) Retinal ganglion cells in the albino rat: revised morphological classification. *J Comp Neurol* 385:309-323.
- Isa T, Endo T, Saito Y (1998) The visuo-motor pathway in the local circuit of the rat superior colliculus. *J Neurosci* 18:8496-8504.
- Jacobs B, Scheibel AB (1993) A quantitative dendritic analysis of Wernicke's area in humans. I. Lifespan changes. *J Comp Neurol* 327:83-96.
- Jacobs B, Schall M, Scheibel AB (1993) A quantitative dendritic analysis of Wernicke's area in humans. II. Gender, hemispheric, and environmental factors. *J Comp Neurol* 327:97-111.
- Jacobs B, Driscoll L, Schall M (1997) Life-span dendritic and spine changes in areas 10 and 18 of human cortex: a quantitative Golgi study. *J Comp Neurol* 386:661-680.
- Jacobs B, Schall M, Prather M, Kapler E, Driscoll L, Baca S, Jacobs J, Ford K, Wainwright M, Treml M (2001) Regional dendritic and spine variation in human cerebral cortex: a quantitative golgi study. *Cereb Cortex* 11:558-571.

- Jakobs TC, Libby RT, Ben Y, John SW, Masland RH (2005) Retinal ganglion cell degeneration is topological but not cell type specific in DBA/2J mice. *J Cell Biol* 171:313-325.
- John SW, Smith RS, Savinova OV, Hawes NL, Chang B, Turnbull D, Davisson M, Roderick TH, Heckenlively JR (1998) Essential iris atrophy, pigment dispersion, and glaucoma in DBA/2J mice. *Invest Ophthalmol Vis Sci* 39:951-962.
- Johnson EC, Morrison JC, Farrell S, Deppmeier L, Moore CG, McGinty MR (1996) The effect of chronically elevated intraocular pressure on the rat optic nerve head extracellular matrix. *Exp Eye Res* 62:663-674.
- Jonas JB, Schmidt AM, Muller-Bergh JA, Schlotzer-Schrehardt UM, Naumann GO (1992) Human optic nerve fiber count and optic disc size. *Invest Ophthalmol Vis Sci* 33:2012-2018.
- Kaas JH, Huerta MF, Weber JT, Harting JK (1978) Patterns of retinal terminations and laminar organization of the lateral geniculate nucleus of primates. *J Comp Neurol* 182:517-553.
- Kabaso D, Coskren PJ, Henry BI, Hof PR, Wearne SL (2009) The electrotonic structure of pyramidal neurons contributing to prefrontal cortical circuits in macaque monkeys is significantly altered in aging. *Cereb Cortex* 19:2248-2268.
- Kapin MA, Doshi R, Scatton B, DeSantis LM, Chandler ML (1999) Neuroprotective effects of eliprodil in retinal excitotoxicity and ischemia. *Invest Ophthalmol Vis Sci* 40:1177-1182.
- Kaplan DR, Miller FD (2000) Neurotrophin signal transduction in the nervous system. *Curr Opin Neurobiol* 10:381-391.
- Karpati G, Carpenter S, Durham H (1988) A hypothesis for the pathogenesis of amyotrophic lateral sclerosis. *Rev Neurol (Paris)* 144:672-675.
- Kass MA, Heuer DK, Higginbotham EJ, Johnson CA, Keltner JL, Miller JP, Parrish RK, 2nd, Wilson MR, Gordon MO (2002) The Ocular Hypertension Treatment Study: a randomized trial determines that topical ocular hypotensive medication delays or prevents the onset of primary open-angle glaucoma. *Arch Ophthalmol* 120:701-713; discussion 829-730.

- Kato T, Hirano A, Donnenfeld H (1987) A Golgi study of the large anterior horn cells of the lumbar cords in normal spinal cords and in amyotrophic lateral sclerosis. *Acta Neuropathol* 75:34-40.
- Katz LC (1987) Local circuitry of identified projection neurons in cat visual cortex brain slices. *J Neurosci* 7:1223-1249.
- Kawai SI, Vora S, Das S, Gachie E, Becker B, Neufeld AH (2001) Modeling of risk factors for the degeneration of retinal ganglion cells after ischemia/reperfusion in rats: effects of age, caloric restriction, diabetes, pigmentation, and glaucoma. *Faseb J* 15:1285-1287.
- Kelly JP, Gilbert CD (1975) The projections of different morphological types of ganglion cells in the cat retina. *J Comp Neurol* 163:65-80.
- Kido N, Tanihara H, Honjo M, Inatani M, Tatsuno T, Nakayama C, Honda Y (2000) Neuroprotective effects of brain-derived neurotrophic factor in eyes with NMDA-induced neuronal death. *Brain Res* 884:59-67.
- Kim BG, Dai HN, McAtee M, Vicini S, Bregman BS (2007) Labeling of dendritic spines with the carbocyanine dye DiI for confocal microscopic imaging in lightly fixed cortical slices. *J Neurosci Methods* 162:237-243.
- Kinoshita D, Cohn DW, Costa-Pinto FA, de Sa-Rocha LC (2009) Behavioral effects of LPS in adult, middle-aged and aged mice. *Physiol Behav* 96:328-332.
- Kirov SA, Harris KM (1999) Dendrites are more spiny on mature hippocampal neurons when synapses are inactivated. *Nat Neurosci* 2:878-883.
- Kisicwa L, Dervan AG, Albon J, Morgan JE, Wride MA (2010) Retinal ganglion cell death postponed: giving apoptosis a break? *Ophthalmic Res* 43:61-78.
- Kitagawa K, Matsumoto M, Niinobe M, Mikoshiba K, Hata R, Ueda H, Handa N, Fukunaga R, Isaka Y, Kimura K, et al. (1989) Microtubule-associated protein 2 as a sensitive marker for cerebral ischemic damage--immunohistochemical investigation of dendritic damage. *Neuroscience* 31:401-411.
- Koester SE, O'Leary DD (1992) Functional classes of cortical projection neurons develop dendritic distinctions by class-specific sculpting of an early common pattern. *J Neurosci* 12:1382-1393.

- Kondo Y, Takada M, Honda Y, Mizuno N (1993) Bilateral projections of single retinal ganglion cells to the lateral geniculate nuclei and superior colliculi in the albino rat. *Brain Res* 608:204-215.
- Kriebel RM (1975) Neurons of the dorsal lateral geniculate nucleus of the albino rat. *J Comp Neurol* 159:45-67.
- Labriola AR, Laemle LK (1977) Cellular morphology in the visual layer of the developing rat superior colliculus. *Exp Neurol* 55:247-268.
- Lacey CJ, Potheary CA, Salt TE (2005) Modulation of retino-collicular transmission by Group III metabotropic glutamate receptors at different ages during development. *Neuropharmacology* 49 Suppl 1:26-34.
- Langer TP, Lund RD (1974) The upper layers of the superior colliculus of the rat: a Golgi study. *J Comp Neurol* 158:418-435.
- Larkman AU (1991) Dendritic morphology of pyramidal neurones of the visual cortex of the rat: I. Branching patterns. *J Comp Neurol* 306:307-319.
- Lavdas AA, Grigoriou M, Pachnis V, Parnavelas JG (1999) The medial ganglionic eminence gives rise to a population of early neurons in the developing cerebral cortex. *J Neurosci* 19:7881-7888.
- Leske MC (1983) The epidemiology of open-angle glaucoma: a review. *Am J Epidemiol* 118:166-191.
- Leske MC (2007) Open-angle glaucoma -- an epidemiologic overview. *Ophthalmic Epidemiol* 14:166-172.
- Leuba G (1983) Aging of dendrites in the cerebral cortex of the mouse. *Neuropathol Appl Neurobiol* 9:467-475.
- Leung CK, Lindsey JD, Chen L, Liu Q, Weinreb RN (2009) Longitudinal profile of retinal ganglion cell damage assessed with blue-light confocal scanning laser ophthalmoscopy after ischaemic reperfusion injury. *Br J Ophthalmol* 93:964-968.
- Leung CK, Lindsey JD, Crowston JG, Lijia C, Chiang S, Weinreb RN (2008) Longitudinal profile of retinal ganglion cell damage after optic nerve crush with blue-light confocal scanning laser ophthalmoscopy. *Invest Ophthalmol Vis Sci* 49:4898-4902.

- Leventhal AG (1979) Evidence that the different classes of relay cells of the cat's lateral geniculate nucleus terminate in different layers of the striate cortex. *Exp Brain Res* 37:349-372.
- Leventhal AG, Rodieck RW, Dreher B (1981) Retinal ganglion cell classes in the Old World monkey: morphology and central projections. *Science* 213:1139-1142.
- Levkovitch-Verbin H, Quigley HA, Martin KR, Valenta D, Baumrind LA, Pease ME (2002) Translimbal laser photocoagulation to the trabecular meshwork as a model of glaucoma in rats. *Invest Ophthalmol Vis Sci* 43:402-410.
- Lewen A, Li GL, Olsson Y, Hillered L (1996) Changes in microtubule-associated protein 2 and amyloid precursor protein immunoreactivity following traumatic brain injury in rat: influence of MK-801 treatment. *Brain Res* 719:161-171.
- Li GL, Farooque M, Holtz A, Olsson Y (1995) Microtubule-associated protein 2 as a sensitive marker for dendritic lesion after spinal cord trauma: an immunohistochemical study in the rat. *Restor Neurol Neurosci* 8:189-197.
- Li GL, Farooque M, Lewen A, Lennmyr F, Holtz A, Olsson Y (2000) MAP2 and neurogranin as markers for dendritic lesions in CNS injury. An immunohistochemical study in the rat. *Apmis* 108:98-106.
- Li Z, Okamoto K, Hayashi Y, Sheng M (2004) The importance of dendritic mitochondria in the morphogenesis and plasticity of spines and synapses. *Cell* 119:873-887.
- Lo DC, McAllister AK, Katz LC (1994) Neuronal transfection in brain slices using particle-mediated gene transfer. *Neuron* 13:1263-1268.
- Lodish H, Berk A, Zipursky S, Matsudaira P, Baltimore D, Darnell J (2000) *Molecular Cell Biology*, 4th Edition. New York: W. H. Freeman.
- Lu CC, Tsai SC, Wang SW, Huang WJ, Wang PS (1998) Age-related differences in the secretion of calcitonin in female rats. *Am J Physiol* 275:E735-739.
- Lund RD (1972) Anatomic studies on the superior colliculus. *Invest Ophthalmol* 11:434-441.
- Ly T, Gupta N, Weinreb RN, Kaufman PL, Yucel YH (2010) Dendrite plasticity in the lateral geniculate nucleus in primate glaucoma. *Vision Res.*

- Machado-Salas J, Scheibel ME, Scheibel AB (1977) Morphologic changes in the hypothalamus of the old mouse. *Exp Neurol* 57:102-111.
- Margalit E, Satta SR (2003) Retinal and optic nerve diseases. *Artif Organs* 27:963-974.
- Martin PR, White AJ, Goodchild AK, Wilder HD, Sefton AE (1997) Evidence that blue-on cells are part of the third geniculocortical pathway in primates. *Eur J Neurosci* 9:1536-1541.
- Masland RH (1986) The functional architecture of the retina. *Sci Am* 255:102-111.
- Matsumoto M, Yamamoto K, Homburger HA, Yanagihara T (1987) Early detection of cerebral ischemic damage and repair process in the gerbil by use of an immunohistochemical technique. *Mayo Clin Proc* 62:460-472.
- Mellwain J (1996) *An Introduction to the Biology of Vision*: Cambridge University Press.
- Meijering E, Jacob M, Sarria JC, Steiner P, Hirling H, Unser M (2004) Design and validation of a tool for neurite tracing and analysis in fluorescence microscopy images. *Cytometry A* 58:167-176.
- Mervis R (1978) Structural alterations in neurons of aged canine neocortex: a Golgi study. *Exp Neurol* 62:417-432.
- Mize RR, Spencer RF, Sterling P (1982) Two types of GABA-accumulating neurons in the superficial gray layer of the cat superior colliculus. *J Comp Neurol* 206:180-192.
- Mizuno K, Koide T, Yoshimura M, Araie M (2001) Neuroprotective effect and intraocular penetration of nipradilol, a beta-blocker with nitric oxide donative action. *Invest Ophthalmol Vis Sci* 42:688-694.
- Molnar Z, Lopez-Bendito G, Small J, Partridge LD, Blakemore C, Wilson MC (2002) Normal development of embryonic thalamocortical connectivity in the absence of evoked synaptic activity. *J Neurosci* 22:10313-10323.
- Morgan JE (2002) Retinal ganglion cell shrinkage in glaucoma. *J Glaucoma* 11:365-370.
- Morgan JE, Uchida H, Caprioli J (2000) Retinal ganglion cell death in experimental glaucoma. *Br J Ophthalmol* 84:303-310.

- Morgan JE, Datta AV, Erichsen JT, Albon J, Boulton ME (2006) Retinal ganglion cell remodelling in experimental glaucoma. *Adv Exp Med Biol* 572:397-402.
- Moriya T, Yamadori T (1993) Correlative study of the morphology and central connections of ipsilaterally projecting retinal ganglion cells in the albino rat. *Exp Eye Res* 56:79-83.
- Morizane C, Adachi K, Furutani I, Fujita Y, Akaike A, Kashii S, Honda Y (1997) N(omega)-nitro-L-arginine methyl ester protects retinal neurons against N-methyl-D-aspartate-induced neurotoxicity in vivo. *Eur J Pharmacol* 328:45-49.
- Morrison JC (2005) Elevated intraocular pressure and optic nerve injury models in the rat. *J Glaucoma* 14:315-317.
- Morrison JC, Moore CG, Deppmeier LM, Gold BG, Meshul CK, Johnson EC (1997) A rat model of chronic pressure-induced optic nerve damage. *Exp Eye Res* 64:85-96.
- Morrison JH, Hof PR (2002) Selective vulnerability of corticocortical and hippocampal circuits in aging and Alzheimer's disease. *Prog Brain Res* 136:467-486.
- Moschovakis AK, Karabelas AB, Highstein SM (1988) Structure-function relationships in the primate superior colliculus. I. Morphological classification of efferent neurons. *J Neurophysiol* 60:232-262.
- Nakamura H, Wu R, Onozuka M, Itoh K (2005) Ventral lateral geniculate nucleus projects to the dorsal lateral geniculate nucleus in the cat. *Neuroreport* 16:1575-1578.
- Nakamura S, Akiguchi I, Kameyama M, Mizuno N (1985) Age-related changes of pyramidal cell basal dendrites in layers III and V of human motor cortex: a quantitative Golgi study. *Acta Neuropathol* 65:281-284.
- Neale EA, Bowers LM, Smith TG, Jr. (1993) Early dendrite development in spinal cord cell cultures: a quantitative study. *J Neurosci Res* 34:54-66.
- Neufeld AH, Gachie EN (2003) The inherent, age-dependent loss of retinal ganglion cells is related to the lifespan of the species. *Neurobiol Aging* 24:167-172.
- Newell F (1991) *Ophthalmology : Principles and concepts* 7th Edition: Mosby Year Book.

- Nguyen MD, Shu T, Sanada K, Lariviere RC, Tseng HC, Park SK, Julien JP, Tsai LH (2004) A NUDEL-dependent mechanism of neurofilament assembly regulates the integrity of CNS neurons. *Nat Cell Biol* 6:595-608.
- Nicholls JG, Martin AR, Wallance BG (1992) *From Neuron to Brain: A Cellular and Molecular Approach to the Function of the Nervous System.*, 3rd Edition: Sinauer, Sunderland, MA.
- Nickells RW (1999) Apoptosis of retinal ganglion cells in glaucoma: an update of the molecular pathways involved in cell death. *Surv Ophthalmol* 43 Suppl 1:S151-161.
- Nimchinsky EA, Hof PR, Young WG, Morrison JH (1996) Neurochemical, morphologic, and laminar characterization of cortical projection neurons in the cingulate motor areas of the macaque monkey. *J Comp Neurol* 374:136-160.
- Nirmalanathan N, Greensmith L (2005) Amyotrophic lateral sclerosis: recent advances and future therapies. *Curr Opin Neurol* 18:712-719.
- Norden JJ, Kaas JH (1978) The identification of relay neurons in the dorsal lateral geniculate nucleus of monkeys using horseradish peroxidase. *J Comp Neurol* 182:707-725.
- Nunomura A, Perry G, Aliev G, Hirai K, Takeda A, Balraj EK, Jones PK, Ghanbari H, Wataya T, Shimohama S, Chiba S, Atwood CS, Petersen RB, Smith MA (2001) Oxidative damage is the earliest event in Alzheimer disease. *J Neuropathol Exp Neurol* 60:759-767.
- O'Brien JA, Lummis SC (2006) Diolistic labeling of neuronal cultures and intact tissue using a hand-held gene gun. *Nat Protoc* 1:1517-1521.
- Pang IH, Clark AF (2007) Rodent models for glaucoma retinopathy and optic neuropathy. *J Glaucoma* 16:483-505.
- Parnavelas JG, Mounty EJ, Bradford R, Lieberman AR (1977) The postnatal development of neurons in the dorsal lateral geniculate nucleus of the rat: a Golgi study. *J Comp Neurol* 171:481-499.
- Parnavelas JG, Lynch G, Brecha N, Cotman CW, Globus A (1974) Spine loss and regrowth in hippocampus following deafferentation. *Nature* 248:71-73.

- Pavlidis M, Stupp T, Naskar R, Cengiz C, Thanos S (2003) Retinal ganglion cells resistant to advanced glaucoma: a postmortem study of human retinas with the carbocyanine dye DiI. *Invest Ophthalmol Vis Sci* 44:5196-5205.
- Paxinos G (2004) *The Rat Nervous System.*, 3rd Edition: Academic Press.
- Paxinos G, Watson C (1998) *The rat brain in stereotaxic coordinates*, 4th Edition. New York: Academic press.
- Payne BR, Peters A (2002) *The Cat Primary Visual Cortex*: Academic Press.
- Pearson RA, Luneborg NL, Becker DL, Mobbs P (2005) Gap junctions modulate interkinetic nuclear movement in retinal progenitor cells. *J Neurosci* 25:10803-10814.
- Peichl L (1989) Alpha and delta ganglion cells in the rat retina. *J Comp Neurol* 286:120-139.
- Perry VH (1979) The ganglion cell layer of the retina of the rat: a Golgi study. *Proc R Soc Lond B Biol Sci* 204:363-375.
- Perry VH, Cowey A (1984) Retinal ganglion cells that project to the superior colliculus and pretectum in the macaque monkey. *Neuroscience* 12:1125-1137.
- Perry VH, Oehler R, Cowey A (1984) Retinal ganglion cells that project to the dorsal lateral geniculate nucleus in the macaque monkey. *Neuroscience* 12:1101-1123.
- Peters A, Moss MB, Sethares C (2001) The effects of aging on layer 1 of primary visual cortex in the rhesus monkey. *Cereb Cortex* 11:93-103.
- Polyak S (1957) *Vertebrate Visual System.* . Chicago: University of Chicago Press.
- Pothecary CA, Thompson H, Salt TE (2005) Changes in glutamate receptor function in synaptic input to the superficial superior colliculus (SSC) with aging and in retinal degeneration in the Royal College of Surgeons (RCS) rat. *Neurobiol Aging* 26:965-972.
- Purves D, Augustine GJ, Fitzpatrick D, Katz L, LaMantia AS, McNamara JO, SM W, editors (2001) *Neuroscience*, 2nd Edition. Sunderland (MA): Sinauer Associates, Inc.
- Qu J, Wang D, Grosskreutz CL (2010) Mechanisms of retinal ganglion cell injury and defense in glaucoma. *Exp Eye Res* 91:48-53.

- Quigley HA (1996) Number of people with glaucoma worldwide. *Br J Ophthalmol* 80:389-393.
- Quigley HA, Broman AT (2006) The number of people with glaucoma worldwide in 2010 and 2020. *Br J Ophthalmol* 90:262-267.
- Quigley HA, Dunkelberger GR, Green WR (1988) Chronic human glaucoma causing selectively greater loss of large optic nerve fibers. *Ophthalmology* 95:357-363.
- Quigley HA, Sanchez RM, Dunkelberger GR, L'Hernault NL, Baginski TA (1987) Chronic glaucoma selectively damages large optic nerve fibers. *Invest Ophthalmol Vis Sci* 28:913-920.
- Ragnarson B, Bengtsson L, Haegerstrand A (1992) Labeling with fluorescent carbocyanine dyes of cultured endothelial and smooth muscle cells by growth in dye-containing medium. *Histochemistry* 97:329-333.
- Ramoia AS, Campbell G, Shatz CJ (1987) Transient morphological features of identified ganglion cells in living fetal and neonatal retina. *Science* 237:522-525.
- Ramoia AS, Campbell G, Shatz CJ (1988) Dendritic growth and remodeling of cat retinal ganglion cells during fetal and postnatal development. *J Neurosci* 8:4239-4261.
- Ramón-Moliner E (1968) The morphology of dendrites. In: *The Structure and Function of Nervous Tissue*. New York: Academic Press.
- Rodieck RW, Watanabe M (1993) Survey of the morphology of macaque retinal ganglion cells that project to the pretectum, superior colliculus, and parvicellular laminae of the lateral geniculate nucleus. *J Comp Neurol* 338:289-303.
- Rodieck RW, Binmoeller KF, Dineen J (1985) Parasol and midget ganglion cells of the human retina. *J Comp Neurol* 233:115-132.
- Ruth E (1935) Metamorphosis of the pubic symphysis. I. The white rat (*Mus norvegicus albinus*). *Anat Rec* 64:1-7.
- Rutledge LT, Duncan J, Beatty N (1969) A study of pyramidal cell axon collaterals in intact and partially isolated adult cerebral cortex. *Brain Res* 16:15-22.

- Rutledge LT, Duncan J, Cant N (1972) Long-term status of pyramidal cell axon collaterals and apical dendritic spines in denervated cortex. *Brain Res* 41:249-262.
- Saini KD, Garey LJ (1981) Morphology of neurons in the lateral geniculate nucleus of the monkey. A Golgi study. *Exp Brain Res* 42:235-248.
- Samsonovich AV, Ascoli GA (2006) Morphological homeostasis in cortical dendrites. *Proc Natl Acad Sci U S A* 103:1569-1574.
- Sappington RM, Carlson BJ, Crish SD, Calkins DJ (2010) The microbead occlusion model: a paradigm for induced ocular hypertension in rats and mice. *Invest Ophthalmol Vis Sci* 51:207-216.
- Sasaki S, Iwata M (1996) Dendritic synapses of anterior horn neurons in amyotrophic lateral sclerosis: an ultrastructural study. *Acta Neuropathol* 91:278-283.
- Sawai H, Fukuda Y, Wakakuwa K (1985) Axonal projections of X-cells to the superior colliculus and to the nucleus of the optic tract in cats. *Brain Res* 341:1-6.
- Schiller PH (1982) Central connections of the retinal ON and OFF pathways. *Nature* 297:580-583.
- Schiller PH, Sandell JH, Maunsell JH (1986) Functions of the ON and OFF channels of the visual system. *Nature* 322:824-825.
- Schwartz M (2001) Harnessing the immune system for neuroprotection: therapeutic vaccines for acute and chronic neurodegenerative disorders. *Cell Mol Neurobiol* 21:617-627.
- Schwartz M, Yoles E (1999) Optic nerve degeneration and potential neuroprotection: implications for glaucoma. *Eur J Ophthalmol* 9 Suppl 1:S9-11.
- Sgobio C, Trabalza A, Spalloni A, Zona C, Carunchio I, Longone P, Ammassari-Teule M (2008) Abnormal medial prefrontal cortex connectivity and defective fear extinction in the presymptomatic G93A SOD1 mouse model of ALS. *Genes Brain Behav* 7:427-434.
- Shapley R, Perry VH (1986) Cat and monkey retinal ganglion cells and their visual functional roles. *Trends Neurosci* 9:229-235.

- Shareef SR, Garcia-Valenzuela E, Salierno A, Walsh J, Sharma SC (1995) Chronic ocular hypertension following episcleral venous occlusion in rats. *Exp Eye Res* 61:379-382.
- Sheldon WG, Warbritton AR, Bucci TJ, Turturro A (1995) Glaucoma in food-restricted and ad libitum-fed DBA/2N^{ia} mice. *Lab Anim Sci* 45:508-518.
- Sherman SM, Koch C (1986) The control of retinogeniculate transmission in the mammalian lateral geniculate nucleus. *Exp Brain Res* 63:1-20.
- Sholl DA (1953) Dendritic organization in the neurons of the visual and motor cortices of the cat. *J Anat* 87:387-406.
- Shou T, Liu J, Wang W, Zhou Y, Zhao K (2003) Differential dendritic shrinkage of alpha and beta retinal ganglion cells in cats with chronic glaucoma. *Invest Ophthalmol Vis Sci* 44:3005-3010.
- Sims PJ, Waggoner AS, Wang CH, Hoffman JF (1974) Studies on the mechanism by which cyanine dyes measure membrane potential in red blood cells and phosphatidylcholine vesicles. *Biochemistry* 13:3315-3330.
- So YT, Shapley R (1981) Spatial tuning of cells in and around lateral geniculate nucleus of the cat: X and Y relay cells and perigeniculate interneurons. *J Neurophysiol* 45:107-120.
- Sommer A (1989) Intraocular pressure and glaucoma. *Am J Ophthalmol* 107:186-188.
- Spear PD (1993) Neural bases of visual deficits during aging. *Vision Res* 33:2589-2609.
- Spear PD, Moore RJ, Kim CB, Xue JT, Tumosa N (1994) Effects of aging on the primate visual system: spatial and temporal processing by lateral geniculate neurons in young adult and old rhesus monkeys. *J Neurophysiol* 72:402-420.
- Sterling P (1971) Receptive fields and synaptic organization of the superficial gray layer of the cat superior colliculus. *Vision Res Suppl* 3:309-328.
- Stone J (1965) A quantitative analysis of the distribution of ganglion cells in the cat's retina. *J Comp Neurol* 124:337-352.
- Sun W, Li N, He S (2002a) Large-scale morphological survey of mouse retinal ganglion cells. *J Comp Neurol* 451:115-126.

- Sun W, Li N, He S (2002b) Large-scale morphological survey of rat retinal ganglion cells. *Vis Neurosci* 19:483-493.
- Szmajda BA, Grunert U, Martin PR (2008) Retinal ganglion cell inputs to the koniocellular pathway. *J Comp Neurol* 510:251-268.
- Terry RD (2006) Alzheimer's disease and the aging brain. *J Geriatr Psychiatry Neurol* 19:125-128.
- Terry RD, Masliah E, Salmon DP, Butters N, DeTeresa R, Hill R, Hansen LA, Katzman R (1991) Physical basis of cognitive alterations in Alzheimer's disease: synapse loss is the major correlate of cognitive impairment. *Ann Neurol* 30:572-580.
- Tezel G, Luo C, Yang X (2007) Accelerated aging in glaucoma: immunohistochemical assessment of advanced glycation end products in the human retina and optic nerve head. *Invest Ophthalmol Vis Sci* 48:1201-1211.
- Tokunaga A, Otani K (1976) Dendritic patterns of neurons in the rat superior colliculus. *Exp Neurol* 52:189-205.
- Turner JP, Salt TE (1998) Characterization of sensory and corticothalamic excitatory inputs to rat thalamocortical neurones in vitro. *J Physiol* 510 (Pt 3):829-843.
- Ueda J, Sawaguchi S, Hanyu T, Yaoeda K, Fukuchi T, Abe H, Ozawa H (1998) Experimental glaucoma model in the rat induced by laser trabecular photocoagulation after an intracameral injection of India ink. *Jpn J Ophthalmol* 42:337-344.
- Urcola JH, Hernandez M, Vecino E (2006) Three experimental glaucoma models in rats: comparison of the effects of intraocular pressure elevation on retinal ganglion cell size and death. *Exp Eye Res* 83:429-437.
- Vickers JC, Hof PR, Schumer RA, Wang RF, Podos SM, Morrison JH (1997) Magnocellular and parvocellular visual pathways are both affected in a macaque monkey model of glaucoma. *Aust N Z J Ophthalmol* 25:239-243.
- Vidal-Sanz M, Bray GM, Villegas-Perez MP, Thanos S, Aguayo AJ (1987) Axonal regeneration and synapse formation in the superior colliculus by retinal ganglion cells in the adult rat. *J Neurosci* 7:2894-2909.

- Vorwerk CK, Lipton SA, Zurakowski D, Hyman BT, Sabel BA, Dreyer EB (1996) Chronic low-dose glutamate is toxic to retinal ganglion cells. Toxicity blocked by memantine. *Invest Ophthalmol Vis Sci* 37:1618-1624.
- Wassle H (1988) Dendritic maturation of retinal ganglion cells. *Trends Neurosci* 11:87-89.
- Wassle H, Illing RB (1980) The retinal projection to the superior colliculus in the cat: a quantitative study with HRP. *J Comp Neurol* 190:333-356.
- Wassle H, Boycott BB, Illing RB (1981) Morphology and mosaic of on- and off-beta cells in the cat retina and some functional considerations. *Proc R Soc Lond B Biol Sci* 212:177-195.
- Watanabe M, Rodieck RW (1989) Parasol and midget ganglion cells of the primate retina. *J Comp Neurol* 289:434-454.
- Weber AJ, Zelenak D (2001) Experimental glaucoma in the primate induced by latex microspheres. *J Neurosci Methods* 111:39-48.
- Weber AJ, Harman CD (2005) Structure-function relations of parasol cells in the normal and glaucomatous primate retina. *Invest Ophthalmol Vis Sci* 46:3197-3207.
- Weber AJ, Kaufman PL, Hubbard WC (1998) Morphology of single ganglion cells in the glaucomatous primate retina. *Invest Ophthalmol Vis Sci* 39:2304-2320.
- Webster MJ, Rowe MH (1984) Morphology of identified relay cells and interneurons in the dorsal lateral geniculate nucleus of the rat. *Exp Brain Res* 56:468-474.
- Weinreb RN, Khaw PT (2004) Primary open-angle glaucoma. *Lancet* 363:1711-1720.
- Whitmore AV, Libby RT, John SW (2005) Glaucoma: thinking in new ways-a role for autonomous axonal self-destruction and other compartmentalised processes? *Prog Retin Eye Res* 24:639-662.
- Wilson JR (1989) Synaptic organization of individual neurons in the macaque lateral geniculate nucleus. *J Neurosci* 9:2931-2953.
- Wilson PD, Stone J (1975) Evidence of W-cell input to the cat's visual cortex via the C laminae of the lateral geniculate nucleus. *Brain Res* 92:472-478.
- Wilson PD, Rowe MH, Stone J (1976) Properties of relay cells in cat's lateral geniculate nucleus: a comparison of W-cells with X- and Y-cells. *J Neurophysiol* 39:1193-1209.

- Wolfs RC, Borger PH, Ramrattan RS, Klaver CC, Hulsman CA, Hofman A, Vingerling JR, Hitchings RA, de Jong PT (2000) Changing views on open-angle glaucoma: definitions and prevalences--The Rotterdam Study. *Invest Ophthalmol Vis Sci* 41:3309-3321.
- Wong-Riley MT (1972) Neuronal and synaptic organization of the normal dorsal lateral geniculate nucleus of the squirrel monkey, *Saimiri sciureus*. *J Comp Neurol* 144:25-59.
- Wong TP, Marchese G, Casu MA, Ribeiro-da-Silva A, Cuello AC, De Koninck Y (2000) Loss of presynaptic and postsynaptic structures is accompanied by compensatory increase in action potential-dependent synaptic input to layer V neocortical pyramidal neurons in aged rats. *J Neurosci* 20:8596-8606.
- Xu Y, Wang H, Chen Q, Zhou Y (2007) Age and sex-related dendritic changes in the visual cortex of the rat. *Zoological Research* 28:297-302.
- Yamasaki EN, Ramoa AS (1993) Dendritic remodelling of retinal ganglion cells during development of the rat. *J Comp Neurol* 329:277-289.
- Yanagihara T, Yoshimine T, Morimoto K, Yamamoto K, Homburger HA (1985) Immunohistochemical investigation of cerebral ischemia in gerbils. *J Neuropathol Exp Neurol* 44:204-215.
- Yoles E, Schwartz M (1998a) Potential neuroprotective therapy for glaucomatous optic neuropathy. *Surv Ophthalmol* 42:367-372.
- Yoles E, Schwartz M (1998b) Degeneration of spared axons following partial white matter lesion: implications for optic nerve neuropathies. *Exp Neurol* 153:1-7.
- Zeyen T (1999) Target pressures in glaucoma. *Bull Soc Belge Ophtalmol* 274:61-65.

Appendix

Comparison of Neuron J Programme to Sholl Analysis

In this thesis, the analysis of dendritic parameters was performed using the Neuron J programme. In order to compare the Neuron J programme (Fig. a1) with the more traditionally used Sholl analysis (Fig. a2), a sample neuron was analyzed using both methods as described below.

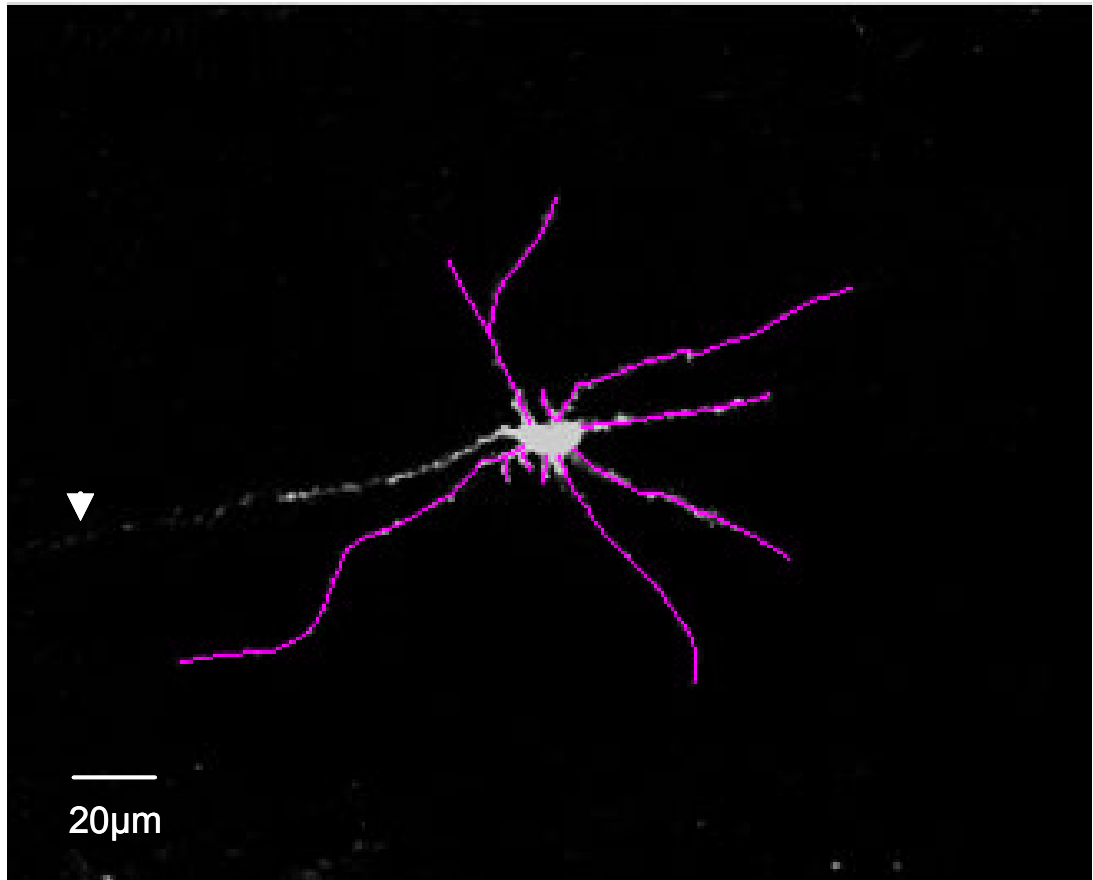


Figure a1: A sample neuron was analyzed using the Neuron J programme.

This figure shows the analysis of dendritic parameters using the Neuron J programme. Dendrites of the sample neuron, as shown in pink, were traced individually and quantified automatically by the Neuron J programme. Both mean dendritic length and dendritic number were measured. The arrowhead indicates the axon.

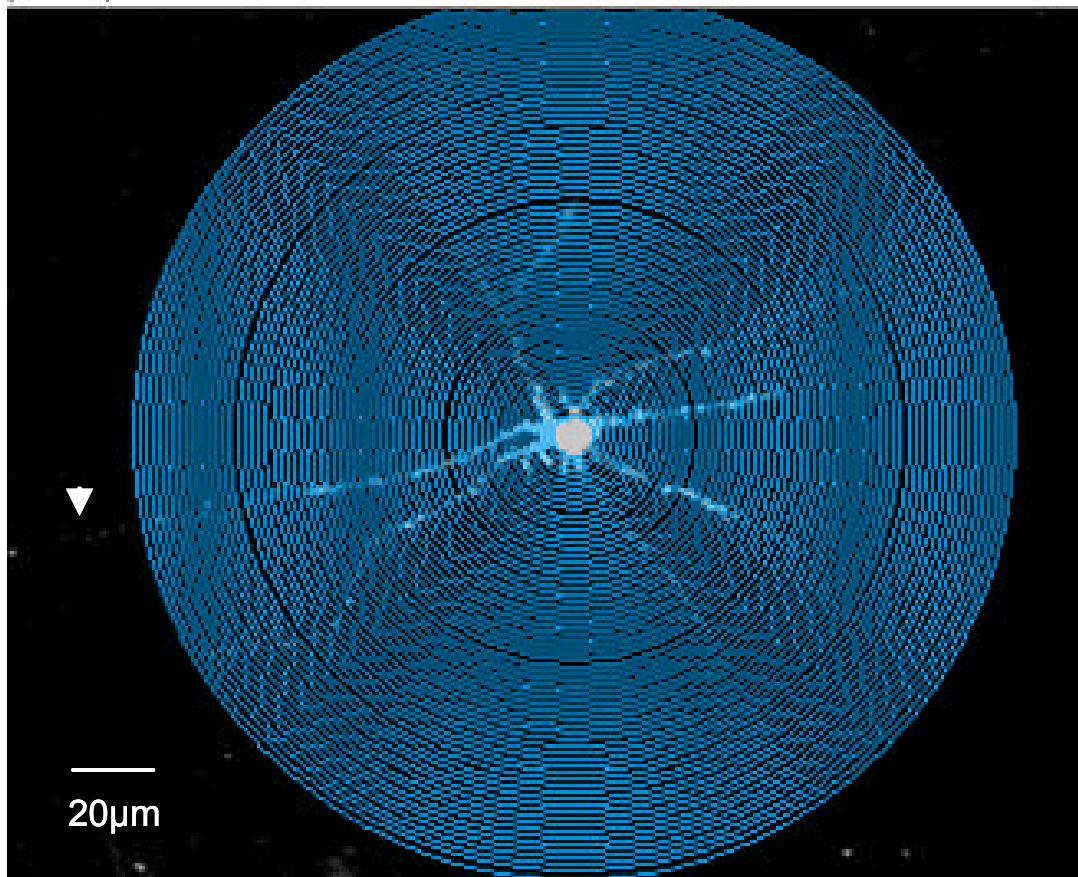


Figure a2: A sample neuron was analyzed using the Sholl analysis.

This figure shows that the same sample neuron shown in Fig. a1 was also analyzed using the Sholl analysis. A series of concentric circles with radii 6.5 to 136.5 μm , spaces at 2 μm increments, were created around the cell body. The cumulative intersections, the relative length of the dendrites and dendritic number were then calculated. The arrowhead indicates the axon.

The paired student T-test was applied to compare the mean dendritic length quantified using the two methods (SPSS 14.0, Chicago, IL) and $p < 0.05$ was considered to be significant. The statistical analysis showed no significant difference ($p > 0.05$) (Table a; Fig. a3).

Image	Dendritic Number	Mean Dendritic Length (μm)	Range of Dendritic Length (μm)	Paired student T-test for the mean dendritic length	
				T value	P value
a1, Sample image-Neuron J	11	52.33	6.71-129.82	2.018	0.071
a2, Sample image-Sholl analysis	11	50.18	4 - 124		

Table a: Comparison of the Neuron J programme to the Sholl analysis on eleven dendrites.

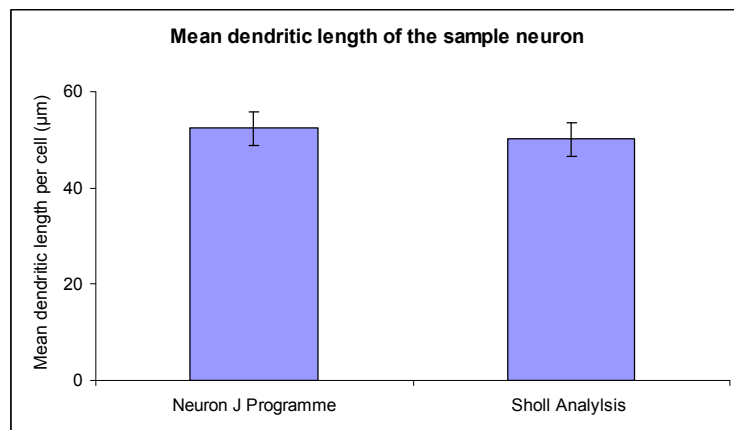


Figure a3: Comparison of the Neuron J programme to the Sholl analysis on eleven dendrites.